UNIVERSITY OF ŽILINA

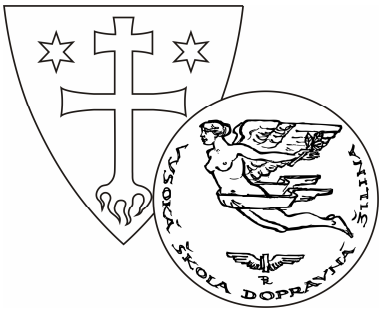

TRANSCOM 2009

8-th EUROPEAN CONFERENCE OF YOUNG RESEARCH AND SCIENTIFIC WORKERS

PROCEEDINGS

SECTION 5

MATERIAL ENGINEERING. MECHANICAL ENGINEERING TECHNOLOGIES

ŽILINA June 22 - 24, 2009
SLOVAK REPUBLIC

UNIVERSITY OF ŽILINA

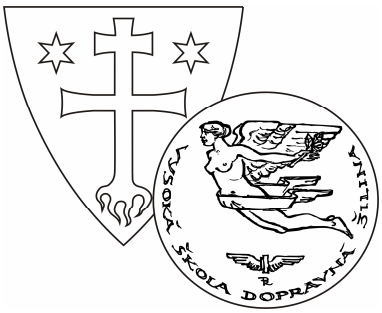

TRANSCOM 2009

8-th EUROPEAN CONFERENCE
OF YOUNG RESEARCH AND SCIENTIFIC WORKERS

under the auspices of

Prof. Ing. Ján Mikolaj, PhD.
Minister of Education, Slovak Republic

&

Prof. Ing. Ján Bujňák, PhD.
Rector of the University of Žilina

SECTION 5

MATERIAL ENGINEERING. MECHANICAL ENGINEERING TECHNOLOGIES

ŽILINA June 22 - 24, 2009
SLOVAK REPUBLIC

Edited by Alan Vaško, Peter Brída

ISBN:….

TRANSCOM 2009
8-th European conference of young research and scientific workers

TRANSCOM 2009, the 8th international conference of young European researchers, scientists and educators, aims to establish and expand international contacts and co-operation. The main purpose of the conference is to provide young scientists with an encouraging and stimulating environment in which they present results of their research to the scientific community. TRANSCOM has been organised regularly every other year since 1995. Between 160 and 400 young researchers and scientists participate regularly in the event. The conference is organised for postgraduate students and young research workers up to the age of 35 and their tutors. Young workers are expected to present the results they had achieved.

The conference is organised by the University of Žilina. It is the university with about 13 000 graduate and postgraduate students. The university offers Bachelor, Master and PhD programmes in the fields of transport, telecommunications, forensic engineering, management operations, information systems, in mechanical, civil, electrical, special engineering and in social sciences.

SECTIONS AND SCIENTIFIC COMMITTEE

1. TRANSPORT AND COMMUNICATIONS TECHNOLOGY

Scientific committee: Baumann S. (D), Cenek P. (SK), Droździel P. (PL), Janáček J. (SK), Jánošíková Ľ. (SK), Kremeňová I. (SK), Novák A. (SK), Palúch S. (SK), Rievaj V. (SK), Řezáč M. (CZ), Schnieder E. (D), Surovec P. (SK), Žarnay P. (SK)

2. ECONOMICS AND MANAGEMENT

Scientific committee: Bartošová V. (SK), Blašková M. (SK), Březinová O. (CZ), Duncan F.H. (USA), Hittmár Š. (SK), Kos B. (PL), Kucharčíková A. (SK), Lyakin A. (RUS), Rostášová M. (SK), Rybakov F. (RUS), Strenitzerová M. (SK), Strišš J. (SK), Tomová A. (SK)

3. INFORMATION AND COMMUNICATION TECHNOLOGIES

Scientific committee: Bärwald W. (D), Dado M. (SK), Drozdová M. (SK), Hanuliak I. (SK), Keil R. (D), Klimo M. (SK), Kolev P. (BG), Kotsopoulos S. (GR), Madleňák R. (SK), Matiaško K. (SK), Spalek J. (SK), Vaculík J. (SK), Vaculík M. (SK), Vrček N. (HR)

4. ELECTRIC POWER SYSTEMS. ELECTRICAL AND ELECTRONIC ENGINEERING

Scientific committee: Altus J. (SK), Blažek V. (D), Čápová K. (SK), Dobrucký B. (SK), Dodds S.J. (GB), Santarius P. (CZ), Vittek J. (SK)

5. MATERIAL ENGINEERING. MECHANICAL ENGINEERING TECHNOLOGIES

Scientific committee: Adamczak S. (PL), Bokůvka O. (SK), Borkowski S. (PL), Dzimko M. (SK), Guagliano M. (I), Kunz L. (CZ), Meško J. (SK), Nicoletto G. (I), Palček P. (SK), Skočovský P. (SK), Takács J. (H)

6. MACHINES AND EQUIPMENTS. APPLIED MECHANICS

Scientific committee: Dekýš V. (SK), Gerlici J. (SK), Kalinčák D. (SK), Malenovský E. (CZ), Medvecký Š. (SK), Merkisz J. (PL), Nemček M. (CZ), Pawelczyk M. (PL), Sága M. (SK), Zapoměl J. (CZ), Žmindák M. (SK)

7. CIVIL ENGINEERING

Scientific committee: Bouchair H. (F), Dmitrovskaja L. (RUS), Garbuz A. (UA), Ižvolt L. (SK), Melcer J. (SK), Ivanov J. (BG), Teleman E.C. (RO), Vičan J. (SK), Zolotov M. (UA)

8. SOCIAL SCIENCES

Scientific committee: Banáry B. (SK), Baštinec J. (CZ), Cabanová V. (SK), Gulová L. (CZ), Kráľová Z. (SK), Růžičková M. (SK), Šindelářová J. (CZ), Vikoren V. (N)

9. SECURITY ENGINEERING. FORENSIC ENGINEERING

Scientific committee: Danihelka P. (SK), Horák R. (CZ), Navrátil L. (CZ), Poledňák P. (SK), Reitšpís J. (SK), Seidl M. (SK), Šenovský M. (CZ), Šimák L. (SK), Vasiliev D. (BG), Zamiar Z. (PL)

ORGANIZING COMMITTEE

CHAIRPERSON Bokůvka Otakar

EXECUTIVE SECRETARY Vráblová Helena

MEMBERS Bábel J., Belan J., Braciník P., Brída P., Brumerčík F., Dobrotková M., Dubcová Z., Frajtová-Michalíková K., Harušinec J., Hnátová Z., Houšková L., Imrišková E., Jánošíková G., Kačiaková B., Kardoš M., Kormancová M., Krasňan M., Kuzmová M., Ladovský T., Ližbetinová L., Mihalov K., Močková M., Mráz M., Murín M., Neslušan M., Ondrejka R., Pachová S., Pavelková I., Pilát P., Potkan T., Remek Ľ., Smetana M., Sršníková D., Stránska S., Štofková K., Tulejová L., Valentíková E., Varmus M., Vaško A., Vaško M., Záborský M.

SECTION 5 MATERIAL ENGINEERING. MECHANICAL ENGINEERING TECHNOLOGIES.

REVIEWERS:

Belan Juraj
Bokůvka Otakar
Fabian Peter
Hadzima Branislav
Konečná Radomila
Kuric Ivan
Liptáková Tatiana
Meško Jozef
Mičian Miloš
Mičietová Anna
Mintách Rastislav
Neslušan Miroslav
Nový František
Palček Peter
Pilc Jozef
Salaj Ján
Skočovský Petr
Sládek Augustín
Tillová Eva
Turek Stanislav
Vaško Alan

Note:

Authors are responsible for language contents of their papers

CONTENTS

Transcom 2009, 22-24 June 2009
University of Žilina, Žilina, Slovak Republic

Welding, Heat Treatment, Microstructure and Vickers Hardness of Austempered Ductile Iron

František Banaš, Jozef Meško *
* F. Banaš Ing., J. Meško, prof., PhD., Ing. – Department of Technological Engineering, University of Žilina, Faculty of Mechanical Engineering, Univerzitná 1, 010 26 Žilina, Slovak Republic, frantisek.banas@fstroj.uniza.sk

Abstract. The article handles with the welding, heat treatment and Vickers hardness of bainitic ductile iron. It includes characteristics of bainitic ductile iron, welding methods, heat treatment and Vickers hardness of ADI (Austempered Ductile Iron), ADI – market overview, application of ADI in automotive, experimental results of ADI welding and graph of Vickers hardness.

Keywords: welding method, austempered ductile iron, tubular electrode cored, bainitic heat treatment, weld pool, bainite annealing, filler metal, Vickers hardness, microstructure.

1. Introduction

ADI has attracted considerable interest in recent years, because of its excellent properties, such as high strength with good ductility, good wear resistance and resistance to fatigue [1,2,3].

2. Characteristics of Austempered Ductile Iron

ADI is a heat treated cast iron with nodular graphite. It is compared with pearlitic cast iron with nodular graphite and it is characterised by significantly higher static and dynamic strength and a higher ductility at the same time. This is proven to be essential, particularly for the required zero damage rate. Also, this material offers better characteristics concerning noise and vibration damping than steel [3].

3. Welding Methods of ADI

Welding is a commonly used fabrication process, which joints materials pieces. This can be accomplished by partially melting of the work pieces, sometimes also by adding of an filler material, to form a pool of molten material that solidifies, cools and subsequently becomes a strong joint [6].

- principles of ADI MMA welding,
- principles of ADI GTAW,
- principles of ADI FCAW [5,6].

4. Heat Treatment of ADI

The initial material for ADI is ductile cast iron. It is subjected to an isothermal heat treatment process called austempering. Austempering process involves the alloy

austenitization in the temperature range of 840 to 940 °C (for 1 – 2 h), then quenching to an intermediate temperature range of 230 – 400 °C and holding there for sufficient time (usually between 2 and 4 h). This results in an unique microstructure in which the matrix is consisting of a mixture of ferrite and high carbon austenite. This microstructure is often referred to as ausferrite [3,4,7].

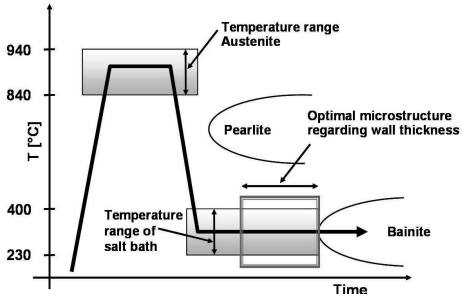

Fig. 1. Diagram of the temperature gradient of the isothermal interstitial transformation

5. Experimental Part

***Base material*:** Austempered ductile iron (ADI), microstructure: nodular graphite type VI 6, bainite matrix

Filler metal: Tubular cored electrode type RD 592/L13 (production in University of Žilina – VUZ – PI Bratislava), ***Preheating***: T_p = 450 ^oC / 30 min.

***Shielding atmosphere*:** Corgon 18 (82 % Ar + 18 % CO2), fy LINDE, k.s. Bratislava

Method of welding: Flux Cored Gas – Shielded Arc Welding (FCAW),

Heat treatment after welding:

• ***HT 1:*** heat treatment 1 – austempering: 910 ^oC / 30 min., heat treatment: 310 ^oC / 90 min. – furnace, following cooling – air,

• ***HT 2:*** heat treatment 2 – austempering: 910 ^oC / 30 min., heat treatment: 270 ^oC / 90 min. – furnace, following cooling – air. ***WOHT:*** without heat treatment.

5.1. Microstructures of Surfacing Welds on the ADI – Cast Irons

a) Without heat treatment after welding

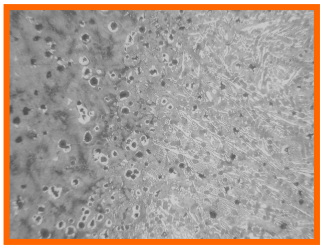

Fig. 2. FCAW: base metal - welded metal
Etch. 1 % Nital, Mag. 100 x

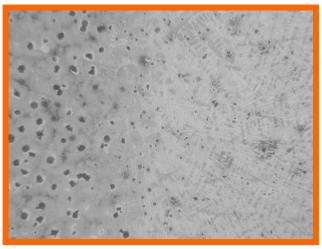

Fig. 3. GTAW: base metal - welded metal
Etch. 1 % Nital, Mag. 100 x

b) Heat treatment 1 after welding

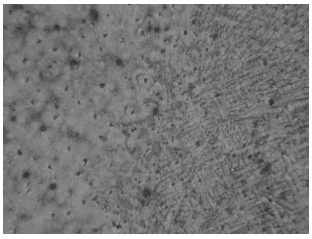

Fig. 4. FCAW: base metal - welded metal
Etch. 1 % Nital, Mag. 100 x

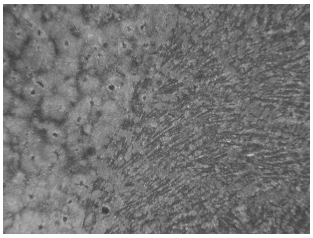

Fig. 5. GTAW: base metal - welded metal
Etch. 1 % Nital, Mag. 100 x

c) Heat treatment 2 after welding

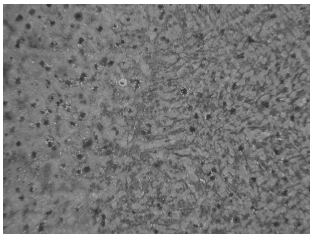

Fig. 6. FCAW: base metal - welded metal
Etch. 1 % Nital, Mag. 100 x

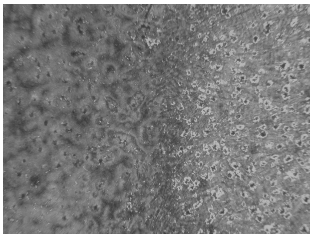

Fig. 7. GTAW: base metal – welded metal
Etch. 1 % Nital, Mag. 100 x

5.2. Vickers Hardness on the ADI – Cast Irons

The measuring of harness was performed on the samples, that were ready for observation of microstructure welding joint. The hardness was measured on the line from FM (filler material) to BM (base material) in different places, for watching the change of hardness. The hardness was measured with the Vickers method STN 420374 (ISO 6507 – 1).

5.3. Experimental Results

The experimental results of microstructure analyses are indicated on the expressive non – homogeneous of weld joints and the creation of phases type as ledeburite, high – low bainite, martensite and remaining austenite.

Vickers method ratings was found, samples without heat treatment under – riding mechanical properties filler metal with base material.

By measuring hardness on welding joint without heat treatment was found filler metal is hardest as base material.

Be possible to imagine high hardness are reason dendrite structure in base material. Big difference hardness between filler metal and base material no be of advantage because uprise internal stress.

Graphic relation between measuring number and HV 10:

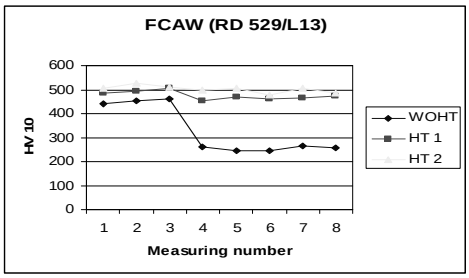

Fig. 8

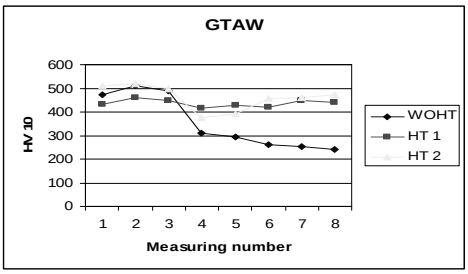

Fig. 9

Fig. 8. Graphic relation between measuring number and HV 10 by using tubular electrode RD529/L13
Fig. 9. Graphic relation between measuring number and HV 10 by using cast iron staff

6. Conclusions

The welding and Vickers method of ADI is in the beginning phase at the present time. The problematic of welding is connected with the difficult weldability of ADI, types of filler metals application, the ranges of preheating and bainitic transformation, following by the heat treatment, etc. The experimental works are in the state of the next research.

This article was created thanks to grant project: K – 08 – 012 – 00. Authors thank to grant agency for the support.

References

[1] PUTATUNDA, S. K.: *Development of austempered ductile iron (ADI) with simoltaneous high yield strenght and fracture touhness by a novel two – step austempering process. Materials Science and Engineering Elsevier. Detroit. USA. 2001. s. 70-80.*

[2] BANNA, E. M.: *Effect of preheat on welding of ductile cast iron. Elsevier, Giza, Egypt, 1999, s. 21-26.*

[3] PUTATUNDA, S. K., GADICHERLA, P. K.: *Influence of austenitizing temperature on fracture toughness of a low manganese austempered ductile iron (ADI) with ferritic as cast structure. Elsevier. Materials Sciense and Engineering. Detroit. USA, 1999, s. 15-31.*

[4] *http://www.aditreatments.com*

[5] MEŠKO, J., VESELKO, J.: *Zváranie a opravy grafitických liatin. 1. vyd. EDIS ŽU, Žilina, 1999, s. 198.*

[6] PLEVA, J.: *Tepelný účinok elektrického oblúka na základný materiál pri TIG – zváraní (The heat influence of electric arc on the base material at the TIG welding.) In: Nekonvenčné technológie NT 06. Elektronický zborník prednášok z vedeckej konferencie. Žilina. 2006. ISBN 80-8070-554-2*

[7] FABIAN, P. KEČKOVÁ, E. BETÁK**,** P.**:** *Tepelné spracovanie. Vydala Žilinská univerzita v Žiline, Univerzitná 1, 010 26 Žilina.Vedecký redaktor: prof. Ing. Augustín Sládek, PhD.Vytlačil: Tlačiareň svidnícka, s.r.o. v decembri 2007 (114 strán, 61 obrázkov, 17 tabuliek). Prvé vydanie, náklad 100 výtlačkov. ISBN 978 – 80 – 969592- 7 –3*

Transcom 2009, 22-24 June 2009
University of Žilina, Žilina, Slovak Republic

Degradation of Advanced Cast Material for Aerospace Industry

[*]Juraj Belan
[*]University of Žilina, Faculty of Mechanical Engineering, Department of Materials Engineering, Univerzitna 1, 01026 Žilina, Slovakia, juraj.belan@fstroj.uniza.sk

Abstract. The Ni – base superalloys are used in aircraft industry for production of aero engine most stressed parts, as are turbine blades. From this reason a dendrite arm spacing, carbides size and distribution, morphology, number and value of γ' - phase are very important structural characteristics for blade lifetime prediction as well as aero engine its self. In this article are used methods of quantitative metallography (software LUCIA for carbides evaluation, measuring of secondary dendrite arm spacing and coherent testing grid for γ' - phase evaluation) for evaluation of structural characteristics mentioned above on experimental material Inconel IN 713LC. The high temperature effect and cooling rate on structural characteristics and application of quantitative methods evaluation are presented in this paper.

Keywords: Ni – base superalloys, turbine blades, quantitative metallography, γ' - phases.

1. Introduction

The structure of polycrystalline Ni – base superalloys, depending form a heat – treatment, is consist of solid solution of elements in Ni (γ – phase, also called matrix), primary carbides MC type (created by element such as Cr and Ti), intermetallic precipitate $Ni_3(Al, Ti)$ (γ' - phase), and secondary carbides $M_{23}C_6$ type (created by elements such as Cr, Co, Mo, W). Shape and size of these structural components have a significant influence on final mechanical properties of alloy.

For instance the precipitate γ' size greater than 0,8 μm significantly decreasing the creep rupture life of superalloys and also carbides size greater than 50μm is not desirable because of fatigue cracks initiation.

For this reason needs of new non – conventional structure parameters methods evaluation were developed. The quantitative metallography, deep etching, and colour contrast belongs to basic methods. The quantitative metallography measuring has statistical nature. The elementary tasks of quantitative metallography are:

- Dendrite arm spacing evaluation.
- Carbide size and distribution.
- Volume ratio of evaluated phase.
- Number ratio of evaluated phase.
- Size of evaluated phase.

The application of quantitative metallography and colour contrast on the Ni – base superalloys are the main objectives discussed in this paper. More detailed analyze are published in previous works [1-6]. These non – conventional methods were successfully used also on the other types of materials [7-8].

2. Experimental methods

The cast Ni – base superalloy Inconel IN 713LC was used as an experimental material. Alloy IN 713LC contains higher amount of Cr, has increased gas corrosion resistance and also high creep rupture life.

This alloy was evaluated after annealing at 800 °C/ 10 and 15 hrs. and followed by cooling with various rate, presented with cooling in water, oil and air. The chemical composition in wt % is in Tab.1.

Specimen	Chemical composition (wt.%)										
	C	Ni	Co	Nb	Ti	Cr	Al	W	Mo	Fe	Mn
IN 713LC	0.047	base	0.06	1.86	0.67	12.6	6.12	0.08	4.43	-	0.02

Tab. 1. Experimental alloy chemical composition (wt. %)

For structural characteristics evaluation were used following quantitative metallography methods:

- Carbide distribution and average size evaluated by software LUCIA Metalo 5.0.
- Secondary dendrite arm spacing measurement.
- For number of γ' - phase particles were used coherent testing grid with area probe of square shape.
- For volume of γ' - phase particles were used coherent testing grid with 50 dot probes made of backslash crossing.

3. Experimental results and discussion

The Inconel IN 713LC microstructure of starting stage is created by carbides in chain morphology situated on grain boundary and large amount of eutectic cells γ/γ' (Fig. 1a). An example of microstructure after annealing at 800°C/15 hrs., focused on carbide distribution is on Fig. 1b.

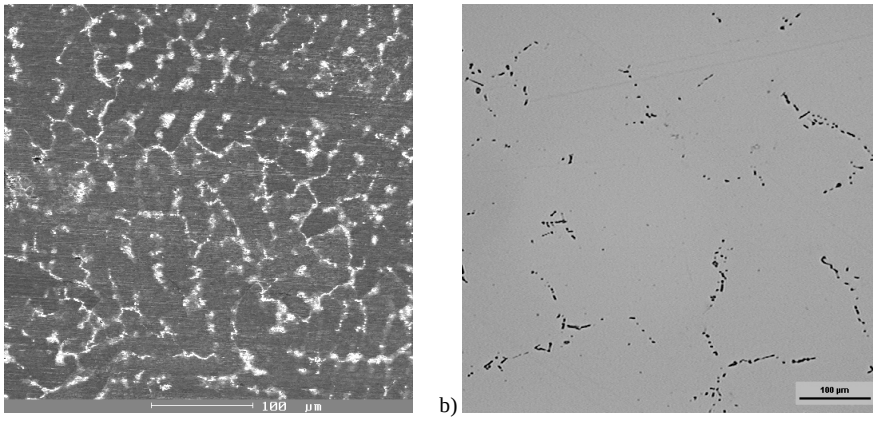

Fig. 1. Superalloy IN 713LC: a) starting stage, b) 800°C/15hrs. cooled in oil , etch. Marble, SEM.

After 800°C / 10 and 15 hrs. the microstructure shows some changes, mainly in number of carbides, its distribution and size. This effect is forced by diffusion mechanism and cooling rate when quick cooling represented by water gives not sufficient time for carbide growth. Results of carbide evaluation are in Fig. 2.

For dendrite structure evaluation was used method of measuring secondary dendrite arm spacing. Results of measuring are in Tab. 2. As cast materials are characterized by dendritic structure, which is result of chemical heterogeneity. With influence of holding on annealing temperature is chemical heterogeneity decreasing. It means that secondary dendrite arm spacing is increasing (dendrites are growing).

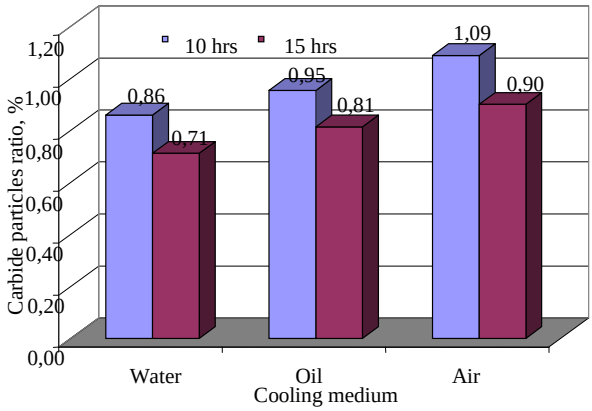

Fig. 2. Carbide particles ratio depended from cooling medium and time of holding

Secondary dendrite arm spacing [μm]					
Alloy	**Air**	**Oil**	**Water**	**Starting stage**	
IN713LC 10h	166.67	151.52	136.99	**IN713LCv**	161.29
IN713LC 15h	172.41	156.25	142.86		

Tab. 2. Results of secondary dendrite arm spacing evaluation.

There were also measured characteristics of γ´ - phase morphology with using of coherent testing grid methods, Tab. 3. As were mentioned above, number and volume of γ´ - phase have significant influence on mechanical properties of this alloy, especially on creep rupture life. Average satisfactory size of γ´ - phase is about 0.35 ÷ 0.45 μm and also carbide size should not exceed size of 5 μm – because of fatigue crack initiation.

Alloy	**Number of γ´ - phase, N [μm^{-2}]**	**Volume of γ´ - phase ,V [%]**	**Size of γ´ - phase , u [μm]**	**Average carbide size [μm]**
IN713LCv	1.68	60.4	0.76	-
IN713LC 10h water	2.14	58.4	0.52	3.629
IN713LC 10h oil	1.84	63.6	0.59	3.695
IN713LC 10h air	1.63	66.6	0.64	3.803
IN713LC 15h water	2.02	61.2	0.55	3.609
IN713LC 15h oil	1.84	65.8	0.60	3.774
IN713LC 15h air	1.58	71.2	0.67	3.608

Tab. 3. The γ´ - phase morphology evaluation including Vickers hardness measuring

4. Conclusion

As cast Ni – base superalloy Inconel IN 713LC was used as an experimental material. The structural characteristics were evaluated from starting stage of sample and after annealing at 800°C / 10 and 15 hrs. with using of quantitative metallography methods. Partial results are as follows:

- Structure of sample is characterized by dendritic segregation. In dendritic areas is segregate fine γ' - phase. In interdendritic areas are segregated eutectic cells γ/γ' and carbides.
- Holding time does not have significant influence on carbide particles size. Size of carbides is under critical level for fatigue crack initiation. Increasing rate of cooling has significant effect on carbide particles ratio.
- Chemical heterogeneity with longer holding time is decreasing. It is reason of sufficient time for diffusion mechanism, which is confirmed by secondary dendrite arm spacing measurement results.
- The volume of γ' - phase with longer holding time is increasing and also γ' - phase size is growing. With higher rate of cooling are γ' particles finer.
- There was not evidence of TCP phase presence even though high annealing temperature.
- Cooling rate have also influence on hardness. At higher rate of cooling are created internal stresses, which caused hardness increasing – changing of dislocation structure.

Cooling rates, represented by various cooling mediums have influence on diffusion processes in structure of alloy. These diffusion processes are the main mechanism for segregation and creating of carbide particles, equalization of chemical heterogeneity, γ' - phase segregation and are responsible for structure degradation of this alloy as well.

Acknowledgement

This work has been supported by Scientific Grant Agency of Ministry of Education of Slovak Republic and Slovak Academy of Sciences, grant No. 1/0208/08 and Culture and Educational Grant Agency of Ministry of Education of Slovak Republic, grant No. 3/6078/08.

References

[1] Copley, S.M., Kear, B.H. Structural characteristics of superalloys, part I, The Minerals, Metals & Materials Society – The American Institute of Mining, Metallurgical, and Petroleum Engineers 239 1967: pp. 977– 983.

[2] Copley, S.M., Kear, B.H. Structural characteristics of superalloys, part II, The Minerals, Metals & Materials Society – The American Institute of Mining, Metallurgical, and Petroleum Engineers 239 1967: pp. 984 – 989.

[3] Donachie, M.J. Superalloy Source Book, ASM, 1984, pp. 102 – 111.

[4] Leverant, G.R., Kear, B.H. Mechanical properties of advanced superalloys, Metallurgical and Materials Transactions 1 1970: pp. 491-498,.

[5] Jackson, J.J. Evaluation of superalloys structural characteristics, Metallurgical and Materials Transactions 8A (10) 1977: pp. 1615 – 1620.

[6] Gell, M., Duhl, D.N. Progressive technologies in superalloys. Advanced high temperature alloys ASM, 1985: pp. 41 – 49.

[7] Skočovský, P., Matejka, M.: Cast iron microstructure – metallography handbook Fompex, Trenčín, ES VŠDS, 1994.

[8] Skočovský, P., Vaško, A. Quantitative evaluation of cast iron structure 1st Edition, EDIS, Žilina, 2007, 73 s.

Transcom 2009, 22-24 June 2009
University of Žilina, Žilina, Slovak Republic

Non-Conventional Methods of Machining and the Sysklass System

*Tomáš Berešík,*Anna Mičietová
* Ing.Tomáš Berešík, ., University of Žilina, Faculty of Mechanical Engineering, Department of Machining and Manufacturing Engineering , Univerzitná 1, 010 26 Žilina, Slovak Republic,
☎ 00421 – 41 – 513 2782, e-mail: tomas.beresik@fstroj. uniza.sk,
prof.Ing.Anna Mičietová, PhD., University of Žilina, Faculty of Mechanical Engineering, Department of Machining and Manufacturing Engineering , Univerzitná 1, 010 26 Žilina, Slovak Republic,
☎ 00421 – 41 – 513 2781, e-mail: anna_micietova@fstroj. uniza.sk.

Abstract. This article displays the options of using of the SYSKLASS system in support of the production preparation in section of non-conventional methods of machining. Described topic is discussed these days in connection with increasing tendency towards practical use of methods in engineering company during machining of hard-to-machine materials and design complicated components.

Keywords: Non-conventional methods of machining, technological preparation of production.

1. Introduction

Expenses, quality and time of the future production can be mostly modified in the pre-production level. Attention should be focused on appropriate methods, supporting information and software products. Pre-production level automation development is specified by moving forward to maximum computer support utilization in all operations realized on this level.

For the technological preparation of production is characteristical using SYSKLASS system (Slovakia), which comes out from using advantages of group technology.

2. The Sysklass System

The SYSKLASS system (system of the classification of components) is a complex system used for computer support technological preparation of production (TPP). Working system principles come out from the concept of the group informative technologies. System is developed by GTSystems2 Detva. It belongs to the most usable TPP support products in Slovakia and Czech Republic.

SYSKLASS provides appropriate computer support, starting with component development through construction and technological preparation. SYSKLASS consists of some program modules (SYSKON, SYSTEP, SYSNORM, SYSNAR, GRAFKLAS, TLGEDIT), which solve the technological – designing process [2]. The system offers an optional consolidated solution on each level .

Components classification in engineering production improves technological preparation of the production (Fig. 1). It is also a necessary operation for using principles of the group technologies in constructional and technological documentary‘s sector. Result of the classification is a model with attributes for the identification and unification of some

components and also for the identification of technological conditions which are necessary for production realization. Geometrical design is the most important attribute.

SYSKLASS's basic data system comes out from four database groups:

- primary database: technological process, piece lists, register of tools, materials etc.,
- indicating database: working stations, centers and tariffs,
- interdepartmental database: data for communication between company's sectors,
- supporting database: catalogues data – parameters of machine, materials, semi-finished products etc..

According to the processing mode, databases could be classified into some groups such as:

- working database: elaborated database,
- valid database: include data about products, which were made in the company,
- indicators, supporting and systems databases: represents basic information source for working in TPP.

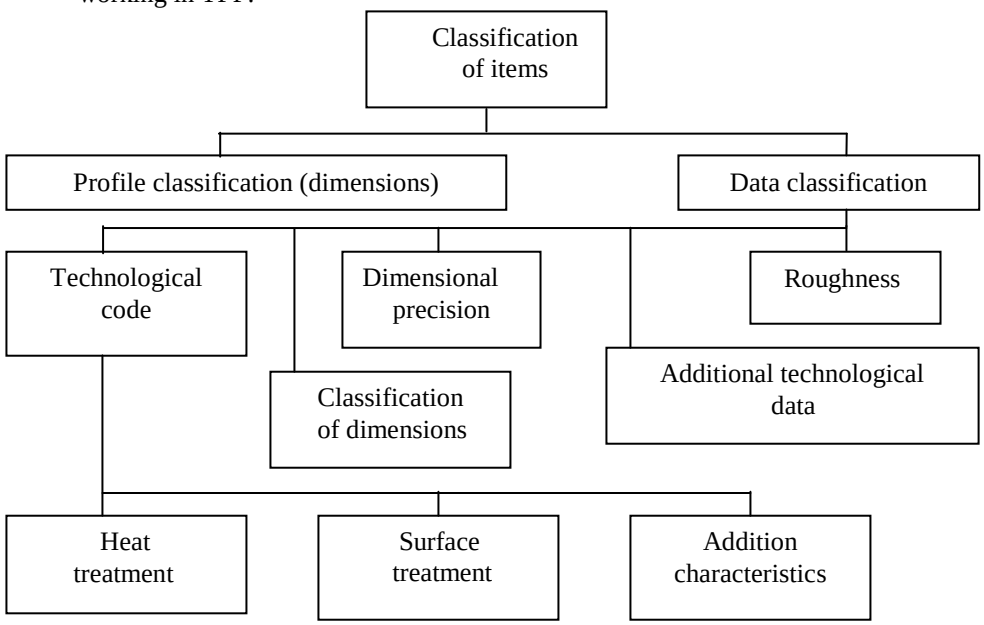

Fig.1. Items clasification in SYSKLASS system.

3. Non-conventional Methods of Machining

The development of harder and difficult ton machine metals and alloys such as tungsten, tantalum, beryllium, hast alloy, nitralloy, wasp alloy, nimonics, carbide, stainless steels and many other high strength temperature resistant (HSTR) alloys.

These materials find wide application in aero space, nuclear engineering and other industries going to their high strength to weight ratio, hardness and heat resisting qualities. The rapid developments in the field of materials has given an impetus to the modern manufacturing technology to develop, modify and is cover newer technological processes with a view to achieve results that are far beyond the scope of the existing conventional or

traditional manufacturing processes. With the developments in the field of materials it has become essential to develop cutting tool materials and processes which can safely and conveniently machine such new materials for sustained productivity, high accuracy and versatility at automation. Consequently, nontraditional techniques of machining are providing effective solutions to the problems imposed by the increasing demand for high strength temperature resistant alloys, the requirement of parts with intricate and compacted shapes and materials so hard as to defy machining by conventional methods. The processes are non traditional or non-conventional in the sense that they don't employ a conventional or traditional tool for material removal, instead, they directly utilize some form of energy for metal machining. Conventional machining methods always produce some stress in the metal being cut. Newer methods have been developed that are essentially stress free. Very thin metals can be cut without distortion or stress. [4]

The industries always face problems in manufacturing of components because of several reasons. This may be because of the complexity of the job profile or may be due to surface requirements with higher accuracy and surface finish or due to the strenght of the materials. This challenge has been accepted and may new materials and unconventional methods of machining have been developed to suit the requirements of industry. The word unconventional means that metals are such that they cannot be machined by conventional methods, but require some special techniques. [4]

These methods do not operate with mechanical working for reduction of material. They are build on some physical or physico-chemical principles for reduction of material using powerless effect on it without producing spoons. [1]

Conventional machining involves the direct contact of tool and work -piece, whereas unconventional machining does not require the direct contact of tool and work piece. Conventional machining has many disadvantages like tool wear which are not present in Non-conventional machining. [5]

Non-conventional methods of machining are: ultrasonic machining, water jet machining, abrasive jet machining, chemical machining, electro-chemical machining, electro-discharge machining, laser beam machining, electron beam machining, ion beam machining and plasma beam machining.

Each method has its own specific attribute. The use of methods is different. Attributes of material (mechanical, chemical and electro-physical attributes), dimensions, roughness, etc. are important for choosing of the optimal method. We need to know all factors which affect the choice of method.

General reasons of usage non-conventional methods:

1. Development of new construction materials and hard-to-machine materials.
2. Design complicated tools.
3. Design complicated components.
4. Increasing productivity.

Disadvantages of non-conventional machining:

1. High cost.
2. Complex set-up.

Non-conventional methods of machining are predicted to be integrated into existed automation production systems and located in CAD/CAM systems. Technical production preparation is a complex operation specialized on processing on constructional, technological and project documentation and documentation for material – technological provision of the production process.

During the *constructional production preparation*, the constructor in cooperation with technologist has to choose the mode of production – classical or non-conventional method of machining. In SYSKLASS are basic data in designing title – number of items, name of the component, material... We need to create a database of hard-to-machine materials with characteristic attributes (mechanical and electro-physical attributes) because of their influence on the optimal selection of non-conventional method of machining.

Technologist selects optimal technology and creates technological process in *technological production preparation.* technological process is influenced by many factors. Production of components is realized in technological process. This fact is used in computer systems for support creation of technological process CAPP, especially by Group technology.

Group technology contains classification and code system for component's configuration into the groups with similar processing attributes represented by design, dimensions, material, technological process, tools.... CAPP systems are created by various database's systems in general [3].

Technological title contains general parameters about component for the whole technological process. Except of this it also contains data about materials of semi – finished product.

Material norm is important for the determination of the conditions and selection optimal semi – finished product. It consists of drawing dimensions of components, additions for cutting. In addition, material norm for non-conventional methods of machining should contain program for calculation additions according to chosen non-conventional method.

Specifying design components, dimensions of all surface (inside and outside) and dimensions of semi – finished product is very important. Except from general drawing dimensions of component, it is necessary to notice secondary parameters (roughness, precision).

Technological production preparations documentary includes technological process. It describes mode and sequence of operations which define component production. Center, working place and tools are parts of the technological process in system's database. Apart from this the system has to contain the production machines database and tool database. From this point of view the material and the tools of dimensions, which are calculated by computer depending on asked dimensions of the component (electro discharge machining, electro-chemical machining, ultrasonic machining) are very important.
After all, each non-conventional method of machining is different and requires special approach.

The conclusion exemplifies the main results and the fundamental ideas presented in the manuscript.

4. Research of Some Aspects when Application of Water Beam Cutting

The cutting process should be evaluated in the complexity of different aspects with their mutual relations. This part of paper provides information about influence of cutting conditions on surface roughness when application water beam cutting as example relation among some parameters. There were analyzed the following dependences:

- Influence of liquid pressure on surface roughness in relation to cutting depth,
- Influence of the mass stream of abrasives on surface roughness in relation to cutting depth,
- Influence of cutting speed on surface roughness.

Increasing of the liquid pressure leads to gentle decreasing of surface roughness (Fig.2). The maximum applied liquid pressure in the practice conditions AWJC is about 400-500 MPa.

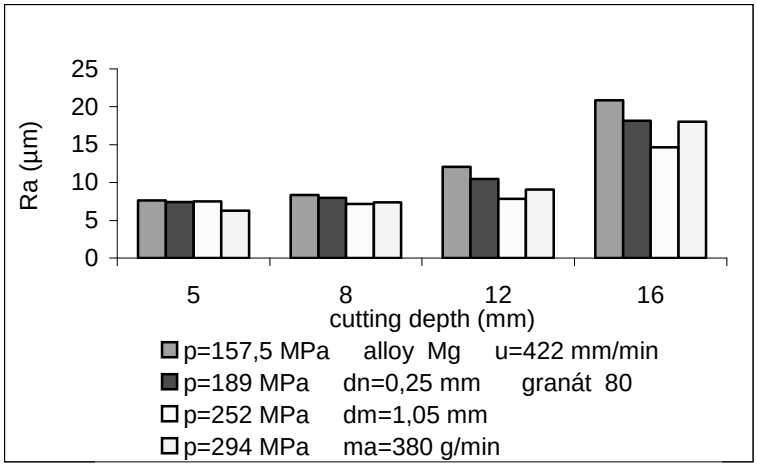

Fig.2. Influence of liquid pressure on surface roughness in relation to cutting depth

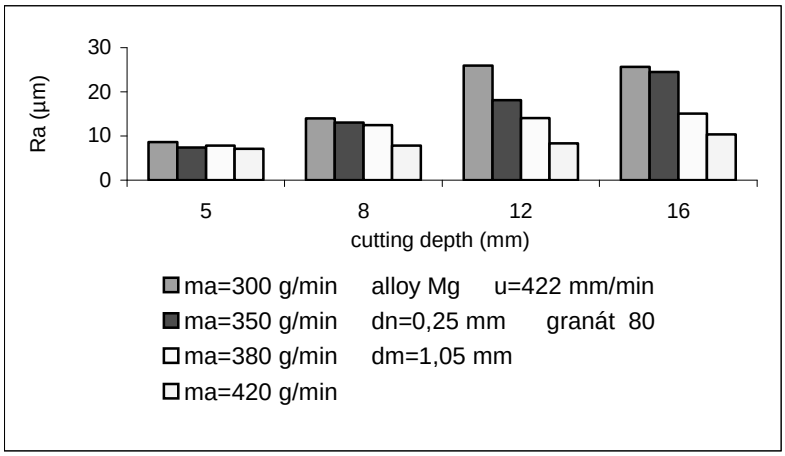

Fig.3. Influence of the mass stream of abrasives on surface roughness in relation to cutting depth

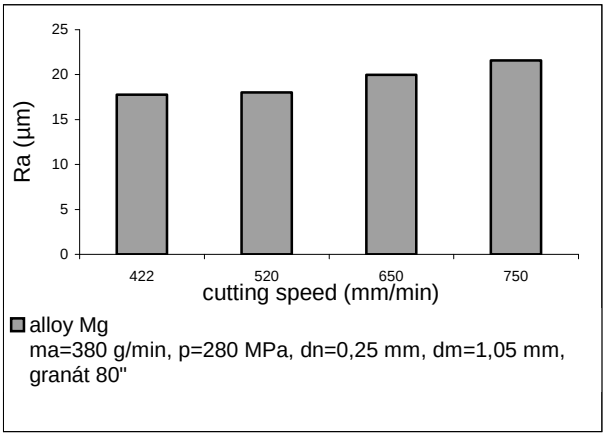

Fig.4. Influence of cutting speed on surface roughness

Increasing of the mass stream of abrasives pressure leads to decreasing of surface roughness too especially under the higher cutting depth (Fig.3). The main reason is he critical mass stream of abrasives. The maximum mass stream was not applied.
Decreasing of cutting speed leads to increasing of the maximum cutting depth and so the surface roughness is decreasing (Fig.4). More abrasives particles are contacting the surface of parts, when application of lower cutting speeds.

Acknowledgement

Automation contributes to modernization of processing technological preparation of the product in a short time. Hereby it helps to adapt to the market swings and news in competitive firms. Existence of SYSKLASS system for the non-conventional methods of machining is very important according to increasing tendency towards using those methods in engineering firms.

References

[1] MIČIETOVÁ, A.: *Nekonvenčné metódy obrábania*. EDIS - vydavateľstvo Žilinskej univerzity, Žilina, 2001.
[2] KURIC, I. – KOŠTURIAK, J. – JANÁČ, A. – PETERKA, J. – MARCINČIN, J.: *Počítačom podporované systémy v strojárstve*. EDIS - vydavateľstvo Žilinskej univerzity, Žilina, 2002.
[3] VASILKO, K. A KOL.: *Výrobné inžinierstvo*. Edícia vedeckej a odbornej literatúry – FVT, Prešov, 2003.
[4] www.123eng.com/projects/non%20conventional.pdf
[5] http://wiki.answers.com/Q/What_is_mean_by_non-conventional_machining

Transcom 2009, 22-24 June 2009
University of Žilina, Žilina, Slovak Republic

Assessing of Experimental Data for Non-Conventional Methods of Machining

[*]Jaroslav Brezáni, [**]Anna Mičietová
*INA Schaeffler Gruppe, Dr. G. Schaefflera 1, 024 01 Kysucké Nové Mesto, Slovakia,
jaroslav.brezani@schaeffler.com
[**]University of Žilina, Faculty of Mechanical Engineering, Department of Machining and Manufacturing Engineering, Univerzitná 1, 010 26 Žilina, Slovakia, anna.micietova@fstroj. uniza.sk.

Abstract. This article covers problems how to assess parameters of product quality and technological parameters of individual non-conventional methods on the one side and their mutual functional dependences on the other side. The article deals with methodology how to proceed with analysis of factors for concrete non-conventional method of machining within scope of planed experiment. There are a criteria for selection of non-conventional machining and aims at thermic procedures of material separation with the assistance of non-conventional methods.

Keywords: Non-conventional methods of machining (NMM), planed experiment, dependent variable, independent variable.

1. Introduction

In the non-conventional methods of machining there are many input parameters that must be taken in to account to reach required product quality indicators. For reason of processional factor analysis and considering of their mutual influence on quality of machining surfaces with using NMM is advantageous to determine specific methodology.

2. Experimental Problem in Selection of Suitable NMM

The experimental problem in selection of the non-conventional method of machining is determination of so-called multifactor functional dependences. Factor experiments allows to analyze these processes. In the experiments are realized tests for all combinations of values of the considered factors. There are empirical dependences in form

$$y=F(x_1,x_2,\ldots,x_n) \tag{1}$$

The experiment is generally described by equation of the experiment

$$y_1,y_2,\ldots,y_s,\ldots,y_{ss}= f(x_1, x_2, \ldots, x_r, \ldots, x_{rr}) \tag{2}$$

where:
y_s – s-th dependent variable (s-th response),
ss – number of dependent variables (responses),
x_r – r-th independent variable (r-th factor), rr – number of independent variables (factors)

2.1. Classification of Factors

From problems and analysis of experimental problem in electrical discharge machining (EDM) method of cutting by wire follows dependent variables – responses that represent requirements on the product quality and they are characterized by significant parameters of surface integrity. The significant quality parameters in the EDM method of cutting by wire

Ra - mean deviation of profile unevenness,
Rz - biggest height of profile unevenness,
Wz - waviness of profile,
u - perpendicularity deviation of cut site,
a - thickness of white layer.

From analysis the EDM method of cutting by wire also follows independent variables – factors. In Tab. 1 are the factors assessed by their trait to variables of qualitative or quantitative trait.

Technological parameters of EDM cutting by wire	Symbol	Measure	Trait of variables	
			qualitatively	quantitatively
Machine:				
- cutting speed	v_c	[$mm^2 \cdot min^{-1}$]		quantitati.
- shift speed	v_f	[$mm.min^{-1}$]		quantitati.
Electric parameters:				
- discharge electric current	I_e	[A]		quantitati.
- generator dry run voltage	U_0	[V]		quantitati.
- capacitor capacity	C	[nF]		quantitati.
- impulse time	t_i	[s]		quantitati.
- impulse frequency	f	[Hz]		quantitati.
- power cutting	P	[kW]		quantitati.
- type of generator impulse	GNI		qualitati.	
Working fluid:				
- dielectric conductance	G_d	[$m .S.m^{-1}$]		quantitati.
- dielectric temperature	T	[ºC]		quantitati.
Rinsing:				
- fluid pressure – coaxial rinsing	p	[Pa]		quantitati.
Tools:				
- wire diameter	d	[mm]		quantitati.
- tension strength of wire	F	[N]		quantitati.
- wire material	M_d			quantitati.
- wire forward speed	v_d	[$m.s^{-1}$]		quantitati.
Workpiece:				
Material of workpiece:	M_o			
- elecrtic conductance	G	[Ω^{-1}]	qualitati.	
- heat conductance	λ	[$W.m^{-1}.K^{-1}$]	qualitati.	
- melt temperature	t_t	[K]	qualitati.	
- chemical structure			qualitati.	
Dimension of workpiece:				
- thickness	h	[mm]		quantitati.
- length x width	d x š	[mm]		quantitati.
- shape of machining site				quantitati.

Tab. 1. Technological parameters of EDM cutting by wire and their trait.

Generally according to the equation (2) we get equation of considered dependences

$$Ra, Rz, Wz, u, a = f(v_c , v_f , I_e , U_0 , C, t_i , f, P, G_d , T, p, d, F, M_d , v_d , h, d \times š) \quad (3)$$

In the next step we again rethink all factors of the experimental equation (3) by classification into constant factors, arbitrary factors and factors with critical influence on the significant quality parameters – experiment responses. Tab. 2.

Independent variables - factors	Classification of factors			
	constant	arbitrary	critical faktors of experiment	Symbol
- cutting speed - shift speed			critical	v_f
- discharge electric current			critical	I_e
- generator dry run voltage - capacitor capacity - impulse time - impulse frequency - power cutting			critical	t_i
- dielectric conductance	constant			
- dielectric temperature	constant			
- fluid pressure – coaxial rinsing	constant			
- wire diameter	constant			
- tension strength of wire			critical	F
- wire material	constant			
- wire forward speed	constant			
- thickness			critical	h
- length x width - shape of machining site		arbitrary		

Tab. 2. Classification of factors and critical faktors of experiment.

On the ground of determining of crucial experiment factors and according to the Tab. 2 and equation (3) follows basic equation of the experiment

$$Ra, Rz, Wz, u, a = f (v_f , I_e , t_i , F, h) \quad (4)$$

According to the (4) we divide experiment to a separate experiment in which is only one dependent variable.

$$Ra = f (v_f , I_e , t_i , F, h) \quad (5)$$

$$Rz = f (v_f , I_e , t_i , F, h) \quad (6)$$

$$Wz = f (v_f , I_e , t_i , F, h) \quad (7)$$

$$u = f (v_f , I_e , t_i , F, h) \quad (8)$$

$$a = f (v_f , I_e , t_i , F, h) \quad (9)$$

Then considered empirical equations of experiments are

$$Ra = C_1 . v_f^{n11} . I_e^{n21.} t_i^{n31} . F^{n41} . h^{n51} \quad (10)$$

$$Rz = C_2 . v_f^{n12} . I_e^{n22.} t_i^{n32} . F^{n42} . h^{n52} \quad (11$$

$$Wz = C_3 . v_f^{n13} . I_e^{n23.} t_i^{n33} . F^{n43} . h^{n53} \quad (12)$$

$$u = C_4 . v_f^{n14} . I_e^{n24.} t_i^{n34} . F^{n44} . h^{n54} \quad (13)$$

$$a = C_5 . v_f^{n15} . I_e^{n25.} t_i^{n35} . F^{n45} . h^{n55} \quad (14)$$

where

C_1, n_{11}, n_{21}, n_{31}, n_{41}, n_{51} are constants of empirical equation (10),

C_2, n_{12}, n_{22}, n_{32}, n_{42}, n_{52} are constants of empirical equation (11),

and similarly for empirical equations (12), (13), (14).

3. Conclusion

This procedure of analysis of process factors in planed experiment can apply to the other NMM. For every individual NMM is needed to consider with specific parameters of given method – with factors and also with specific requirements on the parameters of surface integrity. On the base of acquired empirical dependences can assess selection of non-conventional method in an integrated model.

The article arisen within scope of solving of project VEGA on the Department of machining and manufacturing engineering.

References

[1] MIČIETOVÁ, A. *Nekonvenčné metódy obrábania.* EDIS – vydavateľstvo, Žilina, 2001, ISBN 80-7100-853-2.

[2] MÁDL, J. *Experimntální metody v teórii obrábění.* ČVUT, Praha, 1986.

[3] HARANT, M. *Matematické metódy v experimentálnej praxi.* Žilina, 1970.

[4] VDI 3402 BLATT 4. *Anwendung der Funkenerosion.* März 1994.

Transcom 2009, 22-24 June 2009
University of Žilina, Žilina, Slovak Republic

Computer Aided Runner Optimalization for Aluminim Alloys

[*]Marek Brůna, [*]Dana Bolibruchová
[*]University of Žilina, Faculty of Mechanical Engineering, Department of technological engineering,
Univerzitna 2, 01026 Žilina, Slovakia, brunam@fstroj.uniza.sk

Abstract. Main goal of this article is the effort to improve the quality of aluminium castings poured into sand mould, with the aid by „front tracking indicator" – new function of simulation software ProCAST. Works are focused on optimalization of runner design, thus the mold cavity is filled with minimal devaluation of melt by turbulent flow and entrained oxide films. ProCASTs new function was used to visualize the process, this new function allows to track free surface of melt exposed to air in real time.

Keywords: flow, reoxidation, runner Introduction

1. Introduction

When the gating system is not properly designed, entraining of air bubbles into melt may occur. The area of melt, which is in contact with air bubbles in gating system, behave the same way as melt exposed to air in previos phases of pouring – oxidation (reoxidation) processes begins to absorb surronding melt. This processes could be the main source of porosity in final castings.

One of the most progressive ways to study reactions taking place in gating system is computer simulation of mold cavity filling.

2. Experiments

Horizontal runner and effect of his geometry on melt flow and reoxidation processes during gravity pouring into sand mould was studied with the aid by latest version of ProCAST simulation software.

Virtual geometric model developed for the means of simulations was designed to allow tracking of oxide films throught the whole filling process (Fig.1).

Fig. 1. Geometry of casting.

Aluminium alloy AlSi7Mg0,3 was choosen from software database for purposes of all simulations. To determine effect of runner geometry on flow character, in all simulations was used identical gates and sprues, also conditions of non-presurized gating system with ratio 1:4:4 was realized. Filling time was 4 seconds.
Cross section area of sprue – 93 mm^2
Cross section area of runner – 372 mm^2
Cross section area of gate – 372 mm^2

3. Experiments

Two variants of runner, with equal cross-section area, but different geometries were constructed. Evaluation of simulations was focused on four main parameters.

a) Filling at the beginning of the runner.
b) Filling at the end of the runner.
c) Melt velocity entering the mold cavity (condition of non-critical velocity 0,5 $m.s^{-1}$ was executed in both two variants).
d) Contamination of casting with "new" oxide films, formed in reoxidation phase. Because of limited size of this article, outcomes and vizualizations will be objectives of presentation.

1 VARIANT:

Geometry design

First design comes out from commonly used concept of runner, where dominant dimension is height. Many used runners have ratio of height to width up to 2:1. For the purposes of principal understanding processes taking places in runner is sufficient ratio 1,7:1 (25 mm : 15 mm).

Filling at the beginning of the runner is shown on Fig. 2. From this figure we can see limitation of this concept. Liquid metal entering the runner doesn't have ability to fill whole cross-section area of runner and free surface of melt is exposed to air, which leads to extensive reoxidation processes. This fact is also noticable thanks to changing colours in front of melt (In stages thought purple, blue, green, yellow and red – from melt that is least exposed to air to melt wich is in longest contact with air). The melt reacts with air accompanied by formation of "new" oxide films.

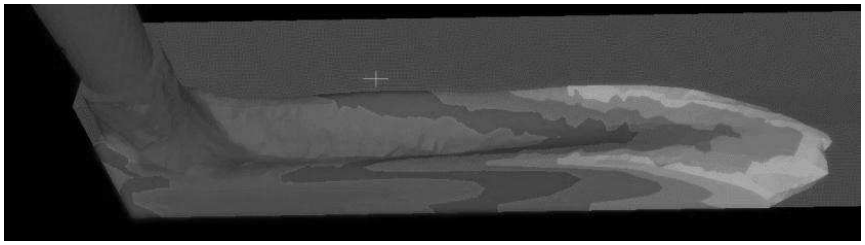

Fig. 2. Filling at the beginning of the runner.

Filling at the end of the runner is shown on fig. 3. Dominant dimension of the runner is height, which gives opportunity to form massive rebounding wave at the end of the runner. Forming wave represent negative phenomenon which causes entraining of surface oxide films into the bulk of melt. This mechanism supports formation of entrained doubled oxide films floating in melt. Yellow colour in front of wave indicates amount of oxides, all these oxides will be consumed into the bulk of melt when the wave colapse to opposing liquid metal flow.

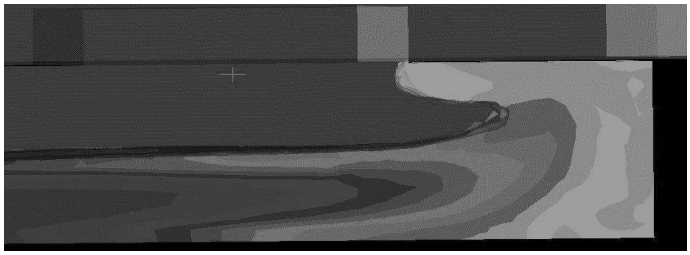

Fig. 3. Filling at the end of the runner.

2 VARIANT:

Geometry design

Second design of runner comes out from concept, where dominant dimension is width. Value of cross-sectional area reamined the same as in the first variant, but ratio "height to width" was changed to 1:2,1 (13 mm : 28 mm). Also sprue base was added.

Filling at the beginning of the runner – Modified design of runner and process of filling is shown on Fig. 4. Simulation demonstrated advantages of this concept. Sprue base is immediately filled with melt, leaving little space for reoxidation processes. Cross-sectional area of runner is completely filled and so only small amount of melt is exposed to air.

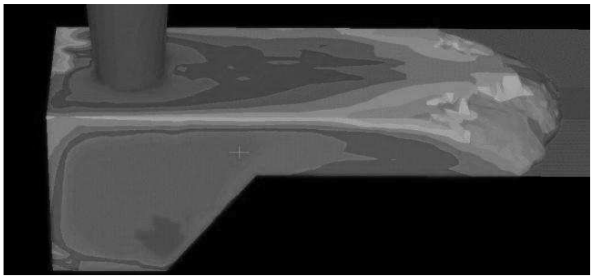

Fig. 4. Filling at the beginning of the runner.

Filling at the end of the runner – Advantages of modified design are also obvious from figure 5. Spectrum of colours demontrate, that only minimum amount of melt is contaminated with oxides, also formation of rebounding wave was supressed.

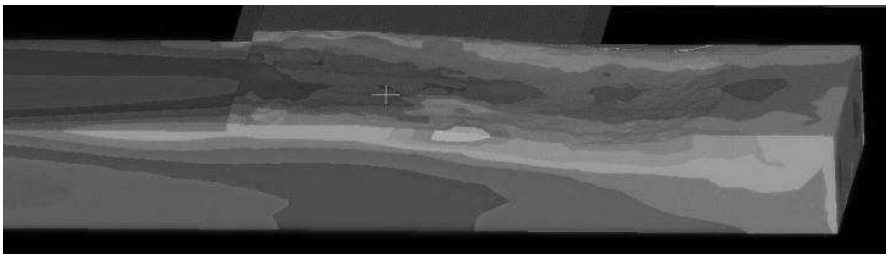

Fig. 5. Filling at the end of the runner.

4. Conclusion

Concept of runner with dominant height (focusing on amount of "new" oxides penetrating the mould cavity) was during our experiments evaluated as inadequate alternative. In second variant we changed orientation of runner from height to width and added sprue base. This modification allowed the melt to completely fill the cross-section area of runner, leaving little space for reoxidation processes. Therefore, it is important to deliberate also geometry of runner, not only value of his cross-sectional area.

Acknowledgement

This work was developed within the grant project KEGA č. 3/5197/07, KEGA 1/0684/08 and VEGA č. 1/4098/07.

References

[1] CAMPBELL, J. - *Castings, 2nd Edition*, United Kingdom: Butterworth Heinemann, 2003.
[2] CAMPBELL, J. - *Castings Practice: The Ten Rules of Castings*, Oxford, United Kingdom: Butterworth Heinemann, 2004.
[3] PASTIRČÁK, R., SLÁDEK, A., BOLIBRUCHOVÁ D. – *Simulácia filtrácie zlievarenských hliníkových zliatin*, 2006, Nekonvenčné technológie, ročník 2006.

Transcom 2009, 22-24 June 2009
University of Žilina, Žilina, Slovak Republic

Fatigue Crack Paths in Nodular Cast Irons and ADI Microstructures

[*]Lukáš Bubenko, [*]Radomila Konečná, [**]Gianni Nicoletto
[*]University of Žilina, Faculty of Mechanical Engineering, Department of Materials Engineering, Univerzitná 1, 01026 Žilina, Slovakia, {lukas.bubenko, radomila.konecna}@fstroj.uniza.sk
[**]University of Parma, Department of Industrial Engineering, Viale G.P. Usberti, 181/A, 43100 Parma, Italy, gianni.nicoletto@unipr.it

Abstract. Considering quality of constructive material, fatigue life is one of the most essential material characteristic. This is influenced particularly by structure of matrix. The way of fatigue crack propagation in the matrix of nodular cast iron (NCI) and austempered ductile iron (ADI) have been investigated in this contribution, while the influence of microstructure is considered and discussed. Experimental material used in presented contribution was pearlitc-ferritic NCI and heat treated ADI 800, whereas pearlitic-ferritic NCI was used as the base for ADI production. Fatigue tests were performed using an Amsler vibrophore on round compact tension (RCT) specimens. After performed tests fatigue crack paths in both materials were investigated and compared. Finally, light microscopy was used to analyze the microstructure, crack initiation and propagation within broken specimens.

Keywords: nodular cast iron, austempered ductile iron, fatigue crack, initiation, propagation

1. Introduction

Cast irons have several manufacturing and engineering advantages compared with steels. These include a 20–40 % lower manufacturing cost, better vibration damping, and lower volume shrinkage during solidification [1]. Austempered ductile iron presents further excellent combination of properties, such as high strength, good ductility, toughness, fatigue strength and wear resistance those are unavailable in other grades of cast iron [2]. The manufacturing cost of ADI is also substantially lower than wrought or forged steel. Furthermore, the density of ADI is lower than cast steel. Thus, ADI has the advantage of higher specific strength than steel. As a result, ADI is considered a very promising engineering material, and an economical substitute for wrought or forged steel in several structural applications in the automotive industry (crankshafts, transmission gears, connecting rods), defense (cannon shells, aircraft landing gears, etc.), earth-moving machinery, railroads, etc [3, 4].

ADI is a heat treated nodular cast iron. The attractive properties of ADI are related to its unique microstructure that consists of acicular ferrite and high carbon austenite. To produce ADI a single-step austempering process is conventionally used. This process consists of austenitizing the casting in the temperature range of 871–982 °C for sufficient time to get a fully austenitic matrix, and then quenching it to an intermediate temperature (austempering temperature) range of 260–400 °C to avoid formation of pearlite. The casting is maintained at this austempering temperature for 2–4 h depending on the section size [5]. Large amount of silicon present in ductile iron suppresses the precipitation of carbides during the austempering reaction and retains substantial amount of stable high carbon austenite. Small amounts of alloying elements, such as nickel, molybdenum and copper are generally added to ADI to avoid formation of pearlite during the austempering process [6, 7].

Considerable work has been done to understand the microstructural characteristics of ADI and their effect on the mechanical properties. However, direct reports on observations of the microprocess of fracture are rare. Further studies are needed to clarify the micromechanism of fracture in ADI, especially the initiation and propagation of microcracks and their interaction with the microstructure [2].

2. Material and experimental procedures

Experimental material used for performing fatigue tests was a pearlitic-ferritic NCI and ADI 800, cast in the form of cylindrical bars of 25 mm diameter and 200 mm long. Pearlitic-ferritic NCI was a basic material for ADI production, while following heat treatment was used: 785°C/30 min – 820°C/135 min – 385°C/90 min. Information about developing pearlitic-ferritic NCI was not supplied.

The AMSLER 421 vibrophore was used for performing fatigue crack propagation tests. Machine was considered due to its high loading frequency and relatively cheap operation and service. RCT specimens with straight through notch, denominated as PER and ADI, were prepared and new grips were developed, according to the standard ASTM E399-06. However, due the load limit of the test machine, dimensions of specimens and grips were adapted [8].

Fatigue crack propagation tests were performed to generate long stable cracks in RCT specimens to investigate the fracture paths through the respective microstructures at different levels of ΔK using light metallographic microscopy. The stress intensity factor range ΔK is given by (1), where a is the crack length, w and t are specimen width and thickness, respectively, $\Delta F = (F_{max} - F_{min})$ is the load range and Y = f(a/w) is the geometry factor for the RCT specimen.

$$\Delta K = \Delta F (\pi a)^{1/2} Y/wt \qquad (1)$$

Fatigue tests were initially at relatively high load (i.e. high □K) to initiate crack from the starter notch. As the fatigue crack propagated, manual reduction of the applied load reduced ΔK to near threshold values to obtain crack arrest.

The structural analysis was carried out applying metallographic techniques and digital image analysis software on polished sections according to the standard EN STN 42 0461.

3. Results and discussion

The microstructures of tested materials are shown in Fig. 1. Specimen PER was characterized according Slovak standard by a pearlitic-ferritic matrix, with content of ferrite from 10 to 20 % (Fe 15), present mostly around regularly distributed graphite nodules. Those were observed as fully globular, with size range from 30 to 60 μm (VI 6).

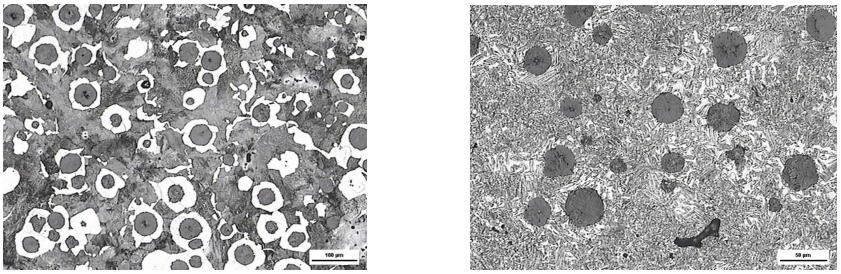

a) PER b) ADI

Fig. 1 Microstructure of PER and ADI specimens, etched with 3% Nital

The ADI specimen presents a matrix formed by thick laths of acicular ferrite, characteristic for upper bainite, and retained austenite. This kind of matrix provides notable improvement of fatigue life of ADI. The character of matrix and distribution of graphite nodules has a significant influence to fatigue properties. Also a multiple micro shrinkages, observed in tested material, may have considerable influence to initiation and propagation of fatigue cracks [9].

Fatigue cracks started to grow from prepared notch in both specimens due to stress concentration. Comparing two kinds of microstructures, difference between crack propagation at different ΔK are noticeable. In pearlitic-ferritic NCI (Fig. 2a, b), crack at high ΔK propagated mainly through the matrix with local secondary cracks and considerable changes in direction, possibly due to the contribution of nodules below the surface. At low ΔK, the crack path changes characteristics and is controlled by the presence of graphite nodules. The crack propagates always at the graphite nodule-matrix interface (Fig. 3a), an indication of the weak nodule/matrix bonding. In case of ADI, both at high and low ΔK (Fig. 2c, d), the fatigue crack path connects neighboring graphite nodules and nodules detach from the matrix. Also local microdefects should influence crack propagation.

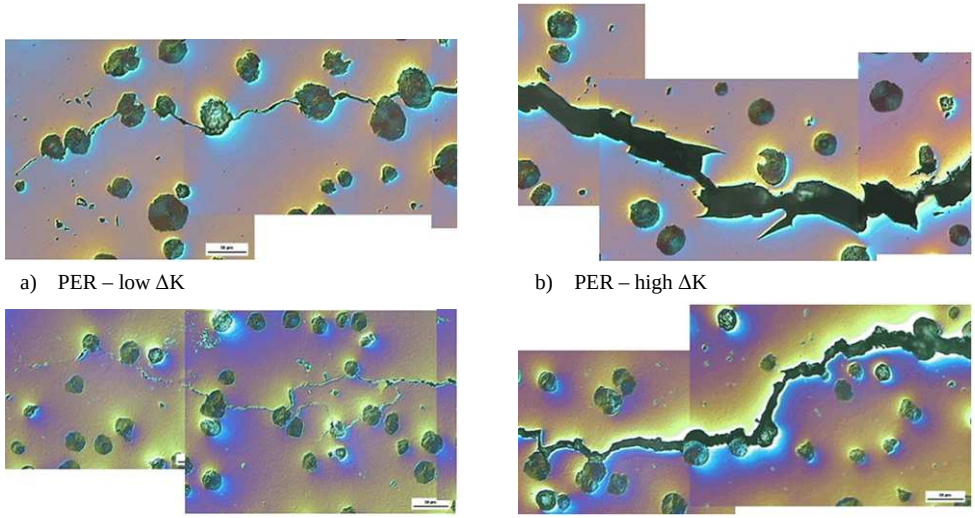

a) PER – low ΔK b) PER – high ΔK

c) ADI – low ΔK d) ADI – high ΔK

Fig. 2 Magnified views of fatigue cracks, no etched, Nomarski

At low ΔK, Fig. 2c, an example of crack branching and reconnection is observed. Since crack branching in ADI is due to crack–nodule interaction, it occurs when a favorable nodule is below the observation plane.

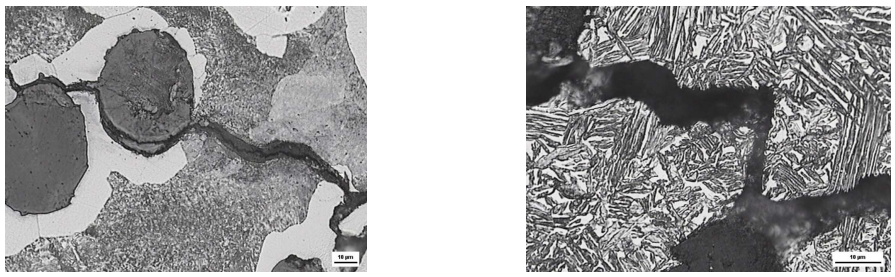

a) crack propagation through G-M interface, specimen PER b) deflection of crack according orientation of bainitic ferrite laths, specimen ADI

Fig. 3 Details of microcracks in tested material

Initiation of microcracks started at the graphite-matrix interface, what is also similar to pearlitic-ferritic NCI, however not every microcrack connected to main crack. Initiation of secondary microcracks was observed in graphite nodules situated close to the main crack. These usually did not connect to the main crack.

The microstructure of ADI consists of bainitic ferrite, retained austenite and graphite. Several bainitic ferrite laths often have the same orientation, forming a cluster of bainitic ferrite laths. The orientation of bainitic clusters is different. Due to described structure, deflection of crack was observed, when fatigue crack propagated according the orientation of bainitic ferrite clusters and propagation of crack changed when the orientation of cluster changed, Fig. 3b.

4. Conclusions

Fatigue crack paths in pearlitic-ferritic NCI and ADI 800 were observed to understand the influence of the microstructure. The following conclusions can be reached:

- Fatigue cracks always propagated from graphite nodule to the next in ADI 800.
- In pearlitic-ferritic NCI fatigue cracks connected graphite nodules only at low ΔK. At high ΔK crack propagation was influenced by the heterogeneous matrix microstructure.
- The fatigue crack path through bainitic ferrite was complex with crack deflection and crack branching due to character of matrix, which consists of clusters with parallel ferrite laths. Cracks propagated along the bainitic ferrite/austenite interface.

Acknowledgement

This work was done as a part of KEGA grant No.3/6110/08 and MATMEC net-lab project funded by Emilia Romagna region.

References

[1] JAMES, M. N., WENFONG, L. *Fatigue crack growth in austempered ductile iron and grey cast irons-stress ratio effects in air and mine water*. Materials Science and Engineering A 265 (1999) 129 – 139.

[2] DAY, P. Q., HE, Z. R., ZHENG, C. M., MAO, Z. Y. *In-situ SEM observation on the fracture of austempered ductile iron*. Materials Science and Engineering A 319 – 321 (2001) 531 – 534.

[3] STOKES, B., GAO, N., REED, P. A. S. *Effect of graphite nodules on crack growth behaviour of austempered ductile iron*. Materials Science and Engineering A 445 – 446 (2007) 374 – 385.

[4] *The application of high – strength cast irons (ADI – austempered ductile iron) in high – performance diesel engines – part I.* Foundry Trade Journal 248 – 250, 2006. http://www.aditreatments.com/pdf%5CADI%20in%20large%20diesel%20engines%20part%201.pdf, obtained on 14th October 2007.

[5] YANG, J., PUTATUNDA, S. K. *Near threshold fatigue crack growth behavior of austempered ductile cast iron (ADI) processed by novel two-step austempering process.* Materials Science and Engineering A 393 (2005) 254 – 268.

[6] YANG, J., PUTATUNDA, S. K. *Influence of novel two-step austempering process on the strain-hardening behavior of austempered ductile iron (ADI).* Materials Science and Engineering A 382 (2007) 265 – 279.

[7] SKOČOVSKÝ, P., PALČEK, P., KONEČNÁ, R., VÁRKOLY, L. *Konštrukčné materiály.* 1. vyd., Žilina, EDIS 2000.

[8] BUBENKO, L., KONEČNÁ, R., NICOLETTO, G. *Fatigue crack paths in NCI and ADI microstructures.* SEMDOK 2009, 14th international of PhD. students´ seminar: Žilina-Súľov, Slovakia, 29-30 January, 2009.- Žilina: Žilinská univerzita, 2009

[9] MURAKAMI, Y. *Metal Fatigue: Effects of Small Defects and Nonmetallic Inclusions.* ELSEVIER, 2002.

Transcom 2009, 22-24 June 2009
University of Žilina, Žilina, Slovak Republic

Effect of Mechanical Surface Treatment Applied to Alloy Az91 on its Electrochemical Properties.

[*]Michal Bukovina, [*]Viktor Škorík, [*]Branislav Hadzima
[*]University of Žilina, Faculty of Mechanical Engineering, Department of Materials Engineering,
Univerzitna 2, 01026 Žilina, {michal.bukovina, viktor.skorik, branislav.hadzima}@fstroj.uniza.sk

Abstract. Article deals with evaluation of corrosion resistance of AZ91 magnesium alloy. Surface of the AZ91 alloy was evaluated in original state, after milling, and after glass balls shot peening state. Corrosion characteristics were measured in 0.1M solution of NaCl at 22°C using electrochemical impedance spectroscopy method.

Keywords: EIS, corrosion resistance, magnesium alloy AZ 91.

1. Introduction

Magnesium and its alloys constitute very interesting material from the practical point of view. Density of magnesium alloys utilized commercially is about 1700 kg/m^3 and it is this low density value that makes them suitable for technical applications mostly in transport industry because by decreasing component weight the overall operational costs decrease. High ratio of toughness to mass, good machinability and casting properties also belong to magnesium alloys‘ benefits. Disadvantages of magnesium alloys lie with low values of Young’s modulus, limited creep resistance at increased temperatures, high contraction and especially high chemical reactivity which causes low corrosion resistance of magnesium alloys. Nowadays the task ahead is to increase resistance to corrosion and to search for new technologies and processes that would bring about higher corrosion resistance of magnesium alloys. This could be achieved either by modifying chemical of composition, i.e. by applying dopant to magnesium alloys, by adjusting the environment utilizing inhibitors, or by treating the surface of components made from magnesium alloys [1].

At present, there is an increasing demand for quality, durability and especially image of components. Out of entire range of surface pre-treatment methods whether chemical or mechanical, shot peening becomes the prominent one being an effective technology able to trim the surface to required quality, i.e. apart from cleaning the surface of basic material it is able to achieve plausible microgeometry and required physical properties of the surface. The shot peening technology is being widely used in practice. Typical applications of shot peening technology are pre-treatment of surface for inorganic and organic films, creation of suitable morphology of the surface, surface hardening, increasing of fatigue and corrosion-fatigue endurance and the like. Shot peening’s positive effect on magnesioum alloys‘ fatigue endurance has been published in works [2, 3]. Questionable remains effect of shot peening on corrosion resistance of magnesium because of its high electrochemical reactivity.

Mechanical surface treatment (shot peening) technology belongs to basic material mechanical surface treatments‘ group where the tool – shot peening agent, upon hitting the surface, brings about qualitative changes thereof, while giving rise to characteristic surface morphology. For example in (Fig. 1) there is a section of shot peened surface STN 41 1375.10 steel [4].

Fig.1 Section of sand shot peened surface of STN 41 1375.10 steel [4]

In the process of shot peening, the shot peening agent hits the surface and plastically deforms the contact points (Fig. 1) [5]. Upon hitting the surface, part of energy converts to heat that removed through component surface and part converts to plastic deformation of the surface. Process of plastic deformation is executed via utilizing one of two deformation mechanisms, i.e. slip or twinning. Mechanism itself depends on conditions of plastic deformation but even more so on a metal’s crystal structure. Each process of plastic deformation, which also includes shot peening, is accompanied with changes in materials‘ mechanical and technological properties. Shot peening causes linear increase of strength limit and yield strength limit, decreases ductility, increases fatigue life-time, edge-notch toughness almost does not change in the process.

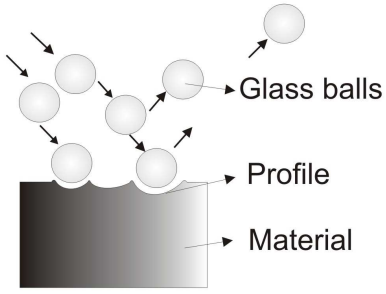

Fig.2 Changes in surface upon impact of shot peening agent. [5]

Fig.3 Experimental device used for assessing electrochemical properties (Voltalab 10)

2. Experimental materials

As an experimental material, a magnesium alloy commercially known as AZ91 being in condition after continuous casting was used. Its chemical composition is in Tab. 1.

element	Al	Zn	Mn	Si	Cu	Fe	Ni	Be
wt.%	8.12	0.68	0.37	0.08	0.030	0.010	0.009	0.003

Tab. 1. Chemical composition (wt. %) of AZ91 magnesium alloy.

2.1. Microstructure analysis

Afer routine metalographic preparation, the microstructure of tested alloy was evaluated by using optical microscope Carl ZEEIS AXIO Imager.A1m. The alloy's microstructure (Fig. 4) is composed of polyedric grains of solid solution of additives in magensium (δ) and areas created by $Mg_{17}AL_{12}$ (γ) phase [11]. Deformation twins in greater numbers are visible in the alloy's surface and sub-surface layer after it has been shot peened with glass balls (Fig. 5), the former having emerged as a result of plastic deformation of surface layer as shown on Fig. 2

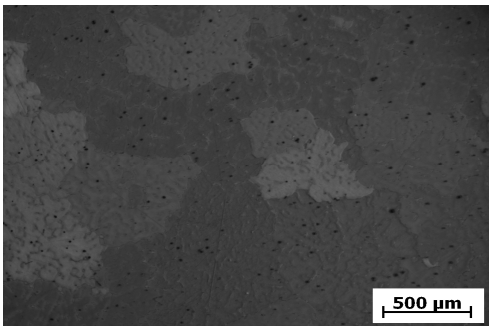

Fig. 4. Microstructure of tested AZ91 Mg alloy Initial state; etch. Acetic picrid.

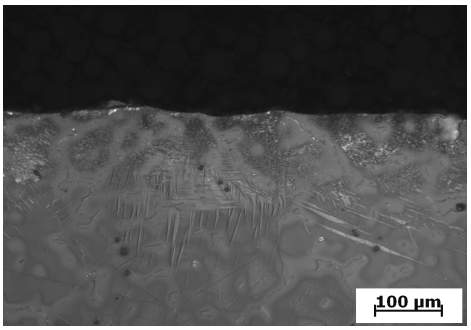

Fig. 5. Microstructure of tested AZ91 Mg alloy, alloy surface shot peened with glass balls; etch. Acetic picrid

3. Results and discussion

The objective of experiments was to discover the effect that shot peening the surface of AZ91 magnesium alloy had on its electrochemical properties by EIS method using VoltaLab 10 laboratory equipment (Fig. 3). Resulting EIS measurings provide values of polarization resistances (R_p), directly proportional to material surface resistance to corrosion in a given environment. Measurements of these properties was taking place in corrosive environment of 0.1 M NaCl solution on non-peened surface (following milling) during 96 hour exposure and on glass balls shot peened surface during 240 hour of exposure. Time for fixation of a sample's free potential in electrolyte prior to EIS measurement was 5 min or 24, 48, 72, 96, 168 and 240 hours respectively. Measurements were taking place at frequency ranging from 100 kHz to 50 mHz with frequency being changed 20 times per decade. Alternating voltage amplitude was 10 mV. Measured sample surface was 0.385 cm^2. The sample rotated on rotating electrode at velocity of 1000 min^{-1}. Connection and measuring principle is described elsewhere [6, 7].

The shot peening was executed at Department of Technologies and Materials at Faculty of Mechanical Engineering of Technical Uuniversity in Košice, on mechanical laboratory blasting device of KP-1 type, from company G. Fischer AG Schaffhausen. A monodispersive BD - STN 42 9823, made by Kovobrasiv Mníšek spol. s r.o. - Mníšek pod Brdy, The Czech Republic, was used. Velocity of grains ejected from projectile wheel was 70.98 $m.s^{-1}$.

Results of EIS measurements in the form of Nyquist diagrams are in Fig. 6 referring to surfaces in initial state and in Fig. 7 referring to shot peened surfaces. It is possible to find out values of polarizing resistances (R_p) by Nyquist diagrams analyzing. Outcomes of analyses are to be found in Tab. 2 referring to alloy AZ91 in its initial state and in Tab. 3 referring to shot peened alloy. This value was determined by employing software analysis using VoltaMaster 4 software based on circural regression. Equivalent circuits were used in analysis performance helping us to model conditions on the electrolyte-sample boundary [9, 10].

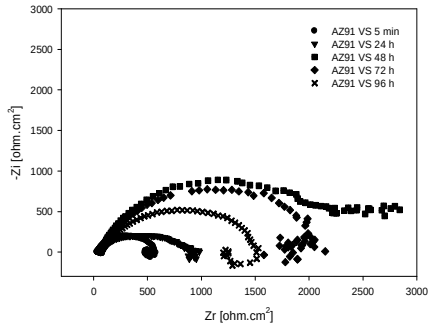

Fig. 6. Nyquist diagrams of AZ91_ VS in 0.1 M NaCl

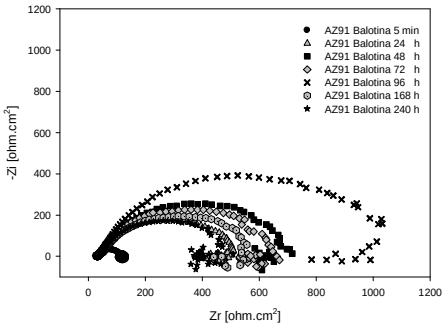

Fig. 7. Nyquist diagrams of AZ91_glass balls (after shot-peening) in 0.1 M NaCl

Time[hour]	Consolidation[V]	Rp[ohm.cm^2]
0	**-1,57393**	**472,6**
24	**-1,54337**	**917,8**
48	**-1,54062**	**2354**
72	**-1,53581**	**1792,6**
96	**-1,55356**	**1628,8**

Tab. 2. Electrochemical properties of AZ91_VS in 0.1 M NaCl

Time[hour]	Consolidation[V]	Rp[ohm.cm^2]
0	**-1,59906**	**60,1**
24	**-1,55412**	**476,2**
48	**-1,54743**	**587,2**
72	**-1,54193**	**598,3**
96	**-1,5123**	**1098**
168	**-1,50456**	**501,9**
240	**-1,48518**	**385,1**

Tab. 3. Elektrochemical properties of AZ91_glass balls (after shot peening) v 0,1 M NaCl

Following analysis of Nyquist diagrams and measured polarizing resistances we are able to observe in reference to AZ91_VS alloy (Fig. 6) that after 24 or 48 hours of fixation in corrosive environment the R_p values doubled and quadrupled in comparison to value of polarizing resistance after 5 minutes of fixation. A curve resulting from measurements taken after 48 hours of fixation notably shows a change of its shape, which points to a different corrosion mechanism after exactly this time of consolidation. After 5 min., 24, 72 and 96 hours the corrosion is controled by charge transfer (chemical reaction), while after 48 hours a mixed corrosion mechanism is observed – charge transfer coupled with diffusion. Moreover, following 5 min, 24 and 96 hours the curve notably shows inductive loop (values on imagery axis below 0), which reduces our values of polarizing resistances. Polarizing resistances values decreasing after 72 and 96 hours against the R_p value after 48 hours is caused by dropping down of protective corrosion products resulting in further active development of corrosion process.

In case of EIS curves measured on glass balls peened surfaces, all measured times showed curves with indutive loop. Maximum value of polarizing resistance was measured after 96 hours of exposure, i.e. after time which was the double of time value recorded with non-blasted surface. After this time, the corrosion products loose their protective property and polarizing resistance is decreasing. Therefore, in reference to shot peened surface, the protective property of corrosion products is double the time. However, value of polarization resistances after individual exposure times is in reference to non-peened surface approximately 1.5 to 3 times higher. Thus shot peened surface is much more reactive and speed of its corrosion in 0.1M NaCl environment is higher.

4. Conclusions

Based on executed experiments and analyses we have arrived at following conclusions:

- Assessing the structure metalographically, it has been discovered the magnesium alloy AZ91 is created by polyedric grains of solid solution of additives in magnesium (δ) and areas of $Mg_{17}Al_{12}$ (γ) phase.
- Following surface shot peening with glass balls and subsequently applying metalographic analysis, it is possible to distinguish deformation twins created as a result of plastic deformation of the surface involving surface and sub-surface layer.
- Upon analysing Nyquist diagrams it became clear the AZ91_VS alloy reached its maximum of R_p value after 48 hours of fixation in corrosive environment at which time there also occurred a change in corrosion mechanism.
- The maximum of R_p value of the surface treated alloy with applied glass balls shot peening was measured after 96 hours of fixation in corrosive environment.
- The R_p values of non-peened surface are 1.5 to 3 times higher in comparison with shot peened surface, i.e. a shot peened surface is substantially more reactive and the corrosion rate in 0.1 M NaCl environment is higher.

Acknowledgement

This work was supported by Science and Technology Assistance Agency under the contract No. APVV-LPP-0144-06. This work has been supported by Scientific Grant Agency of Ministry of Education and Slovak Academy of Sciences, grant No. 1/0203/08. The part of the results of this work was supported by Slovak-Czech cooperation, project No. SK-CZ-0120-07.

References

[1] Kniewald, D.: Original knowledge of mechanical surface treatment. / Habilitation Work /. Košice, TU SjF, 1994

[2] Wagner, L.: Mechanical surface treatments on titanium, aluminum and magnesium alloys. Mat.Sci. Eng. A263 (1999), s. 210.

[3] Zhang, P., Lindemann, J.: Influence of shot peening on high cycle fatigue properties of the high-strength wrough magnesium alloys AZ80. Scripta Mat. 52 (2005), s. 485

[4] Brezinová, J.: Study of change in properties of mechanically treated surface, TU in Košice SjF, Transfer of innovations 7/2004

[5] Ábel, M., Brezinová, J., Draganovská, D.: Properties of a mechanically pre-treated surface, TU in Košice SjF, Transfer of innovations 6/2003

[6] Electrochemical software Voltamaster 4, Radiometer Analytical-Electrochemistry, 2002

[7] Hadzima, B.: Corrosion of alloys Mg-Al-Zn. [Dissertation thesis], ŽU in Žilina, Žilina

[8] Song, Y., L., Liu, Y.,H., Yu, S.,R., Zhu, X.,Y., Wang, Q.: Plasma electrolytic oxidation coating on AZ91 magnesium alloy modified by neodymium and its corrosion resistance

[9] Bragotsky, V., S.: Fundametals of electrochemistry, Hoboken, New Jersey, 2006

[10] Macdonald, D. D.: Application of Electrochemical Iimpedance SpectroHRopy in Electrochemistry and Corrosion HR ience. Techniques for Characterization of Electrodes and Electrochemical Processes. Eds.: Varma, R. and Selman, J. R., John Wiley and Sons, New York, 1991, s. 581.

[11] Hadzima, B.: Metal Mater., 41 (4), 2003, p. 257

Transcom 2009, 22-24 June 2009
University of Žilina, Žilina, Slovak Republic

Aspects Regarding Extracting Gold Through Dissolution Using Cyanides and Implications Upon the Environment

Daniela Cîrţînă
University "Constantin Brâncuşi" of Tg. Jiu, Faculty of Engineering,
street Geneva No.3, 210152, Gorj County, Romania, e-mail *daniela@utgjiu.ro*

Abstract. Extraction through dissolution is a minerals processing technique much rare than hydro-metallurgic processes. For extracting gold through dissolution we either use only this process, either we integrate it in other minerals processing stages, for example after chipping and gravitational separation. Consequently, extraction through dissolution is generally considered a part of minerals process. The use of cyanides in extracting through dissolution is a potential pollution risk for the environment due to cyanides high toxicity, which explains the concern of the public opinion about this procedure in mining.

Keywords: extraction through dissolution, cyanides, minerals process.

1. Introduction

Gold is extracted from the gold ores concentrates through: *amalgamation* and *cyaniding*, when Au from the ore selectively reacts with the NaCN solution:

$$4Au + 8NaCN + 2H_2O + O_2 = 4Na[Au(CN)_2] + 4NaOH \quad (1)$$

Then is extracted from the complex cyanide through Zn cementing:

$$2Na[Au(CN)_2] + Zn = 2Au + Na_2[Zn(CN)_4] \quad (2)$$

Metallic gold as well as its alloys are used for manufacturing devices, serving for researchers in the physical-chemical field, laboratory devices, jewelleries and for coating different objects made of glass, porcelain or metallic material. An extension has been occurred for gold use in the fine industry of electrical engineering and broadcasting engineering, because of its low chemical reactivity. Colloidal gold is used in medicine as antiseptic. Gold has a catalytic role in water synthesis and in some chemical processes [1].

Cyanides use in gold industry. Gold can be found in ores, usually in small concentrations, less than 10 g/t or 0,001%. In these concentrations, the use of hydro-metallurgic extractions processes, like those based on water chemistry, are the only economic reliable methods for extracting gold from the gross ore. Generally, gold recovery through a dissolution extraction stage, where gold is used in watery environment is followed by the separation of the solution including the gold or absorption of the gold on active coal and finally its recovery through precipitation or elution and electrolysis [2,3].

2. The stages of gold recovery from gross ore

2.1. Ore preparation

The purpose of ore preparation is to bring it to a form that would provide an economic and adequate gold recovery. The first step in preparing the ore is chipping and crumbling, which reduces the size of ore particles and releases gold to be recovered. Ores with gold lodes associated with sulphurs or coal-bearing minerals need additional treatments, besides the reduction of their size, before recovering the gold inside them. Gold recovery from sulphur ores is reduced because cyanides preferably dissolute sulphur minerals rather than gold, and cyanides in turn are used by sulpho-cyanides formation. These ores undergo a concentration process, like elutriation, followed by a second process for sulphurs oxidizing, thus limiting the interaction to cyanides during gold extraction through dissolution. Coal-bearing ores absorb gold after it has been dissoluted. This can be prevented by ore oxidizing before beginning the extraction process through dissolution. The extraction process through dissolution could be also altered for preventing this effect, by adding active carbon for preferentially absorbing only the gold.

2.2. Extraction through dissolution using solutions with aqueous cyanides

Gold is recovered either through extraction by dissolution from the mountain of useless rock, either through extraction by dissolution of the nucleus of the mountain of useless rock. Ore or fine agglomerated ore is placed in pits on a bearing provided with a water proof membrane. The cyanides solution is introduced in the pit through a sprinkling system, or irrigation system, the solution is infiltrated in the pit thus diluting the gold in the ore. The resulted solution, which contains gold, is collected on a water proof membrane and discharged to a storage site for a further processing. Ore dissolution is an attractive process due to its low cost, but it is a slow process and gold extraction is not efficient either, it is relatively low. Inside a conventional circuit of selecting and sieving, the ore is processed in mills using balls and sticks for ore crumbling until it reaches the consistency of sand or dust. Crumbled ore is transported using feeding belts under the form of a pulp to the extraction basins through dissolution. The pulp is then mixed in these basins either mechanically, either through compressed air, in order to increase the contact between cyanides and oxygen with gold and increase the efficiency of the extraction process through dissolution. As previously mentioned, cyanide dilutes gold in the ore and forms a complex of gold and cyanide. pH= 10 – 11 is worked using anhydrous lime, at the beginning of the dissolution circuit. The pulp can be also preconditioned in other ways, like peroxidising at the beginning of the circuit, before adding cyanides. Where oxygen is used instead of air as oxidant, there is an advantage of increasing the dissolution rate, decreasing at the same the consumption of cyanides.

In case of using carbon for absorbing gold, the extremely active carbon is introduced in the process, either directly in the dissolution basins or in separate basins after dissolution. Active carbon absorbs the diluted gold in the diluted pulp, thus concentrating it in a smaller mass of solid. Carbon is then separated from the pulp through sieving and undergoes another treatment for recovering absorbed gold.

The solution containing gold could be separated by the pulp's solid components using filtrations or sedimentary equipments. The materials from which the gold has been extracted through absorption or filtration are called sterile. Sterile is either dry for recovering water and any kind of cyanides-based reactive, either treated for neutralizing or recovering cyanides.

2.3. Recovering diluted gold

Gold is recovered from the solution through cementation using zinc dust (Merrill-Crowe process) or by gold concentration using active carbon absorption, followed by elution and zinc cementation or electrolyze. Active carbon in contact to the solution containing gold can generally recover more than 99.5% from the gold in a solution, which may take between 8 and 24 hours.

Gold loaded carbon is then extracted from the solution using sieves cleaned with water or compressed air in order to prevent them from clogging with similar sizes carbon particles. Extremely fine poor ore, like sterile for example, is then either deposited for separating the solution containing cyanides for recovering or destroying cyanides, while the solution containing cyanide is usually recycled at the extraction factory through dissolution. Absorbed gold in active carbon is recovered from the carbon through elution, in general by using a solution of aqueous and hot caustic cyanides. Carbon is then regenerated and introduced in the absorption circuit while gold is recovered from elution using zinc cementation or electrolyze. This gold concentrate is then calcined, if it contains great amounts of main metals, or directly melted and refined in gold bullions generally containing 70 – 90% gold. The bullion is then refined up to 99.99% using chlorides, melting and electric refining. Recently developed processes uses solvents extraction to produce high quality gold directly from active carbon [4].

3. Process implications upon the surrounding environment. Cyanic waters treatment technologies

Waters with cyanides content have the disadvantage of a high toxicity involving special labour safety measures and high costs of their treatment processes. Among the most frequently used treatment procedures, we mention: chemical and electrochemical oxidation, metallic salts complexing, ions changing process, distillation, biologic treatment.

Cyanides chemical oxidation is the most frequently applied procedure at industrial scale and can be made by using different chlorine salts as oxidation agent, like: $CaOCl_2$, NaOCl or fluid chlorine [5,6].

In the first case, simple cyanides oxidation occurs:

$$CN^- + OCl^- = CNO^- + Cl^- \quad (3)$$

Fluid chlorine oxidation is made according to simple cyanides oxidation reactions:

$$CN^- + Cl_2 + 2\ OH^- = CNO^- + 2Cl^- + H_2O \quad (4)$$

Reaction time is maximum 1 minute, and temperature cannot be more than 40°C. Increasing the amount of chlorine and the treatment duration a total decomposition of cyanides occurs, according to the reaction:

$$2NaCNO + 4NaOH + 3C1_2 = 2CO_2 + 6NaCl + N_2 + 2H_2O \quad (5)$$

The reaction speed in this case is 30 minutes (theoretically) and practically, one hour. The excess of chlorine is removed with fixing salt:

$$4C1_2 + Na_2S_2O_3 + 5\ H_2O = Na_2SO_4 + H_2SO_4 + 8\ HCl \quad (6)$$

Cyanates ions (CNO^-) forming in both cases hydrolyze carbonate and ammonium ions, therefore, after the treatment with lime chloride, sodium hypochlorite or fluid chlorine, cyanides are entirely destroyed, and hard metals precipitate under the form of insoluble combinations (hydroxides or carbonates). The theoretical amount of active chlorine necessary for the decomposition of simple and complex cyanides present in waste waters are computed by the formula:

$$X = 2,7A + 3,2B + 2,7C$$

where: A is the concentration of simple cyanides (recalculated at CN^-), in mg/l; B and C is the concentration of complex cyanides of Cu and Zn (recalculated at CN^- in mg/l).

Electrolytic oxidation applies to a high content of cyanide (150-230 mg/l). At the anode, made of graphite or magnetite simple or complex cyanides oxidation occurs. For cathode copper plate is used. Sodium chlorite is introduced in the water. Electric power consumption is 0,2 kW/h for the treatment of 1g cyanides, and the alkaline pH (10-12). The method disadvantage is that it can apply only to small amounts of water, of only a few m /h.

Ionic exchange is used for the treatment of waste waters with low content of cyanides. Anionic complex cyanides Cu, Zn, Au are absorbed on base exchangers, and through further, selective elution, metallic salts solution can result. This recent method consists of absorption, followed by de-absorption of complex cyanides, from the so-called ions exchanging resins. This procedure allows to reach very high extraction outputs (93-98%), in 8-10 hours.

The biological treatment for the waters with high content of cyanides (60-120 mg/l) is also a modern method applied at large scale worldwide. Active mud and biological filtering procedures are applied for the same purpose.

4. Conclusions

Gold is one of the noble metals and that is why it is not soluble into water. The presence of substances like cyanides and an oxidant, like oxygen, is used to dilute gold. The amount of cyanides in a solution necessary for dissolution can have values beginning from 350 mg/l or 0.035 % (from 100 % NaCN).

Other alternative substances for gold extraction, like chlorines, bromides, sulphourea, and fixing salts can be used, but they form less complex substances and thus require harder conditions to dilute gold. These reagents are often more expensive in use and/or reveal risks upon health and surrounding environment. This explains the dominance of cyanides as the main reagent for extracting gold through dissolution from gross ore.

Cyanides under the form of sulphur cyanide or complex cyanides of copper, zinc, iron, etc are the most harmful damaging agents present in waste waters from ores processing. The only complex cyanide without a toxic action is ferric ferro-cyanide, due to its chemical stability. In all the cases of treating the waters containing the cyan ion, one follows to transform CN^- group into a less harmful derivative for organisms.

Cyanides emission sources in the atmosphere are represented by: CN emissions in the air under the form of HCN; infiltrations from treatment pools; discharges of the treatment pools. The attempt to optimize the process economy coincides with the cyanides impact minimization process upon the surrounding environment and with the minimization of the amount of cyanides consumed during the process. Adding too many cyanides can cause a “boomerang” effect, which means high operation costs depending on the amount of cyanide to be bought for processing, as well as due to high amounts of cyanides to be destroyed or recycled after finishing the process. Cyanides classified as “consummated” from the processing point of view can be still active from the point of view of the surrounding environment.

Cyanic waters treatment procedures, like chemical and electrochemical oxidation, ions exchanging procedure or biologic treatment are solutions for decreasing the harmful effects of waste waters with high content of cyanides upon the environment. The elaboration of such procedures is based on good knowledge of chemical and electrochemical processes as well as the properties of cyanic substances.

References

[1] STOICA, L. et all, General chemistry and technical analysis, Didactic and Pedagogic Publishing House Bucharest, 1983.

[2] FODOR, D., BAICAN, G. *Impact of mining industry of environment*, Infomin Publishing House Deva, 2001.

[3] NEGULESCU, M., IANCULESCU, S. *Protection of the environment*, Technical Publishing House Bucharest, 1995.

[4] ROJANSCHI, V. and others, *Protection and engineering of the environment*, Economic Publishing House Bucharest, 1997.

[5] CIOCAN, V., TRAISTA, E., PODARIU, M., *Waste Water Treatment*, Publishing House Universitas Petrosani, 2000.

[6] FORSTER, C.,F., *Biotechnology and wastewater treatment*, New York, NY: Cambridge University Press, 1985.

Transcom 2009, 22-24 June 2009
University of Žilina, Žilina, Slovak Republic

Possibilities of Recycling the Urban and Industrial Wastes With the Purpose of Reducing the Pollution of the Environment

Daniela Cîrţînă
University "Constantin Brâncuşi" of Tg. Jiu, Faculty of Engineering,
street Geneva No.3, 210152, Gorj County, Romania, e-mail *daniela@utgjiu.ro*

Abstract. It is unanimously recognized that Romania is invaded by mountains of wastes that for financial reasons, legislative or technical remain unvalued and continue to degrade the environment. Besides the aspects related to the environment, these occupy enormous spaces and swallow important sums of money, in the conditions where there could constitute valuable sources of recyclable material or un conventional fuels for the energetic department. In the present paper are presented issues regarding the recycling of plastics and technology process for valuing the non metallic wastes through their transformation in an unconventional fuel.

Keywords: industrial wastes, recyclable material, conventional fuels.

1. Introduction

Waste management represents the operations of collect, transport, value and removal of wastes including the supervision of the storage areas after their closing. No matter the adopted solutions in the technological chain of recovery or destruction of wastes, it is noticed that as a necessity the compression operation and reduce huge volumes of waste.

Through the concept of "waste determination" it must be understood primarily a classification of waste material (type of waste) in a category of general waste. It is rational to operate a classification in a group of wastes depending on the mode of formation (generation and collection). For statistical purposes, is necessary also an ordered classification of types of wastes depending on the branches, industry or processes, where is generated the waste.

The management activities of wastes are based on a set of principles [1]:

- the protection of primary resources - brought in the broader context of the concept of "sustainable development" and establishes the need to minimize and streamline the use of primary resources, especially of those non-regenerative, accentuating the use of secondary raw materials;

- the principle of prevention - establishes the hierarchy of waste management, in the descending order of importance to be given to avoid the occurrence, to minimize the quantities, treating for recovery, treatment and removal in a safe conditions for the environment;

- the principle the polutter pays, in line with the principle of producer responsibility and the responsibility of the user – establishes the necessity to create a legislative and economic framework accordingly, so that the management costs to be borne by the generator thereof;

- the principle of substitution - sets out the need to replace the dangerous raw materials with not dangerous raw materials, avoiding this way the occurrence of dangerous wastes;

- the principle of proximity, correlated with the principle of autonomy - determines that the waste must be treated and removed as closer as possible to the generation source, in addition, the export of dangerous wastes is possible only to those countries that have technologies suitable for the removal and in compliance with the conditions of requirements observance for the international trade with wastes;

- the principle of subsidiarity established that the decisions on waste management to be taken at the lowest administrative level.

Developing a National Strategy for Waste Management aimed at creating the necessary framework to develop and implement an integrated waste management, efficient from the ecologically and economically point of view.

The operations of waste management follow a descending order of priorities, namely: the reducing the quantities, recovery and disposal [2].

To meet the national and European goals in the field of waste management is necessary to involve virtually the entire society, represented by the central and local public authorities, wastes generators, professional associations and research institutes, civil society.

2. Recycling of plastics material wastes - a solution for reducing the impact upon the environment

In recent years, plastics have become of great interest, in less than ten years the production of plastics increased greatly. The annual consumption can now be comparable to that of non-ferrous metals. The advantages and disadvantages of using plastic materials are presented synthetically in tab. 1. As regards the pollution, the question is not only pollution becomes greater but that it is permanent because most plastics unlike other materials do not degrade with time.

Collecting and recovering of plastics has advantages both economically and ecologically. Recovery of plastics presents difficulties especially in sorting them into categories, sorting which is made according to density [3,4]. During the valuing, the waste management and recycling companies are responsible for preparing the PET packaging for shipment to the processors. In this sense, there are available installations for:

- perforation of PET containers;
- PET's pressing in the so-called "briketts" or bales.

Advantages	Disadvantages
Small weight	Big volume when unload
Great variety of properties	Biodegradable war
Properties that cannot be attenuated with those of other materials	A large degree of pollution when incinerating
Longevity	A large degree of pollution when incinerating
Easy manufacturing way	A large degree of pollution when incinerating
Reduced energy consumption for manufacture	A difficult manner of recycling (large diversity, difficult decomposing process)
Reduced price	Base substances are partly cancerigen or toxic (ex. PVC)

Tab.1. Plastic materials - advantages and disadvantages of their use.

Recycling of different types of plastic present a problem in terms of the polymer incompatibility. Introducing the so-called "compatiblezers" makes possible the production of a type of alloys of plastic of inferior quality materials.

The technological flow of a standard installation for processing the waste plastics is as follows: in the first phase, flakes (pellets) are transported plastic through a conveyor belt or worm in the drying /crystallization. The material is continuously preheated, dried and

crystallized. From the intermediate silo is directed to the combination of units "cutting / dryer / extruder" through the vacuum valves. Held at low pressure and high temperature, plastic (PET) is decontaminated by volatilization of toxic substances with humidity.

It reaches a viscosity of plastic equal to the initial, before the use. With a system of transducers is enabled the control of the level of residual contamination.

3. Technological process of production of alternative fuel from non-metallic waste

By, “conventional fuel "means a fuel with a calorific value of 700 kcal / kg (corresponding to the inferior coal), the notion of conventional fuels serving different fuels in comparison with the real power through different caloric recalculating their weight in tonnes of conventional fuels [5].

The waste used to produce alternative fuel is: waste wood (wood from demolition, damaged pallets, bark, etc.), textile waste, waste from bags of lime, waste silicon paper, waste plastics, waste of rubber, waste rubber with textile insertion; scrap of waste paper.

Non-metallic waste or non-waste mixtures is collected from different centers of production, this waste collection is done with specialized equipment, in the waste domain, and qualified personnel in accordance with legislation. When the waste arriving at the warehouse is made a qualitative and quantitative receipt, to determine the recycling modality: reuse or recovery. The reusable waste is baled, prepared for recycling, separated by the waste to that follow to be recovered. The waste stored for processing is taken with a front loader and will be taken to a primary chopper equipped with a funnel, not to scatter around and a magnetic belt for metal retention. The waste size after the first grinding is around 150 - 200 mm. These wastes are transported using the conveyor belts to a second machine grind (secondary hacking), where the particle size reaches the maximum 30 mm. After this operation is a sort using a sieve (rotary screen), which has holes of different sizes to choose only those with maximum dimensions of 30 mm. Particles larger than 30 mm fall again in the process of mincing through lanes, the cycle is repeated until the mixture reaches the desired size. This mix of waste contains certain percentages of waste listed above depending to the beneficiaries’ requests.

The obtained material satisfies the requirements of environmental and end-user requirements: high quality, good performance, less polluting and meets the requirements of the European Union. The product of this processing process of waste can be used as an alternative fuel by the cement factories, thermo electric power stations and other beneficiaries who are endowed with special equipment to burn such fuels. Fuel can be produced in smaller sizes of even 20 mm depending on the requirements and activity domain in which is used. Before delivery are taken samples of that mixture to see if it meets certain conditions, for example:

-calorific value must be at least 22 MJ / kg;
-chlorine content should be below 0,5% max 0,75%;
-S content less than 1;
-PVC content less than 50 ppm, etc.

To improve the performance of this fuel, the finished product obtained in the processing plant is treated with various substances depending on the material composition and the further use of the product.

4. Conclusions

Waste Management has an important role because it represents not only a potential source of pollution, but may constitute an important source of secondary raw materials and a source of energy. The choice of priorities in this sector has direct consequences from the economic and environment point of view. It is in touch not only with environmental policies but also with the technological, economic and consumption ones. The current trends on waste are to reduce waste on the one hand the danger of environmental pollution, on the other the danger of environment pollution. The modern strategy on waste management includes a hierarchy of management options where the first accent is upon the prevention of waste production. This is followed by actions of recycling and reuse promotion and then optimization of the methods of final storage of waste.

If we relate to recycling of plastics, it has grown steadily in the last period and was conducted in a wide range in many countries. Rather than pollute rivers or water large areas of soil through their accumulation, PET can be collected and recycled. Recovery of plastic packaging is a big challenge, due primarily to the large number of sites PET (polyethylene terephthalate - is a sophisticated material of high-resistance) used very effectively as a container for beverages. In addition any recovery technologies are not fully finalized and this way the obtained products are of an inferior quality to those obtained directly from the raw materials.

Given that current use of fuel has become a problem both in terms of environmental protection, the degree of pollution is increasingly high, and also from the economic and commercial expenditure, the necessary expenses for their production is high, it was tried an alternative to solve these problems related on one hand to the waste management and on the other hand to their recovery through the production of alternative fuels.

This way, there may be obtained low costs and performances with almost identical alternative fuels that meet the requirements both in terms of quality and standards of environmental protection.

Through processes of non-metallic waste, there can be obtained from mixtures with similar characteristics to the conventional fuels, making it possible to use them as an alternative fuel in cement plants, thermal power stations or in the activity of other beneficiaries who have fitted special equipment to burn such fuels. The maximum where they can produce such blends can provide the necessary fuel for a series of large cement manufacturers in the country.

The afferent costs of acquisition and maintenance of machinery and equipment required for the production of alternative fuel by processing non-metallic waste are quite low, the expenses of personnel also, which constitute significant advantages in diverse areas. The materials are less polluting, do not emit toxic or dangerous compounds into the atmosphere, do not produce ash in large quantity, such as coal land, has a calorific value between 18-24 MJ / kg, being able to replace coal, allows saving the use of conventional fuels and alignment to the EU requirements.

References

[1] Baron V., *Practice environmental management*–ISO 14001, Technical Publishing House Bucharest, 2001.

[2] Bold, O.V. , Marăcineanu, G.A.- *Storage, treatment and recycling of materials and waste*, Publisher Matrix Rom Bucharest 2004.

[3] Gheorghe M.- *Recovery of waste products and industrial construction*, Publisher Matrix Rom Bucharest 2001.

[4] Wehry A., Orlescu, M.- *Recycling and organic waste storage* , Publisher academic horizons Timişoara, 2000.

[5] Antonescu N.- *Valorisation energy waste*, Technical Publishing House Bucharest, 1998.

Transcom 2009, 22-24 June 2009
University of Žilina, Žilina, Slovak Republic

Evaluation of Hydrogen Induced Cracks in Gas Pipeline Steels and Influence of Microstructure

Martin Čipera, Dagmar Mikulová, Jaroslav Málek
SVÚM a.s., Strength Department, Areál VÚ, Podnikatelská 565, 190 11 Praha 9, Czech republic,
{mcipera, d.mikulova, malek}@svum.cz

Abstract. This article deals with evaluation and measurement of hydrogen induced cracks in steel strips from gas pipeline steels with improved yield point L360MB, L450MB, L485MB. Quantitative values of hydrogen induced cracking are given into correlation with microstructure. Main reason for susceptibility of these steels to hydrogen induced cracking was found in pearlite banding.

Keywords: Hydrogen induced cracking, microstructure, pearlite banding.

1. Introduction

Gas is during mining often transported in pipelines with considerable portion of hydrogen sulfide and water. This environment is very aggressive to steels, used in transport and caused around 25 % of equipment failures [1].

During corrosion reaction between steel and water environment, during which is generated hydrogen, on a surface of steel release hydrogen atoms, which, from the most part combine to stable hydrogen molecules. This combining of hydrogen atoms into molecules may be decrease or stop, for example, by hydrogen sulfide. In this case, on the surface of steel is generated high concentration of hydrogen atoms with an ability to enter in to a crystal lattice and diffuse there. If hydrogen atoms during diffusion meet any irregularity, for instance, inclusion or beaded disjunction, they start to cumulate there and combine into a molecular form of hydrogen. This leads to increase of pressure in the disjunction, which further should cause initiation and grow of cracks, usually along rolling direction of steel. Cracks on one plane tend to link up with cracks on adjacent planes to form “steps “ across the thickness. This phenomenon is called hydrogen induced cracking (HIC). Cracking is sometimes accompanied by surface blistering [2, 3, 4].

Resistance against HIC depends on steel cleanliness and on microstructure. Susceptibility to HIC is usually associated with banded structure [5] or with elongated inclusions [6].

This article deals with evaluation of resistance of steel strips from steels with improved yield point L360MB, L450MB, L485MB for gas pipes of interstate and intrastate gas transmission pipelines and susceptibility to HIC correlated with structure aspects.

2. Experimental Procedure

Tests were made according to standard NACE TM0284-87 on specimens from steel strips from steels L360MB L450MB, L485MB. Chemical composition and mechanical properties of tested steels according to standard ČSN EN 10208-2 are in Tab. 1.

Steel designation	Chemical composition [max. %]									Mechanical properties			
ČSN EN 10208-2	C	Si	Mn	P	S	V	Nb	Ti	CE	R_e min. [MPa]	R_m min. [MPa]	A_5 min. [%]	KV 0 °C [J]
L360MB	0,16	0,45	1,6	0,025	0,02	0,05	0,05	0,04	0,41	360	460	20	40 (30)
L450MB	0,16	0,45	1,6	0,025	0,02	0,10	0,05	0,06	0,43	450	535	18	40 (30)
L485MB	0,16	0,45	1,7	0,025	0,02	0,10	0,06	0,06	0,43	485	570	18	53 (40)

Tab. 1. Chemical composition and mechanical properties of tested steels [7].

From every steel strip were parallel to rolling direction taken 3 squared log specimens. These specimens were degreased and putted into test vessel, which was filled by synthetic seawater. Then, hydrogen sulfide gas was bubbled through the synthetic seawater to achieve and maintain saturation. To this corrosion environment were specimens subjected for 96 hour. After exposition was on the surfaces of specimens measured square of blisters per square unit, then were specimens cut and on inner surfaces made sections, which were not etched. Founded cracks were measured according to Fig. 1. For every section was calculated values, which characterized its damage by cracks (1)-(3) [4]. Their common acceptable values are in Tab. 2. Together with it was carried out analyze of segregation of inclusion. Sections were finaly etched in 4% nital for observing of microstructure.

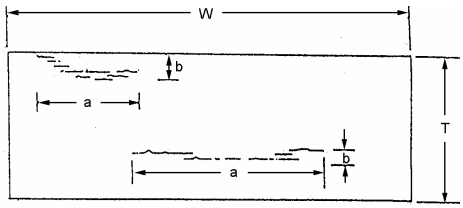

Fig. 1. Measuring of stepwise cracking [4].

$$CSR = \frac{\sum (a \times b)}{W \times T} \times 100 \tag{1}$$

$$CLR = \frac{\sum a}{W} \times 100 \tag{2}$$

$$CTR = \frac{\sum b}{T} \times 100 \tag{3}$$

	CLR	CTR	CSR
Common acceptable values	10 – 15	3	2

Tab. 2. Common acceptable values of quantitative parameters.

3. Results and Discussion

In centerline of specimens from steel L450MB was found high amount of cracks, especially characteristic hydrogen cracks, and on specimen 3 were even quantitative parameters, characterizing damage of steel strips by cracks (Tab. 3), above common acceptable values. These specimens had virtually no blisters.

On Fig. 2a is possible to observed, that microstructure outside of centerline of specimens consisted of ferrite and pearlite, without banding. In centerline of specimens (Fig. 2b), there was segregation of carbon and microstructure was banded. On interfaces and in these bands initiated and grown cracks, because interfaces between pearlite bands and ferrite are hydrogen traps. Hydrogen diffuse in to these interfaces and pressure should reach critical values. Pearlite itself is hydrogen trap, because on interfaces between ferrite and cementite lamellas should be concentration of hydrogen. Initiation and growing of cracks is even facilitated by presence of inclusion, above all sulfides. However in centerline of all specimens from all three steels was not found segregation of sulfides.

Steel designation	Specimen	CLR	CTR	CSR	Blisters [%]
L450MB	1	1,462	0,805	0,003	0,00
	2	4,348	1,594	0,011	0,00
	3	15,145	3,587	0,343	0,03
	Average	6,985	1,996	0,119	0,01
L485MB	4	0,339	0,209	0,001	2,26
	5	1,925	0,707	0,003	2,91
	6	3,292	1,999	0,043	3,97
	Average	1,852	0,972	0,016	3,04
L360MB	7	1,354	0,544	0,002	0,01
	8	0,732	0,590	0,001	0,00
	9	0,776	0,795	0,001	0,02
	Average	0,954	0,646	0,002	0,01

Tab. 3. Quantitative parameters characterizing damage of steel strips by cracks and blisters

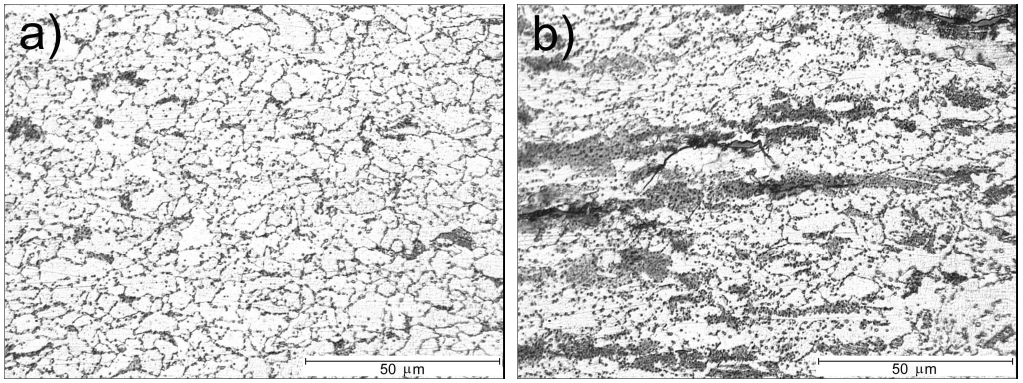

Fig. 2. Microstructure of specimen 3, from steel L450MB, a) outside of centerline, b) in centerline.

Specimens from steel L485MB have values of quantitative parameters quite low, never were above common acceptable values. Amount and size of blisters was high, between 2,26 – 3,97 %. As good are considered values around 1%.

Microstructure outside of centerline of specimens consists of ferrite and was without banding. Centerline of specimens was slightly banded (Fig. 3a) and were there found low amount of characteristic hydrogen cracks. However, their amount and size were significantly lower then in steel L450MB.

Values of quantitative parameters of cracks and blisters in specimens from steel L360MB were significantly under common acceptable values.

Microstructure outside of centerline and in centerline of specimens (Fig. 3b) consists of ferrite and pearlite, without any pearlitic banding.

There was not found correlation between average values of quantitative parameters characterizing damage of steel strips by cracks and blisters (Tab. 3). There should be correlation between single specimens from same steel strip. It is clear for steel strip from

L485MB, but steel strips from L450MB and L360MB have values of blisters to low to prove this correlation.

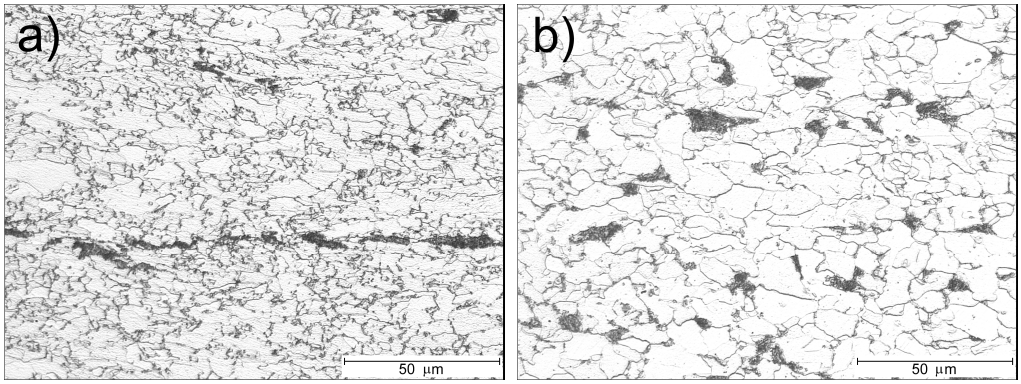

Fig. 3. Microstructure in centerline of specimens: a) L485MB, b) L360MB.

4. Conclusions

- Steel strip from steel L450MB shows significant susceptibility to HIC.
- Steel strips from steel L485MB and L360MB show acceptable resistance to HIC.
- In examined steel strips were proved relation between enhanced susceptibility to HIC and pearlitic banding in centerline of strips.
- It was not found clear correlation between quantitative parameters characterizing damage of steels by cracks and blisters .

Acknowledgement

The work was carried out under the grant MSM 2579700001 of the Czech Ministry of Education, Youth and Sports.

References

[1] BEYERRA, P. S. A., JÓIA, C.J.B.M., ASSUNCAO, F. C. R. *Proceedings of 18 Congresso Brasiliero de Corrosao.* ABRACO, 1995.

[2] FRIDRICH, R. *Vodíková koroze a křehkost kovů.* SNTL, 1963.

[3] *ČSN EN 10229.* ČNI, 2000.

[4] *NACE Standard TM0284-87*. NACE, 1987.

[5] Mazancová, E. *Strukturně metalurgické charakteristiky vodíkem indukované křehkosti.* Hutnické listy, no. 11-12, 2001.

[6] Domizzi, G., Anteri, G., Ovejero-García, J. *Influence of sulfur content and inclusion distribution on the hydrogen induced blister cracking in pressure vessel and pipeline steels.* Corrosion Science, 43, 2001.

[7] *ČSN EN 10208-2.* ČNI, 1999.

Transcom 2009, 22-24 June 2009
University of Žilina, Žilina, Slovak Republic

Programming Measurements with Coordinate Measuring Machines

[*]Mário Drbúl, [*]Stanislav Turek, [*]Ivan Litvaj
[*]University of Žilina, Faculty of Mechanical Engineering, Department of Machining and Manufacturing Engineering, Univerzitna 2, 01026 Žilina, Slovakia, { mario.drbul@fstroj.uniza.sk, stanislav.turek @fstroj.uniza.sk, litvaj@fel.uniza.sk}

Abstract. In this article we deal with making offline programs for measuring machines. Such programming of the measurement process involved the creation of a mathematical model in the test computer, which for example helps to verify the appropriateness and effectiveness of different measurement strategies, to identify various states of conflict and the measurement of contact.

Keywords: measurement program, offline programming, coordinate measuring machine, CAD, CAM.

1. Introduction

Current CNC measuring machines can be programmed offline or directly at the machine. Measuring programs for coordinate measuring machines (the machines SMS) containing a large number of modules, the simplest is intended to manually measure the object. Course measurement is the entry in the tree window. This course can be saved and reused at the next measurement, measured in the same parts. This type of measurement is called the ". "Teach in" mode and is among the most commonly used methods of measurement automation. It is used mainly its simplicity and low requirements for operator qualification measurement.

Another mode is the offline programming. This is done by a computer or workstation, independent of SMS machine. Such programming may be an integral function in the CAD / CAM system or a separate system using geometric data are transferred from the CAD system. These programs include: Delmas V5 INSPECT, Metrology V5 R16, Silmo CimStation Inspection, LK Camio Studio Inspect and others. Conventional systems are often a combination of CAD and the independent monitoring program (this will eliminate the problem of interoperability between CAD systems and offline programming [1]) for example. WinWerth, Inca and other 3D.

1.1 Metrology V5 R16

It is fully integrated into CATIA V5. This allows him direct access to geometry and FTA modules (FD & T) CATIA V5 [3]. S Metrologie V5 (Fig.1) can control a CMM uses DIIS and analyze the results of directly comparing the components with CATIA V5 data in real time. The program allows for a direct link between design and quality control.

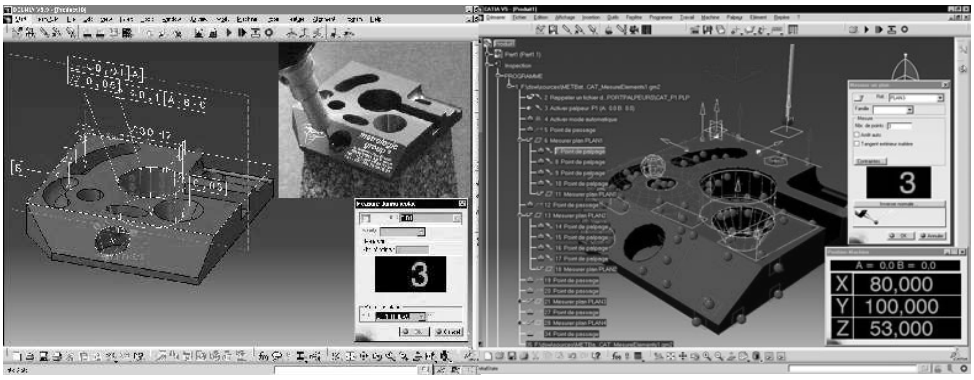

Fig.1. Metrology V5 R16 - practical applications [5]

2. Delmia V5 INSPECT

The ranks of an interactive 3D graphics incentive tools, which are intended for design, evaluation and analysis of the measurement. It contains a library of coordinate measuring machines. With these modules can be performed following [2]:
- Automates the creation of coordinate measuring machine
- Incentive check routes and measuring the probe rather than the programmed operation is performed on the CMM
- During the simulation we can determine the status of a collision, measure the dimensions of CAD models and other (Fig. 2).

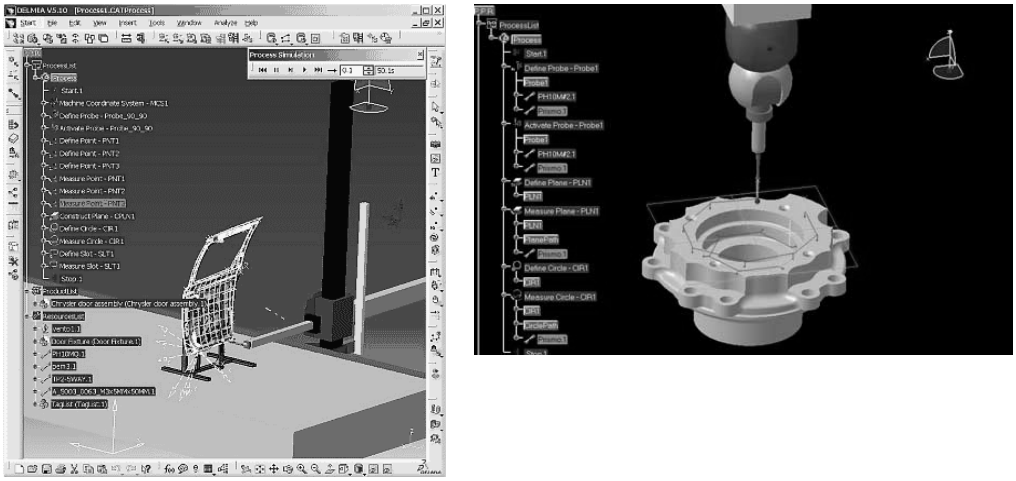

Fig.2. Digital Process Manufacturing [8]

3. Silmo CimStation Inspection

3D graphics is an incentive program, which allows the form of SMS programs directly from CAD model. It contains a library of kinematic models of SMS and sensors. The program has direct links with CATIA, PTC Pro / ENGINEER. and enable off-line and on-line programming SMS [4]. CAD models of components are imported into CimStation Inspection (Fig. 3,4) in their own format, via a direct link geometry data integrity is protected.

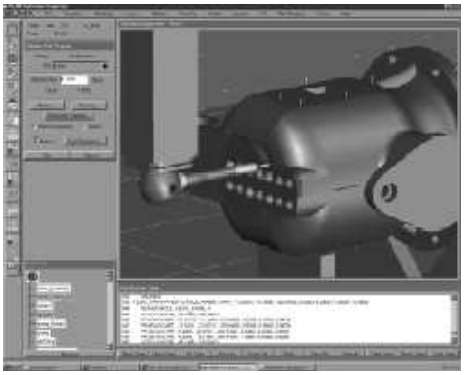

Fig.3. Detection of conflict situations. [6]

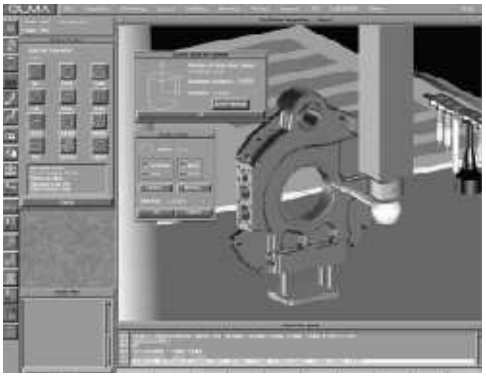

Fig.4. CMM- Programs generated on Silmo CimStation Inspection. [6]

4. LK Camio Studio Inspect

That measurement is an internationally certified program in the Institute PTB Braunschweig, meet EUR 10901 EN and EUR 13417 EN of CMM. LK DMIS allows measurement program launch from measuring machines of other manufacturers compatible with standard DMIS (Dimensional Measurement Interface Standard). LK Cami (Fig. 5) is built on a platform of ACIS (Spatial Technology, part of Dassault Systems, which supplied and Catia CAD system). Library Catia are directly integrated into the Studio.

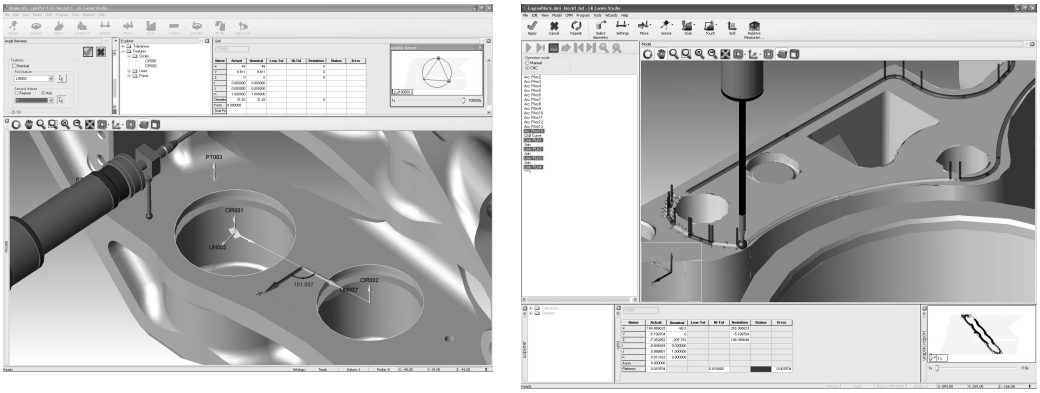

Fig.5. On-line Inspection [7]

5. Standards for Programming Measuring Machines using CAD Systems

The transition from the CAD geometry for offline programming systems is usually done the classic standard CAD exchange formats such as IGES and VDA. The biggest shortages of these key standards that contain variations that are an important parameter for evaluation of measured control components, as well as for automation of many tasks of planning control. SMS machines usually have its own programming language, which shall be subject to offline programming.

DMIS (Dimensional Measuring Interface Specification) is the standard format used for bidirectional communication between CAD systems and SMS machines. DMIS is a very important programming language with a structure similar to automatic programming tool APT (Automatically Programed Tool). Obtained results of the checks are usually processed into a format usable SMS or CAD systems [1].

6. Benefits of Offline Programming

Offline programming offers many advantages, such as.:

- Eliminate unproductive SMS machine programming time and a potential increase in use of the measuring machine.
- Avoiding unexpected operating problems and thereby eliminate unproductive time spent re-SMS.
- The possibility of minimizing the time necessary for the control element and thus increase the production SMS.
- Reduction control sequences, thereby enabling better utilization of working time of the inspection staff.

7. Conclusion

To make more effective control of products, manufacturers are forced to constantly upgrade their control facilities. Coordinate measuring machines that are controlled by computer technology, provide space to the automated measurements but also offer opportunities while offline programming. Thanks to the automation can not only shorten the time of the measurements, but to streamline the process of checking that, in Automated CMM machine is not needed constant supervision throughout the duration of handling of the measurement process and to allow staff to address the other control activities.

References

[1] LEGGE D. I.: Off-line Programing of Coordinate Measurinng Machines
[2] http://www.delmia.com/gallery/pdf/DELMIA_v5Inspect.pdf
[3] http://www.metrologic.fr/news_letter/news_March_2006_uk.htm#V5
[4] http://www.agendapr.com/quality_today_editorial.pdf
[5] http://www.metrologic.fr/news_letter/news_March_2006_uk.htm
[6] http://www.acel.co.uk
[7] http://www.topmes.cz/cz/lk_software.html
[8] www.delmia.com

Transcom 2009, 22-24 June 2009
University of Žilina, Žilina, Slovak Republic

On the Statistical Description of Porosity Effect on Fatigue of Al-Si Cast Alloys

[*]Stanislava Fintová, [*]Radomila Konečná, [**]Gianni Nicoletto
[*]University of Žilina, Faculty of Mechanical Engineering, Department of Materials Engineering, Univerzitná 1, 01026 Žilina, Slovakia, {stanislava.fintova, radomila.konecna}@fstroj.uniza.sk
[**]University of Parma, Department of Industrial Engineering, Viale G.P. Usberti, 181/A, 43100 Parma, Italy, gianni.nicoletto@unipr.it

Abstract. During the casting process the porosity formation is current event. Porosity is the main factor influenced the mechanical properties and increased the fatigue behavior of castings. Due to this fact the prediction of the fatigue life from the knowledge of the casting porosity is very interesting opportunity. In this contribution for the statistical description of porosity in Al-Si cast alloy and largest defects sizes prediction the Murakami's statistical method was used. Two different approaches of statistical evaluation of largest defect sizes measured by metallography were compared here in this paper with results from fatigue tests. The threshold size of casting defect for fatigue crack initiation was also considered.

Keywords: porosity, Al-Si cast alloy, Murakami's statistical method

1. Introduction

Aluminum alloys are increasingly used in structural applications controlled by low weight requirements, (i.e. aircraft and automotive industry) for their excellent specific strength (i.e. strength-to-density ratio). The Al-Si alloys are the most used Al–alloys when the casting process is considered [1].

Formation of porosity and microshrinkage cavities are almost inevitable in the sand casting process [2]. The defects often result in poor mechanical properties including limited strength and ductility, variable fracture toughness, irregular crack initiation and crack propagation characteristics, potentially accompanied by a lack of pressure tightness [3]. Compared with porosity, the eutectic structure and intermetallic phases play a minor role in crack initiation. The effect of porosity on fatigue life has been summarized as follows: pores reduce the time for crack initiation by creating a high stress concentration in the material adjacent to the pores; because of this, most of the fatigue life is spent in crack growth [4]. There exists a critical defect size, [5], (in Sr modified cast A356 alloy, the critical defect size is in the range of 25-50 μm) for fatigue crack initiation, below which the fatigue crack initiates from other intrinsic initiators such as eutectic particles and slip bands.

The present work is aimed to compare the two different approaches of statistical evaluation of largest defect sizes measured by metallography and to find the correlation with fatigue tests results. Fatigue experiments were performed on specimens of Al-Si alloy modified by an optimal amount of Sr. Light microscopy was used to analyze the material microstructure and porosity after fatigue testing. The method proposed by Murakami, [6], for the statistical description of equivalent largest defect sizes in materials is then used.

2. Experimental material

As the experimental material the Al-Si cast alloy AlSi7Mg delivered from the University of Parma was used. The specimens for the fatigue tests were extracted from real castings and they were tested for fatigue. The metallographic specimens were extracted from specimens failed during the fatigue tests under rotating bending loading. The structural analysis was carried out applying metallographic techniques and digital image analysis software on polished cross sections according the Slovak standard STN 42 0491.

3. Results and discussion

3.1. Fatigue test results

The fatigue tests at different stress levels (from 80 to 60 MPa) according to the rotating bending configuration at 50 Hz frequency were performed and the results are shown in Tab. 1. Since the objective was the correlation of stress amplitude, number of cycles and predicted largest pore sizes was carried out. The relation between stress amplitude and fatigue life shows quite high scatter that it is not generally unexpected for cast Al-Si alloys because of the inhomogeneity of the cast material and also because of the cast defects. One-order-of-magnitude difference in number of cycles to fracture at the same stress amplitude is observed in Tab. 1 and similar fatigue lives are associated to quite different stress amplitude. Interestingly, SDAS was fairly constant in all specimens.

Specimen	S [MPa]	N [cycles]	SDAS [μm]	Estimated largest pore size for S = 10 mm^2 [μm] predicted from LEVD plots for	
				all measured values	values above thresholds
1B	60	2 041 210	64	89	79
2B	70	10 388 728	58	51	48
3B	80	2 074 770	53	60	14
4B	60	223 080	55	53	52
5B	70	669 562	56	71	70
6B	60	870 745	58	113	30

Tab. 1. Fatigue tests results and estimated largest pore sizes

3.2. LEVD

The size of casting porosity was studied on metallographic specimens in a light optical microscope. For the statistical description of porosity the Murakami's statistical method, [6], and for the statistical description of porosity the Largest Extreme Value Distribution (LEVD) were used. The equivalent sizes, area$^{1/2}$, of the largest pore within each control area S_0 on the polished cross section of the metallographic specimen using the image analysis program were measured. The fitted distribution was then used to estimate the size of the largest defect size in a given region S larger than the control area S_0, through the return period $T = S/S_0$, or to compare largest defects from control areas of different sizes. For pores size evaluation the 50 x magnification was used here. The control area was $S_0 = 1.86$ mm^2 [2]. The largest defect sizes were predicted in this paper for the area S = 10 mm^2, representative of the highly stressed area of the rotating bending fatigue specimen.

On the LEVD plots on the Fig. 1 the distributions for the largest defect sizes for measured specimens are shown. The values in the plots don't fill the linearity condition necessary for using of Gumbel distribution [6]. It is evident that the distribution for smaller defects is different as the one for bigger largest defect. There exist a threshold between smaller

and bigger largest defects in all cases and it is evident that in all cases is the threshold size of largest defect different.

Using the thresholds following from distributions changes the predicted largest defect sizes are smaller (Tab. 1). The difference between largest defect sizes predicted from LEVD plots using all measured values and LEVD plots using just values above the threshold sizes are in each case variously due to the differences in distributions. In all cases the defects predicted from LEVD plots using just sizes of largest defects above the threshold are smaller.

The size of largest defects predicted from LEVD plots for all measured values was in all cases bigger than critical defect size, [5], for fatigue crack initiation (25-50 μm). The predicted largest defects sizes and the predictions of fatigue lives of specimens quite correlate with the fatigue tests results except specimen 4B. The longest fatigue lives were predicted for the specimens 2B, 4B and 3B and then shorter for the specimens 5B, 1B and 6B. The numbers of cycles to the fracture measured during the fatigue tests was the highest for the specimen 2B and then lower for the specimens 3B and 1B and the lowest number of cycles to the fracture was measured for the specimens 6B, 5B and 4B.

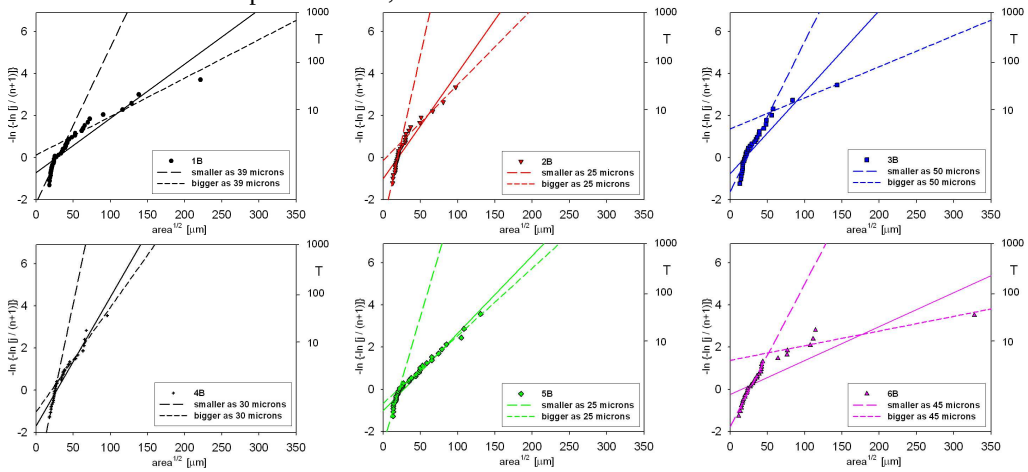

Fig. 1. LEVD plots

The predicted largest defects sizes from LEVD plots for values above the threshold sizes were in some cases smaller as the critical defect size. In cases of specimens 2B, 3B and 6B were the predicted sizes of largest defects smaller as 50 μm and it is possible, that they did not cause as the fatigue crack initiation places, [5]. They reached quite long fatigue life due to the loading during fatigue tests. Specimens 4B and 5B reached shorter fatigue life, but the predicted defect sizes were larger as the critical defect size. The fatigue life of specimen 1B is comparable with fatigue lives of specimen 3B, even though the predicted largest defect size was higher. The longest fatigue lives predicted from the LEVD plots plotted just for values of defects bigger than the thresholds for change of the defects distributions were predicted for the specimens 3B, then smaller 6B, 2B, 4B, 5B and 1B. Prediction of fatigue life of the specimens 1B and 2B does not correlate with fatigue tests results completely. But the specimens 3B and 6B reached higher number of cycles to the fracture than specimens 4B and 5B.

The differences between the largest defects sizes predicted from LEVD plotted for all measured values and from LEVD plots plotted for values above the thresholds were the biggest in case of specimens 3B and 6B (Tab. 1). Anyway, the fatigue lives predicted by both methods correlate with the real results obtained from fatigue tests just partially. Using the LEVD plots with thresholds the predictions of fatigue lives for the specimens 6B and 3B and also 4B and 5B correspond with the fatigue test results but in case of the specimens 2B and 1B disappeared.

The fatigue life of the specimens predicted from LEVD plots with thresholds correlate with the fatigue tests results more than the fatigue life predicted from the LEVD plots for all measured values. The differences between the assumed and the determined fatigue life can be explained by the influence of other casting defects characteristics as number and location of defects in the volume of specimens with respect to the free specimens' surface. In addition in some cases the unambiguous definition of a pore size was problematic due to possible cavity ramification typical of shrinkage pores. Colonies of small shrinkage pores observed on the polished cross section, [7], can be branches of one single shrinkage pore. Therefore, metallographic measurements should not be used as direct inputs to predict the lower bound fatigue performance of the material and to estimate the upper bound pore size using the extreme value statistic method can be used. For the pore size characterization, [7], not only the equivalent sizes, $area^{1/2}$, but also the maximum Feret diameter can be used. This issue will be addressed with an on-going study.

4. Conclusion

Prediction of the largest defect size in an Al-Si casting is a key-step in the prediction of its fatigue strength. The following conclusions are reached from this study:

- In all cases the largest defects sizes predicted from LEVD plots for all measured values were bigger as the critical defect size for fatigue crack initiation.
- The largest defects sizes predicted from LEVD plots with thresholds were for the specimens 2B, 3B and 6B smaller than the critical defect size 50 µm (the critical defect size for fatigue crack initiation) and for the specimens 1B, 4B and 5B bigger than critical defect size.
- The fatigue lives of the specimens predicted from both LEVD plots do not correspond with the fatigue test results completely.
- The population and also the location of casting defect towards the free surface of the specimens have the influence on the fatigue life.

Acknowledgement

This work was done as a part of the KEGA grant No.3/6110/08. It is also consistent with the objectives of MATMEC, an Emilia-Romagna regional net-lab (http://www.matmec.it/).

References

[1] BRYANT, J. D. -. WHITE, D. R: *Aluminium and magnesium for automotive applications*. The Minerals Metals and Materials Society; 1996.

[2] KONEČNÁ, R. – NICOLETTO, G. – MAJEROVÁ, V.: *Largest extreme value determination of defect size with application to cast Al-Si alloys porosity*. METAL 2007.

[3] AMMAR, H. R. – SAMUEL, A. M. – SAMUEL, F. H.: *Porosity and the fatigue behavior of hypoeutectic and hypereutectic aluminium-silicon casting alloys*. International journal of Fatigue, 2007.

[4] AMMAR, H. R. – SAMUEL, A. M. – SAMUEL, F. H.: *Effect of casting imperfections on the fatigue life of 319-F and A356-T6 Al–Si casting alloys*. Mater. Sci .Eng. A, 2007, doi:10.1016/j.msea.2007.03.112.

[5] WANG, Q. G., APELIAN, D., LADOS, D. A.: *Fatigue behavior of A356-T6 aluminum cast alloys. Part I. Effect of casting defects.* Journal of Light Metals 1, 2001, pp. 73-84.

[6] MURAKAMI, Y.: *Metal Fatigue: Effects of Small Defects and Nonmetallic Inclusions*. Elsevier, Oxford, 2002, pp. 320.

[7] WANG, Q.G., JONES P.E.: *Prediction of Fatigue Performance in Aluminum Shape Castings Containing Defects.* The Minerals, Metals & Materials Society and ASM International, 2007, DOI: 10.1007/s11663-007-9051-4

Transcom 2009, 22-24 June 2009
University of Žilina, Žilina, Slovak Republic

The Influence of the Rate of Laser Beam Feed on the Cutting Front Shape for Stainless Steel

[*]Marta Garbala
[*]University of Technology, Centre of Laser Technology, Aleja Tysiąclecia Państwa Polskiego 7, 25-314 Kielce, Poland, martaaa7@o2.pl

Abstract. The experimental analysis of the influence of the rate of laser beam feed on the shape of the cutting front for stainless steel 304 is presented. The aim of the research was to determine the influence of the rate of laser beam feed on the process and to facilitate construction of engineering models. The experiment was carried out on TRUMPF TLF 6000 Turbo laser. The variable parameter was the rate of laser beam feed, and constant parameters were: laser beam power, pulse frequency, working gas pressure, head distance from the metal sheet surface, and the focus position. It has been found that the change of the rate of the laser beam feed has a significant influence on the cutting front shape of stainless steel.

Keywords: Laser cutting; stainless steel;

1. Introduction

Laser cutting is a process in which the energy of continuous or pulse laser beam causes local melting and in some cases evaporation of the material being cut. The melt is then removed out of the cutting kerf by a strong gas jet applied coaxially with the laser beam [2]. Laser cutting is used to process a very wide range of materials: metals, wood, glass, ceramic, cloth even stone. The advantages of laser technique in comparison with other methods of cutting are: speed, flexibility, safety, cleanness of a workplace, simplicity, ease of work and above all cost-effectiveness.

Several methods of laser cutting are used: vaporisation cutting, fusion cutting, active gas melt shearing (reactive fusion cutting), chemical degradation („cold" cutting), scribing and thermal stress cracking (controlled fracture)

There has been a lot of experimental work aimed at improving the cutting quality and efficiency. The purpose of the present research was to examine the influence of the rate of the laser beam feed on the shape of the cutting front of stainless steel. The fusion cutting was applied, which is standard method of processing of this kind of steel. In this method the material melted within the cutting zone is removed by the high pressure jet of inert gas.

2. Description of the Experiment

The experiment was carried out with the use of laser TRUMPF TLF 6000 Turbo at Centre of Laser Technology of Metals (joint Kielce University of Technology and Polish Academy of Sciences unit) in Kielce (Poland). In this type of laser, the active medium is carbon dioxide (CO_2). The laser can work in a continuous mode or in a pulse mode. Its

maximal power is 6 kW and the wavelenght 10,6 μm. The material used in the experiment research was stainless steel AISI 304 (1.4301). It is commonly used stainless steel containing 18 % of chromium and 9 % of nickel [3].

In order to obtain the cutting front shape, the method of interrupted beam action was used. The specimens were covered with copper plate (Fig.1).

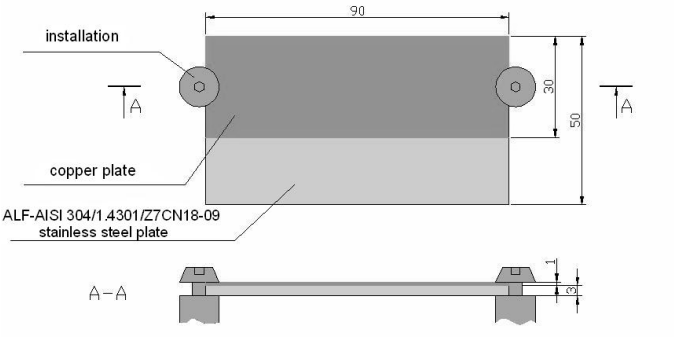

Fig. 1. The way in which the specimen is installed.

Next, the specimen was cut every 15 mm with different values of the rate beam feed (Fig.2). In the places where the laser beam comes across copper plate, the laser beam was blocked due to high reflectivity and conductivity of copper and the process of cutting of the underneath specimen was suddenly interrupted. Thus the instantaneous shape of the cutting front could be obtained.

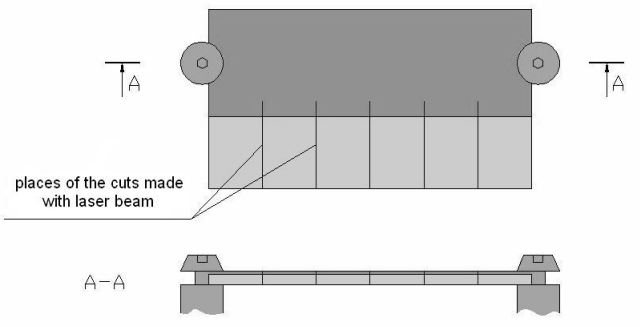

Fig. 2. The way in which the specimen are cut.

Then the specimen were cut and milled in the way shown in Fig. 3, in order to expose the shape of the cutting front.

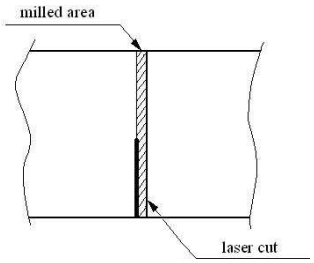

Fig. 3. Preparation of the specimen for measuring

In this way, 19 specimen are processed with the variable rate of the laser beam feed. Constant parameters were the following:

— power 2500 W
— pulse frequency 10000 Hz
— process gas – nitrogen, pressure 12 atm
— distance between the cutting head and the surface 1 mm
— focal position h = –3 mm, (at the bottom surface of the metal sheet cut)

3. Results analysis.

The position of consecutive points on the cutting front shape for each specimen were measured every 0.2 mm with the use of optical microscope. The shapes of all profiles are shown in Fig. 4.

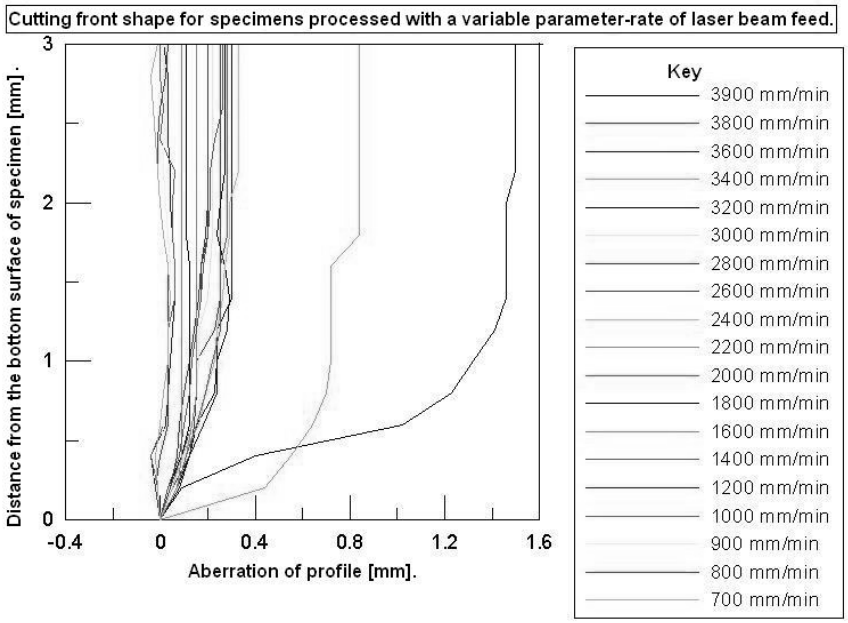

Fig. 4. Cutting front shape for all 19 specimens processed with a variable rate of the laser beam feed.

For the sake of clarity, every third point measured has been plotted and the scale of the x-axis has been enlarged.

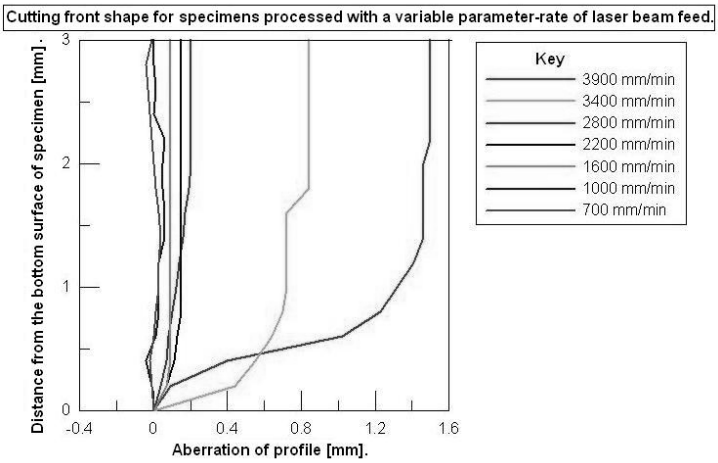

Fig. 5. Cutting front shape of the specimens processed with a variable rate of the laser beam feed (every third result showed).

4. Conclusion.

The rate of the laser beam feed has significant influence on the cutting front shape of stainless steel and therefore influences the whole process of laser cutting.

As can be easily seen the higher value of the rate of the laser beam feed, the inclination of the cutting front shape is larger. When the value of this parameter attains 3900 mm/min, the inclination is about 1.6 mm.

The cutting front shape influences the appearance and coarseness of the surface of the cut.

Too high value the rate of the laser beam feed can cause chipping of the material as well as uncutting the desired gauge of the material.

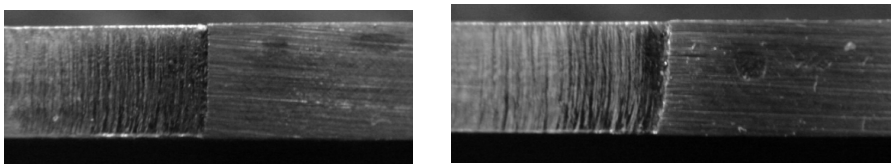

Fig. 6. The cut front shapes for the rate of laser beam feed of 3000 mm/min (left) and 3800 mm/min (right)

References

[1] Garbala, M. *The influence of the parameters of processing on the cutting front shape for stainless steel* [in Polish], master thesis (prof. W. Zowczak), Kielce University of Technology, Kielce 2006.

[2] Klimpel A.: *Welding and cutting of metals* [in Polish], WNT, Warszawa 1999.

[3] Przybyłowicz K.: *Metallography* [in Polish], WNT, Warszawa 2003.

Transcom 2009, 22-24 June 2009
University of Žilina, Žilina, Slovak Republic

Application Quantitative Assessment by Study Cu-Rich Intermetallic Phases in Recycled Alsi9cu3 Cast Alloy

[*]Lenka Hurtalová, [*]Eva Tillová
[*]University of Žilina, Faculty of Mechanical Engineering, Department of Material Engineering, Univerzitná 1, 010 26 Žilina, Slovakia, E-mail: lenka.hurtalova{eva.tillova}@fstroj.uniza.sk

Abstract. The contribution is deal with influence of solution treatment by 505°C, 515°C and 525°C with different holding times 2, 4, 8, 16 and 32 hours on changes in morphology Cu-rich intermetallic phases (Al-Al2Cu-Si) in recycled AlSi9Cu3 cast alloy used especially in automotive and aerospace industry. Cu-rich phases were observed by optical and electron (SEM) microscopy. Quantitative study of changes in morphology cooper intermetallic phases was carried with used Image Analyzer software NIS - Elements. During solution heat treatment was observed the spheroidization, gradual disintegration and melting of this intermetallic phases on base Al-Al2Cu-Si. Temperature 525°C made secretion cooper phases in form homogeneous particles at the edge those was make annealing cavities, because this temperature is declare as temperature dissolving of Al-Al2Cu-Si intermetallic phase.

Keywords: AlSi9Cu3 cast alloys, solution treatment, quantitative assessment, Al_2Cu phase.

1. Introduction

Al-alloys represent an important category of materials used especially in aerospace and automotive industries in heat treated state. The alloys of the Al-Si-Cu system have become increasingly important in recent years, mainly in the automotive industry that uses recycled aluminium in the form of various motor mounts, pistons, cylinder heads, heat exchangers and so on [1].

Al-Si-Cu systems usually contain a certain amount of Fe, Mn, Mg and Zn that are present either undeliberately, or they are added deliberately to provide special material properties. These elements partly go into solid solution in the matrix and partly form intermetallic particles during solidification:

Fe-rich intermetallic phases. The dominant phase is plate-shaped Al_5FeSi (know as beta- or β-needles phase). Al_5FeSi needles are more unwanted, because adversely affect mechanical properties, especially ductility. The deleterious effect of Al_5FeSi can be reduced by increasing the cooling rate, superheating the molten metal, or by the addition of a suitable "neutralizer" like Mn, Co, Cr, Ni, V, Mo and Be. The most common addition has been Mn. Excess Mn may reduce Al_5FeSi phase and promote formation Fe-rich phases $Al_{15}(FeMn)_3Si_2$ (know as alpha- or α-phase) in form „skeleton like" or in form „Chinese script" [2, 3]. If Mg is also present with Si, an alternative called pi-or π-phase can form, $Al_5Si_6Mg_8Fe_2$. $Al_5Si_6Mg_8Fe_2$ has script-like morphology.

Cu-rich intermetallic phases. In Al-Si-Cu alloys was detected variously types cooper phases: Al_2Cu, Al-Al_2Cu-Si and $Al_5Mg_8Cu_2Si_6$ [1, 2]. In unmodified alloys copper is present primarily as Al_2Cu or Al-Al_2Cu-Si phase, in modified alloys as $Al_5Mg_8Cu_2Si_6$. The average size of the copper phase decreases upon Sr modification. The Al_2Cu phase is often observed to precipitate both in a small blocky shape with microhardness 185 HV 0.01. Al-Al_2Cu-Si phase

is observed in very fine multi-phase eutectic-like deposits (Fig. 1) with microhardness 280 HV 0.01 [4].

Influence of intermetallic phases to mechanical and fatigue properties depends on size, volume and morphology this phases [2].

2. Experimental

As an experimental material was used secondary AlSi9Cu3 alloy [6 - 8]. The melt was not modified or refined. Experimental cast samples were given a heat treatment - solution treatment for 2, 4, 8, 16 or 32 hours at three temperatures (505, 515 and 525°C); water quenching at 40°C and natural aging for 24 hours at room temperature. After heat treatment were samples subjected for mechanical test (strength tensile, ductility, hardness).

The alloy and its heat treatment presented in this work is part of a larger project and the microstructural (Si morphology, DAS, Fe-rich phases) and mechanical property details of which have already been published [6 - 8]. Present work is focused on study of the effect of solution heat treatment to the Cu-rich intermetallic phases.

Metallographic samples were prepared from selected tensile specimens (after testing) and the microstructures were examined by optical and electron (SEM) microscopy. Samples were prepared by standards metallographic procedures (wet ground, DP polished with diamond pastes and etched by Dix-Keller, HNO_3 or H_2SO_4). To determine the chemical composition of the intermetallic phases was employed scanning electron microscopy with EDX. The formation of these phases should correspond to successive reaction during solidification [2, 3].Structure hypoeutectic AlSi9Cu3 cast alloy consists of dendrites α-phase (light grey), eutectic (dark grey) and intermetallic Fe- and Cu-rich phases [1, 4, 5 and 8]. The cooper-rich phases form towards the end of solidification [1] and consequently may be nucleated on other interdendritic particles (Si, Fe-rich phases) Fig. 1a or Fig. 2.

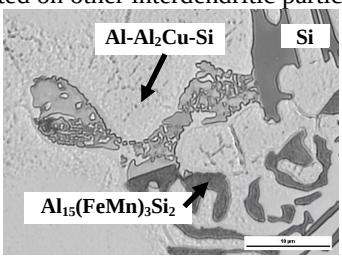

Fig. 1. Cu-rich (Al-Al_2Cu-Si) intermetallic phase etch. Dix-Keller

The effect of heat treatment on morphology of Cu-rich phases was followed by optical and electron microscopy. Morphology of Al-Al_2Cu-Si is demonstrated in Fig. 2.

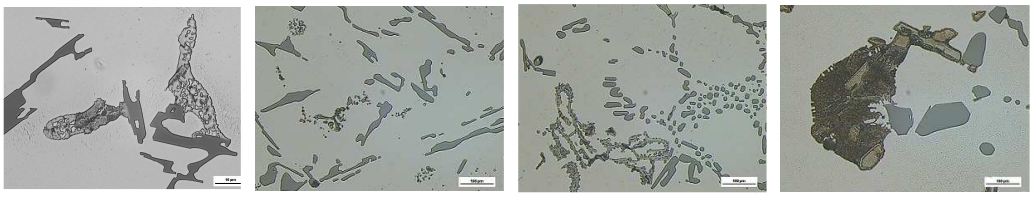

a) untreated state b) 505°C, 4 hours b) 515°C, 4 hours b) 525°C, 4 hours

Fig. 2. Influence of heat treatment on morphology of Cu-rich phases (Al-Al_2Cu-Si), etch. HNO_3

The changes of morphology of Al-Al_2Cu-Si observed after heat treatment are documented for holding time 4 hours. Al-Al_2Cu-Si phase without heat treatment (untreated state) occurs in form compact oval troops (Fig. 2a). After solution treatment by temperature 515°C these phase disintegrated into smaller segments. The amount of Al-Al_2Cu-Si phase decreases. This phase is gradually dissolved into the surrounding Al-matrix with an increase in solution treatment time (Fig. 2b). By solution treatment by 515°C is this phase observed in the form coarsened globular particles and these occurs along the black needles, probably

Fe-rich Al_5FeSi phase (Fig. 2c) [6]. By solution treatment 525°C is this phase documented in the form molten particles with homogenous shape (Fig. 2d) [7].

Quantitative metallography [9] was carried out on an Image Analyzer NIS - Elements to quantify the Cu-rich intermetallic phases (surface fraction and average Cu-phases particle area by magnification 250 and 500 x).

Fig. 3 shows the amount of Al-Al_2Cu-Si phase obtained in solution heat treated samples, calculated as a percentage of the average value. Fig. 4 shows the average Al-Al_2Cu-Si phase particle area obtained in solution heat treated samples. It is evident that heating at temperatures below the final solidification temperature (505°C, 515°C and 525°C) results in a dissolution of Al-Al_2Cu-Si phase. Dissolution is accelerated as soon as the holding time is increased to 4 hours, where the dissolution exhibits a relatively linear behaviour with holding time. Further heating does not bring about much change in the amount or surface of Al-Al_2Cu-Si phase. Maximum average Al-Al_2Cu-Si phase particle area was observed by temperature solution treatment 525 °C with holding times 2 hours (9 995.5 μm^2). Minimum average Al-Al_2Cu-Si phase particle area was observed by temperature solution treatment 515°C (0.277 μm^2).

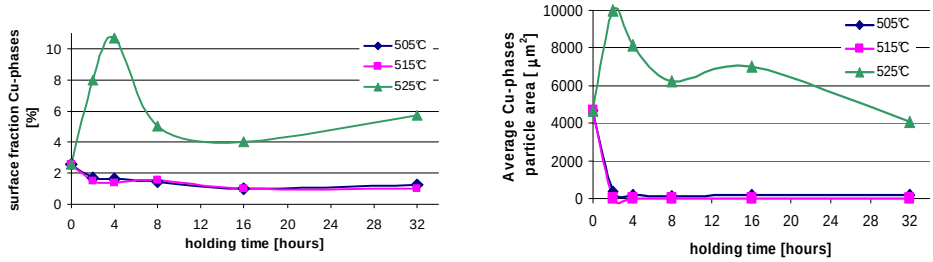

Fig. 3. Percentage changes and surface changes of Cu-rich phases during the heat treatment

Solution treatment at 525°C apparently causes a marked change. This, however, is attributed to the melting of the Al-Al_2Cu-Si, rather than to its dissolution.

Dissolution and melting of Al_2Cu phase in AlSi9Cu3 alloy has been studied in detail by Samuel [10]. During solution heat treatment, incipient melting of a binary alloy can occur when the alloy composition exceeds the critical composition and the alloy is annealed at a temperature higher than the eutectic temperature. In alloys with segregation of the alloying elements, the composition may locally exceed the critical composition, even thought the mean composition is lower, and incipient melting occurs in this case [10]. When the AlSi9Cu3 alloy is solution treated at temperature about the melting point of the eutectic (Al + Al_2Cu) phase, e.g. 525-540°C, the Al-Al_2Cu-Si particles may undergo incipient melting even after periods as 4 hours as evidenced by the black spots observed within the Al-Al_2Cu-Si particles.

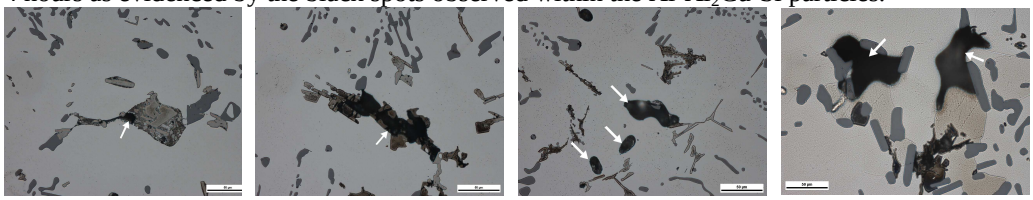

a) after 2 hours b) after 8 hours c) after 16 hours d) after 32 hours

Fig. 4. Melting process of Al-Al_2Cu-Si particles in samples solution heat treated at 525°C, etch. Dix-Keller

Microstructure of test bars solution treated at 525°C is documented in Fig. 4. Melting process of Al-Al_2Cu-Si particles has 4 stages: after 2 hours (Fig. 5a) is observed initiation of melting (arrowed →); after 8 hours showing massive Al_2Cu coexisting with Si and Fe-phase; next showing structureless phase – note the presence of the previously existing Al_2Cu eutectic

at the outer fringes; finally showing the presence of cavities and structureless phase particles. Heat treatment is one of the major factors used to enhance the mechanical properties of heat-treatable Al-Si alloys, through an optimization of both solution and aging heat treatments. The solution treatment homogenises the cast structure and minimizes segregation of alloying elements in the casting. Segregation of solute elements resulting from dendritic solidification may have an adverse effect on mechanical properties.

Fig. 5 shows the influence of heat treatment on the Brinell hardness. Hardness of solution treated test bars are increased by increasing the solution temperature and time. Highest hardness was observed by temperature 515°C for times 2 hours (122 HBS) [6]. At 525°C, test bars show hardness reduction due to melting of the Al-Al_2Cu-Si phase.

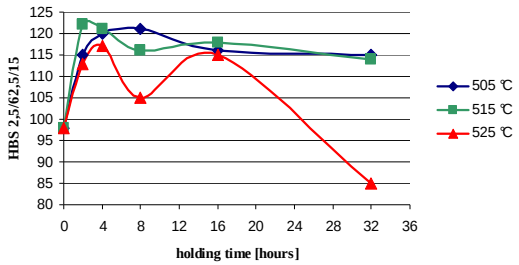

Fig. 5. Influence of heat treatment on hardness of recycled AlSi9Cu3 alloy

3. Conclusion

- Solution heat treatment at 505 and 515°C caused homogenization of as-cast structure. Al-Al_2Cu-Si phases are fragmented, dissolved and redistributed within α-matrix (surface fraction decreases from 10.7 % to 1 % and average Cu-phases particle area decreases from 9 995.5 μm^2 to 0.277 μm^2). Hardness by increasing the solution temperature and holding time increased.
- Solution heat treatment at 525°C can end in melting process of Al-Al_2Cu-Si particles and finally caused showing the presence of cavities and structureless phase particles.
- The control of heat treatment temperature is very critical, because if the melting point is exceeded, there is localized melting at the grain boundaries (cavities) and the mechanical properties are reduced.

Acknowledgement

This work has been supported by Scientific Grant Agency of Ministry of Education of Slovak republic and Slovak Academy of Sciences, No 1/0208/08 and No Kega 3/5196/07.

References

[1] RIOS, C. T. et al.: *Acta microscopia*, Vol. 12, No. 1, (2003), p. 77-82.

[2] TAYLOR, J. A.: *The effect of iron in Al-Si casting alloys*.

[3] SEIFEDDINE, S., JOHANSSON, S., SVENSSON, I.: Materials Science and Engineering, A 490, (2008), pp. 385-390.

[4] TILLOVÁ, E., PANUŠKOVÁ, M.: Materials Engineering, Vol. 14, No. 2, (2007), pp. 73-76.

[5] TILLOVÁ, E., PANUŠKOVÁ, M.: Mettalurgija, METABK 47 (3) 133-137 (2008), pp. 1-4.

[6] PANUŠKOVÁ, M., TILLOVÁ, E., CHALUPOVÁ, M.: Strength of Materials, No.1, 391, (2008), pp. 109-112.

[7] HURTALOVÁ, L., TILLOVÁ, E., PANUŠKOVÁ, M: *Vplyv rozpúšťacieho žíhania na vybrané štruktúrne parametre zliatiny AlSi9Cu3*. In Letná škola únavy materiálov, Vol. 9, (2008), pp. 195-198

[8] TILLOVÁ, E., CHALUPOVÁ, M., PANUŠKOVÁ, M.: Material Engineering, Vol. 13, No. 1, (2006), pp.25-30.

[9] SKOČOVSKÝ, P., VAŠKO, A.: *Quantitative evaluation of structure in cast iron*. EDIS ŽU Žilina, (2007),

[10] SAMUEL, F. H.: Journal of Materials science 33, (1998), pp.2283-2297.

Transcom 2009, 22-24 June 2009
University of Žilina, Žilina, Slovak Republic

Phenomena on Screw Drill at Drilling of Steel Cr17Ni15Mo3Ti

[*]Jozef Jurko, [**]Mário Gajdoš, [***]Anton Panda
[*]Technical university of Košice, Faculty of Manufacturing Technologies, Department of Manufacturing Technologies, Štúrova 31, 080 01 Prešov, Slovakia, jozef.jurko@tuke.sk
[**]ELBA a.s. Kremnica, ČSA 264/58, 967 01 Kremnica, Slovakia, e-mail: mgajdos@elba.sk
[***] Technical university of Košice, Faculty of Manufacturing Technologies, Department of Manufacturing Technologies, Štúrova 31, 080 01 Prešov, Slovakia, anton.panda@tuke.sk

Abstract. Precise and reliable information on the machinability of a material before it enters the machining process is a necessity, and hypotheses must be tested through verification of actual methods. This article presents conclusions of machinability tests on stainless steels Cr17Ni15Mo3Ti and describes appropriate parameters for the cutting zone during the process of drilling. The article focuses on the analysis of selected domains through four basic indicators of steel machinability: dynamic and surface quality, with the goal of proposing recommendations for stainless steels, and to integrate current knowledge in this field with drilling theory and praxis.

Keywords: drilling, cutting zone, plastic deformation, stainless steels, cutting tool, tool wear, surface

1. Introduction

Automated production of, in the sense of, machine production has characteristic features: a reduction of production costs, stimulation of the development of cutting tools, and changes in the construction of machine tools, all of which work against the creation of optimal technological methods, which thrusts the technological process of cutting into a more important position. These trends confirm that the cutting process remains one of the basic manufacturing technologies. A condition of the economic usage of modern, automated programmed turning machines is the optimal course of the cutting process, i.e. the use of optimal work conditions. A summary of optimal work conditions requires knowledge of the laws of cutting theory and knowledge of the practical conditions of their application. This article presents the results of experiments that concerned the verification some parameters of machinability of work pieces of difference types of stainless steel Cr17Ni15Mo3Ti.

2. Evaluation and Experimental Results

This article described with the evaluation of selected domains of machinability. The experiments were performed in laboratory conditions and verified in real conditions during manufacture. The set-up used contained the following components: a VR 6A drilling machine, a screw drill from SC. The materials to be machined were type of stainless steel Cr17Ni15Mo3Ti with chemical composition listed in Tab. 1. The cutting process employed was dry machining (DM), and the cutting frequency was defined at intervals of v_c =30 to 120 m/min, the feed was advanced from intervals of f=0.05 to 0,12 millimetres, and cutting depth a_P=5.0 mm. One of the associated phenomena in the measurement of dynamic characteristics is the testing of thermal effects in the cutting zone, mainly measured on the cutting section of the tool. Heat in the cutting zone influences deformation and friction in the removal of the cut

layer. The magnitude of the heat depends on the cutting time, but after a certain interval it no longer increases in the tool. This effect of heat has an important significance in the study of damage to the tool cutting edge and cutting wedge wear. The creation of heat has a basic influence on the temperatures of the chip, the cutting edge of the tool, and on the machined surface (5-10% into the air, 5-10% into the tool, 10-15% into the work piece, 65-80% chip)

Steel	Chemical composition [%]							
	C	Cr	Ni	Mn	Ti	Mo	P	S
Cr17Ni15Mo3Ti	0,08	17,0	15,0	2,0	0,5	3,0	0,045	0,030

Tab. 1. Chemical composition of steel Cr17Ni15Mo3Ti

The heat produced is associated with the heat field distribution in the chip, on the machined surface, and on the tool cutting edge. The law of constant optimal cutting temperature (as a function of average temperature) was formulated by Makarov as follows: "Optimal cutting speeds (for a given material of the tool cutting edge) in various combinations of cutting process conditions correspond to a constant temperature in the cutting zone-the so-called optimal cutting temperature. Through experimental tests of temperature effects during cutting we find that temperature measurement is a problematic field, because the continuous dissipation of the temperature field (on the tool, chip, and work piece) does not fall gradually, that is, on a gradient, but the temperature field is variable according to the motion of the cutting wedge and the chip (as it corresponds to the work piece) and cutting time. A method of temperature measurement was used involving a thermal camera that depicted the temperature field in the form of an figure. The final markings document a temperature range from 300 to 900° C. Tab. 2 shows the measured and calculated values for Cr17Ni15Mo3Ti steel. Fig. 1 shows the dependency of average cutting wedge temperature (measured by thermocouple) during drilling of steel Cr17Ni15Mo3Ti in defined cutting conditions.

Feed f [mm]	Steel Cr17Ni15Mo3Ti
0,05	$\Theta_m = 4{,}8933.v_c^{0,7956}$
0,08	$\Theta_m = 8{,}6542.v_c^{0,7568}$
0,1	$\Theta_m = 11{,}9854.v_c^{0,7165}$
0,12	$\Theta_m = 11{,}5562.v_c^{0,7589}$

Tab. 2. Average cutting wedge temperature, screw drill HSCo, d=10 mm

The generation of heat during the cutting process causes a change in temperature. The temperature field is defined in spite of the lack of temperature gradient, as described in Wei Yen, Wright. Temperature gradient means a change in temperature along one precise dimension in the direction of the greatest change (fall) of temperature. An understanding of the significance and interpretation of the temperature gradient is indispensable to describe momentary temperature and temperature fields in cutting geometrically-defined cutting edge, as described by the Fourier-Kirchhoff Equations. The average temperature grows under the influence of cutting speed only in the zone of secondary plastic deformation (the interaction of the chip with the face plate of the tool cutting edge)-on the chip and the machined surface the change in average temperature is less marked.

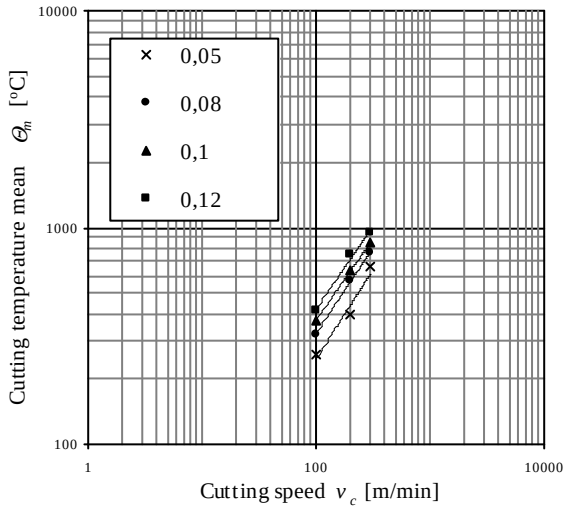

Fig. 1. Average temperature Θ_m for the defined cutting conditions for steel Cr17Ni15Mo3Ti

The variant values (none greater than 100° C) can be explained mainly by the chemical composition of each steel (the creation of complex carbides at fibre boundaries) that results in a worsening of steel thermal conductivity, by Oxley-1963. From the standpoint of temperature effects in the cutting process, the cutting zone comprises a thermodynamic system whose state changes through heat transfer as a form of energy transfer. Thermal conductivity A[W/K]=[kg.m^2.s^{-3}.K^{-1}] expresses the capacity to diffuse heat in a specific environment. The specific thermal conductivity λ[W.m^{-1}.K^{-1}]=[kg.m^2.s^{-3}.K^{-1}] as a material quality (or constant) expresses the capacity to diffuse heat through convection. It is especially characteristic for stainless steels that they have rather low values of specific thermal conductivity. For example, for C45 steel, λ=60[W.m^{-1}.K^{-1}] and for austenitic stainless steels λ=18.7 to 22.8 [W.m^{-1}.K^{-1}], so its conductivity is three times worse in comparison with the reference material (C45 steel), which is often used in actual work. The variable temperature field appears mainly in the formation of individual chips, whose deformation is not homogenously concentric in the individual pieces connected to the later of intensively deformed material, e.g. steel Cr17Ni15Mo3Ti. The individual pieces of chips are formed in cycles of gradual deformation. Temperature at chip-face plate contact underlies the cyclical changes. The subsequent area of interaction between the chip and the face plate of the tool cutting edge is dependent on the cutting process conditions and on the geometry of the instrument cutting edge. The diffusion of the temperature field in the zone of secondary plastic deformation at the spot of maximum temperature corresponds to the localized spot of wear on the cutting tool face plate. Temperature maxima at the area of interaction between the chip and the cutting tool face plate, and the time of cutting wedge “cooling” both depend on cutting speed. At lower values of cutting speed, there is a longer time of “cooling,” and as cutting speed grows, the area of “localized spot heating” intensifies, but the “cooling” time only shortens. The diffusion of the temperature field in the zone of secondary plastic deformation at the spot of maximum temperature corresponds to the localized spot of wear on the cutting tool face plate. Temperature maxima at the area of interaction between the chip and the cutting tool face plate, and the time of cutting wedge “cooling” both depend on cutting speed. At lower values of cutting speed, there is a longer time of “cooling,” and as cutting speed grows, the area of “localized spot heating” intensifies, but the “cooling” time only shortens.

3. Conclusion

The variable temperature field appears mainly in the formation of individual chips, whose deformation is not homogenously concentric in the individual pieces connected to the later of intensively deformed material, e.g. steel Cr17Ni15Mo3Ti. The individual pieces of chips are formed in cycles of gradual deformation. Temperature at chip-face plate contact underlies the cyclical changes. The subsequent area of interaction between the chip and the face plate of the tool cutting edge is dependent on the cutting process conditions and on the geometry of the instrument cutting edge. The diffusion of the temperature field in the zone of secondary plastic deformation at the spot of maximum temperature corresponds to the localized spot of wear on the cutting tool face plate. Temperature maxima at the area of interaction between the chip and the cutting tool face plate, and the time of cutting wedge "cooling" both depend on cutting speed. At lower values of cutting speed, there is a longer time of "cooling," and as cutting speed grows, the area of "localized spot heating" intensifies, but the "cooling" time only shortens. The diffusion of the temperature field in the zone of secondary plastic deformation at the spot of maximum temperature corresponds to the localized spot of wear on the cutting tool face plate.

Acknowledgement

The authors would like to thank in words the VEGA grant agency at the Ministry of Education SR for supporting research work and co-financing the projects: Grant work VEGA #01/0406/2003 with the title: "Research concerning the machinability of stainless steels in automated production" and Grant work #01/3173/2006 with the title "Experimental investigation of cutting zones in drilled and milled stainless steels."

References

[1] JURKO, Jozef: *Monitoring and Diagnosis of Drill Wear and the Thermodynamic Phenomenas of Material Removal by drilling of Stainless Steels.* Book: Experimental Analysis of Nano and Engineering Materials and Structures. Springer Netherlands, 10.1007/978-1-4020-6239-1_37, 2007, p.77-78, ISBN 978-1-4020-6239-1

[2] LUKOVICS, I.: *Research of High Speed Cutting. In.: COM MAT TECH 2004, 12-th International Scientific Conference,* 14.-15.10.2004 Trnava, SK, STU Bratislava, SK, p. 124, ISBN 80-227-2121-2, p.809-814, ISBN 80-227-2117-4.

[3] MAKAROV,A.D.: *Optimizacija processov rezania metallow*. Mašinostrojenie, Moskva, 1976

[4] MÁDL,J.-TESNER,L.: *Tool Wear Monitoring in Machining. Zborník z medzinárodného kongresu MATAR*, Praha : ČVUT Praha, 1996, s.169

[5] MRKVICA, I.-MORAVEC, V.: *Úpravy břitů a povrchů řezných nástrojů. MM Průmyslové spektrum,* 6/2007, s.58-59. ISSN 1212-2572.

[6] NESLUŠAN, M.-CZÁN, A.: *Obrábanie titánových a niklových zliatin,*EDIS Žilina 2001, ISBN 80-7100-933-4

[7] OXLEY, P.L.B.: *Mechanics of Metal Cutting.* International conference in production engineering, Pittsburg, 1963, pp.50

[8] PALČEK, P.-CHALUPOVÁ, M.: *Fraktografia a mikro-fraktografia konštrukčných materiálov*. Materiálové inžinierstvo, ročník 9, č.3/2002, s. 57-66, ISSN 1335-0803

[9] PILC, J.-STANČEKOVÁ, D.-MIČIETOVÁ, A.-SALAJ, J.:*Jednoúčelové stroje a výrobné linky*, 2001, Žilina EDIS: p.142

[10] WEI YEN,D.-WRIGHT,P.K.: *A Remote Temperature Sensing Technique for Estimating the Cutting Interface Temperature.* Journal of eng. For industry trans. Of the ASME, 113, 1986, pp.251-264

[11] ZABOROWSKI, T.: *Ekowytwarzanie*. Gorzow Wlkp. : IBEN Gorzow Wlkp., ETE Gorzow Wlkp., 2007, p.100, ISBN 978-83-925108-0-2

Transcom 2009, 22-24 June 2009
University of Žilina, Žilina, Slovak Republic

Dimension Change of Gating System and its Influence on Oxide Films Formation by Aluminium Alloys Pouring

Radoslav Kantorík, Dana Bolibruchová, Richard Pastirčák
*University of Žilina, Faculty of Mechanical Engineering, Department of Technological Engineering, Univerzitna 1, 01026 Žilina, Slovakia, {radoslav.kantorik, danka.bolibruchova, richard.pastircak}@fstroj.uniza.sk

Abstract. This article deals with simulation and design of gating system for a simple casting of plate. For this casting was designed constant-pressure, overpressure and underpressure gating system with overpressure sprue. Simulation calculation was realized in software ProCast. Free surface of melt was observed with help of simulation which was exposed to effect of atmosphere in casting mould.

Keywords: Simulation, aluminium alloys, reoxidation

1. Introduction

Oxide films, how is well-known, induce violation of continuity in metal matrix, they decrease mechanical properties of casting and lower fluidity. Oxide films form in 0,01 s and after 1 s have 1 μm and after 10 s are thick 10 μm. Therefore it is necessary to shorten connection time of melt with atmosphere or provide, those parts of melt, which were in the longest connection with atmosphere, were not in casting. Simulation software ProCast offers possibility to observe free surface of melt, which is subject to an atmosphere in cavity of casting mould and so ProCast is a complex software for observing the flow in casting mould. Function "junction" observes free surface of melt, which is in connection with atmosphere in cavity of mould. With the help of this function it is possible to anticipate places where oxide films can probably exist. Simulation helps to optimalize gating system in terms of reoxidation.

2. The design of casting

Casting which serves to observing of melt free surface is in Fig. 1. Casting has a simple shape of plate, therefore was chosen for experimental casting. It is possible to anticipate which places of metal flow are the longest subject in connection with atmosphere on a simple shape.

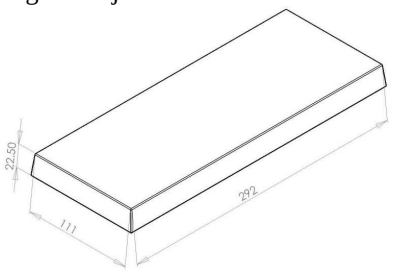

Fig. 1. Casting of a plate.

3. The Computation of Gating System

The gating system was calculated by two methods, calculation by Sobolev and calculation according to velocity of melt rising in cavity of mould.

First way assigned the time of filling on 10 s and second way on 2 s. With the help of these two calculating methods were assigned operative sections of gating systems. For each calculation was designed three gating systems and that is constant-pressure, overpressure and underpressure system with overpressure sprue. Section ratio of individual parts of gating system is in Tab. 1.

Gating system	Section ratio Sk : St : ∑Sz
Constant-pressure	1 : 1 : 1
Overpressure	1,4 : 1,2 : 1
Underpressure	1 : 2 : 4

Tab. 1. Section ratio of individual parts of gating system

4. Simulation

The simulation was calculated by the software ProCast. One function of this software is "junction". This function enables observing of melt free surface which is in connection with atmosphere in casting mould cavity. This function can be used to assign places, where is most probable appearance of oxide films which are formed by pouring of casting mould. Unit of this function is cm^2.s. However this entry does not show number of formed oxide films, but it shows places in melt which were longest in connection with atmosphere in casting mould. Higher entry of function "junction" means longer time for connection with atmosphere in mould and shows places where are most probably formed oxide films.

The merits of function "junction" are at the filling time 10 s, between 9 and 67 cm^2.s and at the filling time 2 s are between 1 and 2 cm^2.s. From this is possible to conclude that longer filling time causes higher index of function "junction" and so higher probability of oxide films presence.

Calculation by Sobolev found out that the filling time was 10 s, following this merit was set operative section of gating system which was 50,1 mm^2. Sections of individual parts of gating system were computed with the help of section ratio from Tab. 1.

In Fig. 2 is showed constant-pressure gating system. With the help of function "junction" we can see places which were longest in connection with atmosphere, where index reached 67 cm^2.s, which is caused by long filling time. This merit is high in comparison with castings pouring during 2 s. The slow filling of mould cavity occured what caused the raise of this merit. During the filling of mould cavity big part of melt was in connection with atmosphere in casting mould.

For casting was designed overpressure gating system too, which is in Fig. 3. By overpressure gating system decreased index of function "junction" to 9 cm^2.s, what could cause higher velocity of metal flow. Problem of higher flow rate is in turbulence creation. Turbulence causes entrainment of oxide films in mould cavity.

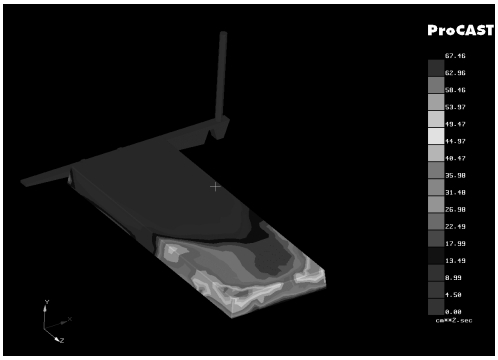

Fig. 2. Constant-pressure gating system.

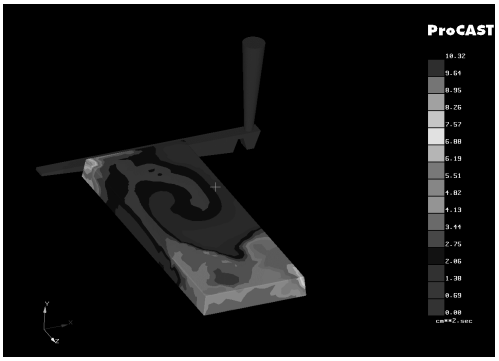

Fig. 3. Overpressure gating system.

Casting of plate pouring by underpressure gating system with overpressure sprue is in Fig. 4. Index of function "junction" reached merit 38 cm^2.s, but only in overrun of slag trap runner. The mostly spoiled is the front of metal flow and this front is the longest in connection with atmosphere in mould cavity. First part of metal flow which entered in slag trap runner stands in overrun of a channel and did not reach mould cavity. In casting was entry 15 cm^2.s. Plate was filled slowly and still, but the front of metal flow which entered through the ingates to mould cavity was in longer connection with atmosphere. Part of casting near the ingates was filled as last and in this place was reached the highest entry of function "junction".

According to velocity of melt raising in mould cavity was computed filling time in 2 s and with the help of this time was calculated operative section 227,2 mm^2. Dimensions of individual parts of gating system were computed by following ratio from Tab. 1. For this filling time were created three gating systems as in the previous case.

By constant-pressure gating system was found out index of function "junction" 0,99 cm^2.s (Fig. 5.). The front of metal flow was shorter time in connection with atmosphere in mould cavity than in previous cases. The possibility of oxide films forming decreased, but the risk of turbulence creation raised. Turbulence causes entrainment of originated oxide films. These films can be transported with metal flow in mould cavity.

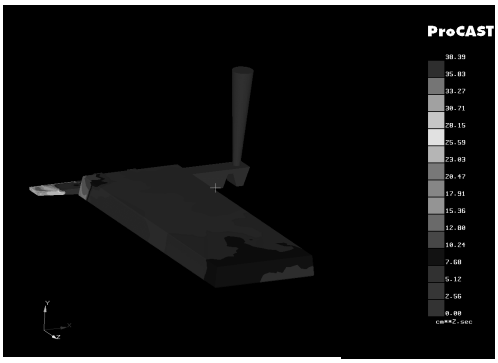

Fig. 4. Underpressure gating system with overpressure sprue..

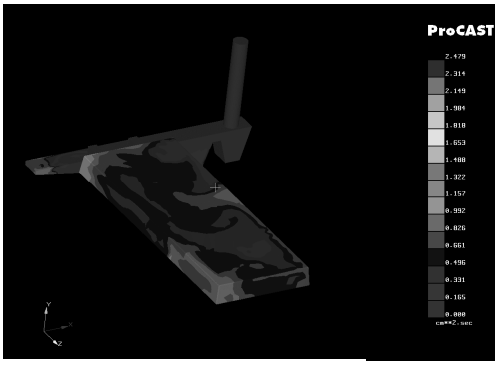

Fig. 5. Constant-pressure gating system.

Simulation of plate pouring through overpressure gating system is in Fig. 6. With the help of this simulation was found out merit of function "junction" 1 cm^2.s. By overpressure gating system raises the velocity of metal flow by passage to other parts of gating system and

so the danger of turbulence creation raises. The turbulence can cause that oxide films can be found in places where is the entry zero.

Last simulation was simulation of pouring through underpressure gating system with overpressure sprue where was found index of function "junction" 1,8 cm^2.s (Fig. 7). Cavity filling was performed in slower velocities of flow. In the figure it is possible to see that entry of function "junction" was the highest at the front of the flow, which was longest in connection with atmosphere in mould cavity because the pouring was slow.

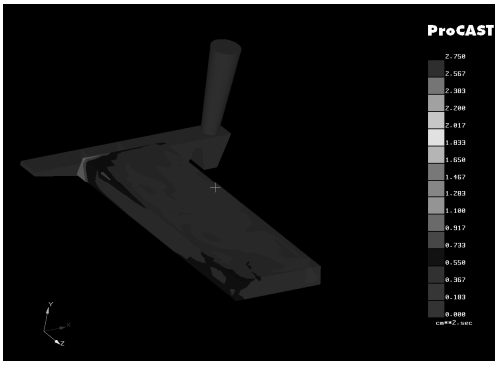

Fig. 6. Overpressure gating system.

Fig. 4. Underpressure gating system with overpressure sprue..

5. Conclusion

With the help of simulation it was found out that for this casting is better constant-pressure or overpressure gating system. By using the overpressure gating system there is a real risk of turbulence creation in places where the metal flow is quickest and it is in ingates. Turbulence can cause transport of oxide films to places which have merit of function "junction" zero. By slow filling of casting mould is metal flow in the longest connection with atmosphere in mould cavity and it causes forming of oxide films. By the constant-pressure gating system occurs air entrainment in sprue and oxide films are formed which are transported to mould cavity.

Acknowledgement

This research was partially supported by the grant No. KEGA 3/5197/07, KEGA 1/0684/08 and VEGA 1/4098/07. The authors gratefully acknowledge this support.

References

[1] BECHNÝ, L. – GEDEONOVÁ, Z. – MÄSIAR, H.: *Teória zlievania*., 1. vyd. ALFA Bratislava, 1990, s. 320. ISBN 80-05-00489-3.

[2] MURGAŠ, M. – POKUSA, A. – POKUSOVÁ, M. – PODHORSKÝ, Š.: *Teória zlievarenstva*., 1. vyd. Vydavateľstvo STU Bratislava, s. 291. ISBN 80-227-1684-7.

[3] GEDEONOVÁ, Z.: *Teória zlievarenských pochodov*., 2. vyd. ALFA Bratislava, 1990, s. 360. ISBN 80-05-00491-5.

Transcom 2009, 22-24 June 2009
University of Žilina, Žilina, Slovak Republic

Internal Damping of AZ31 Alloy in Dependence on Temperature

[*]Martin Kasenčák, [*]Rastislav Mintách , [*]Peter Palček
[*] University of Žilina, Faculty of Mechanical Engineering, Department of Materials Engineering, Univerzitna 2, 01026 Žilina, Slovakia,{martin.kasencak, rastislav.mintach, peter.palcek}@fstroj.uniza.sk

Abstract. Experimentally determinated damping curves of magnesium alloy AZ31 are presented in this paper in a dependence on temperature. The damping measurements were performed in range from 35 to 250 ^{o}C. The damping curves for initial state of alloy (i.e. without heat treatment stage) are compared with the damping curves for annealed alloy. The damping maximums were measured in both cases. They cold by explained by relaxation processes appeared in material. The damping values of annealed alloy AZ31 were three times higher then those for initial state of alloy.

Keywords: AZ31 magnesium alloy, high frequency damping, damping peak, dislocation damping

1. Introduction

The damping capacity is a critically important material property from the viewpoint of vibration suppression, noise control and instrument stability enhancement in automotive industry, architectural industry and aerospace [1]. So it is important to seek for highdamping capacity materials to eliminate the damage and noise caused by mechanical vibration. From among the commercial metallic materials that exhibit a high damping capacity belong magnesium alloys [2].

Magnesium alloys have attracted significant interest due to their low density, high specific strength and stiffness, good damping capacity, excellent machinability and good castability, etc., which make them potentially suitable candidates for replacing heavier materials in some automobile parts, portable personal computers and cellular phones [2, 3]. The demand for magnesium alloys in such applications has increased rapidly in recent years.

However magnesium alloys also generally exhibit low ductility near room temperature due to the limited slip systems of hexagonal crystal structure and poor elevated temperature properties, especially creep or oxidation resistance above 150 °C. In the case of Mg–Al system alloys such as AZ91 and AZ31 there is a discontinuous grain boundary precipitation of $Mg_{17}Al_{12}$ phase and the coarsening of $Mg_{17}Al_{12}$ phase in the interdendritic eutectic region. The stability of microstructure and mechanical properties at elevated temperature is based on the presence of stable precipitates [3, 4].

Current knowledge about internal damping behavior of Mg alloys is predominantly related to investigation in the region of low frequency loading (from 0.5 to 300 Hz) [5]. Results of high frequency damping are practically missing in open literature.

The aim of this paper is to present results of a study of internal damping measurement of Mg alloy AZ31 in dependence of temperature at load frequency 20 kHz.

2. Material and experiments

AZ31 magnesium alloy was used for experimental measurement of internal damping. The chemical composition of the material is shown in the Tab. 1. The magnesium alloy AZ31 was produced by the squeeze-casting method. The experimental material was delivered without the heat treatment.

Alloy	Al	Zn	Fe max	Mn	Cu	Mg
AS41	2.5-3.5	0.6-1.4	0.005	0.2	0.05	base

Tab. 1: Chemical composition of the magnesium alloy AZ31 (wt. %)

The microstructure of the original material is shown in Fig. 1a. The structure is dendritic and coarse-grained. In interdendritic regions there are occurred inhomogeneities and phase colonies of different types. The most important is the intermetalic phase $Mg_{17}(Al, Zn)_{12}$. Thereafter, homogenization annealing at temperature T = 415 °C, holding time at this temperature for 3 hours and consequential slowly cooling in the furnace was performed in order to removing the original dendritic structure.

The microstructure of the magnesium alloy AZ 31 after heat treatment is shown in Fig. 1b. Microstructure consists of polyhedral grains of the solid solution of aluminum and zinc in magnesium and other added elements. Metallographic analyze detected precipitated phases on grain boundaries or within the grains. It was observed that the $Mg_{17}(Al, Zn)_{12}$ phase was preferentially segregated on the grain boundaries what strengthen the boundaries.

The method of resonant system quality determination was used for the internal damping measurement at high frequency loading. For this method it is necessary to use the specimen, which frequency is similar to the frequency of the resonant system, consisted from piezoceramic transducer, adapter and specimen. The frequency of the resonant system was 20 360 Hz. Sequentially the characteristic of the resonant system at different levels of entered exciting voltage U_a was measured, namely frequency and response of voltage U_{pu} at constant entered exciting voltage U_a, [6]. The size of the entered exciting voltage U_a was chosen as 0.07 V.

The internal dumping of the material can be determined by reciprocal value of the resonant system coefficient Q^{-1} and it is possible to express it by formula:

$$Q^{-1} = \left(\frac{\Delta f_{r3dB}}{f_r} \right)_{12} . \qquad (1)$$

where Δf_{r3dB} is threedecibel varince of resonant peak. This method is specified in [6].

The internal damping was measured in dependence of the temperature in temperature interval from 35 to 250°C. The internal dumping was measured on cylindrical specimens with gauge length 60 mm and specific diameter 3 mm. The heating of the specimens was performed in the furnace with regular speed of heating 0-9°C/min. Temperature of the experiments was measured by thermocouple, type K (Ni-Cr a Ni-Al).

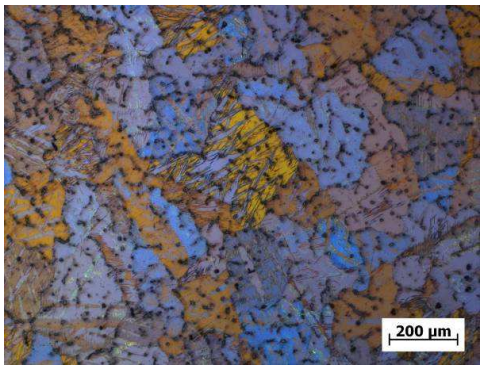

a) original material

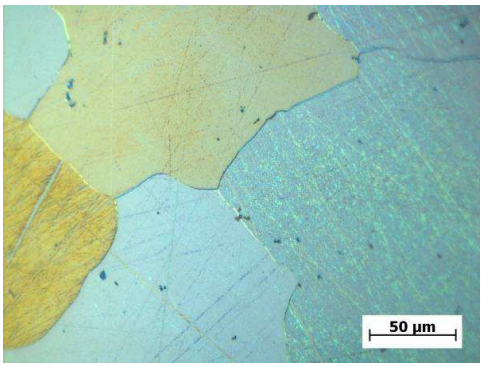

b) after heat treatment

Fig. 1 Microstructure of AZ 31, etched by picric acid, polarized light

3. Experimental results and discussion

Experimental results of damping tests for Mg alloy AZ 31 obtained at the continuously heating of the specimen are presented in Fig. 2 and 3. The results are expressed in the form of the dependence of the damping on temperature for alloy without heat treatment (Fig. 3) and after heat treatment (Fig. 4). In Fig. 3 two damping curves marked as the 1th and the 2th measurement are compared. The measurements were performed only in one test bar. It can be seen that the damping does not considerably depend on the temperature up to 200 °C for both measurements. However significant damping maximum was detected at 150 °C with other considerable smaller damping peaks in this temperature interval. Concretely the damping value at the temperature 150 °C was 1.75×10^{-4} for the 1th measurement and 1.8×10^{-4} for the 2th measurement. As can be seen from both damping curves the damping further increases from 200 °C with increasing of the temperature. It can be further seen from Fig. 3 that the 2th measurement has damping phone (i.e. zone without phase transformation) moved to higher value than for the 1th measurement. Higher damping value for 2th measurement can be probably explained by partial annealing of test bar during 1th damping measurement performed to 250 °C.

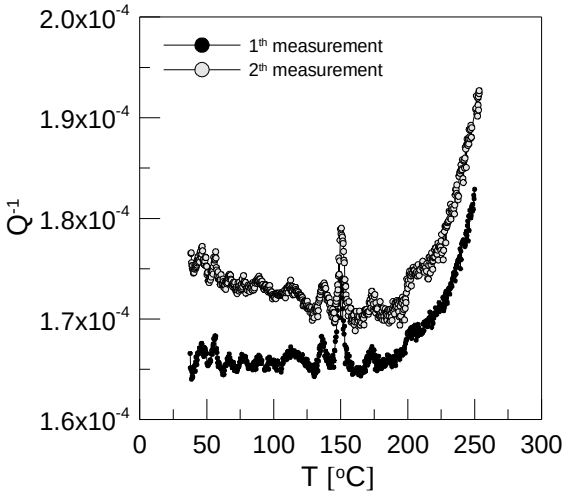

Fig. 2 Damping curves for non-heat treated AZ31 alloy.

The damping curves for annealed alloy are shown in Fig. 4. A couple of damping measurements after heat treatment was performed in same test bar as in the case of original state of Mg alloy (without heat treatment) and is marked as the 3th and 4th measurement. These results are compared together with damping curves for original state (1th and 2th measurement). It can be seen that the heat treatment considerably influenced the character of damping curves, namely by occurrence of two damping maximums at the temperatures 173 °C and 230 °C. The damping value was 2.8×10^{-4} for the 3th measurement, and 3.1×10^{-4} for the 4th measurement at 173 °C and

approximately $4.5x10^{-4}$ for both measurements at 230 °C. From Fig. 4 can be seen that maximum damping values measured for heat treated alloy are almost three times higher than that for non-heat treated alloy. That is why the maximum peaks for original state of alloy nearly disappeared.

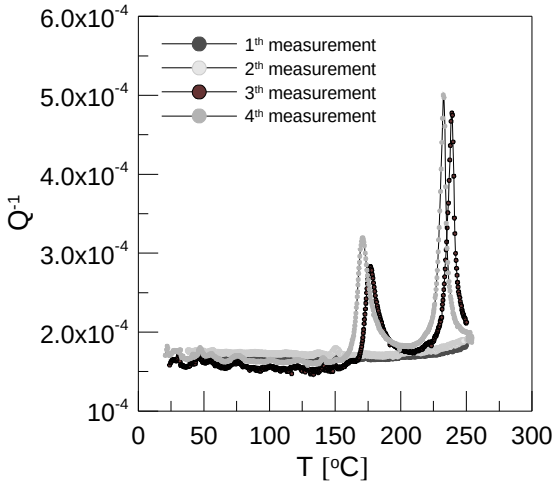

Fig. 3 Damping curves for heat treated AZ31 alloy.

Measured damping maximums can be explained by relaxation processes took place in material for both original and heat treated state of AZ31 alloy. The relaxation processes can be connected with dislocation motion and their interaction with vacancies, impurities, secondary phases or grain boundaries [7]. For lower temperatures (to 120 °C) the internal damping process is probably a result of dislocation motion in basal planes whereas at higher temperatures grain boundary sliding plays dominant role.

4. Conclusion

Internal damping measurement of AZ31 magnesium alloy provided:

- The dependence of internal damping on temperature was measured for original and heat treated magnesium alloy AZ31 in the temperature range from 35 to 250 °C.
- In both cases the damping maximums were measured that can be explained by relaxation processes taking place in material.
- The damping values for heat treated alloy were three times higher than that for original state.

Acknowledgement

This was supported by Science and Technology Assistance Agency under the contract No. APVV SK-CZ-0085-07. This resource has been supported by Scientific Grand Agency of Ministry of Education of Slovak Republic and Slovak Academy of Science, grant No. 1/3155/06.

References

[1] Bishop J. E., Kinra V. K., Metall. Trans. A 26 (1995) p. 2773.

[2] Ritchie I., Pan Z. L., Sprungann K. W., H. K. Schmidt, R. Dutton, Can. Metall. Q. 26 (1987) p. 239.

[3] Kainer K. U.: Magnesium Alloys and Technology, WILEY-VCH Verlag GmbH & Co. KG aA (2003).

[4] Mabuchi M., Kubota K. and Higashi K., Mater. Trans. JIM. 36 (1995), p. 1249.

[5] Wu S.K., Chang S.H., Chou T.Y., Tong S.: Journal of Alloys and Compounds 465 (2008) p. 210.

[6] Nishiyama K., et.al.: In: Journal of Alloys and Compounds 355 (2003) p. 22.

[7] Hu X. S., et. al: Scripta Materialia 54 (2006) p. 1639.

Transcom 2009, 22-24 June 2009
University of Žilina, Žilina, Slovak Republic

Tribological Properties of Ductile Cast Iron

Elena Kečková, Peter Fabian
University of Žilina, Faculty of Mechanical Engineering,, Univerzitna 1, 01026 Žilina, Slovakia,
elena.keckova@fstroj.uniza.sk, peter.fabian@fstroj.uniza.sk

Abstract. This article deals with tribological properties of cast iron with nodular graphite. It was observed and compared wear of cast irons by identical extreme conditions of loading according to way their heat treatment. Principe of this work was demonstration that materials with identical hardness have not equal wear because they have different structure.

Keywords: Cast iron with nodular graphite, austempered ductile iron, heat treatment, tribological properties

1. Introduction

Lifetime of mechanical components and machines is connected with knowledge of regularity and principles wear of metal material in real conditions. Despite of positive results of science in field of tribology is practical problems solution of reliability and technical lifetime raising only partial. We increase fastidiousness on properties of used materials in machine industry especially in connection with the specific condition of mechanical parts work, which influence can we characterize with degradation processes on wear surfaces with activity of various factors.

2. Heat Treatment of Cast Iron with Nodular Graphite

Cast iron with nodular graphite offers big possibilities of mechanical properties variability because of development in foundry industry direct to using this material. Cast iron with nodular graphite differs from grey cast iron with structure and properties, mainly mechanical. Grey cast iron is most widespread material on castings in term of using, however cast iron with nodular graphite is undepreciated foundry material for complicated and more stress parts, where substitute partly steel castings. After heat treatment cast iron with nodular graphite is possible obtain ausferrit structure, which has comparable mechanical properties like a steel and its production is less difficult on energy and raw material.

Heat treatment of cast iron with nodular graphite is important part of production because it defines final properties of material. Isothermal refinement has dominant standing in heat treatment process of cast iron with nodular graphite, which result is austempered ductile iron (ADI). ADI is given with its properties for condition of highly stress working, it introduces new type of cast iron for production of high strength castings. ADI have extraordinary wear resistance and endurance strenght, what allows decrease part weight. Extraordinary properties of ADI are obtained with exactly controlled progress of heat treatment – isothermal refinement. Results of previous researches show that with this technology of heat treatment we

obtain ausferritical and in some case ausferritical-martensitic structure. Practical experiences with this technology show that is possible to reach asked hardness of parts, but with increased toughness. Highly toughness is assumption for achievement of ADI higher wear resistance.

3. Tribologic Tests

We determine with tribologic tests mainly frictional properties of chosen materials and so size of wear in frictional processes. Contact between active items of tribologic system is by serving of asked technical function sign of system behavior. Is necessary to regard number of bodies, their dimensions and physical, chemical and mechanical properties with regard to big variability of contact situation. Prevailing kind of deformation, scale of stress and velocity of relative motion is important too.

We have to compute by tribologic tests with mechanical effects of abrasive elements on surface layers. This active layer has high intensity enter to corrodent processes. In general we can talk about reactivity of material. The influence of wear environment on degrading process we can evaluate only in connection with wear material. Intensity of degrading processes we evaluate with wear size – decrease of material, change of dimension. The question how can participate the frictional processes on general wear will be subject of experimental program which is oriented on abrasive and adhesive wear.

4. Experimental Part

The objective of experiment was design tribologic test which allows observes tested material in conditions which correspond to practical utilization. Three samples were compared and so non heat treated cast iron with nodular graphite, heat treated on sorbitic structure and isothermal refined on ausferritic structure. Both of samples were treated on equal hardness 54 HRC. The preparation of material and measuring device (scanner, thermocouple, speedometer, data bus). The method is used to describing tribologic properties of system and definition of surface resistance volume by contact stress.

Sample width [mm]	Stress [N]	Velocity [$m.s^{-1}$]	Temperature [°C]	Time [hod.]
4	20	0,26	20	24

Tab. 4.1. The parameters used for observation.

By valuation of tribologic processes on surfaces of abrasive wear parts we accept processes, which occur with influence of abrasives mechanical effects. We can choose wear resistance material on base of mechanical properties criterion against of introduced elements effect, therefore was produced abrasive wear cylinder from material STN 14 209, heat treated on hardness 62 HRC that is hardest like tested samples.

By relative motion of surfaces of tested disk and tested sample, which are press to itself with fixed force, occur to adhesive wear. Because of microundulation of both surfaces don´t occur to contact of surface on all surface, but only on small contact surfaces, whereaby the tops of undulation deform elastic and plastic. By relative motion of both surfaces occur friction and the tops of undulation can break and on broken contact surfaces create microwelds with influence of adhesive forces. Adhesive wear occur with breaking of this microwelds. Torn off elements stay between contact surfaces a create scratches on surface of sample $\Rightarrow$ abrasive wear.

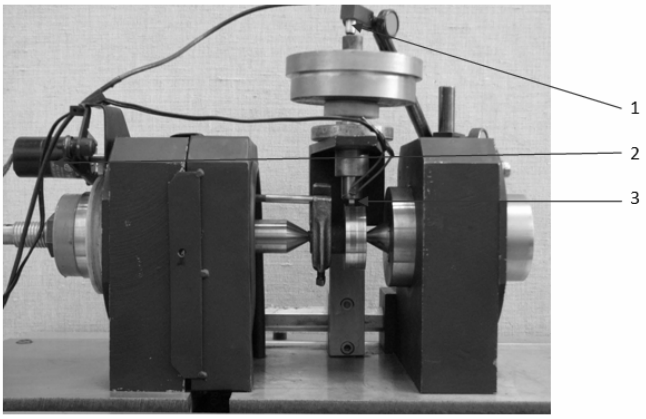

Fig. 4.1 Detail of tested part, 1-measuring part TESA, 2-speedometer, 3-sample with thermocouple.

It is possible to reach high hardness with heat treatment by sorbitic structure and so use this casting to construction parts with abrasive and adhesive wear (with refinement we reach higher impact value). Isothermal refinement by compared hardnesses with sorbitic structure offers higher impact value and possibility to use products for dynamic stress. Advantage ausferritic structures against sorbitic structures could decrease number of defective products with influence of surface crack creation by heat treatment on sorbit.

The most advantageous are samples treated on ausferritic structure like refined or non heat treated cast iron with nodular graphite in term of measuring data (Fig.4.2). The reason is smaller dependence of sample wear in temporal horizon by same stress 20N. We reach higher strength characteristics with isothermal refinement like by conventional treatment, by same hardness both structures. By tough samples occur smaller crumbling of elements from surface like and smaller wear. Both heat treated materials show smaller wear, lifetime like non heat treated base material. The results of measuring incite to use heat treatment of both ways by mechanical parts, segments (gear-wheels, crankshaft, piston-rod), which are stressed adhesive or abrasive wear.

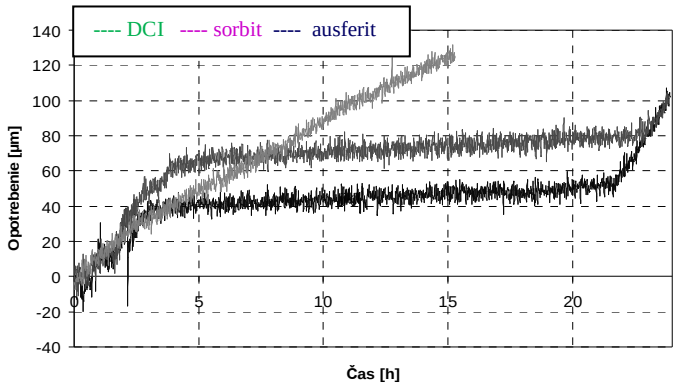

Fig. 4.2 Wear of cast iron with different structure by stress 20N

5. Conclusion

Increased wear resistance have cast irons with increased mechanical value, they are mostly cast irons with martensitic or ausferrtic structure, obtained direct by casting or by heat treatment. Heat treatment of samples used by measuring was inspirited with these structures a their advantageous properties resist of wear and therefore was choosen by ausferritic sample lower temperature of isothermal refinement salt bath and by sorbitic sample lower termperature of martensitic structure refinement. Result was hard needle structures, homogeneous divided in all section of sample.

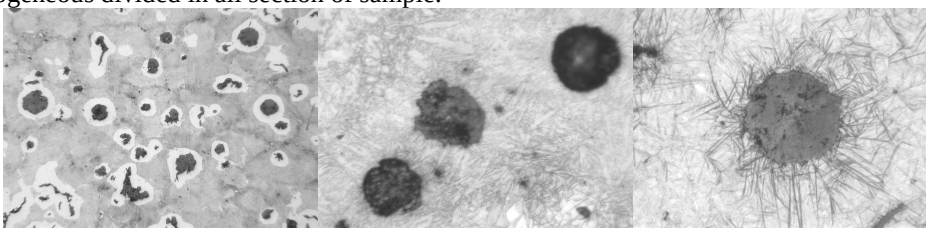

a b c

Fig. 5.1 Structures of samples a) DCI, 100x, b) sorbit 500x, c) ADI 500x.

Change of wear character, which show only by needle morphology, can be connected with redistribution of harder needles in soft base or with their abrasive effect after release from softer structural component. Verify wear mechanism will be possible after next experiments.

Advantage of originated structures after heat treatment is in decreasing of wear by deformation, what results from higher toughness. Advantages can we reason with lower structural stresses and higher homogeneity of structure.

In term of economy will production of ADI perform definitive task by their application to practice. Isothermal refinement is difficult on production like a classical refinement (hardening and tempering) however by financial costingness is better for higher wear resistance. Ausferritic structure is advantageous and has lower inclination to crack creating like a sorbitic structure, it follows possibility of application ausferritic materials on shape difficulty parts without fear of early wear. They have a lot of advantages against others (differently treated) cast irons and could replace in some cases and so by dynamic stress parts, where are not proper non heat treated cast irons because of their high fragility.

Acknowledgement

This research was partially supported by the grant No. VEGA 1/0228/09 The Prediction of Tribological Properties of Selectively Heat Treated Cast Materials for Automobile Industry. The authors gratefully acknowledge this support.

References

[1] KONEČNÁ, R – SKOČOVSKÝ, P.: Porušovanie liatin s prechodovými tvarmi grafitu. Materiálové inžinierstvo, roč. 5, 1998, č. 11, s. 69-74.

[2] GEDEONOVÁ, Z. – JELČ, I. : Metalurgia liatin, 1 vyd. HFTU Košice 2000.

[3] BLAŠKOVIČ, P. a kol. : Tribológia, Alfa Bratislava 1990.

[4] http://www.ateam.zcu.cz/

Transcom 2009, 22-24 June 2009
University of Žilina, Žilina, Slovak Republic

Mechanical Properties and Fracture Behaviour of Laminated Iron-Intermetallic Composites

[*]Marek Konieczny, [*]Michał Kopciał
[*]Kielce University of Technology, Faculty of Mechatronics and Machine Building, Department of Metals Science and Materials Technologies, Al. 1000-lecia P.P. 7, 25-314 Kielce, Poland,
{mkon}@interia.pl, {michalkopcial}@gmail.com

Abstract. Laminated composites were fabricated through reactive synthesis in vacuum using Fe, Cu and Ti foils with controlled temperature, treating time and pressure. The copper and titanium layers were completely consumed by forming intermetallic and the final microstructure consisted of alternating layers of intermetallic phases and unreacted iron. The mechanical properties and fracture behaviour of the fabricated composites were investigated through tensile and three-point bending tests. The yield and ultimate tensile strengths of the Fe-intermetallics composite were higher than of commercially pure iron: ~109% and ~125%, respectively. Shear deformation of the metal layers of the Fe-intermetallics composite was initiated by transverse cracking in the layers of intermetallics. Results also showed that these composites exhibited anisotropy of mechanical properties during three-point bending test. Delamination of layers occurred during three-point bending test, especially when the load perpendicular to the laminates was applied.

Keywords: laminated composite, mechanical properties, deformation behaviour

1. Introduction

Metal – intermetallic composites can be fabricated *via* many different techniques. They are known to be very attractive for a number of potential applications: electronic devices, armour and other structural components. As a distinct class of materials, intermetallics have good high-temperature strength, high resistance to corrosion and oxidation, high stiffness, good creep resistance and relatively low density. On the other hand, most intermetallics exhibit brittle fracture and low tensile ductility at room temperatures, because of limited dislocation mobility and insufficient number of slip or twinning systems resulting in little to no plastic deformation at the crack tip. Several composite reinforcement concepts involve material combinations consisting of one brittle and one ductile constituent. Examples include metal matrix composites and laminated composites comprised of alternate layers of intermetallics with metals. The intermetallic phases give high hardness and stiffness to the composite, while unreacted metal provides the necessary high strength, toughness and ductility for the system to concurrently be flexible. The multilayered structure of the composite allows for variations in the layer thickness and phase volume fractions of the components simply through the selection of initial thickness, which consequently allows for the optimisation of mechanical properties for practical applications. Methods for the production of laminated metal-intermetallic composites include magnetron sputtering [1], electron beam evaporation [2] and synthesis reactions between dissimilar elemental metal foils [3-7]. In the present study, a reaction process was developed to fabricate laminated Fe-intermetallic composites. This paper summarises mechanical properties (microhardness, tensile properties, flexural strength) and fracture behaviour of Fe-intermetallic laminated composites.

2. Experimental procedure

The rectangular samples with the dimensions of 50 mm length and 10 mm width of 0.6 mm thick sheets of iron (99.89 wt. %), 0.1 mm thick foil of copper (99.99 wt. %) and 0.1 mm thick foil of titanium (99.02 wt. %) were used to fabricate a laminated Fe-intermetallic composite. The joining surfaces of the samples were prepared by conventional grinding techniques using 800-grit abrasive paper and polished on diamond paste using Struers polishing machine. Rinsed first with water and then with ethanol and dried rapidly, the foils were placed alternately to form multilayer sandwiches of iron/copper/titanium/copper/iron (5 Fe, 8 Cu and 4 Ti layers), which were then treated in a vacuum furnace under vacuum of 10^{-2}Pa. A pressure of 5 MPa was applied at room temperature to ensure good contact between the foils. The temperature was initially raised to 850 ^{0}C and then the pressure was released to avoid an expulsion of liquid phases. Subsequently, the temperature was increased to 900 ^{0}C, which was necessary for the initiation and rapid development of the structural processes at the interfaces of iron, copper and titanium. The samples were held at a temperature of 900 ^{0}C for 2 hours and then furnace-cooled to room temperature. Detailed information concerning the synthesis of Fe-intermetallic laminated composite has been published previously [8]. After fabrication Vickers measurements were conducted using a Hanemann microhardness tester. Samples 50 mm x 8 mm x 4 mm, made from fabricated composite, were subjected to tension test on a screw machine at the strain rate of 0.1 mm·min^{-1}. The flexural strength measurements were performed using a three-point bending test on the specimens with dimensions of 50 mm x 4 mm x 3 mm where the loading span was 40 mm. Two loading directions were used: one perpendicular and another parallel to the laminates. The tests were carried out under displacement control at a rate of 0.5 mm·min^{-1}. Slip traces, shear bands and cracks produced during deformation were observed using Nomarski contrast.

3. Results and discussion

A picture of the lateral wall of a specimen prepared for the study of the deformation process during mechanical tests is shown in Fig. 1.

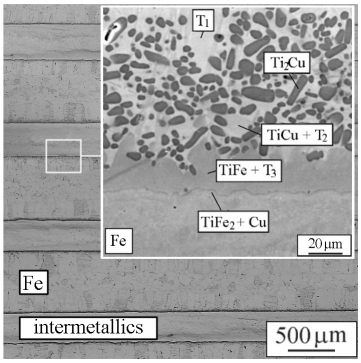

Fig. 1. Optical and scanning electron micrographs showing a typical microstructure of the laminated composite produced from Fe, Cu and Ti foils.

It was evident from earlier metallographical examination [8] that the predominant part of intermetallics had been synthesised in the region passing from a liquid state to a solid state. The inhomogeneous reaction zone contained intermetallic compounds: Ti_2Cu, TiCu, Ti_3Cu_4, TiFe, $TiFe_2$, T_1 ($Ti_{33}Cu_{67-x}Fe_x$; 1<x<2,5), T_2 ($Ti_{40}Cu_{60-x}Fe_x$; 5<x<17) and T_3 ($Ti_{43}Cu_{57-}$

$_xFe_x$; 21<x<24). The study also revealed that titanium could migrate to iron through copper layer, hence, copper layer couldn't hinder the formation of brittle Ti-Fe base intermetallics.
Properties of the laminate composites are sensitive to the thickness of the metal and intermetallics layers. When the iron-to-intermetallic layered thicknesses are optimised, the mechanical properties of the layered composites can be tailored to produce a composite that is both strong and tough. Table 1 summarises the mechanical properties the fabricated Fe-intermetallics composites.

Microhardness	Copper-rich regions	520÷572 HV
	$TiFe + T_3$	681 HV
Tensile properties	Yield tensile strength	187 MPa
	Ultimate tensile strength	280 MPa
	Average elongation	4.9 %
Flexural strength	Parallel to layers	173 MPa
	Perpendicular to layers	215 MPa

Tab. 1. Summary of mechanical properties of investigated composites.

The fracture behaviour of the Fe-intermetallic laminates is typical of ductile-phase-toughened matrix composites, with the ductile metal layers bridging the many cracks that form in the brittle intermetallic layers during plastic deformation [6]. The failure of this composite during tensile test can be described in the following way. Cracking first occurs in the brittle TiFe intermetallic layers. Fortunately, the Cu-Ti and Cu-Ti-Fe-based intermetallics have a good capacity for plastic deformation and they are capable of effectively arresting microcracks (Fig. 2a).

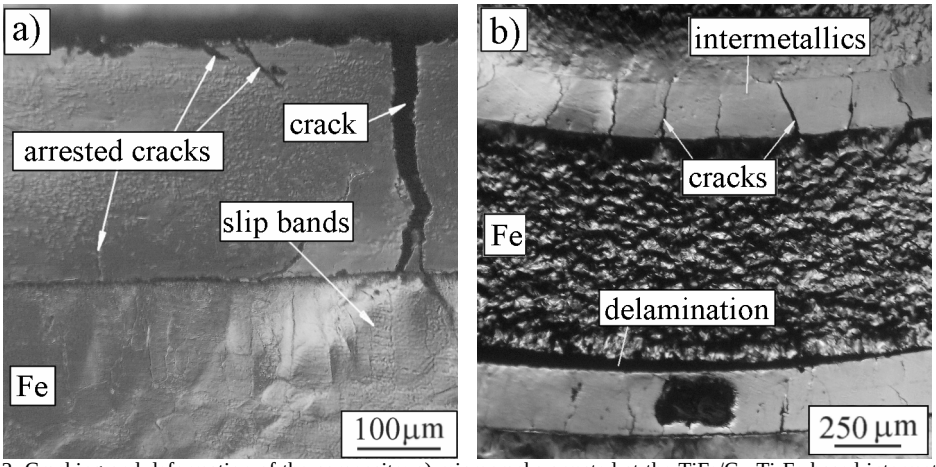

Fig. 2. Cracking and deformation of the composite: a) microcracks arrested at the TiFe/Cu-Ti-Fe-based intermetallic border during tensile test, b) transverse cracking and delamination during three-point test.

Formation of transverse cracks in the layers of intermetallic phases is the characteristic feature of the prolonged composite deformation (Fig. 2a). These cracks debond the metal layer from the intermetallic layer, thereby allowing the ductile metal layer to plastically deform but the plastic flow that take place is restricted to the small regions between opposite cracks in the neighbouring layers of intermetallic phases. As a result a plastic strain of iron is localised firstly in slip bands and then in shear bands. When many loads are transferred to the metal, the metal layer undergoes microvoid formation and coalescence, leading to a ductile rupture of the layer. The final fracture of the composite occurs through the linkage of many cracks, which is indicative of tough composite behaviour. It should be added

that the composite exhibits a good cohesion between iron layers and layers of intermetallics during tensile test. The brittle TiFe layers break first but the TiFe/Cu-Ti-Fe-based intermetallic interfaces do not delaminate.

During three-point bending test, when the load perpendicular to the laminates was applied, the iron layer deformed plastically causing delamination of the neighbouring TiFe intermetallic layer. Further loading caused transverse cracking of the copper-rich regions and deformation in the next Fe layer (Fig. 2b). This process was repeated until all intermetallic layers cracked and delaminated. This failure mechanism has been shown in the literature to be typical of laminated composites [9]. When the load direction was parallel to the laminates, the failure occurred by cleavage mode. Therefore, it is evident that there was solely one main crack that grew gradually in the through-thickness direction and finally travelled across the specimen. Delamination was not observed. The flexural strengths are listed in Table 1.

4. Conclusions

The mechanical properties and fracture behaviour of the Fe-intermetallic laminated composites were investigated through tensile and three-point bending tests. The yield and ultimate tensile strengths of the Fe-intermetallics composite are higher than of commercially pure iron: ~109% and ~125%, respectively. Investigations showed that the Cu-Ti-Fe-based intermetallics in the composite are capable of effectively stopping microcrack propagation. Shear deformation of the metal layers of the Fe-intermetallics composite is initiated by transverse cracking in the layers of intermetallics. Results also show that these composites exhibit anisotropy of mechanical properties during three-point bending test. Delamination of layers occurs especially when the load perpendicular to the laminates is applied.

Acknowledgements

The author would like to thank Ms Danuta Kępka for her assistance with sample preparation. Discussions and help from Dr. Renata Mola in SEM are greatly appreciated.

References

[1] TIXIER-BONI, S.,SWYGENHOVEN, H. *Hardness enhancement of sputtered Ni_3Al/Ni multilayers*, Thin Solid Films, 342, 1999, p. 188.

[2] DYER, T.S., MUNIR, Z.A. *The synthesis of nickel aluminides by multilayer self-propagating combustion*, Metall. Mater. Trans, 26B, 1995, p. 603.

[3] BANERJEE, R., FAIN, J.P., ANDERSON, P.M., FRASER, H.L. *Influence of crystallographic orientation and layer thickness on fracture behaviour of Ni/Ni_3Al multilayered thin films*, Scripta Mater., 44, 2001, p. 2629.

[4] MOLA, R., DZIADOŃ, A. *Formation of Al-intermetallic phases layered composite - growth of intermetallics at the Al-Ni, Al-Cu, Al-Fe and Al-Mg interface*, Proc. TRANSCOM'05, Zilina, Slovak Republic, 2005, p. 81.

[5] CHUNG, D.S., ENOKI, M., KISHI, T. *Microstructural analysis and mechanical properties of in situ Nb/Nb-aluminide layered materials*, Sci. Technol. Adv. Mater., 3, 2002, p. 129.

[6] ALMAN, D.E., DOGAN, C.P., HAWK, J.A., RAWERS, J.C. *Processing, structure and properties of metal-intermetallic layered composites*, Mater. Sci. Eng., A 192-193, 1995, p. 624.

[7] KONIECZNY, M. *Deformation mechanisms in copper-intermetallic layered composite at elevated temperatures*, Kovové Mater., 45, 2007, p. 313.

[8] KONIECZNY, M., MOLA, R. *Fabrication, microstructure and properties of laminated iron - intermetallic composites*, Steel Research Int., 79, 2008, p. 499.

[9] ODETTE, G.R., CHAO, B.L., SHECKHERD, J.W., LUCAS, G.E. *Ductile phase toughening mechanisms in TiAl-TiNb laminate composite*, Acta Metall. Mater., 40, 1992, p. 2381.

Transcom 2009, 22-24 June 2009
University of Žilina, Žilina, Slovak Republic

Austempered Ductile Iron fatigue behaviour in ultra high cycle region

[*]Peter Kopas, [**]Alan Vaško, [*]Andrej Udvorka
[*]University of Žilina, Faculty of Mechanical Engineering, Department of Applied Mechanics, Univerzitná 1, 010 26 Žilina, Slovakia, {peter.kopas, andrej.udvorka}@fstroj.uniza.sk
[**]University of Žilina, Faculty of Mechanical Engineering, Department of Materials Engineering, Univerzitná 1, 010 26 Žilina, Slovakia, alan.vasko@fstroj.uniza.sk

Abstract. For attractive technical applications such as cars and trains, the durability sought for some components is between 10^8 and 10^{10} cycles. However, only few experimental results beyond 10^7 cycles are available. The S–N curve in the ultra-wide life region must be determined in order to guarantee the real fatigue strength and safe life of components. This paper presents a study of the fatigue behaviour of the austempered ductile iron (ADI) between 10^6 and 10^{11} cycles. These tests were carried out using the high-frequency tension-compression loading. Based on the experimental results, the shape of the S–N curves are discussed.

Keywords: Austempered ductile iron (ADI), fatigue, ultra high cycle region, S-N curve.

1. Introduction

Mechanical failures have caused many injuries and much financial loss. However, relative to the large number of successfully designed mechanical components and structures, mechanical failures are minimal. Mechanical failures involve an extremely complex interaction of load, time, and environment, where environment includes both temperature and corrosion. For these reasons, there is a need to continually invent new materials with improved resistance to wear, high strength, hardness and the next progressive physical, mechanical and chemical properties. One such material is ductile iron. The nodular cast irons (LGG) belong among very important construction materials, which are considered as materials of future. The great advantage is a favourable shape of graphite what enable to utilize excellent mechanical properties of metal matrix [1]. Research efforts on this material, have mainly, focused on possible improvements of its mechanical properties by according it appropriate heat treatments. One such heat treatment is austempering and the resultant product is called austempered ductile iron (ADI).

Austempered ductile irons are rapidly being developed for an increasing number of engineering aplications. The reason for the recent interest in ADIs is that they offer excellent combinations of high strength, ductility, toughness, fatigue strength and wear resistance that are unavailable in other grades of cast iron. These diserable mechanical properties of ADI are comparable or in some cases superior to those of forget steel. A variety of combinations in the mechanical properties of ADI can be achieved by proper austempering treatments in relation to a unique microstructure consisting of acicular, carbide-free ferrite with carbon-enriched austenite. Minor amounts of martensite and carbides may also be present [2].

Fatigue resistance is one of the most important engineering properties, that plays a significant role in machine design. Fatigue testing is usually performed to estimate the relationship between the stress amplitude and the cycles to failure (σ-N curve). Majority of

published experimental works shows [3, 4] that the number of cycles of stress that the metal can endure before failure increases with decreasing stress amplitude and for some engineering materials the σ-N curve becomes horizontal at a certain limiting stress known as the fatigue limit or endurance limit. Below the fatigue limit, the material will not fail in an infinite number of cycles. Up to date researches gives some arguments, that this representation of the fatigue resistance can not be true because infinite fatigue endurance does not exist. And so fatigue design based on the usual fatigue limit ($N = 1.10^6 \div 1.10^7$ cycles) cannot provide the safety design data of mechanical structures [5].

2. Material and experimental procedures

The material used in an experimental works was ADI (Austempered Ductile Iron) with different microstructures respectively tensile strength R_m (Tab. 1). The microstructures of ADI after heat-treatment were characterized by upper or lower bainite, retained austenite and graphite, Fig. 1 ÷ Fig. 4. For the study were selected experimental physical metallurgy methods-quantitative chemical analysis (chemical composition), metalography analysis (microstructures), tensile test (tensile strength R_m) and high-frequency fatigue tests (fatigue lifetime). High-frequency fatigue tests (HFFT) were carried out with using an ultrasonic testing apparatus KAUP-ZU [5-7] for high-frequency sinusoidal cyclic push-pull loading (working frequency f ≈ 20 kHz, temperature T = 20 ± 5 °C, load ratio R = –1, forced specimens cooling with distilled water with anticorrosive inhibitor). Smooth 4-mm-dia round bar specimens polished in the working area by metalography procedures were used (12 to 15 specimens for each testing programme). The fatigue lifetime, stress amplitude vs. number of cycles to failure, was investigated in the region from $N \approx 5.10^6$ cycles to $N \approx 2{,}5.10^{10}$ cycles of loading. The fatigue tests were realized with using methods authors [7, 8].

C	Mn	Si	P	S	Cu	Ni	Mo	Cr
3.57	0.67	2.72	0.05	0.022	0.93	0.74	0.037	0,08

sign.	heat – treatment austenitization * isothermal transformation	R_m [MPa]
◊	920 °C, 30 min * 420 °C, 50 min	980
Δ	920 °C, 30 min * 380 °C, 60 min	1040
●	920 °C, 30 min * 320 °C, 90 min	1164
■	920 °C, 30 min * 250 °C, 240 min	1551

Tab. 1. Chemical composition, heat-treatment and mechanical properties, ADI (◊ Δ ● ■).

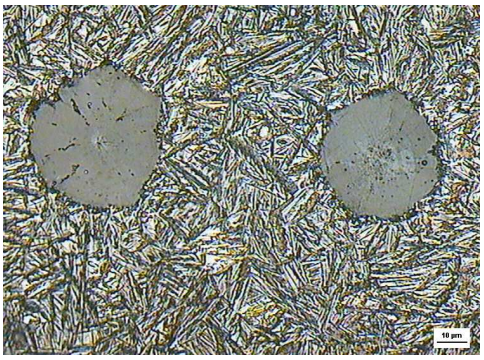

Fig. 1. Microstructure, ADI 420 °C / 50 min, mag. 500x, etch. Beraha-Martenzit

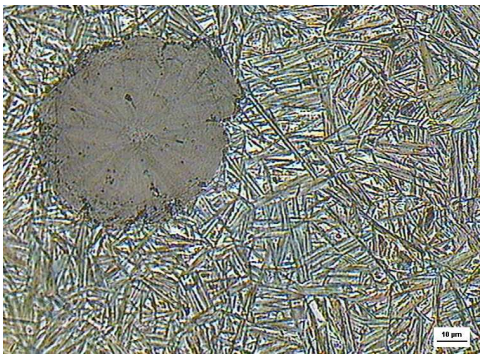

Fig. 2. Microstructure, ADI 380 °C / 60 min, mag. 500x, etch. Beraha-Martenzit

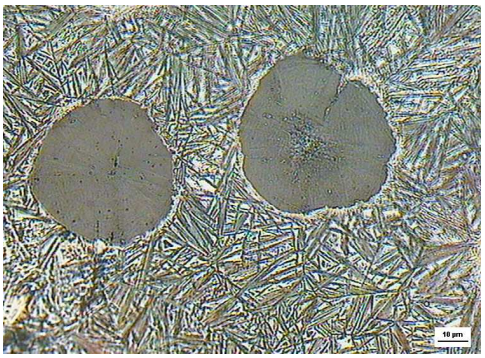

Fig. 3. Microstructure, ADI 320 °C / 90 min, mag. 500x, etch. Beraha-Martenzit

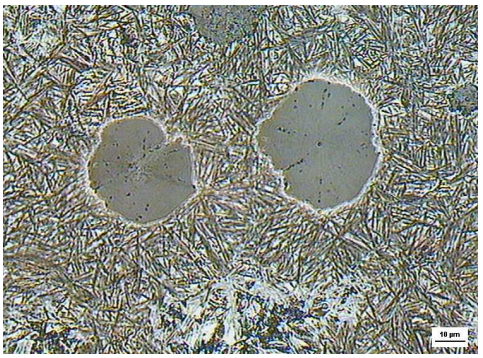

Fig. 4. Microstructure, ADI 250 °C / 240 min, mag. 500x, etch. Beraha-Martenzit

3. Result and discussion

The results, fatigue durability of ADI with different microstructures (stress amplitude vs. number of cycles to failure) in the very high cycle regime are presented in Fig. 5. The obtained results can be discussed i.e. from the point of view of ultimate tensile strength and microstructure (texture and different of phase influence). Generally, we can say, that stress amplitude continually decreasing with number of cycles to failure increasing after conventional limit of cycles number ($N_C = 2.10^6$ cycles to $N_C = 1.10^7$ cycles) used to fatigue limit σ_C determination.

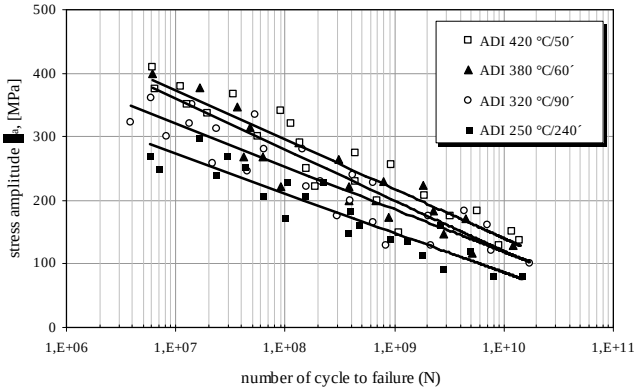

Fig. 5. Fatigue lifetime, ADI, high – frequency fatigue testing.

The tensile strength increasing is not accompanied with correspond of fatigue properties increasing. The suitable fatigue properties we can observe in the upper bainite structures with lower tensile strength with compare of lower bainite structures. Results are with a good agreement with authors' conclusions [6] about fatigue limit σ_C versus ultimate strength R_m parabolic dependence, Fig. 6. These specific behaviour of the bainite structures is possible explain with the some factors effect, e.g. content of retained austenite in matrix, plastic properties of matrix, retained austenite transformation to martensite during cycles loading, size of critical defects for fatigue crack initiation, fatigue cracks growth mechanisms, and fatigue crack growth rate and K_{ath} ... [6, 10, 11]. These factors have different effect of intensity with regard on the level of transformation temperature and length of isothermal transformation dwell.

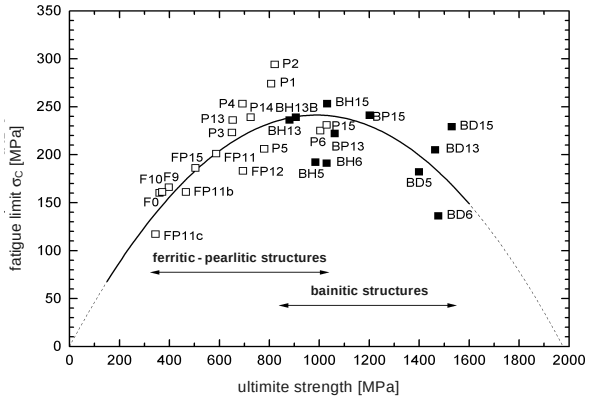

Fig. 5. Fatigue limit σ_C vs. ultimate strength R_m, parabolic dependence push – pull loading (R = -1), nodular cast iron and ADI [6].

4. Conclusion

- The fatigue lifetime of nodular cast iron incl. ADI increases with decreasing stress amplitude continuously in the cycles of number region ($3.10^6 < N < 2{,}5.10^{10}$ cycles).
- The fatigue properties of ADI strongly depends on transformation conditions, e.g. temperature and the length of isothermal transformation dwell.

Acknowledgement

The research was supported by the grant of VEGA No. 1/0441/08 and VEGA No. 1/4099/07. The authors gratefully acknowledge this support.

References

[1] KOPAS, P., NOVÝ, F., BOKŮVKA, O. *Únavová odolnosť ADI v oblasti veľmi vysokého počtu cyklov do lomu.* SEMDOK 2005, Súľov, SR, 2005.

[2] KOVACS, B. V. AFS Trans., 1994.

[3] BATHIAS, C. *Fatigue in the very high cycle regime.* Vienna, Austria 2001.

[4] VOIGT, R. C. *Austempered ductile iron-processing and properties.* Cast Metals, 1989.

[5] BOKŮVKA, O., NICOLETTO, G., KUNZ, L., PALČEK, P., CHALUPOVÁ, M. *Low & high frequency fatigue testing.* CETRA and Univerzity of Žilina, Žilina 2002.

[6] VĚCHET, S., KOHOUT, J., BOKŮVKA, O. *Únavové vlastnosti tvárné litiny.* EDIS ŽU Žilina, SK, 2001.

[7] PUŠKÁR, A. *Vysokofrekvenčná únava materiálov.* EDIS ŽU Žilina, SK, 1997.

[8] PUŠKÁR, A., BOKŮVKA, O., NICOLETTO, G., PALČEK, P. *Berichte und Informationen.* No. 1/97, D, 1997.

[9] STANZL-TSCHEGG, S., MAYER, H. *Fatigue in the Very High Cycle Regime.* Vienna, Austria, July, 2001.

[10] VĚCHET, S. Mechanika 52, No. 217, Opole, PL, 1996.

[11] NOVÝ, F., KOPAS, P., BOKŮVKA, O., CHALUPOVÁ, M. *Vplyv zlievarenských chýb na únavovú životnosť perliticko – feritickej LGG.* Materiálové inžinierstvo, 3, 10, SK, 2003.

Transcom 2009, 22-24 June 2009
University of Žilina, Žilina, Slovak Republic

Off-line Programs for Robotic Cells

[*]Peter Kovačič, [**]Darina Kumičáková
[*]University of Zilina, Faculty of Mechanical Engineering, Department of Automation and Production Systems, 010 26 Žilina, Slovakia, {peterkovacic}@hotmail.com
[**]University of Žilina, Faculty of Mechanical Engineering, Department of Automation and Production Systems, 010 26 Žilina, Slovakia, darina.kumicakova@fstroj.uniza.sk

Abstract. Companies which production factories use robotic cell are trying to answer a question how to increase the effectiveness and competitiveness of decreasing series production. Part of the solution are the off-line program tools, which are becoming necessary nowadays.

Keywords: simulation, robot, off-line programing

1. Introduction

The current situation on the world market can be briefly characterized by words like global crisis, cleaning of the market, a big pressure of competition and suppression of the prices. Innovation is a key to sustain the competition. There are different methods, tools and practices that focus on increasing effective productivity. The way to increase the productivity is through using suitable software applications allowing creating real simulations and analysis of robots and their periphery mechanisms in work place. These applications allow offline robot programming what contributes to reduction of wait time and to increase production.

These days we need a high flexibility in factory and sale products made on robotics cell. User must use robot, which allow fast and easy programming. This target is possible to reach with off-line programs, as virtual reality, visualization, simulation etc. From this aspect the future of robotic welding relies on consistent improving of these methods. [1]. In simulation real of situations there are used virtual 3D model system, created in CAD/CAM/CAE systems.

1.1. Off-line programovanie výrobného procesu

Off-line programming is executed in computer 3D model real robotics cell with accessories. Programming is made in advance. Programming system makes direct import of objects from different CAD systems. Disadvantage is that this process request extra investment apart of the robot. However, on the other hand, some important information is known beforehand. With this tool we know effective use of robotic work space. For designer is off-line programming also proposition, because he can it use for creating of welding jig and simulation in virtual reality and collision protection. Off-line programming robots go out virtual model robotics cell. Standard is working on different programming language as robots, what requires postprocessor which generates program for specific robot.

Virtual model of robot has 3 parts: manipulator model, control system model and program. Model of manipulator it represents 3D solid model. Model of control system represents real control system of robot and program specific task, which robot will do. For machinery (e.i. NC machine, jig, and conveyer) can create same virtual model as for robot. Communication among parts is modelled by link models [2]. Exchange of information among models of programming systems and CAD/CAM system is supported by natural formats step, igs and sat. Systems from robotic manufactures contain robotics library, positions, and peripheral equipments; these are directly imported into simulation system. Simulations run in real time in 3D simulation. Resolution model of solution are realized in base simulations. After reaching of optimal variant, the program is generated into robot language and imported into real system (Fig. 1).

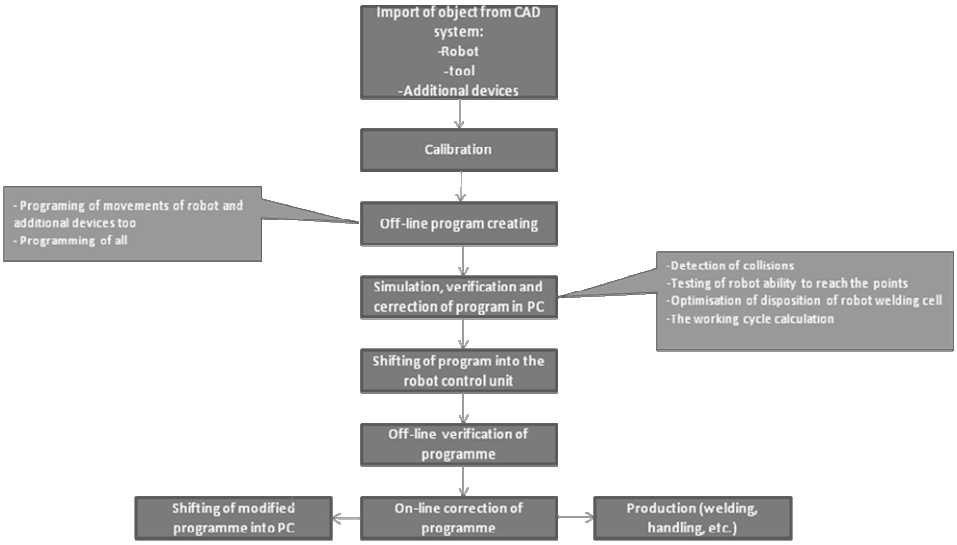

Fig. 1. Procedure of pri off-line programming

Off-line programming allows for using of all types of interpolation as for example PTP, LIN or CIRC. In addition, 3D detailed simulation, collision detection in simulation and verification of innovation in process, testing access of robot on welding and manipulation points and other. This allows user to find not just the optimal layout of robotic cell but also optimal manipulation of operation cycle. Many off-line program systems follow real time behaviour activity of robot, support select advantages of tools or welding parameters process. Important rule to real program is creating real model with all property and behaviour. On picture 2 it is virtual model and reality.

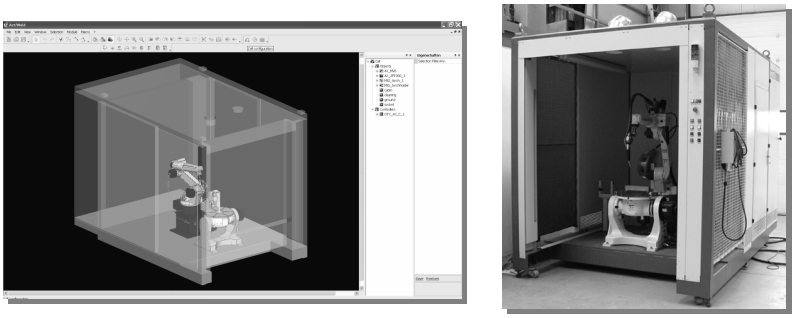

Fig. 2. Virtual workplace for off-line programming Act/weld (ALMA) and real workplace

Advantages of off-line programming focus on simulation of complete process:

- Detection of collision on robotic cell prior to real of production
- Automatic search of trajectory with axoidance to part
- Programming of all parameters important for real technology
- Optimal work cycle and make all process more effectrive.

For selection of simulation software is important price. While a few years ago hardware represented the biggest financial barrier, nowadays purchasing of the software is the most expansive.

2. Off-line programy

Commercial market currently offers an extensity variety of off-line programs. When choosing the right program it is important to take the same steps as during choosing CAD/Cam systems and their functions. Also it is important to remember that there are differences among off-line. Offline program can be applied from different aspects:

- Support of technology for simulation - which technologies the program supports: for example circle welding (MIG/MAG, TIG, LASER) cutting (by plasma, laser, oxygen-acetylene, watter jet), manipulation, mechanical working, *(milling, griding), or painting.*
- Universal – ability offline program to simulate robot activity from multiple manufactures.
- Full-value – the ability to generate fully capable program for robot. Except the simulation of the movement activity of the robot it is possible to implement into the program also all necessary technological parameters.

2.1. Problems in the Robot off-line Programming

The development in off-line programming field has brought some problems that have to be yet solved. From this point of view the problems of off-line programming can be specified as follows:

- *Robot workplace calibration.* Quality of the created program and accuracy of executed operations depend on calibration. There are a few factors which influence inaccuracy of this one. Faulted calibration of *TCP* and workplace dimensions are some of them. The problem is we do not have a verified process of calibration in big robotized workplaces. Technicians have to rely on their own knowledge and practical experience. One of the companies that tries to resolve this problem is *Robotec*, Sučany. Robotec integrates of off-line programme *Arc/weld* of *ALMA* Company. *Optimisation of algorithm during the simulation.* This problem is appeared in frame of programmes on lower development level than advanced off-line programmes (i.e. *Arc/weld, Delmia, RobotStudio).*
- *Fidelity of 3D model in comparing with reality.* The problem appears to be in if off-line program with simple graphics. In this case it is not possible to create 3D model of the component with detailed features which can interact in the robot working space and can not be implemented into virtual environment. In addition, un-detected collisions can appear in the real workplace.
- *Solution of cable join collisions during simulation.* The solution of this problem is very difficult. The alternative ways how to solve this problem have to be yet found. One of the possible solutions is to limit the movements of the robot end axes according their position.
- *Robot singularities.* Identification of the robot singularities is very important for the correct execution of the required technological or manual operation. Lowe level off-line programs are not able to detect these critical areas.
- *Simultaneous controlling of external axes* is a special function which connects a few functions into single function block. Problems can appear if the off-line program is used for simulation of another type of robot system with the different structure. Therefore the research is focused on the creation of single universal set of instructions suitable for broad spectrum of robots.

3. Conclusion

The off-line programming field is developed very dynamically. On one hand, different programming tools are still improving but on the other hand, new problems that are appearing have to be yet solved. From the view of practical application, the solution of collision states of the end effector cable pack is one of the biggest problems. My dissertation work will focus on resolving some of the off-line problems.

References

[1] SEMJON, J. *Simulation with welding Fixture*. Acta Mechanica Slovaca., KOŠICE, 2-A/2008, ISBN 1335-2393.

[2] PALASCAKOVA, D. *Useing virtual reality for robotic cells design*. Acta Mechanica Slovaca., KOSICE, 2-A/2008, ISBN 1335-2393.

[3] KOVACIC, P. *Off-line programation of welding robots*. Acta Mechanica Slovaca., KOŠICE, 2-A/2008, ISBN 1335-2393

[4] PALASCAKOVA, D. *Simulation of The Robotic cells in a Virtual Robotics environment*, NOVUS SCIENTIA 2007

[5] www.robotec.sk

[6] www.almacam.de

[7] http://www.odbornecasopisy.cz/index.php?id_document=28901

Transcom 2009, 22-24 June 2009
University of Žilina, Žilina, Slovak Republic

Dynamic Tensile Characteristic and Fracture Behavior of UFG Copper

[*]Andrea Kovacova, [**]Tibor Donic, [**]Milan Martikan
[*]Technical University in Kosice, Faculty of Metallurgy, Department of Metal Forming, Vysokoskolska 4, 04200 Kosice, Slovakia, {Andrea.Kovacova}@tuke.sk
[**]University of Zilina, Faculty of Mechanical Engineering, Velky Diel, 01026 Zilina, Slovakia {Tibor.Donic}@fstroj.uniza.sk

Abstract. In the present study behavior of ultrafine-grained (UFG) oxygen free high purity (OFHP) copper prepared by equal channel angular pressing (ECAP) was investigated during dynamic loading at the ram speed 2, 2,5, 3, 4 m/s. The dynamic tensile test was conducted by high speed tensile machine in room temperature and obtained loading-elongation curves clearly show existence of dynamic upper yield stress $R_{eH,}d$, dynamic lower yield stress $R_{eL,d}$ (dynamic tensile properties) and loading oscillation in material. The $R_{eH,}d$, $R_{eL,d}$ investigations in different deformation rates suppose their increase with deformation rate increasing. The deformed area observations of dynamically fractured surface show a typical ductile fracture mode in every ram speed regime. The dimple size measurements indicate their decrease with ram speed increasing. Following dynamic tests reduction of area shows its increase with dimple size increasing.

Keywords: ECAP, UFG Cu, dynamic tensile tests, dynamic tensile properties, fracture behavior.

1. Introduction

Ultrafine-grained materials represent a new generation of advanced materials exhibiting unique and technologically attractive properties due to the size of grains. Ultrafine-grained materials exhibit extremely high strength and good fatigue resistance and at the same time they are rather ductile [1]. There are many methods to achievement ultrafine-grained materials, nowdays. Equal-channel angular pressing is method, which was developed by Segal and his co-workers. The main goal is introducing severe plastic deformation (SPD) into materials without changing the cross section area of billets [2].

The dynamic tensile properties of ultrafine-grained samples are important since the dynamic behavior of material is different from quasi-static behavior. The most material data depend on the strain rate during plastic deformation process and it is much higher than the rate obtained in conventional tensile testing machines. Lately, several studies on quasi-static and dynamic deformation properties of ultrafine-grained or nanograined Fe, Cu and Ni have been conducted using a hydroservo system or a compressive Kolsky bar [3, 4, 5].

Deformation and fracture behaviors of UFG materials under dynamic loading are studied at the present time in limit area because the most of studies are related to phenomena occuring under quasi-static loading. The progress of dynamic deformation and fracture behavior is important to know owing to designing and applying ultrafine-grained materials to parts used under high-speed loading conditions.

2. Experimental Material and Methods

The material used in this study was a oxygen free high purity copper (OFHP-99, 99%), its initial mechanical properties and grain size are given in Tab.1. Afterwards, the ECAP was carried out in order to achievement ultrafine-grained structure of copper. It was realized 5 passes by route C at room temperature, obtained subgrain diameter was 200 nm.

$R_p0.2$ [MPa]	R_m [MPa]	A_5 [%]	Z [%]	HV	d_z [µm]
275	282	11,5	82	125	7

Tab.1. OFHP Cu properties before ECAP

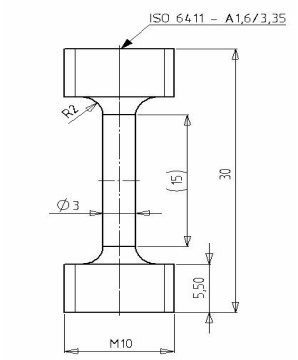

Fig.1. Shape and dimensions of the specimen for dynamic tensile test

The next analyse was realized via dynamic tensile loading at the room temperature and fracture investigation. In dynamic tensile test a high speed tensile machine was used. The parameters of Cu samples with UFG structure which were used during dynamic tests are displayed in Fig.1. It was investigated dynamic behavior of UFG copper during four different ram speed conditions. Fracture surfaces were observed using a scanning electron microscope after the test. The mean dimple size was measured from around 200 dimples group.

3. Results

3.1. Dynamic Tensile Tests

Following [6, 7] dynamic upper yield stress $R_{eH,}$d and dynamic lower yield stress $R_{eL,d}$ were found in dynamic tested materials. Room-temperature dynamic tensile stress-strain curve of UFG copper is presented in Fig.2 with $R_{eH,d}$, $R_{eL,d}$ description. The sample and dynamic tensile system during loading oscillate following [7, 8] as shown in Fig. 3.

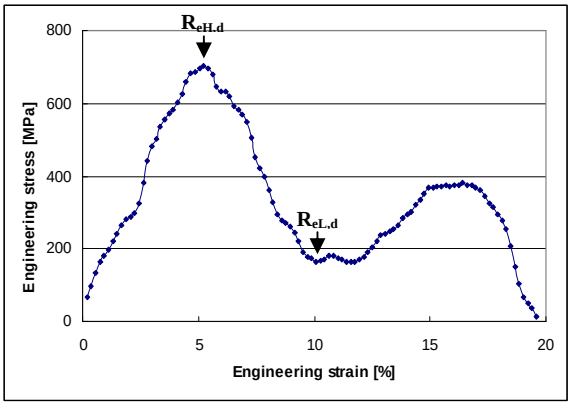

Fig.2. Stress-strain curve obtained from dynamic tensile test in ram speed 3 m/s

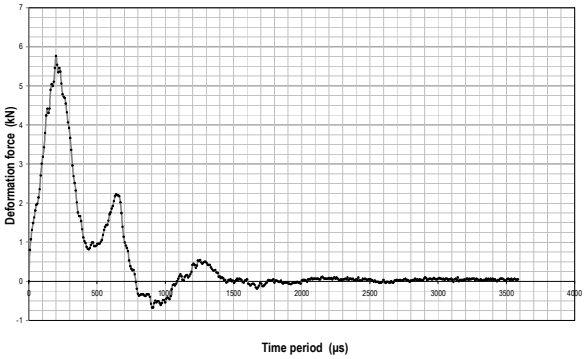

Fig.3. Dependence deformation force on time period during dynamic loading

In the Tab.2 $R_{eH,d}$, $R_{eL,d}$ values for every ram speed are determined and in Fig.4 engineering stress dependence on ram speed is plotted, where increase of $R_{eH,d}$ with deformation rate increasing is visible after 3 m/s by reason of strengthening.

Ram speed [m/s]	**$R_{eH,d}$ [MPa]**	**$R_{eL,d}$ [MPa]**
2	686	141
2,5	672	184
3	577	177
4	744	102

Tab.2. UFG copper dynamic tensile properties

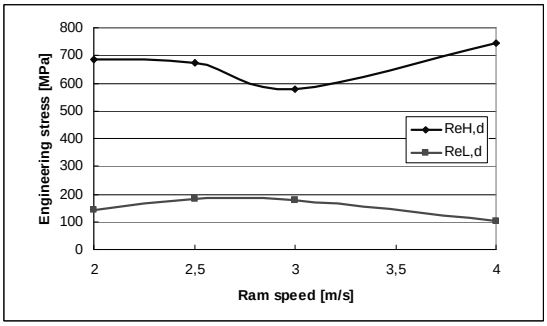

Fig.4. Engineering stress dependence on ram speed

3.2. Fracture Observations

Fracture characteristic observation using scanning electron microscopy was made. The SEM micrographs of dynamically fractured tensile UFG copper specimens clearly show a typical ductile fracture mode in every ram speed regime, Fig.5. The ductile fracture mode based on Gourland-Plateau theory suppose three stages dimple creation before the fracture: initiation, increase and coalescence of dimple. The Fig.6 clearly shows, that if ram speed increased dimple size would decrease in UFG copper after dynamic loading owing to high speed deformation, when progress of dimple increase and coalescence is not fully achieved. The reduction of area is very important plastic characteristic of material, following dynamic tensile tests it was determined and obtained results are also plotted in the Fig.6.

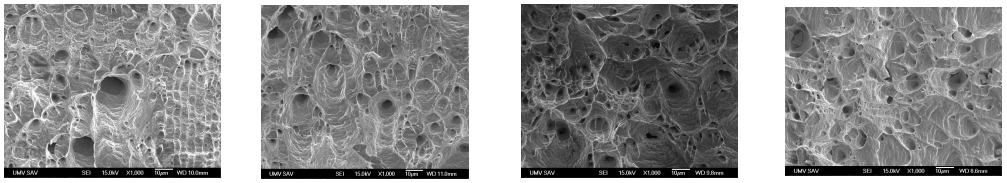

a) b) c) d)

Fig.5. SEM micrographs of UFG copper fractured area in a) 2 m/s b) 2,5 m/s c) 3 m/s d) 4 m/s (1000x)

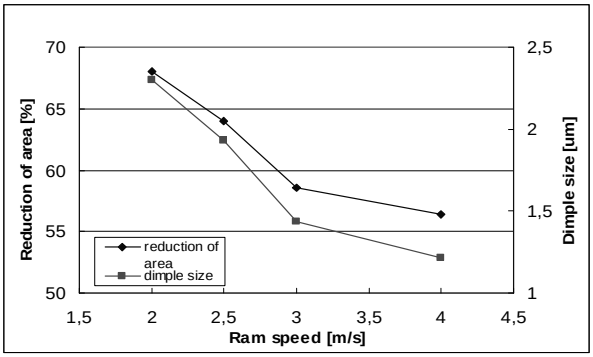

Fig.6. Reduction of area and dimple size dependences on deformation rate

4. Conclusion

In the present study, dynamic tensile tests were conducted on ultrafine-grained copper and its deformation and fracture behavior were analyzed.

1) According to the dynamic tensile test results, dynamic upper yield stress $R_{eH,d}$ and dynamic lower yield stress $R_{eL,d}$ were found in tested materials.
2) Following obtained results from dynamic tests, oscillation in dynamically loaded samples was found.
3) Fracture characteristic observation dynamically fractured samples show a typical ductile mode in every deformation rate regime. The dimple size measurements indicate its decrease in dependence on deformation rate increasing.

Acknowledgement

This work is supported by Slovak agency APVV-20-027205.

References

[1] GUTKIN, M. YU., OVIDKO, I.A., PANDE, C.S. *Theoretical models of plastic deformation processes in nanocrystalline materials.* Rev. Adv. Mater. Sci. 2 (2001) 80-102.
[2] SEGAL, V.M., REZNIKOV, V.I., DROBYSHEVSKIY, A.E., KOPYLOV, V.I. *Russian Metall.* 1981; 1:99.
[3] SHIN, D.H., KIM Y.S., LAVERNIA E.J. *Acta Mater.*, 2001, vol. 49, pp. 2387-93.
[4] GRAY G.T., LOWE T.C., CADY C.M., VALIEV R.Z., ALEKSANDROV I.V. *Nanostruct. Mater.* , 1997, vol. 9, pp. 477-80.
[5] WEI, Q., KECSKES, L., JIAO, T., HARTWIG, K.T., RAMESH, K.T., MA, E. *Acta Mater.*, 2004, vol. 52, pp. 1859-69.
[6] FARLIK, A., ONDRACEK, E. *Teórie dynamického tváření.* STNL-Nakladatelství technické literatúry, Praha 1968, 04-010-68.
[7] KUSSMAUL, K., SCHUELE, M. *Dynamic tensile tests on ferritic and austenitic steels with improved testing and measuring technique.* Journal De Physique III., Volume 4, Septembre 1994.

Transcom 2009, 22-24 June 2009
University of Žilina, Žilina, Slovak Republic

Destructive and non Destructive Methods for Testing of the welding joints on the thermoplastic

[*]Ivana Kulíková, [*]Viliam Leždík, [*]Jaroslav Bohinský, [**]Miloš Mičian
[*]SPP, a.s. Bratislava, 825 11 Bratislava 26, viliam.lezdik@spp.sk
[**]University of Žilina, Faculty of Mechanical Engineering, Department of Technological Engineering, Univerzitná 1, 010 26 Žilina, Slovak Republic, milos.mician@fstroj.uniza.sk

Abstract. The products of the plastic materials, which are used in industry, are the boom. It is growing mainly by the distribution or transport of different mediums (for example gas, water ...). It is important to deal with the quality of the welding joints of the thermoplastic material. This text describes the methods for testing of the welding joints of thermoplastic. We write about destructive and non destructive methods. Quality assurance of the welding joint is giving mostly of the customer request.

Keywords: the thermoplastic, the methods, the defect, destructive and non destructive, the welding joint.

1. Introduction

Quality assurance of the welding joint is giving mostly of the customer request. The data in generally valid instructions have to meet requirement. It is possible to use the following standards and regulations for the qualification and ranking the defects:

- the standard STN EN 14 728. The defects of welding joints of the thermoplastics. The qualification. The subject of this standard is qualification and description the defects. We can meet these defects in the welding joint of the thermoplastics,
- for ranking the quality of the welding joint of the gas pipeline, for example the standard STN EN 12 007-2,
- in year 2006 the company "Prvá zváračská, a.s. Bratislava (PZ, a.s.)" has published the technical rule TR 701 for creating the conditions for qualification of defects and for identification the degrees of quality of welding plastic joints. TR 701: The welding joints of thermoplastics. The defect qualification and identification the degrees of quality. The subject of this rule is to specialize a marginal values by appraisal the joints, to knot on STN EN 13 100-1 and STN EN 473, with take account on STN EN ISO 17659.

2. The visual test

The visual test is one of the most important methods of non destructive testing for materials and products. We use this test generally before other non destructive methods. The advantage of this method is a fact, that the information about defects of materials and products are immediate and we don´t need the interpretation of their indications, like in the other non destructive methods.

The visual test is the basic method for detection of external defects and profile defects. Its purpose is to make the activity, which can find and rank the qualitative properties of tested

surface, like an external defect, a profile defect, a position defect, a defect of finish. For this method we need to use just eyes, optical and other tools.
The basic requirement is sufficient knowledge of worker, who is practising the audit, about technology of production of checked product, about formation, kind, position of the defect, about methods of metering and knowledge of the criteria of assurance by decision about their acceptability. Apart from professional knowledge is important specification the workers vision properties, which need to be regular testing (standard STN EN 13100-1). The welding joints, which don´t answer of these criteria, don´t find useful and they need to be corrected.
On the Figure 1 are the examples of the most frequently effects by abutting welding, which were find by visual test on welding joints.

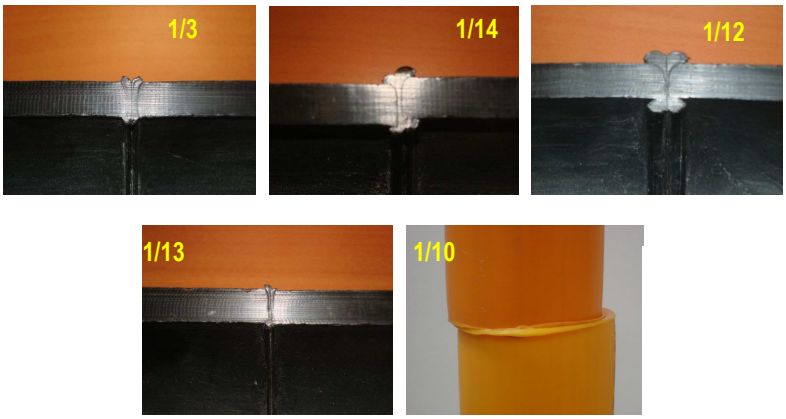

Fig. 1 The examples of the most frequently defects by abutting welding, which were find by visual test on welding joints.

Nr. of fault	The name of fault	The figure	The limits	
1/3	Notch during the production	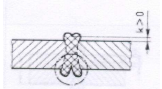	Not allowable	*The anotation: The clasification of defects of welding joints and the borders of accessibility are in the harmony with the technical rule TR 701 for quality degree „B“ high.* *e – the defect size [mm]* *b – the largeness of strapped weld [mm]* *b_1 – the largeness of strapped weld [mm]* *b_2 – the largeness of strapped weld [mm]* *s – the depthof the basic material [mm]*
1/10	The displacement of the connecting areas	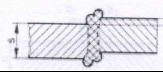	Allowable, when e ≤ 0,1.s, but max. 2 mm	
1/11	The angled yaw	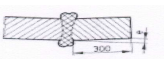	Allowable, when e ≤ 1 mm	
1/12	The tight camber effluence		Not allowable	
1/13	The under created effluence	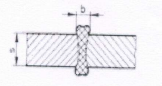	Allowable, when 0,6 s ≤ b ≤ 1,2 s	
1/14	The irregular welding effluence	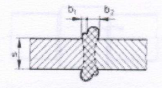	Allowable, when $b_1 \geq 0,7 . b_2$	
1/15	The high temperature destructive	X	Not allowable	

Tab. 1 Legend to Figure 1

3. The compressed test

Technical supervision from investor and incoming investor need to be by realization this compressed test. Gas pipeline must be clean before this test. The protocol about mode and final result of control needs to be given. This test must be realized with atmospheric pressure 600kPa on the smother gas pipeline, which is stored in the ground. The armatures and the demountable joints need to be uncovered. The pressure test is successful, if the pressure will not drop. The pressure can drop, because of the escape of experimental medium or the leakage of demountable joints. The pressure audit is also successful, if the leakages will repair.

4. The tensile test

We can use the tensile test for checking of front joints and flashing. The thermoplastic material can be filled, not filled or reinforced. The tensile test can we use for all welding modes.

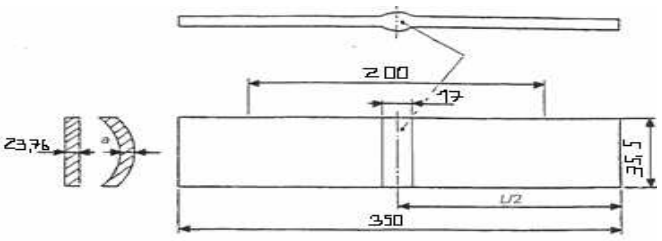

Fig. 3 The experimental body following the standart STN EN 12814-2

Experimental body is pulling in the line of its longitudinal axis by the constant speed to the moment, when this body will be broken or the material will creeping.
On the Figure 4 and 5 we can see the experimental machine LabTest 4.100 SP1 for the tensile test and the sample after the tensile test.

Fig. 4 The experimental Machine LabTest 4.100 SP1

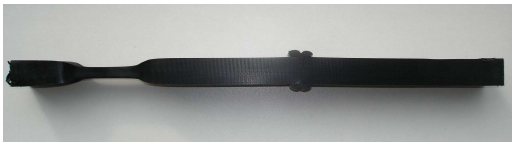

Fig. 5 The sample after the tensile test

5. The test by pressing

We can use the test by pressing for the appraisal of the characteristic of flashing in the plate and the pipe. The basic of this test is it, that we will split a forked joint on two same

parts. The samples are pressed for the appraisal of the characteristic of welding joint. We need to take two samples of every welding joint. The example of samples is on the Figure 6.

The audit by pressing is using just for the pipes, which were welding by adapting pipe. Standard STN EN 12814-4 is defining this audit.

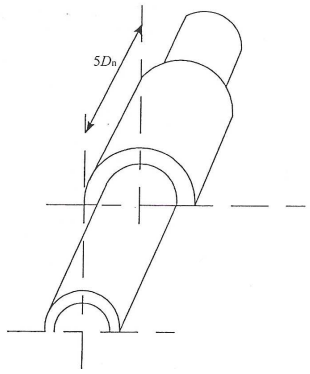

Fig. 6 The experimental sample for test by pressing

Fig. 7 The process of pressing

6. The macroscopic test

The macroscopic test is the exam of samples with eye or we can enlarge the samples just little. We use the macroscopic test for qualitative determination of macroscopic characteristic of welding joint.

7. Conclusion

The data in generally valid instructions for the quality of the welding joints have to meet requirement. Quality assurance of the welding joint is also giving of the customer request. The allegations of the welding joints must be in the project documentation or must be written by the worker, who has the certificate of the higher welding staff – The technologist of the plastic welding. The workers, who want to get this certificate, have to know everything about destructive and non destructive methods for testing the welding joints on the thermoplastic. We were described these methods in this article. The workers for visual test need to be qualified and certificate by the allegation of the standard STN EN 473 a STN EN 13100-1.

References

[1] Loyda, Šponer, Ondráček a kolektív: *Svařování termoplastů, Praha*, 2001.
[2] STN EN 13067: *Personál pre zváranie plastov. Skúšky odbornej spôsobilosti zváračov. Zváranie spojov z termoplastov*, 2004.
[4] STN EN 12814-2: *Skúšanie zvarových spojov. polotovarov – Časť 2 : Skúška ťahom*, 2002.
[5] STN EN 12814-4: *Skúšanie zvarových spojov. polotovarov – Časť 4 : Odlupovacia skúška*, 2002.

Transcom 2009, 22-24 June 2009
University of Žilina, Žilina, Slovak Republic

Analytical Model of Thermal Bending of Bars

Piotr Kurp
Kielce University of Technology, Centre of laser technologies for metals, Aleja Tysiąclecia Państwa Polskiego 7, 25-314 Kielce, Poland, E-mail: dominik_dudek@op.pl

Abstract. Thermal forming is a method of changing the shape of an element by heating with a moving source of heat e.g.: laser beam or flame head. In this method expected changes of shape will occur by thermal expansion phenomena. The plastic deformations which will appear after cool down the material are named real or permanent deformations. Permanent thermal deformation will occur only when the element or its part will be treat by thermal cycle. During this cycle element must be heated to specific temperature, and after cooled down to the beginning temperature.

During each of thermal treatment of materials e.g. welding, coating, laser hardening, heat treatment, heat cutting etc. this kind of deformations will occur. Shape changes in this types of treatment are objectionable and should be minimized. For the other hand we are interested in purposeful shape change of material by heat influence. Elaboration of analytical model of laser forming give us opportunity to control and predict the effects of this process.

In this paper analytical model of laser forming will be presented by use of laser upsetting mechanism. The experimental results of laser bending will be presented as well. It should be noticed that previously experiments were curried out using thickness of plate. In this experiment plate was bended in perpendicular direction to beam incidence surface. Further experiments should give us opportunity to elaborate analytical model of thermal forming of construction materials like: angle bars, T-bars, I-bars, C-bars etc.

Keywords: laser bending, laser forming, laser machining

1. Introduction

Homogeneity upsetting of material along path of heat source beam with minimal bending according to specific shortening is named forming by upsetting mechanism. Field of temperature should has possibly small gradient in perpendicular direction to beam. Zone of higher temperature shouldn't be to much vast simultaneously (because of thermal buckling conditions will appear) and surrounding area must be stiff enough. According to this conditions almost hole material under the beam will be straining during heating phase. Because of both short time of heat and stiffness of element it won't strain but will upset in strain zone. This upset induce its shortening. During cooling down bending torque will appear just after beam incidence point. This torque will make minimal deformation due to small temperature gradient presence.

Fig. 1 presents example of flat bar bending by using triangle (wedge) heat zone. Because of upsetting the material is shortening in perpendicular direction to heating path.

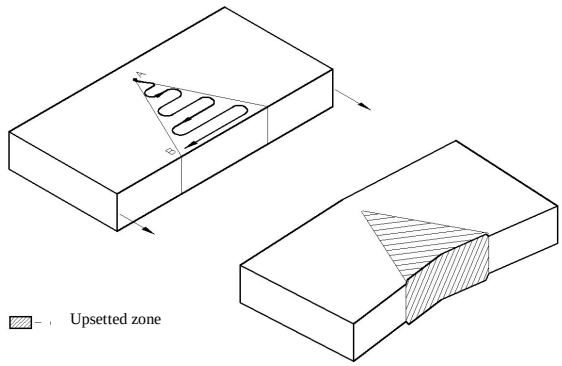

Fig. 1. Flat bar bending by upsetting mechanism.

2. Analytical Model for Laser Bending by Upsetting Mechanism by using Rectangular Cross-section Beam

Considering plate bending in its surface with using moving laser beam rectangular cross-section which dimensions are $b \times l$. Local heating of material makes upsetting of element. Plastic deformations appear (Fig. 2).

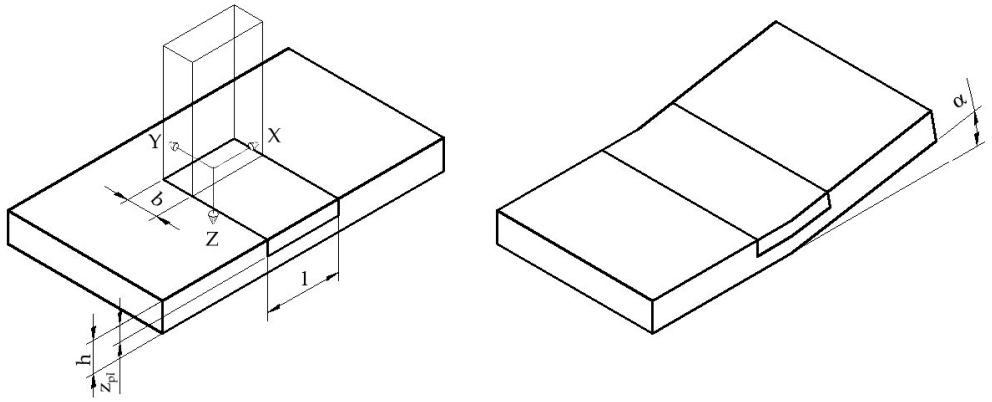

Fig. 2. Model of laser bending with rectangular beam cross-section and rectangular zone of plastifying.

Employed assumptions are:

- the temperature field is quasi-stationary related to the heat source,
- material parameters are not depended on temperature, with the exception of the yield limit, which is assumed to drop to zero at critical temperature T_{pl},
- continuous distribution of temperature is take into account in the strain zone,
- the bend angle is small,
- the Fourier number: $F_0=(\kappa b)/(\nu h^2)<1$.

where: h – plate thickness, κ - thermal diffusivity, ν - velocity of laser beam, b – wide of moving laser beam.

The plate is modeled as the Bernoulli-Euler beam. The stress distribution for elastic-plastic phenomena with imposed inherent strain due to material upsetting is described by the following equation [1]:

$$\sigma_x(z)=ER_r^C[\varepsilon_{0X}+(z-h_0)C+R_r^H \alpha_{th} \Delta T(z) H(z_{pl}-z)] \quad (1)$$

where: E – Young modulus, ε_{0X} – strain component characterizing material uniform shortening; $(z-h_0)C$ – strain component characterizing bending deformation, where C is the plate curvature in x direction from the center of gravity $z=h_0$; α_{th} – thermal coefficient of expansion; $\Delta T(z)=T(z)-T_0$; H(z) – Heaviside's unit function (H(z)=0 for z<0, H(z)=1 for z>0), z_{pl} – depth of the inherent strain zone; R_r^H i R_r^C – restrain rigidity coefficient at the heating stage and the cooling stage [2]. Plate's centre of gravity is $h_0=h/2$ – half of plate thickness.

The colder material in front of and on both sides of the heated area provides stiffness necessary for production material thermal upsetting during heating stage. Converse the whole heat source path contracts during cooling, which results the deformation. This effect can be express using this relation: $R_r^C << R_r^H$. In the considered model $R_r^H=1$ is assumed.

The moving heat source for sufficiently high velocity ν could be treated as a line heat source, which is thin in direction of velocity and finite width in the perpendicular direction (x) [3]. Dependence of peak temperature in material for rectangular cross-section beam is described by equation:

$$\Delta T(z) = T(z) - T_0 = \sqrt{\frac{2}{\pi e}} \frac{2AP}{\nu \rho cl(z + z_0)} \quad (2)$$

where:

$$z_0 = \sqrt{\frac{\kappa b}{2e\nu}} \quad (3)$$

where: A – laser beam absorption coefficient; P – power of the laser beam; l – width of rectangular cross-section laser beam; ρ - density of material; c – specific heat; λ - thermal conductivity coefficient.

Equilibrium conditions on the plate cross-section are described by equations:

$$\int_0^h \sigma(z)dz = 0 \qquad \int_0^h \sigma(z)zdz = 0 \quad (4)$$

This two above equations allow to find strain ε_0 and curvature C. from equilibrum conditions (4) we obtain solutions for the plate curvature, bend angle and shortening of the plate in the case of the fast moving heat source. This describes below formula:

$$C = \frac{3}{h}\alpha_{th}\Delta T_{pl}\theta_s\sqrt{\frac{2}{e}F_0}\left\{\ln\theta_s - \sqrt{\frac{2}{e}F_0}[\theta_s - \ln(e\theta_s)]\right\} \quad (5)$$

Formula for bend angle:

$$\alpha = Cl = 3L\alpha_{th}\Delta T_{pl}\theta_s\sqrt{\frac{2}{e}F_0}\left\{\ln\theta_s - \sqrt{\frac{2}{e}F_0}[\theta_s - \ln(e\theta_s)]\right\} \quad (6)$$

Formula for longitudinal deformation:

$$\varepsilon_{0X} = -2\alpha_{th}\Delta T_{pl}\theta_s\sqrt{\frac{2}{e}F_0}\ln\theta_s = \varepsilon_{0Z} \quad (7)$$

where ε_{0Z} – strain component characterizing material upsetting

The Fourier number is defined as:

$$F_0 = \frac{\kappa b}{\nu h^2} = \frac{\tau_h}{\tau_d} \qquad (8)$$

where: $\tau_h=b/\nu$ - the interaction time between the heat source and material; $\tau_d=h^2/\kappa$ - time of heat diffusion thru thickness of the material; L=l/h – dimensionless width of the rectangular laser beam; h – thickness of plate.

Surface temperature θ_s is expressed in dimensionless form as:

$$\theta_s = \frac{T_s - T_0}{T_{pl} - T_0} = \frac{2AP}{l\lambda(T_{pl} - T_0)}\sqrt{\frac{\kappa}{\pi\nu b}} \qquad (9)$$

where: $T_s=T(z=0)$ acc. To equation (2)

3. Modeling of bend in perpendicular direction to heat source incidence.

Previous chapter presented modeling of plate bending in parallel direction to moving heat source (according to thickness) with rectangular area of straining isotherm – this is the most simple model of bending. In real world area of straining isotherm could have any other shape. To simplify the calculations it is assumed that area cross-section could be triangle, ellipse, circle or any other shape which allow us to make calculations.

If we considering to bend plate in perpendicular direction to heat source incidence (in plate surface), we will assume that plate is heating using triangle straining area (Fig. 3). It is assumed that the temperature of straining is constant in heat zone thru whole thickness of plate also.

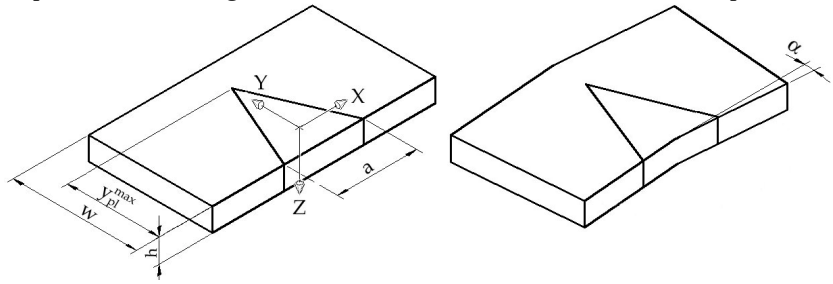

Fig. 3. Model of laser plate bending thru surface by using triangle zone of straining

Using equation (1) stress distribution could be described as [4]:

$$\sigma_x(x)=ER_\Gamma^C[\varepsilon_x+(y-w_0)C-R_\Gamma^H\varepsilon_{0X}\,H(y_{pl}(x)-y)] \qquad (10)$$

where: ε_x – strain component characterizing material uniform shortening in x direction; ε_{0X} – strain described by formula (7); w_0 – center of gravity of plate on their width w, $w_0=w/2$; other components are the same like in formula (1).

Using equilibrium equations (4) in y direction:

$$\int_0^w \sigma(y)dy = 0 \qquad \int_0^w \sigma(y)ydy = 0 \qquad (11)$$

From (11) we found formula for strain:

$$\varepsilon_x(x) = \varepsilon_{0X}\frac{y_{pl}(x)}{w} \qquad (12)$$

and curvature:

$$C(x) = -\frac{h\varepsilon_{0X}}{2J}[wy_{pl}(x) - y_{pl}^2(x)] \qquad (13)$$

where: J – moment of inertia in relation to center of gravity $J=hw^3/12$.
With the formula [4]: $$\alpha = \int_0^x C(x)dx \qquad (14)$$

The overal equation for bending angle is:

$$\alpha = -\frac{h\varepsilon_{0X}}{2J}[w\int_0^a y_{pl}(x)dx - \int_0^a y_{pl}^2(x)dx] \qquad (15)$$

Because of integrand $y_{pl}(x)$ describes geometry of strain zone, we could calculate bending angle. For triangle strain zone it is:

$$\alpha_\Delta = -h\varepsilon_{wz} a y_{pl}^{max} \frac{3w - 2y_{pl}^{max}}{12J} \qquad (16)$$

After substitution ε_{0X} (7) and $J=hw^3/12$:

$$\alpha_\Delta = 2\alpha_{th}\Delta T_{pl}\theta_s\sqrt{\frac{2}{e}F_0}\ln\theta_s a y_{pl}^{max}\frac{3w - 2y_{pl}^{max}}{w^3} \qquad (17)$$

If obtuse angle is constant, α_Δ will be maximum for $y_{pl}=w$
We can calculate equation for rectangle strain zone in the same way:

$$\alpha_\square = 2\alpha_{th}\Delta T_{pl}\theta_s\sqrt{\frac{2}{e}F_0}\ln\theta_s a y_{pl}^{max}\frac{w - y_{pl}^{max}}{w^3} \qquad (18)$$

$\alpha_\square$ will be maximum for $y_{pl}=w/2$

4. Experimental plate bending in perpendicular direction to beam incidence surface.

The aim of experiment was laser's plate bending in perpendicular direction to beam incidence surface and comparison results with theoretical model. The probes were made from St3 steel (carbon steel). Dimensions of probes: 100x50x2 [mm]. Probes were heated by laser rectangle beam 2x10 [mm] by triangle (Fig 4a) and rectangular mask (Fig 4b) two times both one and second side (four times per one probe). Experiment was performed by Trumpf TLF-6000 laser with segmented mirror head.

For triangle zone $y_{pl}=w$ (probe No 1), for rectangle zone $y_{pl}=1/2w$ (probe No 2). After experiment the bended angle were measured.

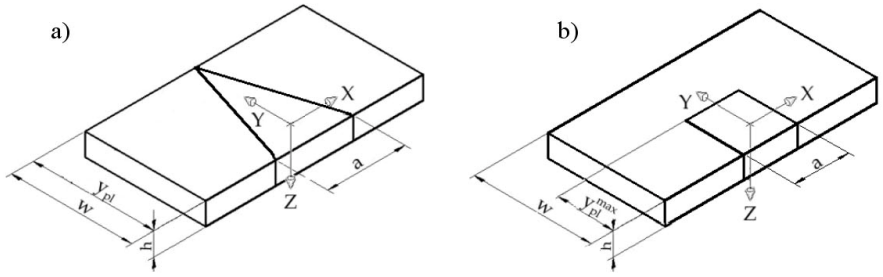

Fig. 4. Probe with triangle a) and rectangular b) strain zone.

Measured bend angle for probe No 1 is α_Δ=3,18°, and for probe No 2 $\alpha_\square$=2,03°. For one path of laser heating α_Δ=0,795°, $\alpha_\square$=0,508°.

The theoretical bending angle was calculated. Probe number 1 – triangle strain zone, equations: (17), (8) and (9).

Parameters:

Dimensions of probe: a=0,027 [m]; y_{max}=0,05 [m]; w=0,05 [m]; h=0,002 [m].

Material constants: λ=40 [W/mK]; ρ=7850 [kg/m^3]; c=452 [J/kgK]; α_{th}=0,013 [mm/mK]

Laser material processing parameters: A=0,6; P=1500 [W]; ν=0,0125 [m/s]; ΔT_{pl}=600 [K]; b×l=0,002 [m] × 0,01 [m]

Using heat diffusion equation $\kappa=\lambda/\rho c$: $\kappa=1{,}13\times10^{-5}$ [m^2/s]

After substitution F_0, θ_s and other data to equation (17), and after recalculation onto degrees we have α: α_Δ=0,82°.

Probe number 2 – rectangle strain zone, equations: (18), (8) and (9).

Parameters:

Dimensions of probe: a=0,025 [m]; y_{max}=0,025 [m].

Other parameters are exactly the same like for probe number 1.

After substitution F_0, θ_s and other data to equation (18), and after recalculation onto degrees we have α: $\alpha_\square$ =0,38°.

5. Conclusions:

1. Real measured angles are: α_Δ=0,795°, $\alpha_\square$=0,508°, and theoretical angles are: α_Δ=0,82°, $\alpha_\square$ =0,38°. According to this data it is concluded that applied model to bend simple bars describes real bend angle very well.

2. There is opportunity to model compound bars by specific heating zone.

3. Experiment was performed by laser as an heating source, but another heating sources could be used to bend.

References:

[1] Mucha Z., *Efficiency of Material Laser Forming*, International Workshop on Thermal Forming and Welding Distortion, Bremen, Germany, 2008, p. 55-64

[2] Taira S. Ohtani R., *Theory of high temperature resistance of materials*, Metallurgija, Moskwa, 1986

[3] M.F. Ashby, K.E. Easterling, *The transformation hardening of steel surfaces by laser beams – I. Hypoeutectoid steels*, Acta Metall, Vol. 32, No 11 (1984), p. 1935-1948

[4] Mucha Z., *Modelowanie i eksperymentalne badania kształtowania laserowego materiałów konstrukcyjnych*, Kielce, 2004

Transcom 2009, 22-24 June 2009
University of Žilina, Žilina, Slovak Republic

FEM Simulations of ECAP Process with Backpressure

[*]Michal Kvačkaj, Róbert Kočiško
[**] Tibor Donič
[*]Technical University of Košice, Faculty of Metallurgy, Department of Metal Forming, Vysokoškolská 4 040 00 Košice, Slovakia, michal.kvackaj@tuke.sk
[**]University of Žilina, Faculty of Mechanical Engineering, Department of Applied Mechanics, Univerzitná 1, 01 026, Žilina, tibor.donic@fstroj.uniza.sk

Abstract. The purpose of equal channel angular pressing (ECAP) is obtaining the ultra-fine grained (UFG) materials. For practical application, it is important to understand the sample deformation behavior which is affected by many parameters, such as geometry, friction between sample and die, corner gap shape, back pressure and back pressing plunger shape. Because most deformation occurs during the pass at the die corner, we used finite element analysis (FEM). The effects of external force (friction, back pressure) and die corner shape on sample deformation were studied to improve the quality of the ECAP process. A new index factor was defined and suggested from the analysis of sample deformation during ECAP to get the strain homogenity and uniform microstructure. Variation of the suggested index factor is also studied to account for the effects of material properties and back pressure produced by friction and back pressing plunger. In this study it showed that the influence of back pressure shape was one of the strongest factors to be controlled for the improvement of ECAP process.
ECAP is one of the most promising processes to form UFG materials. The material deformation is affected by die geometry, material behavior, friction and back pressure. The effect of back pressure on deformation behavior, effective strain and deformation load were analyzed by using finite element software named DEFORM 3D.

Keywords: equal channel angular pressing; αfinite element analysis; back pressure; strain distribution

1. Introduction

Severe plastic deformation (SPD) is an effective method for strengthening of metals and alloys.

UFG materials are currently of great scientific interest due to their unusual mechanical and physical properties. It is possible to develop the UFG structures in metallic materials by a process of severe plastic deformations (SPD) [1]: very high plastic deformations (true strain >4) are required at ambient temperature [2]. It is advantageous to produce such materials relatively cheaply in bulk form. For the bulk production of highly strained samples, ECAP technique was initially developed by Segal et al. [3].

The material deformation during the ECAP is affected by the nonlinearity of metallic materials, the geometry of die, the temperature, the friction between the sample and the die, and the shape of plungers. The early researches were executed only for basic die design parameters such as the internal angle, ϕ; between the two die channels and corner curvature angle, ψ (Fig. 1) [3].

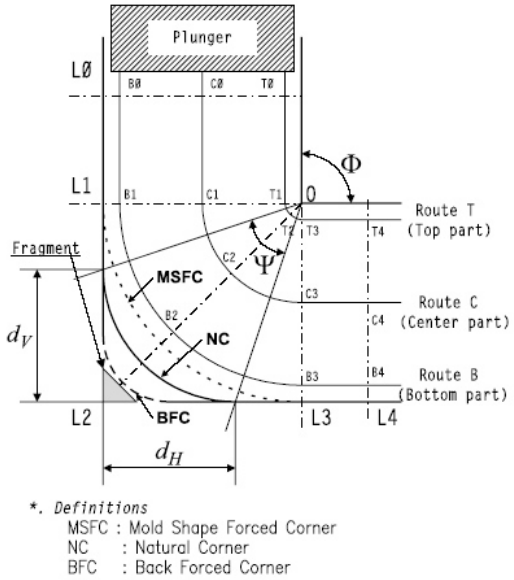

Fig.1[3]. The state of corner during the ECAP process

According to Segal [3], the deformation behavior during ECAP was thought to be homogeneous in shear plane within the majority of the sample. The plastic strain per pass, Δε; is given by Eq. (1):

$$\Delta\varepsilon = \frac{2}{\sqrt{3}} \cot\left(\frac{\Phi}{2}\right) \tag{1}$$

However, the estimated plastic strain value (/Φ=90°,Δε=1,155) is only an average value, and it can not explain the actual deformation material behavior and their strain heterogenity in cross-section of sample.

To understand the material behavior under ECAP, various researches were performed by computer simulation technique. Prangnell et al. [4] presented a simplified finite element model, which had been used to investigate the ECAP process. Bowen et al. [5] studied the deformation of ECAPed sample under various conditions by both FEM analysis and experiments. Kim et al. performed the computer simulation of ECAP by using DEFORM-2D software. Kim et al. used the DEFORM software to understand stress, strain variation during the ECAP [6], die gap corner formation which affected by material strain hardening rate in ECAP [7], and die geometry effect during ECAP [8].

For practical application of ECAP process, it is important to find the best working condition. Finite element method is an effective tool to predict the material behavior and design of ECAP mold. Liu et al. [9] performed finite element simulation of changing channel pressing to design changing channel mold which can avoid tensile mode of straining. Many researches [4_/8] have been done for the study of ECAP process and material behavior but not for a quality criterion of the ECAPed sample. The criterion is a basis for the practical application. The geometry of die corner is also an important factor for the control of sample microstructure, and the application of the back pressing plungers should be considered to develop further the technology of ECAP process.

2. Experiments and Analysis

In this study was used DEFORM 3D software for simulation of ECAP process with back pressure. Focusing on the angle of back pressure plunger in diferent orientation and also various pressure of plunger. Material used for FEM simulation was Brass alloy CDA - 110 (20°C - 900°C). Pressure power of upper spine was 64kN, constantly. Fig.2 shows ECAP process without back pressure. Fig.3 represent FEM simulation of ECAP process with back pressure power of F=5kN and back pressure inclination α=90° . ECAPed sample with back pressure power of F=3,6kN a inclination α=60° is showed on Fig.4.

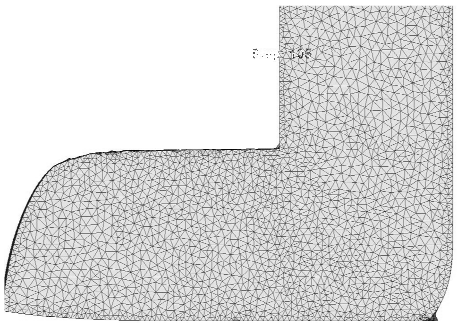

Fig.2. ECAP process without back pressure

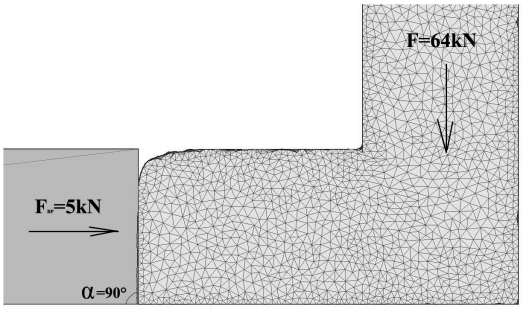

Fig.3. ECAP process with back pressure of 5kN and angle 90°

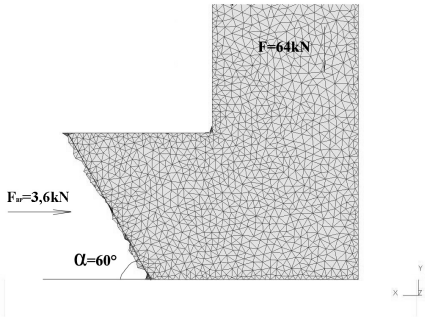

Fig.4. ECAP process with back pressure of 3,6kN and angle 60°

3. Conclusion

Finite element analysis and experiment on the sample deformation during the ECAP has been carried out to understand the effects of material flow, with and without back pressure application.

The following conclusions were made; The corner gap of the sample was influenced by material properties, temperature, friction and back pressure. The deformed sample has corner shapes of parabolic and the size is varied with the material and back pressing force. The die corner shape with circular corner and larger radius than that of NC (natural corner) affected the deformation behavior.

References

[1] K. Nakashima, Z. Horita, M. Nemoto, T.G. Langdon, Mater. Sci. Eng. A281 (2000) 82_87.
[2] K. Nakashima, Z. Horita, M. Nemoto, T.G. Langdon, Acta Mater. 46 (5) (1998) 1589_1599.
[3] V.M. Segal, Mater. Sci. Eng. A197 (1995) 157_164.
[4] P.B. Prangnell, C. Harris, S.M. Roberts, Scripta Mater. 37 (7) (1997) 983_989.
[5] J.R. Bowen, A. Gholinia, S.M. Roberts, P.B. Prangnell, Mater.Sci. Eng. A287 (2000) 87_99.
[6] H.S. Kim, Mater. Sci. Eng. A315 (2001) 122_128.
[7] H.S. Kim, M.H. Seo, S.I. Hong, Mater. Sci. Eng. A291 (2000) 86_90.
[8] H.S. Kim, M.H. Seo, S.I. Hong, J. Mater. Process. Tech. 113 (2001) 622_626.
[9] L. Zuyan, L. Gang, Z.R. Wang, J. Mater. Process. Tech 102 (2000) 30_32.

Transcom 2009, 22-24 June 2009
University of Žilina, Žilina, Slovak Republic

Observation of Surface Temperature of Acrylic Bone Cement During Polymerization

[*]Henrietta Lelovics, [*]Róbert Seewald, [**]Libor Nečas
[*] University of Žilina, Faculty of Mechanical Engineering, Department of Materials Engineering, Univerzitná 1, 01026 Žilina, Slovakia, {henrietta.lelovics, robert.seewald}@fstroj.uniza.sk
[**] Orthopedics and Traumatology Clinics, Teaching Hospital in Martin, Kolárova 2, 03659 Martin, Slovakia, necas@mfn.sk

Abstract. Today's surgical bone cements are mainly based on acrylic polymers and copolymers. After mixing the liquid and powder components together the radical exothermal polymerization begins when the PMMA beads are gradually covered with polymerizing monomer. It was shown, that the amount of generated heat depends on the cement mantle thickness and may cause destruction of the surrounding tissues. In this paper the maximum (peak) surface temperatures during the polymerization of differently thick acrylic bone cement samples and times pertaining to this values are presented.

Keywords: bone cement, polymerization, temperature.

1. Introduction

Acrylic bone cements are used in orthopedic surgery (arthroplasty) since the 60's of the last century, when Charnley used it first for fixation of the acetabular and femoral prosthesis components. The main role of the bone cement is to transfer the loads from the prosthesis to bone and tissues [1].

The carefully cleaned bone canal, where the prosthesis component is inserted, is filled with the prepared viscous cement dough which exothermally polymerizing in vivo. Free radicals break the covalent C=C bonds of the monomer, allowing them to bind to the lengthening polymer chains. This reaction releases 52 KJ/mole of monomer, equating to heat production of 1,4 to 1,7 x 10^8 J/m^3 of cement [2].

Collagens denature with prolonged exposure to temperatures in excess of 56°C and the risk of causing thermal damage to bone has been raised by several authors [3, 4].

2. Material and Experimental Methods

2.1. Bone Cement SmartSet HV

Bone cement SmartSet HV was used as an experimental material, its composition is specified below in the Tab. 1.

The liquid component is a colorless, flammable liquid with a distinctive odor. Its major component is the monomer Methyl Methacrylate. Hydroquinone is a stabilizer preventing premature polymerization which may occur when the liquid is exposed to heat or light. N,N-Dimethyl-p-toluidine is added to promote cement polymerization following mixing of the powder and liquid component.

The powder component is a white, finely divided powder composed of a Polymethyl Methacrylate based polymer. Di-Benzoyl Peroxide initiates cement polymerization when the powder and liquid components are mixed. The powder component moreover contains the radiopaque agent Zirconium Dioxide.

Bone Cement Powder			Bone Cement Liquid		
Methyl Methacrylate/ Methyl Acrylate Copolymer	Di-Benzoyl Peroxide	Zirconium Dioxide	Methyl Methacrylate	N,N-Dimethyl-p-toluidine	Hydroquinone
84 (%w/w)	1 (%w/w)	15 (%w/w)	97,5 (%w/w)	≤ 2,5 (%w/w)	0,0075 (%w/w)

Tab. 1. Quantitative composition of the bone cement SmartSet HV

2.2. Sample Preparation

The cement samples were prepared by hand mixing technique with exact timing under the next conditions: temperature: 21oC, mixing time: 30s, waiting time: 60s, frequency of mixing: 1Hz.

The bag containing the powder component was opened and the entire contents were emptied into a suitable, clean, dry mixing ceramic bowl. Then the ampoule containing the liquid component was opened and the entire contents were evenly poured onto the powder in the mixing bowl. The dough was then mixed carefully to minimize the entrapment of air. After 90 seconds from the beginning of mixing procedure the dough was taken into hands and kneaded for a few seconds. After that the cement mass was put into the rotational rheometer preheated to 37oC with a cylindrical parallel plates about 25mm diameter, and was trimmed to 1, 2, 4 and 5mm high (the optimal cement mantle thickness in vivo is 2-5mm). Then 4 surface temperature measurements were made on the differently thick samples. The sample straining and heating options were during the measurements turned off, only the temperature courses were monitored.

3. Results

The measured surface temperature courses of the 1, 2, 4 and 5mm thick samples are represented in Fig. 1 to Fig. 4 and the averaged values of peak temperatures and times required to obtain the peak temperatures are represented in Tab. 2.

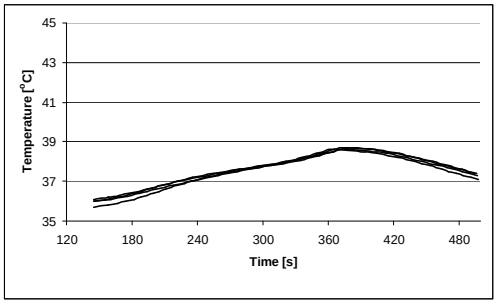

Fig. 1. Surface temperature courses of the samples with 1mm thickness

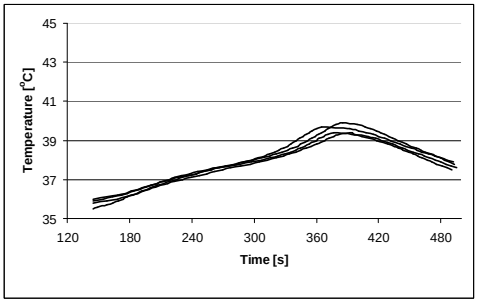

Fig. 2. Surface temperature courses of the samples with 2mm thickness

Before the measurement the measuring system was preheated to 37°C but opening the chamber, positioning and trimming the samples caused drop of the default temperature of the system to 35,5 – 36,1 °C at the beginning of the measurements.

It's clear, that the amount of produced heat during the cement polymerization depends on the sample thickness. The lowest peak temperature was recorded for the samples with 1mm thickness and the highest for the 5mm thick samples.

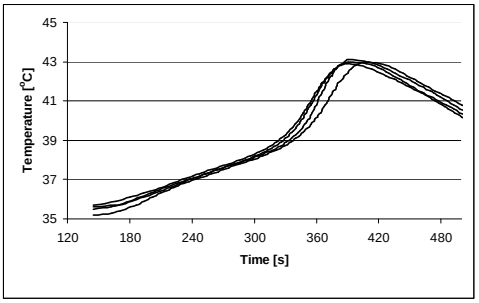

Fig. 3. Surface temperature courses of the samples with 4mm thickness

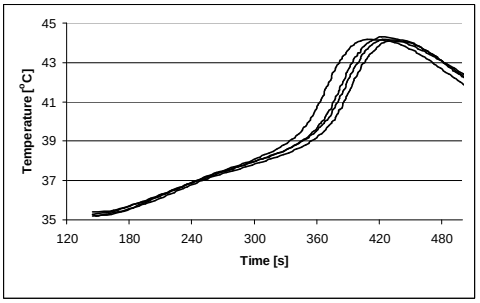

Fig. 4. Surface temperature courses of the samples with 5mm thickness

Sample thickness [mm]	Peak temperature [°C]	Time [s]
1	38,65 ± 0,03	373 ± 4
2	39,6 ± 0,12	381 ± 6
4	43 ± 0,04	394 ± 4
5	44,2 ± 0,04	421 ± 4

Tab. 2. Averaged values of peak temperatures and times required to obtain the peak temperatures

The measured highest peak temperature under the selected conditions was 44,2 ± 0,04 °C which cannot cause bone tissue destruction. The time required to obtain the peak temperature from the beginning of mixing procedure is also different and raises by the sample thickness. It can be due to the low thermal conductivity of the polymerizing cement. The required time to obtain the peak temperature was 373 ± 4 s for the samples with 1mm thickness up to 421 ± 4 s for the samples with 5mm thickness.

There was no distinct correlation observed between the rising peak temperatures, time and the sample thickness. For exact explanation of the obtained temperature and time results is necessary to attend to the chemical and physical processes during the polymerization of the tested bone cement.

4. Conclusions

In this study the temperature courses of polymerizing acrylic bone cement were monitored on the surfaces of the samples using a parallel plate measuring system of the rotational rheometer.

It was shown, that the lowest peak temperature was 38,65 ± 0,03 °C and it rose with increasing sample thickness up to 44,2 ± 0,04 °C but this value still can not cause bone tissue necrosis.

Moreover was determined, that the coarser the cement sample, the longer the time required to obtain the peak temperature on its surface.

Acknowledgement

This research has been partially supported by the Cultural and Educational Agency of the Ministry of Education of the Slovak Republic, grant No 3/5/5200/0, Scientific Grand Agency of the Ministry of Education of the Slovak Republic and the Slovak Academy of Sciences, grant No 1/4096/07 and grant SK - MAD – 01506. This support is gratefully acknowledged.

References

[1] LELOVICS H, LIPTÁKOVÁ T. *Comparison of some mechanical and rheological properties of bone cements.* 25th Danubia-Adria Symposium on Advances in Experimental Mechanics, 2008, 157-158.

[2] J. C. J. WEBB, R. F. SPENCER. *The role of polymethylmethacrylate bone cement in modern orthopaedic surgery*. Journal of Bone and Joint Surgery - British Volume, Vol 89-B, Issue 7, 851-857.

[3] DIPISA JA, SIH GS, BERMAN AT. *The temperature problem at the bone-acrylic cement interface of the total hip replacement*. Clin Orthop 1976;121:95–8.

[4] MJOBERG B, PETTERSSON H, ROSENQVIST R, RYDHOLM A. *Bone cement, thermal injury and the radiolucent zone*. Acta Orthop Scand 1984;55:597–600.

Transcom 2009, 22-24 June 2009
University of Žilina, Žilina, Slovak Republic

Presence of Inclusion Trapped in Ceramic Pressed Filters

Vladimír Magát, Dana Bolibruchová
*University of Žilina, Faculty of Mechanical Engineering, Department of Technological Engineering,
Univerzitna 2, 01026 Žilina, Slovakia,
{ vladimir.magat, danka.bolibruchova }@fstroj.uniza.sk

Abstract. In last few years was published many articles about filtration, but many of those articles are advertising stuff. However, the question of real efficiency of filtration is still not completely answered. Influence of filtrtion proved on tenslile properties and mikrostrukrures. The aim of this article is analyse of presence of inclusion in top, middle and bottom part of filter and causes of their ceration.

Keywords: filter, filtration, aluminium alloy

1. Introduction

Increasing of quality of castings and decreasing of fail castings in last few years is possible only with using new and effective technolies. One of these new technologies is filtration. Filtration is defined as a process of catching inclusions in filters, while pure metl flow into the gating system. Filters can be placed in gating system and in some special cases can even replace one of the basic part of gating system, for example the sprue. Because many of articles published about filtration are advertising, the objectivity of those articles is not sure. Therefore is the aim of this work to analyze ability of filters to catch inclusions and observating the mirsostructure of ally at the top, in the middle and at the bottom part of filter .

2. Experiment

For experiment was used material: : $AlSi_{12}MgMn$ (STN 42 4330).

This alloy has an extraordinary good mechanical properties, good stain resistance and cast properties. Thanks to these properties is widely used for thin wall castings in automobile industry and aircraft industry. Chemical composition of used alloy is listed in Tab. 1.

	Si	Fe	Cu	Mn	Mg	Ni	Pb	Sn	Ti
[%]	11,28	0,1971	0,0026	0,2316	0,3313	<0,0016	0,0411	<0,0024	0,021

Tab. 1. Chemical composition of $AlSi_{12}MgMn$.

For filtration was used ceramic pressed filter. Characteristics of this ceramic pressed filter is listed in Tab. 2.

Thickness of filter [mm]	Number of holes	Diameter of hole [mm]	Surface area of holes [mm^2]
10	314	$2,2^{\pm 0,15}$	1194

Tab. 2. Characteristics of used filter.

Samples were poured at temperature 730°C into the metal form. Aluminium metl was few times remelted. The reason for remeltig was regulated pollution of the melt. The melt was filtered in 1, 3 and 6 melting. Filter was placed in filler at the entrance into the gating system, as it is shown in Fig. 1.

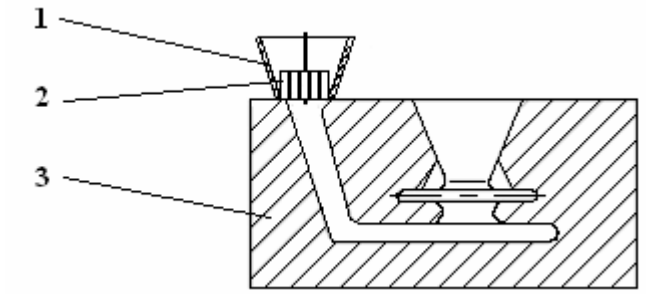

Fig. 1. The placing of filter: 1 – filler, 2 – filter, 3 – metal form.

After solidification were filters ready for taking of samples. Samples for observating of microstructure were carefully taken from the top, middle and bottom part of filter,as it is shown in Fig. 2.

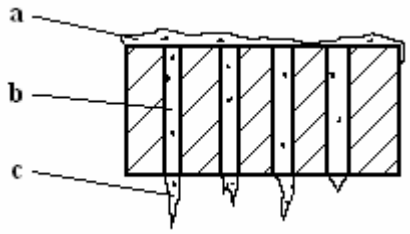

Fig. 2. The areas of taking samples: a – top of the filter, b – middle of the filter, c – bottom of the filter.

From mentioned melts were perfomed tests of mechanical properties, like a tenslile strenght. Test bars were poured with and without filters. This can give as informations about influence filtration to the mechanical properties. The results of these tests are listed in fig. 3 and Fig. 4.

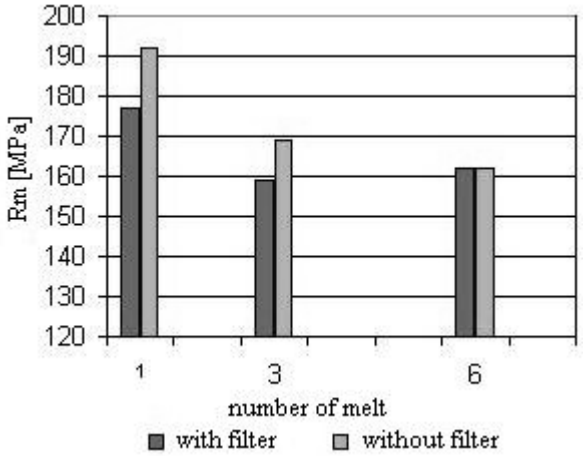

Fig. 3. The results of tensile tests.

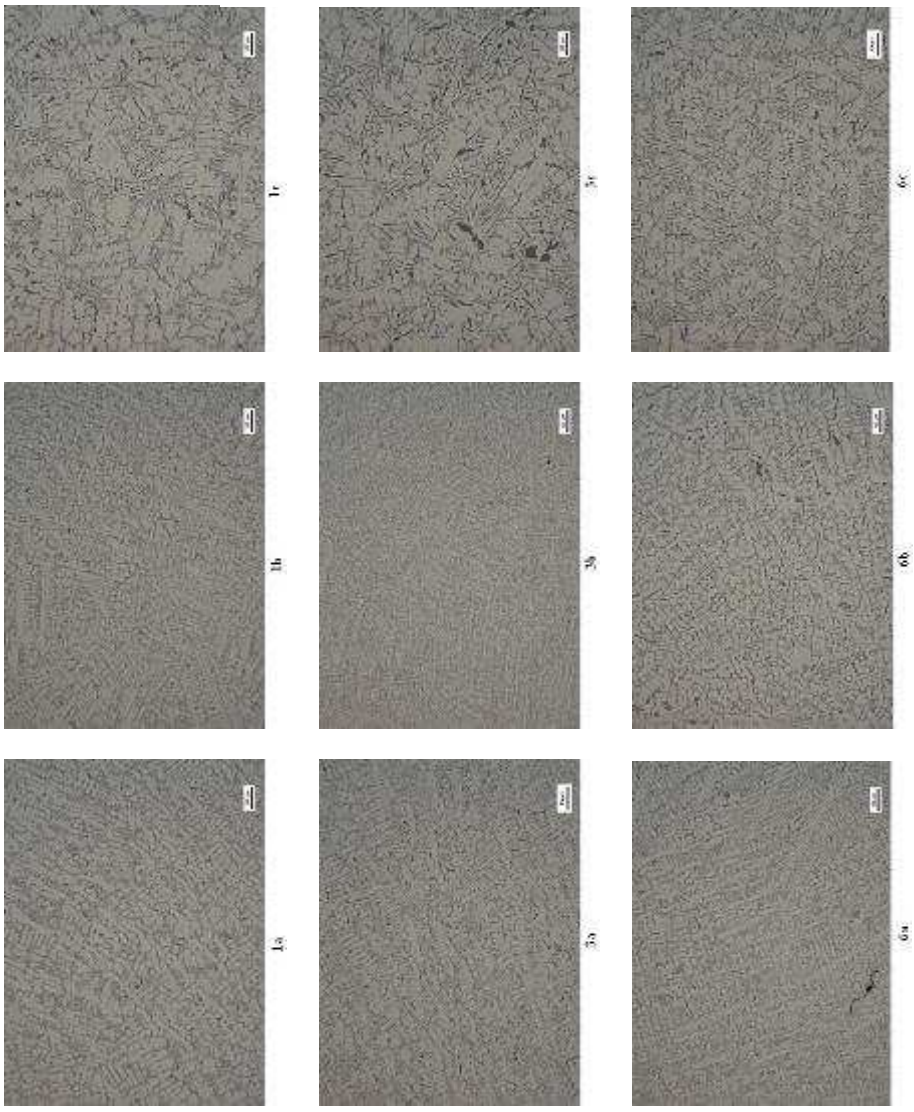

Fig. 4. Microstructures of melted alloy

Microstructure of once melted samples from the top (Fig. 4 – 1a) and middle (Fig. 4 – 1b) of filter is similar. There are small dendrites of alpha phase and small needles of eutectic silicon. The sample taken from the bottom (Fig. 4 – 1c) of once melted alloy is typical with biger size dendrites of alpha phase and biger needles of eutectic silicon. Observed places of samples from once melted alloy were without inclusion. In the case of three times melted alloy is the microstructure similar as in the case of once melted alloy. There are small dendrites of alpha phase and small needles of eutectic silicon at the top (Fig. 4 – 3a) and in the middle (Fig. 4 –

3b) of filter. At the bottom of filter of three times melted sample was the increase of size of structural elements observed again. In the figure made at the top of six times melted alloy (Fig. 4 – 6a) is obvious inclusion. This inclusion with its apperance looks as oxidic inclusion. This oxidic inclusion could be pulled down with the flow of melt during pouring. The microstructure of six times melted alloy at the bottom of filter (Fig. 4 – 6c) is with its appearance similar as microstructures in the figures 4 – 1a and 4 – 3a.

3. Conclusion

Microstruktures made at the top of once, three times and six times melted alloy is similar. There was not observed ares with inclusions, so this fact does not prove the theory about creation of filtration cake at the top of the filter. But there is chance that our places of observation does not interfered with places with filtration cake. It stands to reson that filtration has an influence on the microstructure. The samples taken from the bottom of filters have biger size of dendrites of alpha phase and biger needles of eutectic silicon in all cases. This increace of structural elements could be casued by different area of solidification of melt. The samples taken from the top and middle of filter have solidificated in the filter, while the samples taken from the bottom of filter have solidificated behind the filter. However, filtration has good influence to the mechanical properties. In all cases filtration caused increase of tensile strenght while non filtrated samples has the amount of tensile strenght lower.

Acknowledgement

This wokr was created thanks to grant project KEGA n. 3/5197/07, KEGA n. 1/0684/08 and VEGA n. 1/4098/07.

References

[1] BOLIBRUCHOVÁ, D. – TILLOVÁ, E.: *Zlievarenské zliatiny Al-Si*., 1. vyd. EDIS – ŽU v Žiline, 2005

[2] BRUNA, M. – KANTORÍK, R. – BOLIBRUCHOVÁ, D.: *Komplexné metalografické hodnotenie hliníkovej zliatiny po filtrácií*., Slévarenství, 2008, č.7-8, s. 337-339. ISSN 0037-6825

[3] FUOCO, R. - CORREA, E. R. – BASTOS, M. A. – ESCUDERO, L. S.: *Characterization of Some Types of Oxide Inclusions in Aluminium Alloy Castings*. AFS Transactions, n.85, 1999, s. 287 - 284

Transcom 2009, 22-24 June 2009
University of Žilina, Žilina, Slovak Republic

Determinative Factors in Thermic Metal Cutting

*Ing. Michal Maťko, **prof. Ing. Anna Mičietová, PhD.
*Univesity of Žilina, Faculty of Mechanical Engineering, Department of Machining and Manufacturing Technique, Univerzitná 1, 010 26 Žilina, Slovakia, michal.matko@gmail.com
** Univesity of Žilina, Faculty of Mechanical Engineering, Department of Machining and Manufacturing Technique, Univerzitná 1, 010 26 Žilina, Slovakia, anna.micietova@fstroj.uniza.sk

Abstract. This paper deals with factor affecting the cutting process when appliocation progressive non-conventional methods of maching as Electro Discharge Machining, Plasma beam machining, Laser beam machining, Electron beam machining. The paper presents the survey of the most significant aspects of these processes.

Keywords: metal cutting, plasma, laser

1. Introduction

Electrothermal or thermal proceeding use for stock removal like a primary source heat energy, which is providing highenergic jets of electron, photons, ions and plasmas. For this group belong these types of progressive machining as Electro Discharge Machining, (EDM), Plasma beam machining (PBM), Laser beam machining (LBM), Electron beam machining (EBM) [2]. In the present are uncoverable also progressive machining, of which plasma beam machining and laser beam are the most often using and they have uncoverable place, mainly for material cutting and in the case of plasma for application of different coatings in mechanical production. A big expansion of plasma and laser machining became in 80th years of last century and continue till today. At the begining it was computer equipment, which let use a great opportunities of laser machining and do better plasma machining. Later on, with production growing and elevating congruence between producters these manufacturing establishment and also between companies, which are using these progressive machining, became price-cutting and quality elevating. This all had and still have a big expansion of plasma machining and from the end of 90th years of last century mainly laser machining. Plasma and laser machining have their anvantages and disadvantages. Each can be used for machining for other material, form and get by them different quality of machined work surface. And these differents together with different machining costs are giving possibility of right choice machining methods.

2. Affecting Factors by Laser Cutting

Also by laser beam cutting exist factors, which have effect on finish cut quality.

• Laser power:

Alone laser power doesn´t define just what a material width is possible to cut, but also what a cut quality. For bigger thickness laser has to cut by impulse mode instead of continual mode, what make cut quality worse.

• Constant power:

During whole period of roughing work piece is necessary to provide constant laser power. Power variaton make worse cut quality. Very important is also, that laser power can´t come down during whole duration. We are talking about long-lasting laser power.

• Divergent angle:

Divergence *1 mrad* means to widen laser beam about *1 mm* for length *1 m*. This angle has a big importance on machine with flying optics. When we want to get a linear cut quality in different distances, we have to keep divergence on the lowest figure.

• Kind of gas and his pressure :

Kind of gas is one from the most importnat factors, which are affecting cut quality. Axcept for a right choice cutting gus is very important gas cleanness and his pressure. For example nitrogen cleanness to require *99,999%*, because already minimum oxigen quantity induce creating from oxidate layer on cutting edge. Gas pressure isn´t change only with material thickness, but also depending up used gas. Pressure of activ gas will be different than inert gas.

• Focus point position: Focus point position has basic affect on cutting quality. For every cutting method is choosen different focus point position.

• Cutting speed: Used cutting speed affect mainly thickness and material of work piece, laser power too. Cutting speed is always compromise, by which come to the best quality of cut with the highest productivity. Low cutting speed affecting low productivity and big thermal affected locality, by contrast high cutting speed is reason of low class face on cutting edge.

• Laser´s optic: On the cut quality have a big effect whole optic compilation of laser cutting machine. The troubles can become mainly if operating mirrors or focus lens are dirty and for setting laser beam toward of nozzle hole.

• Choice of the right nozzle: Choice of the right nozzle for concreit processing is very important. For highpressure cutting are using nozzles with bigger hole than for normal cutting.

• Material assigned for laser cutting: For secured cut quality, assigned material has to be up to standard, which producer of laser machine requires. These requirement can to split as follows:
- content of alloying elements, material structure, material surface, working of surface, beams reflectiveness, heat conduction, fusion point.

• Geometery of work piece: Geometery of work piece influence for finish required geometery exactness and abrasiveness of cutting surface. The troubles causes acute angles and small holes (diameter $\geq$ thickness of metal plate). These elements are cutting with reduced laser power, with reduced moving, when in urgent cases are other parameters modified.

3. Affecting Factors by Plasma Cutting

• Choice the right plasma and secondary gas (for burnets with gas stabilization): For different qualities and material thickness is adequate different kind of plasma and secondary gas.

• Cutting parameters: Also for cutting metal materials by plasma, as for all machinings, cutting parameters are very important. Important is cutting speed and current intensity and also gas pressure. Mainly cutting speed and current intensity are parameters, which are affecting a cut quality in big size. These cutting parameters are setting depends by material quality and his thickness. In general deal, that for heightening cutting current is possible to make cutting speed higher and by this reach to improve a productivity.

• Choise the right nozzle of plasma burnet: Choose the right nozzle is very important and depends on material quality.

• Material assigned for cutting: When we want make the best cut quality, can parameters to split as follows material surface, working of surface, eletrical conductivity, heat conduction, fusion point.

4. Laser Cutting of Metal

Cutting process proceed on basic interaction of laser beam, cutting gas and cutting material. Laser, which effects on cut face, must melting-down material on heat, which is become to change from solid phase to liquid phase and faseous phase. Cutting of material is the most expanded and the most popular laser technology for almost all sorts of constructions materials. For cutting steels are prioritizing CO_2 lasers, which are the most economical for material thickness from *6 to the 7 m*m, however technical is possible to cut also bigger thickness to the *20 mm*. For cutting of steel materials are differentiate sort of steel (soft steel, low alloy steel, alloy steel, stainless steel a.t.c.), processing history (metal plates cold-rolled, hot-rolled) and additional modification (metal plates surface treatment, jet surface metal plates, galvanized metal plates a.t.c.), which is necessary to deliberate with application laser technology. Thickness status after last operation is effecting application laser cutting, the same like a rests oils and lubricants, contaminated products, corrosive combustion gas and strong oxidate layers, which can for cutting evocate enviroment contamination. Oxidate layers slow down cutting speed and make worse cut quality with creating solid drops on the bottom place of cut. Metal plates surface treatment like a galvanized, coloured, jet is posible to cut by laser in definite limitary conditions.

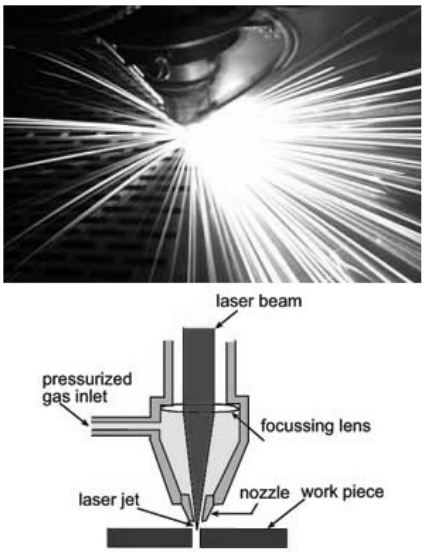

Fig. 1. Laser cutting. [5]

5. Plasma Cutting of Metal

In the present is metal cutting by plasma broadly exploited and so in carbon steels, low alloyed steels, so in stain steels, coppers and aluminiums. Steels is possible to cut to the material thickness *100 mm*, but the most often to the *30 mm*.
Advantages of plasma cutting:
• Against laser cutting:
- lower operaton costs = lower work piece price,
- for small work piece thickness (to the *3 mm*) is comparable abrasiveness of cut surface,
- higher flexibility for handling and machine,

- there are a smaller claims for quality of metal plate surface, which from will become work piece.

• Against autogen:
- higher cutting speed,
- smaller heat affected zone,
- lower fired,
- without preheating.

Disadvantages of plasma cutting:
- chamfer of the cut edge *1°- 5°* depending from material thickness,
- limiting cut thickness to the maximum *100 mm* (structural steel),
- hight operation costs for consumption parts in gas cooled burnet.

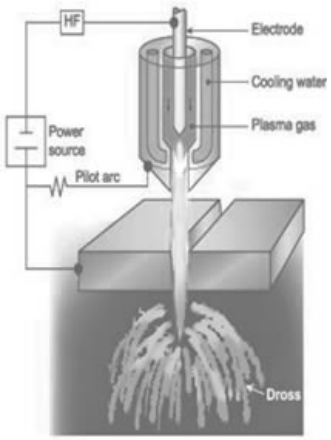

Fig. 2. Plasma cutting. [4]

6. Conclusion

From economic side is important produce the highest posible quality in the shortest time. High cutting speed, which is possible to procure laser, are the best results, how to improve manufacture productivity. Operation costs for cutting are always higher for laser than for plasma cutting. Important is to give to depend operation costs for cutting from material thickness with required abrasiveness surface *Ra*, or required correctness. Plumbless factor for appraisal plasma or laser cutting technology availability is ekological statement. Let´s say, that laser to charge working and environment lesser than plasma. It means, that choice progressive cutting methods (plasma, laser), cut condition, economical and ekological factors are connected together and affect each other.

References

[1] MIČIETOVÁ, A.: *Nekonvenčné metódy obrábania*, EDIS, Žilina 2001.
[2] MAŇKOVÁ, I.: *Progresívne technológie*, Vienala - vydavateľstvo, Košice 2000.
[3] KÖNIG, W.: *Fertigungsverfahren Band* 3, VDI-Verlag, Düsseldorf 1990.
[4] http://www.aviationmetals.net/images/laser-cutting(unc8f2).jpg
[5] http://structuralcarbonsteelplate.com/images/PlasmaCuttingTorch.jpg

Repair Mold Active Components by Micro-welding

*Borislav Melo **Ján Moravec
*Viena international s.r.o., Kráčiny 2, 036 01 Martin, melo@viena.sk,
**Žilinská univerzita Žilina, Univerzitná 1, 010 26 Žilina, jan.moravec@fstroj.uniza.sk

Abstract. The article deals with to handle of concrete problem of active components of molding tools by micro-welding in company area. The presents contribution hint as served view applied materials, equipments and technologies for materials two kinds.

Keywords: micro-welding, repair, molds

1. Introduction

When the molding tool is working in production process, its active components by stamping die, which are produced from tool – steel, must be repaired or restored. Since molds and active components have been produced from high-alloyed tool steel, there is the need for tool welding. Active tools components are the most expensive part of stamping die. The exact reason for using the welding process is to eliminate fabrication of a new part or parts affected by engineering changes, wear, damage from equipment malfunction, or even an occasional metallurgical defect. Welding is also the most often used option to reduce cost and reduce lost time when compared to making new mold components.One of resolutions is *micro-welding*.

2. Micro-welding Process

Micro-welding is the name given to the process that has evolved from traditional TIG welding (or more recently termed GTAW), using the technology of electric current being applied to the workpiece to generate heat at the point of the *arc gap.* GTAW (TIG) Arc Micro-welding uses a non-consumable tungsten electrode in inert gas. At the point of the arc gap, a molten pool is established and the filler rod (the additional material) is introduced into the molten pool. The inert gas protects molten pool, tungsten electrode and the nearest welding surround before atmosphere effects (mainly oxygen and nitrous from the air) – Fig. 1 The non-consumable electrode is from clear tungsten or with activate admixture and as shielding gas are used argon, helium, eventually their cocktails.[1]

Fig.1. Method of melting-down of basic and additional material

The difference between traditional TIG and micro-welding is that micro-welding is done at extremely low amperages (usually less than 10 A) in combination with fine control of the amperage range, along with the aid of a high-powered (10-20X or more) microscope. [2] In the micro-welding process the technique performing the weld repair—in combination with the welding equipment controls and the weld wire selection—is absolutely critical to end results - Fig.2

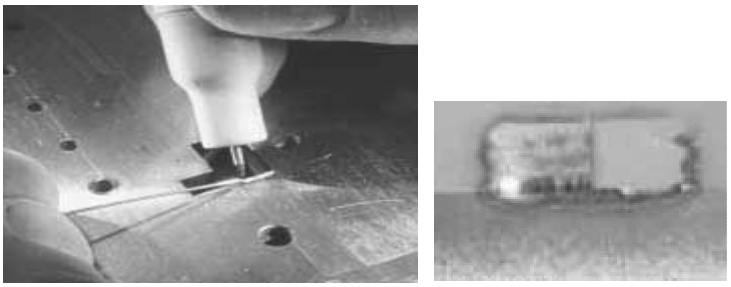

Fig. 2. Cutting edge repair and repair point quality

Micro-welding is process which is minimally changing mechanical properties of repaired components. Therefore this method is suitable for repair or renovation of accurate, small and thin components - Fig.3.

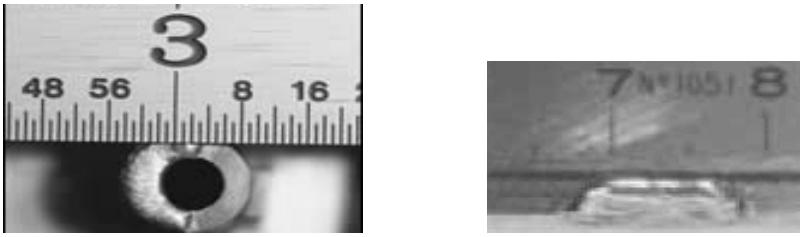

Fig. 3. Examples of repair area dimension

Additional materials

Selection of suitable form and qualities of the additional materials is important to reach required result after welding. The additional material can be deposited in a few layers on the repair area and every layer itself is keeping nearly the same properties as a base material. Additional materials are delivered in various forms – filler rods, flat strap, dust, metallic wave etc. Their application is determined by according repaired area. The most of the additional materials are machinable, hardenable, eventually can be nitrided. For different sorts of the basic materials can be used different sorts of the additional materials – Fig. 4 and Tab. 1.

Fitting rods

Flat straps

Metallic dust

Metallic wave

Fig. 4. Form of additional materials

Basic material	Additional material – properties and applying	Normative values
1.2307, 1.2313, 1.2341, 1.2343	Additional material alloy Cr-Mo-W-V with stability elements. At short time melting down resorts fast hardening welding area. Additional material can create structure, is polishable, nitridable and heat – conductive. There is possible hardening and tempering, in certain paroles is possible chrome plate. It has close structure resistant toward crack, high temperature and stable on edge. Additional material is used for repair and restore of high - temperature working steel. It is applied for die, form for metal pressing, ejectors and close edges forms. It is used for stamping die for stamping thin metal plate.	Hardness1.layer cca 56 – 59 HRc Hardness 2.layer cca 54 – 57 HRc Hardness 3.layer cca 53 – 56 HRc Hardening to cca 58 HRc
1.2601, 1.2201, 1.2376, 1.2379, 1.2362, 1.2880, 1.2884	High-alloyed additional material of alloy Cr-Mn-Si-V with stabily elements. Material is possible nitridable and EDM machinable. Chrome plating is not possible. It is used for cold working steel. It can be used in soft condition for next machining and hardening. Hardness of layers may be up to 58 HRc	Hardness 1.layer cca 58 – 60 HRc Hardness 2.layer cca 56 – 58 HRc After hardening cca 62 HRc

Tab. 1. Additional materials – example to use [3]

3. Repairing of Cutting Edge by Micro-welding

Arrangement of workplace and suitable selection of welder devices is important for right and error-free micro-welding repairs – Fig. 5. Welding devices are generally multifunctionally and consists of:

- soft welding for repairs and changes on finished forms and tools,
- TIG – manual welding with energy - storage or interval welding for medium or little layers,
- welding with extrude electrode – for high layers.

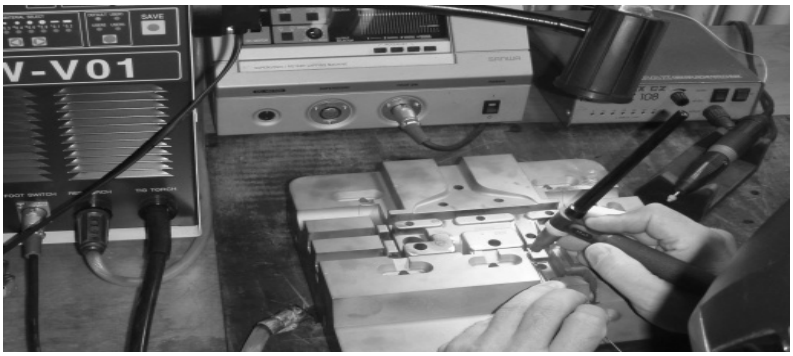

Fig. 5. Workplace arrangement for micro-welding

Method for repairing or restoring of broken components (method for repairing of cast iron and steel components is presented by on Fig. 6. and Fig.7.) is following:

a. Clean damaged area from contamination and grease (clean only eco - friendly cleaner)
b. Spot the additional material on basic material at repair area
c. Melt down the additional and basic material by arc gap
d. Trim, lap and polish the welding place

3.1. Method of repairing cast iron components – Fig. 6.

Material: cast iron 1.7140

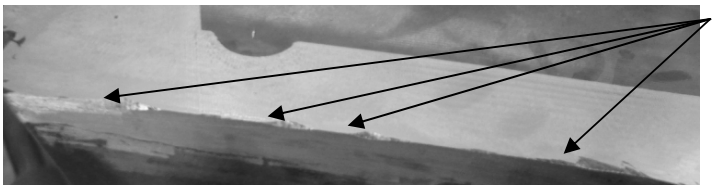

Edge before repair

Spoting

Fitting rod: 697 405 (RC 44)

Diameter : Ø0,8

Amperage: 650A Time: 010 ms

Micro-welding *TIG*

Fitting rod: 697 405 (RC 44)

Diameter: Ø0,8

Amperage: 84A Time: 084

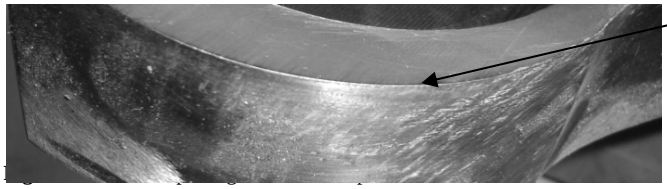

3.2. Method of repairing tool steel components – Fig. 7.

Material: tool steel 1.2379

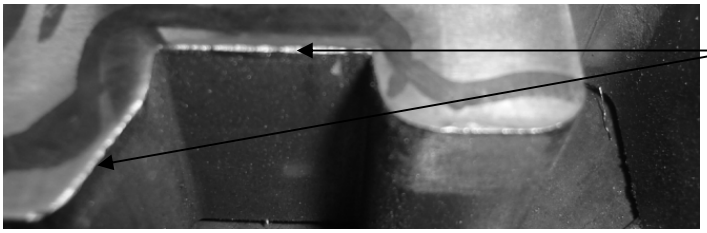

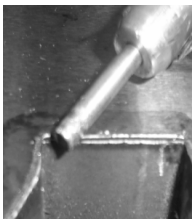

Spoting
Fitting rod: 697 405 (RC 44)
Diameter : Ø0,8
Amperage: 650A Time: 010 ms

Micro-welding *TIG*
Fitting rod: 697 405 (RC 44)
Diameter: Ø0,8
Amperage: 84A Time: 084

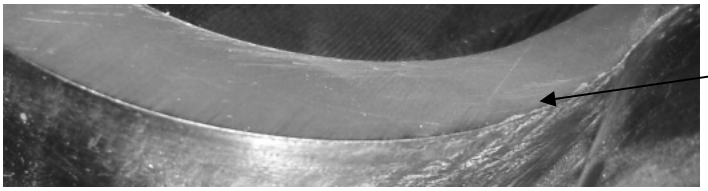

Fig. 7. Method of repairing tool steel components

4. Summary

Molding tools have increasing participation in production of finished products in various spheres of industry – automobile industry, electrical engineering, consumer industry etc. Molding tools are exposed to enormous load, so the bigger demands on period of service and cutting life are required from the active components in tools. Active components belong to the most expensive segments in the molding tools; they are produced from the most expansive materials – high - alloyed tool steel – financially and time - consuming technologies. When they are defective or worn, it is necessary to search the methods to repair and renovate them. And here the place for welding technologies is opening.

Micro-welding is one of wide spectrum of welding technologies which is being used increasingly for repairs and renovations of pressing and molding tools. *Micro-welding* means quick and cheap method to save expensive components of molding tools without influencing their added properties – hardness, strength, adhesive and abrasive resistance, machinability, hardenability etc. Therefore it begins to represent ideal method for cost reduction at repair and renovation of components from high - alloyed tool steel.

References

[1] DRASLÍK, F. a kolektív*: Strojnícka príručka*, zväzok 4. 11/2004
[2] MOBERG, C.: *Laserwelding versus microwelding*, Moldmaking Technologies June 2006
[3] Catalogue NOVAPAX, 2008

Transcom 2009, 22-24 June 2009
University of Žilina, Žilina, Slovak Republic

Effectiveness Analysis for The Rolling Mill Exploitation

[*]Krzysztof Mielczarek, [**]Stanisław Borkowski
[*]mgr inż., Czestochowa University of Technology, Faculty of Management, Department of Production Engineering, e-mail: k.mielczarek@wp.pl
[**]prof. n. techn. i n. ekon. dr hab. inż., Czestochowa University of Technology, Department of Management, Division of Production Engineering, email: bork@zim.pcz.czest.pl

Abstract. In this article the approach to maintenance of technical objects TPM was introduced. Chosen TPM coefficients were calculated. Standstill in machines work was divided on the fallowing kinds: break-down time (TA), instrumentation change (ZO), regulation (R). The period of research embraced one year and the object of the analysis is the rolling mill.

Keywords: TPM, exploitation condition, standstill

1. Introduction

TPM (Total Productive Maintenance) is an approach to services of technical objects and its equipment. TPM is the workings, which depends on the maintenance service of technical objects, which is realized by staff responsible for its maintenance inside the whole enterprise through operators and the staff responsible for its maintenance. One of the most important aims of introducing TPM is the identification and aspiration for elimination the losses caused by uneconomical maintenance of technical objects. These losses are concerned: time, speed and the quality. Through elimination of these losses it is possible to improve the productivity of plant and equipment [1, 2].

The TPM coefficients are the measuring instruments that are designed for evaluating effectiveness work machine and they are calculated on the base of their performance. They are applying to accessibility in the meaning of active work of machine, utilization in the meaning of planned in percentages loading and the quality of produced by the machine articles. They are concerns of settings of shift time [3, 4].

2. TPM Coefficients as a Measure of Effectiveness Working Machine

The TPM coefficients are the measuring instruments that are designed for evaluating the effectiveness of work machine and they are calculated on the base of their performance. They are applying to accessibility in the meaning of active work of machine, utilization in the meaning of planned in percentages loading and the quality of produced by the machine articles. They are concerns of settings of shift time. The structure of individual time in TPM coefficient calculation was introduced on Fig. 1.

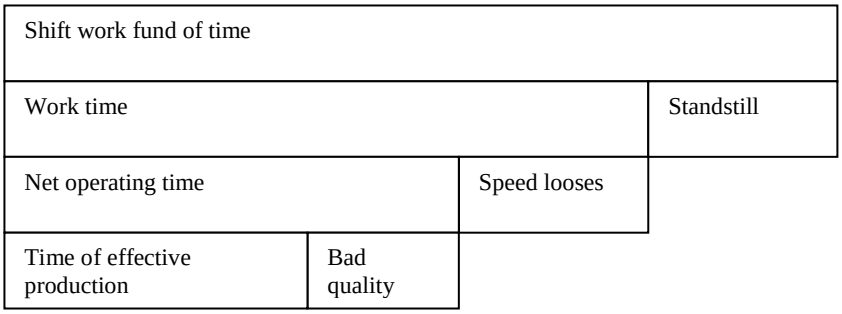

Fig. 1. Settings of shift time for TPM coefficients calculation.

To calculate TPM coefficients the following type of times are used:

- shift work fund of time (TZ), it is accessible work time machine in every working day,
- standstill (TP), it is standing time of technical object cause by down-time such as: survey, technological pauses, break-downs, changing of instrumentation,
- ideal time per unit (ICJ), it is a time, in which one unit of product should be manufactured,
- actual time per unit (RCJ), it is time in which in given condition one unit of product is manufactured.

Moreover, to calculate the following quantity are used:

- production (PR), it is a number of manufactured products during the given time,
- quality level (PJ), it is percentage of defective products.

To evaluate effectiveness exploitation the coefficients which formulas are introduced in [1, 5] have to be calculated.

The next part of the analysis is the standstill time structure. Standstill in machines work was divided on the fallowing kinds: break-down time (TA), instrumentation change (ZO), regulation (R). The level of individual shutdown for researched rolling mill was presented on Fig. 2.

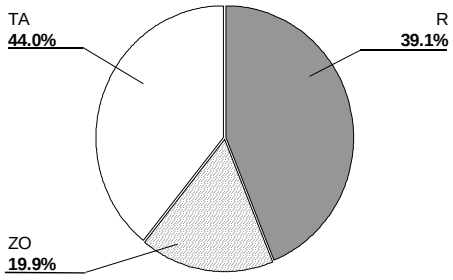

Fig. 2. Shutdowns level in rolling mill work in one - year period.

The most share of shutdown during the whole year presented the shutdowns caused through break-down (44%). The cause of frequent break-downs was detraction process of machine elements and also insufficient conservation quality. Elimination of above-mention losses can contribute to significant rise effectiveness of researched device.

3. TPM Coefficients Structure

Assessment of actual effectiveness was carried out in 12 month period. In the evaluation of maintenance performance, the overall equipment effectiveness (OEE) is used as metric to evaluate the manufacturing capability and is a function of equipment availability, performance efficiency and the quality. For researched rolling mill the average result about 75% means that from machine we can obtain ¾ of products, which can be received in an ideal condition. An 85% OEE is considered as being world class and enterprises should try to reach it.

The value of chosen TMP coefficients and the quality level (number of defective product) for rolling mill was introduced in Tab. 1.

Period of research	TPM coefficient				PJ [%]
	WE [%]	UCD [%]	WW[%]	OEE [%]	
1	96,00	85,28	85,25	79,78	2,38
2	98,25	68,34	68,50	65,29	2,50
3	96,25	79,95	80,00	75,02	2,38
4	97,75	76,11	75,75	72,36	2,25
5	95,50	83,17	83,25	77,64	2,00
6	99,25	76,04	76,00	73,62	2,50
7	96,50	78,24	78,00	73,51	2,50
8	95,75	85,31	85,50	79,42	2,38
9	96,75	84,50	84,50	79,52	2,25
10	97,50	83,81	83,75	79,88	2,25
11	99,00	82,54	82,50	79,80	2,50
12	96,50	79,31	79,25	74,75	2,00

Tab. 1. Average value of TPM coefficients for rolling mill in one-year period.

On Fig. 3 was introduced average value of the coefficient of exploitation (WE), the performance coefficient (WW) and the overall equipment effectiveness (OEE), in following research period.

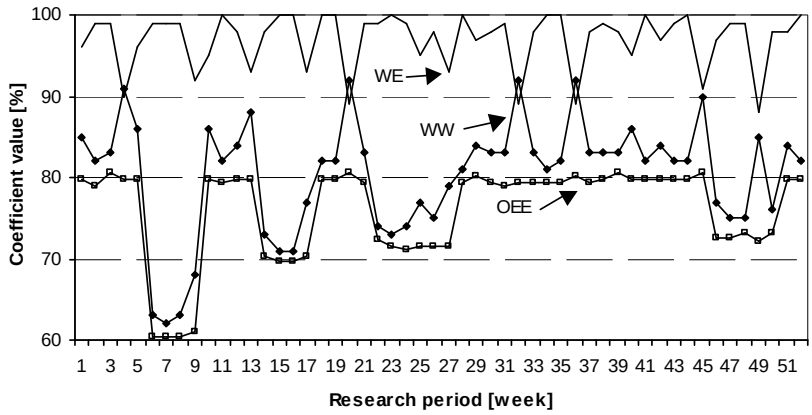

Fig. 3. TPM coefficients value for rolling mill in individual research periods.

Value of individual coefficients is not subjected to a big fluctuation in research period. For first six weeks the value of coefficients were on high and rather stable level. In next weeks there was a gradual fall of value the performance coefficient (WW). It was caused by decreasing of production efficiency. It also finds reflection in significantly lower value of OEE. Since ten weeks the value of coefficient again was on high and stable level. It shows that the value of individual coefficients reached optimal values.

4. Conclusion

If we want to improve production effectiveness we should know what the current situation is. Information about it delivers TPM coefficients. As a result of conducted investigations for rolling mill it was affirmed that the general effectiveness of machine is on a suitable level. Despite good results, the values of individual coefficients should be constantly monitored. It will allow quickly reacted while wrong effect of working machine will be noticed.

As a result of conducted research for rolling mill it was affirmed that overall effectiveness of machine is shaped on good level because analyzed TPM coefficients reached optimal values. Nevertheless, the average value of quality level more than 2% shows that researched rolling mill manufactured a high level of incompatible products. It is caused among other things by shutdowns of machine work that results from break-down. It should be remembered that also other factors such as: experience of workers, bad quality of materials and other factors can have decisive meaning in creating quality.

References

[1] BORKOWSKI, S., SELEJDAK, J., SALAMON, S. *Efektywność eksploatacji maszyn i urządzeń*. Wydawnictwo Wydziału Zarządzania Politechniki Częstochowskiej. Częstochowa, 2006.

[2] BORKOWSKI, S., SELEJDAK, J. *TPM and PAMCO Exploitation factors as quality determinants.* Advanced manufacturing and repair technologies in vehicle industry. 24th International Colloquium. Czech Republic. Svitavy, 2007.

[3] MIELCZAREK, K., BORKOWSKI, S. *Correlation analysis between quality level and TPM coefficients. Chapter 8.* In: *Quality and Production Management in Practice*. BORKOWSKI, S., KOVALENKO, V.S. (red.). Press Association of Universities Russia. Saint Petersburg, 2008.

[4] BORKOWSKI, S., ULEWICZ, R. *Zarządzanie produkcją. Systemy produkcyjne*. Oficyna Wydawnicza „Humanitas". Sosnowiec, 2008.

[5] SALAMON, S. *Wskaźniki w kompleksowym utrzymaniu maszyn (TPM). Rozdział 13.* In: *Efektywność eksploatacji maszyn i zdolność jakościowa procesu*. HRUBEC, J., BORKOWSKI, S., (red). Wydawnictwo Instytutu Organizacji i Zarządzania w Przemyśle ORGMASZ. Warszawa, 2006.

Transcom 2009, 22-24 June 2009
University of Žilina, Žilina, Slovak Republic

Computation Methods for Travelling Salesman Problem

Miroslav Michalco, Nadežda Čuboňová
University of Žilina, Faculty of Mechanical Engineering, Department of Automation and Production Systems, Univerzitná 1 , 01026 Žilina, Slovakia,
{miroslav.michalco, nadezda.cubonova}@fstroj.uniza.sk

Abstract. This paper deals about a very complex combinatorial optimization problem named "Travelling Salesman Problem". In this article you can find simple description of the problem and several strategies used to solve it. These strategies are divided into exact and heuristics methods and they are used for different variations and sizes of the problem.

Keywords: Travelling Salesman Problem, algorithm, optimum, city

1. Introduction

The travelling salesman problem (TSP) is one of the most widely studied combinatorial optimization problems, with links to many fields of pure and applied mathematics like graph theory and integer programming (Lawler et al. 1985). Simply stated, a salesman has to visit TV cities, visiting each city exactly once and return back to the starting city with minimum cost. Search space is then permutation of *n* cities and every permutation is a possible solution and a permutation with shortest path is the optimal solution. Size of the search space is then *n!*.

TSP is relatively old problem: firstly described by Euler in 1759. Name "Travelling salesman" was first used in 1932. A lot of techniques were designed for TSP solving in last years, using different methods and strategies.

2. Computing a Solution

The traditional lines of attacking for the NP-hard problems are the following:

- Devising algorithms for finding exact solutions (they will work reasonably fast only for relatively small problem sizes).
- Devising "suboptimal" or heuristic algorithms, i.e., algorithms that deliver either seemingly or probably good solutions, but which could not be proved to be optimal.
- Finding special cases for the problem ("subproblems") for which either better or exact heuristics are possible.

2.1. Exact Algorithms

The most direct solution would be to try all permutations (ordered combinations) and see which one is cheapest (using brute force search). The running time for this approach lies within a polynomial factor of $O(n!)$, the factorial of the number of cities, so this solution

becomes impractical even for only 20 cities. One of the earliest applications of dynamic programming is an algorithm that solves the problem in time $O(n^2 2^n)$[10]

The dynamic programming solution requires exponential space. Using inclusion–exclusion, the problem can be solved in time within a polynomial factor of 2^n and polynomial space.

Improving these time bounds seems to be difficult. For example, it is an open problem if there exists an exact algorithm for TSP that runs in time $O(1.9999^n)$

Other approaches include:

- Various branch-and-bound algorithms, which can be used to process TSPs containing 40-60 cities.
- Progressive improvement algorithms which use techniques reminiscent of linear programming. Works well for up to 200 cities.
- Implementations of branch-and-bound and problem-specific cut generation; this is the method of choice for solving large instances. This approach holds the current record, solving an instance with 85,900 cities.

An exact solution for 15,112 German towns from TSPLIB was found in 2001 using the cutting-plane method proposed by George Dantzig, Ray Fulkerson, and Selmer Johnson in 1954, based on linear programming. The computations were performed on a network of 110 processors located at Rice University and Princeton University. The total computation time was equivalent to 22.6 years on a single 500 MHz Alpha processor. In May 2004, the travelling salesman problem of visiting all 24,978 towns in Sweden was solved: a tour of length approximately 72,500 kilometers was found and it was proven that no shorter tour exists.

In March 2005, the travelling salesman problem of visiting all 33,810 points in a circuit board was solved using *Concorde TSP Solver*: a tour of length 66,048,945 units was found and it was proven that no shorter tour exists. The computation took approximately 15.7 CPU years. In April 2006 an instance with 85,900 points was solved using *Concorde TSP Solver*, taking over 136 CPU years.

2.2. Heuristic and Approximation Algorithms

Various *heuristics* and *approximation algorithms*, which quickly yield good solutions have been devised. Modern methods can find solutions for extremely large problems (millions of cities) within a reasonable time which are with a high probability just 2-3% away from the optimal solution. Several categories of heuristics are recognized:

2.2.1. Constructive Heuristics

The nearest neighbour (NN) algorithm (or so-called greedy algorithm) lets the salesman choose the nearest unvisited city as his next move. This algorithm quickly yields an effectively short route. For N cities randomly distributed on a plane, the algorithm averagely yields length = 1.25 * exact_shortest_length.

However, there exist many specially arranged city distributions which make the NN algorithm gives the worst route. This is true for both asymmetric and symmetric TSPs.

Recently a new constructive heuristic, Match Twice and Stitch (MTS) has been proposed. MTS has been shown to empirically outperform all existing tour construction heuristics. MTS performs two sequential matchings, where the second matching is executed after deleting all the edges of the first matching, to yield a set of cycles. The cycles are then stitched to produce the final tour.

2.2.2. Iterative Improvement

- **Pairwise exchange** or **Lin-Kernighan** heuristics.

The pairwise exchange or '2-opt' technique involves iteratively removing two edges and replacing these with two different edges that reconnect the fragments created by edge removal into a new and shorter tour. This is a special case of the k-opt method. Note that the label 'Lin-Kernighan' is an often heard misnomer for 2-opt. Lin-Kernighan is actually a more general method.

- ***k*-opt Heuristic**

Take a given tour and delete k mutually disjoint edges. Reassemble the remaining fragments into a tour, leaving no disjoint subtours (that is, don't connect a fragment's endpoints together). This in effect simplifies the TSP under consideration into a much simpler problem. Each fragment endpoint can be connected to $2k - 2$ other possibilities: of $2k$ total fragment endpoints available, the two endpoints of the fragment under consideration are disallowed. Such a constrained $2k$-city TSP can then be solved with brute force methods to find the least-cost recombination of the original fragments. The k-opt technique is a special case of the V-opt or variable-opt technique. The most popular of the k-opt methods are 3-opt, and these were introduced by Shen Lin of Bell Labs in 1965. There is a special case of 3-opt where the edges are not disjoint (two of the edges are adjacent to one another). In practice, it is often possible to achieve substantial improvement over 2-opt without the combinatorial cost of the general 3-opt by restricting the 3-changes to this special subset where two of the removed edges are adjacent. This so-called two-and-a-half-opt typically falls roughly midway between 2-opt and 3-opt, both in terms of the quality of tours achieved and the time required to achieve those tours.

- ***V'*-opt Heuristic**

The variable-opt method is related to, and a generalization of the k-opt method. Whereas the k-opt methods remove a fixed number (k) of edges from the original tour, the variable-opt methods do not fix the size of the edge set to remove. Instead they grow the set as the search process continues. The best known method in this family is the Lin-Kernighan method (mentioned above as a misnomer for 2-opt). Shen Lin and Brian Kernighan first published their method in 1972, and it was the most reliable heuristic for solving travelling salesman problems for nearly two decades. More advanced variable-opt methods were developed at Bell Labs in the late 1980s by David Johnson and his research team. These methods (sometimes called Lin-Kernighan-Johnson) build on the Lin-Kernighan method, adding ideas from tabu search and evolutionary computing. The basic Lin-Kernighan technique gives results that are guaranteed to be at least 3-opt. The Lin-Kernighan-Johnson methods compute a Lin-Kernighan tour, and then perturb the tour by what has been described as a mutation that removes at least four edges and reconnecting the tour in a different way, then v-opting the new tour. The mutation is often enough to move the tour from the local minimum identified by Lin-Kernighan. V-opt methods are widely considered the most powerful heuristics for the problem, and are able to address special cases, such as the Hamilton Cycle Problem and other non-metric TSPs that other heuristics fail on. For many years Lin-Kernighan-Johnson had identified optimal solutions for all TSPs where an optimal solution was known and had identified the best known solutions for all other TSPs on which the method had been tried.

2.2.3. Randomised Improvement

- Optimised Markov chain algorithms which use local searching heuristic sub-algorithms can find a route extremely close to the optimal route for 700 to 800 cities.
- Random path change algorithms are currently the state-of-the-art search algorithms and work up to 100,000 cities. The concept is quite simple: Choose a random path, choose four nearby points, swap their ways to create a new random path, while in parallel decreasing the upper bound of the path length. If repeated until a certain number of trials of random path changes fail due to the upper bound, one has found a local minimum with high probability, and further it is a global minimum with high probability (where high means that the rest probability decreases exponentially in the size of the problem - thus for 10,000 or more nodes, the chances of failure is negligible).

TSP is a touchstone for many general heuristics devised for combinatorial optimization such as *genetic algorithms, simulated annealing, Tabu search, ant colony optimization,* and *the cross entropy method*.

3. Conclusion

There are many different applications and different TSP variations in the real world, therefore it is necessary to know, what kind of problem we are going to solve. First we have to study it, think about the results we demand, if we need the optimal solution or we need solution close to the optimal one, how close and how much time do we want to spend on computation. All these factors can lead us to different optimization techniques. Some of these techniques are universal and can be used for several tasks or several modifications; some are very special, designed for only one task. Genetic algorithms are used for a modification of TSP in a doctoral thesis *"Implementation of genetic algorithms into optimization of technological processes"*. In this thesis, GA based on TSP task are used as an optimization tool for improving the rapid move efficiency and reducing the length of toolpaths. This work deals with common problems of GA's like comparison of several techniques and searching for method, good enough for our purpose.

References

[1] ZBIGNIEW, M., *Genetic algorithms + data structures = evolution programs.* Berlin: SPRINGER, 1999,

[2] http://www.talkorigins.org/faqs/genalg/genalg.html

[3] http://en.wikipedia.org/wiki/Travelling_salesman_problem

Transcom 2009, 22-24 June 2009
University of Žilina, Žilina, Slovak Republic

An Insight into the Behaviour of a Mathematical Model for Predicting Roughness of Surface Face Milled with the Coromill 390

[*]Edward Miko, [*]Łukasz Nowakowski
[*] Kielce University of Technology, Chair of Mechanical Engineering and Metrology, Aleja Tysiąclecia Państwa Polskiego 7, 25-314 Kielce, Poland, E-mail: emiko@tu.kielce.pl, lnovak@poczta.fm

Abstract. The paper discusses the results of a computer simulation focusing on the influence of selected factors on the process of surface roughness formation during face milling with a CoroMill 390. The factors considered include the edge corner radius, vibrations in the machine-tool-workpiece system, and the minimum undeformed chip thickness. The analysis were conducted basing on the mathematical model for predicting surface roughness discussed in Ref. [1].

Keywords: machining parameters, face milling, modeling of the surface roughness

1. Introduction

Face milling is considered to be one of the most efficient methods of surface formation. However, the process is very costly and requires determining the most optimal conditions. In many a case, it is essential to apply milling as a final operation. In which a workpiece is first sculptured according to the designer's requirements and then finished to obtain the appropriate geometry and surface properties [2,3].

Surface roughness is characterized by parameters that are determined by measuring its irregularities. It is one of the most important factors affecting the functional properties of machine components represented by: friction in the contact area, contact stress, fatigue toughness, corrosion resistance, tightness of joints, conditions of the flow of liquids and gases around the surface, electrical and thermal contact resistance, and thermal radiation from magnetic surfaces [1,4].

The models for predicting roughness of face-milled surfaces found in the literature analyze the effect of only one factor, for instance: vibrations, tool run-out and sometimes also tool wear. An overview of the research on the subject shows that these factors have an enormous effect on surface roughness in face milling. The model for predicting surface roughness in face milling is based also on the results of the previous research by the authors [5,6].

2. Predicting the Roughness of Surfaces Face Milled with a Coromill 390

The mathematical model presented in Ref. [1] was used to develop a Mathcad application, perform simulation calculations, and, finally, create graphs for predicting the values of surface roughness *Ra* during a face milling operation with a CoroMill 390 equipped with rounded corner inserts. The milling was conducted under the conditions recommended by the producer.

The simulation was carried out to analyze the effect of:

– the feed,
– the number of inserts,
– the tool corner radius,
– the vibrations in the tool-workpiece system,
– the minimum undeformed chip thickness.

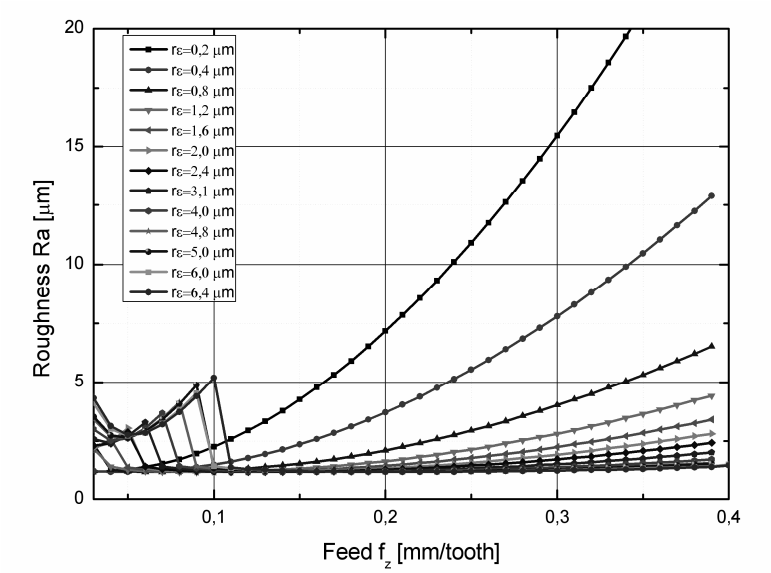

Fig. 1. Influence of the tool corner radius and the feed on the parameter *Ra* for D(ξ)= 1 μm and h_{min}= 1 μm

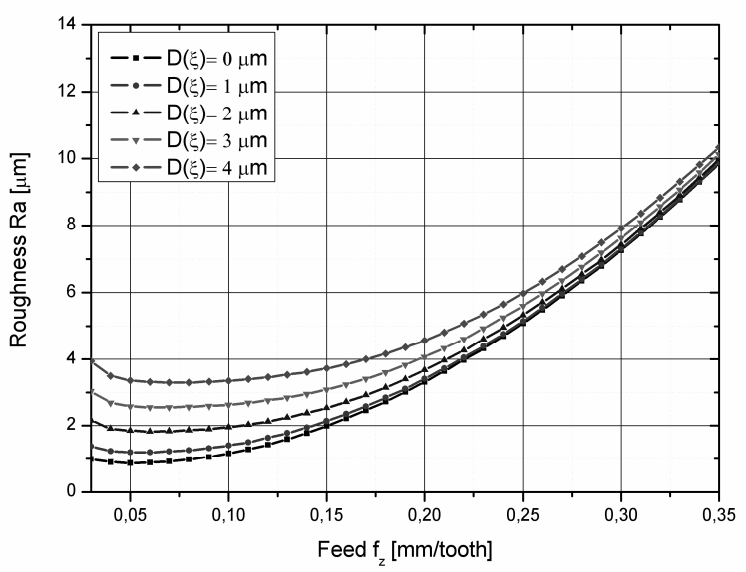

Fig. 2. Roughness *Ra* vs vibrations and feed for h_{min}= 2 μm, and r_{ε}= 0.4 mm

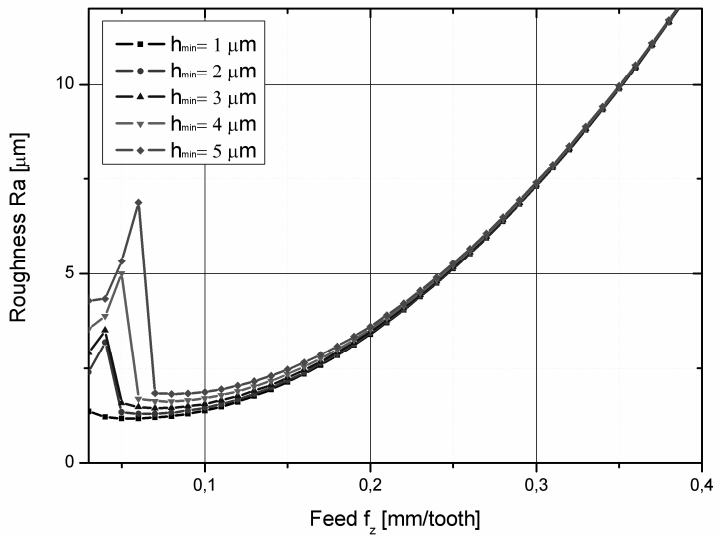

Fig. 3. Influence of the minimum undeformed chip thickness h_{min} and the feed f_z on the parameter *Ra* when D(ρ)=1 μm, D(ξ)= 1 μm, r_ε= 0.4 mm

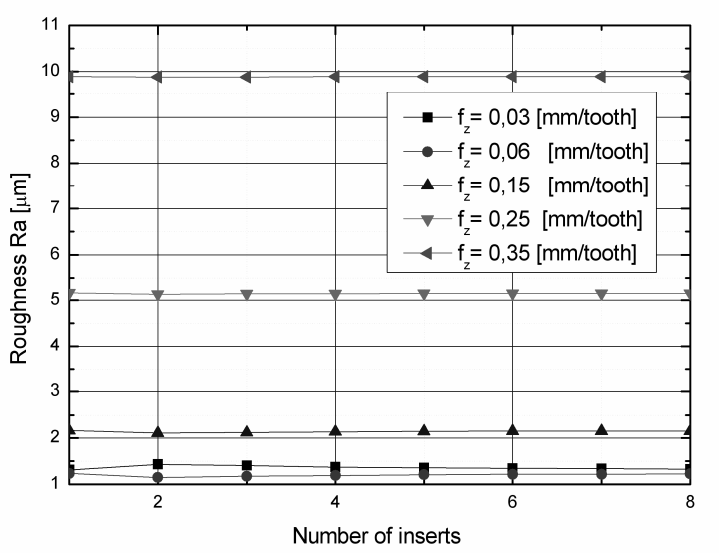

Fig. 4. Roughness *Ra* vs number of inserts at D(ρ)=1 μm, D(ξ)= 1 μm and r_ε= 2.4 mm, for five selected values of the feed.

Analyzing the curves in Fig. 1, one can see that the impact of the feed f_z on the value of *Ra* becomes less and less significant, when the length of the corner radius r_ε decreases. Applying feeds of 0.03-0.10 mm/tooth results in the instability of the milling operation, and, accordingly, high values of the surface roughness parameters *Ra*. At higher feeds, the tool corner radius has an important effect on the surface roughness *Ra*. Applying high feeds and cutting tools with large corner radii, it is possible to obtain a multiple decrease in the parameter *Ra*, an increase in the machining capacity, and as a consequence, a reduction in production costs.

As can be seen from Fig. 2, the higher the value of the feed f_z, the less effect the vibrations D(ξ) have on the roughness *Ra*. When feed ranges 0.25 to 0.35 mm/tooth, the influence of the vibrations on the process of microhardness formation becomes negligible.

Figure 3 shows the influence of the feed, f_z, on the parameter *Ra* for five different values of the minimum undeformed chip thickness h_{min}.

The simulations show that the minimum undeformed chip thickness h_{min} has a significant effect on the surface roughness *Ra* in face milling at small values of the feed. For feeds higher than 0.15 mm/tooth, the influence is small; and for lower feeds it becomes negligible.

Finally, it was essential to simulate the influence of the number of inserts on the parameter *Ra* during face milling for five ranges of the feed. The results show that the number of inserts is important, yet only to a certain extent.

From Fig. 4 it is clear that by applying two inserts we obtain the lowest value of the parameter *Ra*. Increasing the number of inserts to more than four does not cause any changes in the geometrical surface structure.

3. Conclusion

1. The roughness of face-milled surfaces is dependent on the following factors: the stereometric and kinematic representation of the cutting edge, the minimum undeformed chip thickness, relative vibrations of the tool-workpiece system, face run-out and the edge wear.
2. The feed is reported to influence surface roughness considerably only if tool with small corner radii are used. Applying small values of the feed leads to the instability of the milling process and, in consequence, high surface roughness. The simulations show that the most optimal are feeds of 0.1–0.25 mm/tooth.
3. When tools with large corner radii r_ε are used for milling at high feeds, there is a multiple decrease in the value of the parameter *Ra* and an increase in the machining capacity.
4. The roughness parameter *Ra* is dependent on the number of inserts only if two to five inserts are used. If six or more inserts are applied, no considerable influence on the surface microroughness is observed.

References

[1] MIKO E. *Konstytuowanie mikronierówności powierzchni metalowych obrobionych narzędziami zdefiniowanej stereometrii ostrzy*, Monografie, Studia, Rozprawy Kielce 2004 No. 46.

[2] ŻEBROWSKI, H. *Konstytuowanie technologicznej warstwy wierzchniej w procesie toczenia z podwyższonymi prędkościami skrawania*, Mechanik No 11, 1998, pp. 686-692.

[3] PETERKA, J. *A New Approach to Calculating the Arithmetical Mean Deviation of a Profile during Copy Milling.* Journal of Mechanical Engineering, Vol. 50, No. 12, 2004, pp. 594-597.

[4] GRZESIK W. *Podstawy skrawania materiałów metalowych*, WNT, Warszawa 1998.

[5] KAWALEC M. *Skrawanie hartowanych stali i żeliwa narzędziami o określonej geometrii ostrza.* Wydawnictwo Politechniki Poznańskiej, seria Rozprawy, No 234, Poznań 1990.

[6] BONIFAĆIO M., DINIZ A.E., *Correlating tool wear, tool life, surface roughness and tool vibration in finish turning with coated carbide tools.* Wear, Vol. 173, 1994, pp. 137-144.

The scientific work funded from resources on the science in years 2007-2010, as the research and developmental project .

Stability of Microstructure of UFG Copper after Fatigue Loading and Thermal Exposition

*Lucie Navrátilová, *Libor Pantělejev, *Ondřej Man, **Ludvík Kunz
*Institute of Material Science and Engineering, Faculty of Mechanical Engineering, Brno University of Technology
**Institute of Physics of Materials, Academy of Sciences of the Czech Republic

Abstract. The objective of the present work was to study the stability of microstructure of ultra fine-grained (UFG) copper under high-cycle and very high-cycle fatigue loading and under thermal exposition. UFG Cu was prepared by equal channel angular pressing. No grain coarsening was observed after fatigue resulting in failure in the interval from 104 to 1010 cycles. Similarly, no grain coarsening was detected after thermal exposition at a temperature of 180 °C for 6 min. The microstructure was examined by electron backscattering diffraction (EBSD) and transmission electron microscopy (TEM).

Keywords: UFG copper, ECAP, stability of microstructure, EBSD.

1. Introduction

Ultrafine-grained (UFG) materials prepared by severe plastic deformation have been systematically studied since the last 15 years. The equal channel angular pressing (ECAP) is one of the most frequently used techniques to produce UFG materials in bulk [1]. The safe engineering application of these materials exhibiting generally improved tensile properties requires also sufficient resistance of UFG structures to cyclic loading and resistance to grain growth at elevated temperatures. Hence, the detailed knowledge of both phenomena is important from the engineering point of view.

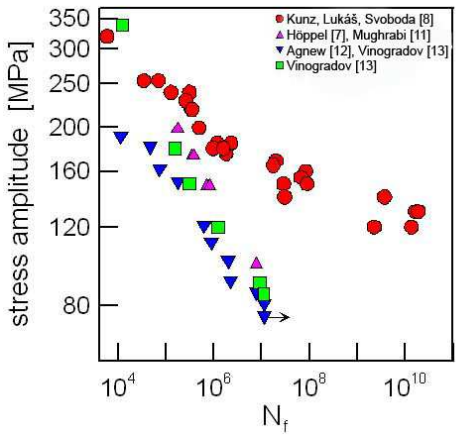

Fig. 1. Comparison of S-N plots of UFG Cu determined by different authors.

One of the most intensively studied UFG materials is Cu. It has been shown that the grain structure is sensitive to elevated temperatures. Grain growth [2][3] and changes in texture were already observed at 170 °C [4][6]. Höppel et al. [7] reported formation of bimodal grain structure responsible for changes of mechanical properties as a result of post-ECAP annealing at 170 °C. Instability of UFG microstructure substantially influences fatigue performance. It has been shown in previous publications by one of the authors [8][10] that the fatigue strength of UFG Cu in high and very high cycle region is higher than that reported in literature. This finding is shown in Fig. 1. The S-N curve determined by Kunz et al. [8] is shifted towards higher lives in high-cycle and in very high-cycle region when compared to the results published by Höppel et al. [7], Mughrabi et al. [11], Agnew et al. [12] and Vinogradov et al. [13]. The explanation of low fatigue performance of UFG Cu in high cycle region examined in the last mentioned four studies was based on instability of UFG structure and formation of bimodal one. The fatigue crack initiation in large grains of the bimodal structure is easier and results in shorter fatigue life. Contrary to that no changes of microstructure in terms of grain size were observed

in [8]. The reasons for different stability of UFG structures in particular cases are not entirely clear. The most often considered reason is material purity. Low purity UFG Cu is expected to be more stable than the pure one.

The aim of this work was to examine and discuss the structure stability of UFG Cu. Observation was conducted on specimens fatigued in previous work [8]; the corresponding S-N data are shown in Fig. 1. Moreover, annealing experiments were performed to determine the stability of UFG structure under thermal exposition.

2. Material and experiments

UFG copper of commercial purity (99.9%) was used in this study. The chemical composition is given in Table 1. The material was processed by eight passes of ECAP process using B_C route (after each pressing the billet was rotated around its longitudinal axis about 90°).

Cu, no less than	Impurity (%), no more than										
	Bi	Sb	As	Fe	Ni	Pb	Sn	S	O	Zn	Ag
99.9%	0.001	0.002	0.002	0.005	0.002	0.005	0.002	0.004	0.05	0.004	0.003

Tab. 1. Chemical composition of Cu.

The basic tensile characteristics of UFG Cu determined on four specimens are the following: $R_m = 387 \pm 5$ MPa, $R_{p0,1} = 349 \pm 4$ MPa, a $R_{p0,2} = 375 \pm 4$ MPa [8].

Microstructure of the original material, material after fatigue tests performed in previous works [8] and after thermal exposition was examined by electron backscattering diffraction (EBSD) and transmission electron microscopy (TEM). EBSD analysis was carried out by means of two systems; SEM Philips XL 30 electron microscope with EBSD detector and Oxford INCA crystal EBSD system in JEOL 6460 SEM.

Specimens for EBSD observations were electropolished in phosphoric acid-ethanol-water-isopropyl alcohol solution at 10 V and holding time 60 s. The temperature of the electrolyte varied between 9 and 13 °C.

Annealing of the material after ECAP at 180°C for 6 min total time in inert argon atmosphere was carried out in Heraeus ROS 4/50 tube furnace. Small specimen with dimensions 15×5×2.5 mm was inserted into the fully thermally stabilized heating zone of the furnace, then retracted after the specified time and cooled down in the argon flow.

TEM observation of dislocation structures was carried out on thin foils.

3. Results

Microstructure of UFG Cu after ECAP process as observed by means of EBSD and expressed in terms of a grain map is shown in Fig. 2a. An example of a structure after fatigue loading at stress amplitude of 255 MPa in symmetrical cycle is shown in Fig. 2b. From the comparison of structures revealed in Figs. 2a and b, which represent a set of at least ten micrographs of both material conditions, it can be concluded that the fatigue loading does not result in substantial grain growth. Similar results were found for stress amplitudes resulting in the fatigue failure in the interval of number of cycles shown in Fig. 1.

Microstructure of material before and after fatigue loading as observed by TEM is presented in Fig. 3. It can be seen that the grains (dislocation cells) are nearly equiaxed (Fig. 3a.). Fig. 3b shows dislocation microstructure after fatigue. It is very similar to that after ECAP process. No substantial grain coarsening is observed. This again witnesses for stability of the material in terms of grain size.

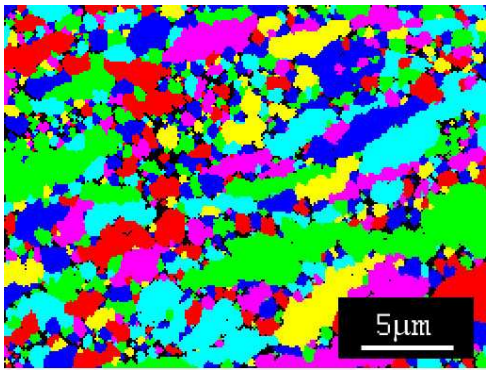

a)

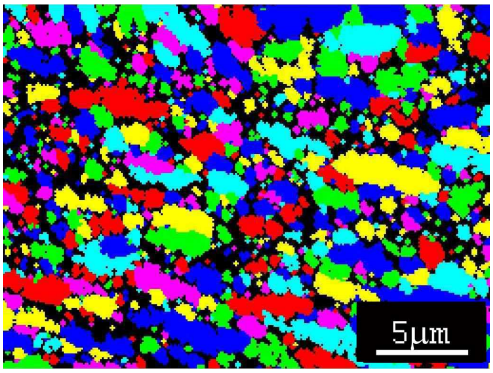

b)

Fig. 2. Grain maps of UFG Cu a) before and b) after fatigue loading.

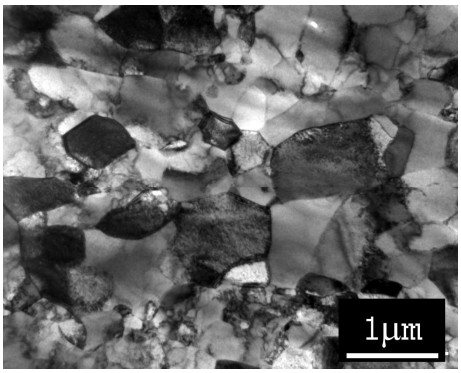

a)

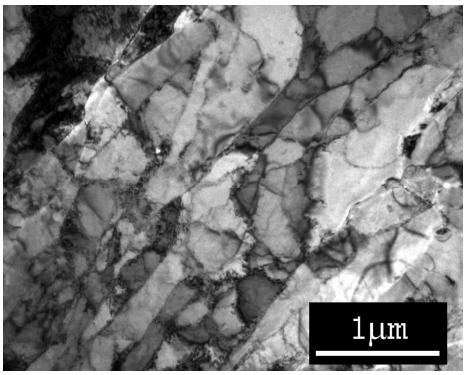

b)

Fig. 3. Dislocation microstructure: a) before and b) after fatigue loading.

Microstructure before and after annealing is shown in Figs. 4 and 5. In this particular case, the EBSD observation was performed on the same area before and after annealing. The exact position of the analyzed area on the specimen surface was marked by Vickers micro indents. From simple optical comparison of both grain maps it can be concluded that the thermal exposition did not result in a significant grain growth. Histograms presented in both Figures yields similar result. Detailed quantitative evaluation of the average grain size provides small increase of about 3%. This negligible difference in grain size is documented by the Misorientation Angle (MA) histogram (Fig. 8) which shows almost no change in misorientation angle distribution. The distribution corresponding to the UFG structure before thermal exposure is denoted as NAN and distribution after exposure as AN. This result means that - in global average - there was detected no profound rearrangement of the grain boundary network.

Minor changes in local orientation spread due to thermal exposition were detected by Kernel Average Misorientation (KAM) analysis, which provides information about average misorientation angle among each pixel and its second closely neighboring data points. Physical meaning of this parameter is the amount of local lattice distortion. The results of this analysis are shown in Fig. 9.

The stability of UFG microstructure under applied thermal exposition was confirmed also by texture analysis. Pole figures characterizing the texture of UFG Cu before thermal exposition are shown in Fig. 6 and after it in Fig. 7. Pole figures are obviously very similar which again indicates stability of UFG microstructure, in this case in terms of global orientation distribution.

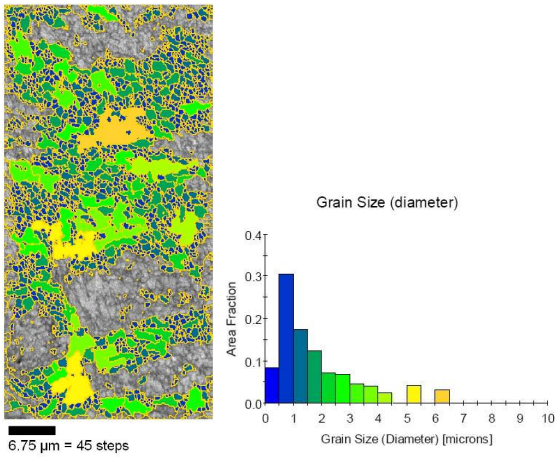

Fig. 4. Microstructure of UFG Cu before thermal exposition (grain size map and histogram). Edge grains omitted.

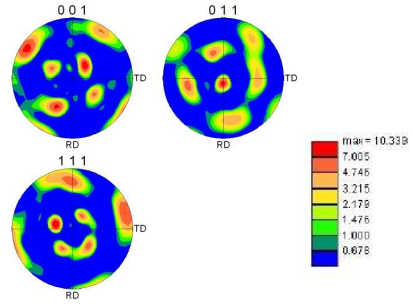

Fig.6. Pole figures for selected plane systems (before thermal exposition).

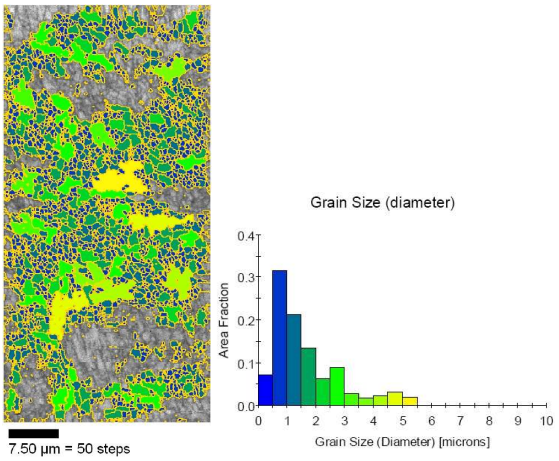

Fig. 5. Microstructure of UFG Cu after thermal exposition (grain size map and histogram). Edge grains omitted.

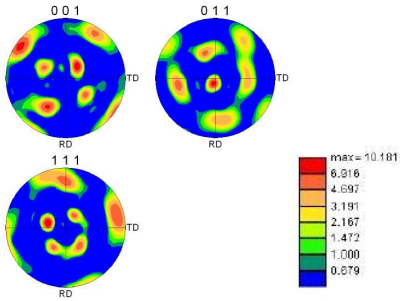

Fig.7. Pole figures for selected plane systems (after thermal exposition).

4. Discussion

The experimental results of this work confirm stability of UFG microstructure of Cu studied in [8] and exhibiting better fatigue performance than coppers studied by other authors. Good stability was proved both for fatigue loading at room temperature and for thermal exposition without mechanical loading at temperature of 180°C for 6 minutes. No substantial grain growth or development of bimodal structure was found. This result is in agreement with high fatigue performance of UFG Cu documented in Fig. 1.

The above mentioned results are in agreement with the determination of texture changes after thermal exposition. The texture is in the first approximation not influenced by annealing at 180°C for 6 minutes. Only minor changes in plane {001}, Figs.6 and 7, and in the texture intensity can be detected. This finding is different from that published in [4] where annealing of UFG Cu after 2 ECAP passes at 170 °C resulted in apparent weakening of texture. After

annealing at 200 °C the components of the deformation texture had almost completely disappeared. Similar results were found [5] for UFG Cu after 12 ECAP passes.

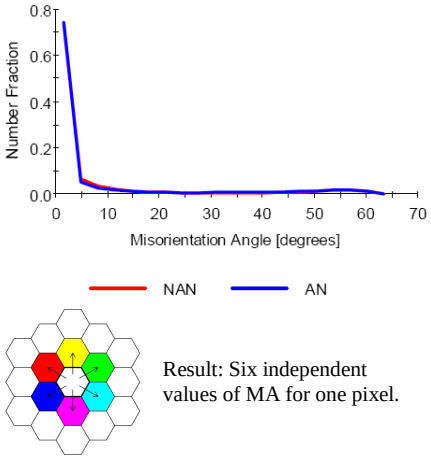

Fig.8. Changes in MA before and after thermal exposition. Insert: scheme of MA calculation.

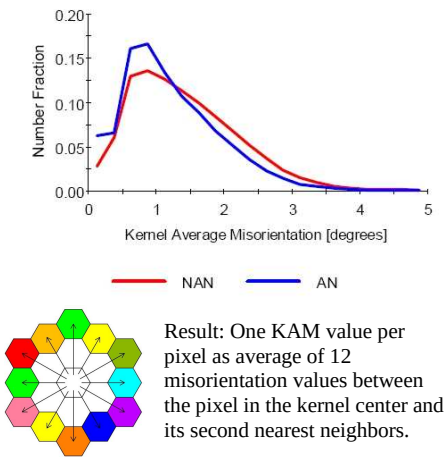

Fig.9. Changes in KAM before and after thermal exposition. Insert: scheme of KAM calculation.

5. Conclusion

Microstructure of UFG Cu studied in previous work [8] and exhibiting better fatigue performance than that reported for UFG coppers in literature is stable after fatigue loading in high- and very high-cycle region and also after thermal exposition at 180 °C for 6 minutes. No substantial grain growth or development of bimodal structure was observed. Also the texture remained stable.

Acknowledgement

This work was financially supported by the Academy of Sciences of the Czech Republic under the contracts 1QS200410502 and AV0Z20410507. This support is gratefully acknowledged.

References

[1] M. Zehetbauer, Y.T. Zhu, eds., Bulk Nanostructures Materials, Wiley-VCH Verlag (2009).
[2] N.A.Akhmadeev, N.P. Kobelev, R.R. Mulyukov, Ya. M. Soifer and R.Z. Valiev, *Acta Metall. Mater., 41* (1993) 1041.
[3] J. Lian, R.Z. Valiev and B. Baudelet, *Acta Metall. Mater., 43* (1995) 4165.
[4] X. Molodova, S.Bhaumik, M. Winning, G. Gottstein, *Mater. Sci. Forum, 503-504* (2006) 469.
[5] X. Molodova, S.Bhaumik, M. Winning, R.J. Hellmig, *Mater. Sci. Eng., A 460-461* (2007) 204.
[6] X. Molodova, G. Gottstein, R.J. Hellmig, *Mater. Sci. Forum, 558-559* (2007) 259.

[7] H.W.Höppel, M. Brunnbauer, H. Mughrabi, R.Z. Valiev, A.P. Zhilyaev, *Materials week 2000*, Frankfurt, 25-28 September 2000, Munich, 2001, [online]. http://www.materialsweek.org/proceedings/.
[8] L. Kunz, L., P. Lukáš, M. Svoboda, *Mat. Sci. Eng. A424* (2006) 97.
[9] L. Kunz, L., P. Lukáš, Z. Zúberová, *Materálové inžinierstvo 14* (3/2007) 8.
[10] L. Kunz, L., P. Lukáš, M. Svoboda, *Mater. Sci. Forum 567-568* (2007) 9.
[11] H. Mughrabi, H.W. Höppel, M. Kautz, *Scripta Mater. 51 (2004)* 807.
[12] S.R. Agnew, A.Y. Vinogradov, S. Hashimoto, J.R. Weertman, *J. Electron. Mater. 28* (1999) 1038.
[13] A. Vinogradov, S. Hashimoto, *Mater. Trans. 42* (2001) 74.

Transcom 2009, 22-24 June 2009
University of Žilina, Žilina, Slovak Republic

Influence of the Reheating Conditions on Structural Change of C-Mn-Nb-V Steel

Lenka Némethová[1], Martin Fujda[2], Imrich Pokorný[1]
[1] Technical University of Košice, Faculty of Metallurgy, Department of Metal Forming, Letná 9, 042 00 Košice
[2] Technical University of Košice, Faculty of Metallurgy, Department of Materials Science, Park Komenského 11, 042 00 Košice

Abstract: The heating of C-Mn-Nb-V steel was realized for different temperatures and times. The structural changes were observed after the exceeded of some temperature (precipitation dissolution temperature) such as 1100ºC, where the austenite grain size (AGS) was from 63 to 162 μm. This temperature is a threshold temperature for the abnormal austenite grain size. It is caused by a drag effect of carbides and nitrides Nb and V to grain boundary nearby this temperature. Experimental data were compared with calculated. Part of the experimental material was submitted to dilatometers test. The results of this test were compared with simulation by software Hardenability Database. Good coincidence was observed between the dilatometers test and the simulation data.

Keywords: heating temperature, holding time, average austenite grain size (AGS), dilatometers, precipitation

1. Introduction

The C-Mn-Nb-V steel (according to the ULSAB classification) is HSLA steel with the R_e=210-550 MPa. This steel is characterized by [1-4] as steel with high strength, good toughness and weldability. Perfect mechanical properties are obtained by balanced chemical composition with the controlled thermomechanical processing. HSLA is alloying separately with Nb, Ti and V or in their combination [1,5]. One of the important parameters for ensuring of uniformity and uncoarsening austenite microstructure is the heating temperature. This temperature influences on a grain size, precipitation dissolution degree and austenite stabilization. Hence we need to know the heating temperature for the required dissolution for the following microalloying elements: carbides, nitrides and carbonitrides. Guarantee of uniformity and uncoarsening can be achieved by delaying of austenite grains growing during the heating process in the furnace. Delay effects are making by non-soluble particles of carbides, nitrides or carbonitrides which show a strong drag effect to grain boundary. These particles lose their function of delay whereby they enter to solid solution after exceeding the specific temperature (precipitation dissolution temperature) and AGS begin to grow [6,7]. The strong influence of temperature on the grain size can be interpreted as a measure for dissolution of carbonitrides Nb and V [8]. Next parameter to ensure the uniformity and uncoarsening austenite microstructure is the time, which has a weak effect [6,7].

2. Experimental Procedure

Material: The chemical composition of the CMnNbV steel is shown in Tab. 1.
Experiment: The samples were heated from 950 to 1250ºC with a holding time on temperature from 10 to 60 min and the process was finished by their quenching.

Microstructure: The experimental material microstructure was investigated by optical microscopy Vanox-T. For optical microscopy to original austenite grain size the etching of picric acid was used.
Simulations: Thermomechanical simulations were carried out by Hardenability Database [9] and dilatometers experiment by Ernst Leintz Wetzlar. For the dilatometers test Φ 4mm and 50mm length samples were used.

Element	C	Mn	Si	P	S	V	Nb	Ti	Al	B	N	O	H
[wt.%]	0,12	1,54	0,12	0,004	0,001	0,18	0,048	0,010	0,015	0,0005	0,0042	0,0015	1,30 [ppm]

Tab.1. Chemical composition of tested steel

3. Results and Discussion

3.1 Influence of Heating Temperature on Average AGS

An average AGS increased with the increasing temperature as is shown in the Fig.1. Temperature above 1100ºC represented the strong influence of NbC, Nb(CN) to an abnormal growth of the AGS. AGS is between 35 μm (at the lowest temperature and holding time) to 600 μm (at the highest temperature and holding time to temperature). According to [10] grain coarsening during reheating occurs at a temperature significantly (100-150ºC) below the solubility temperature calculated for coarse particles.

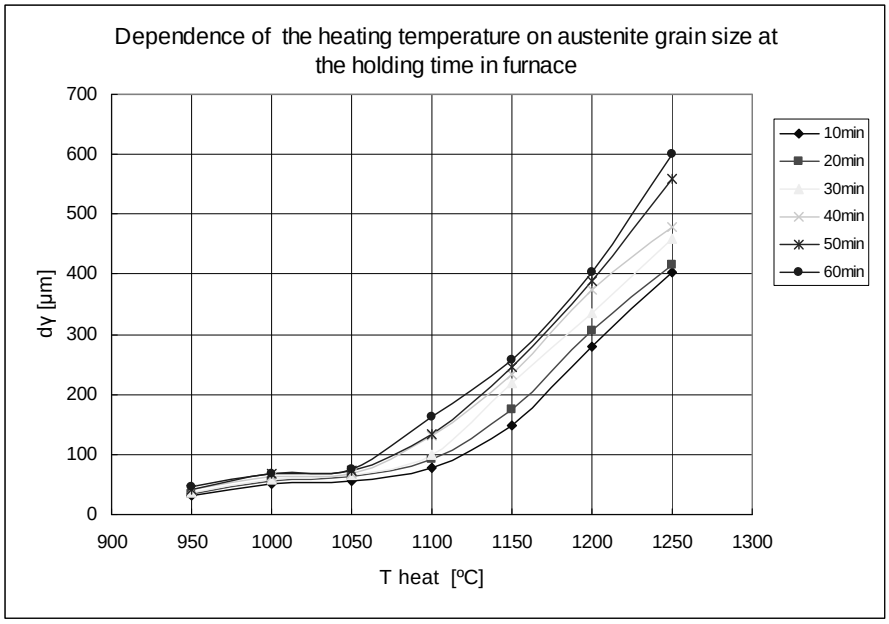

Fig.1. Dependance of heating temperature on the average austenite grain size

From experimental data was derived regression Eq.1 describing dependence of AGS on reheating parameters:

$$d_\gamma = 6{,}589.10^{-28} * T_{heat}^{\ 9{,}51} * t_{hold}^{\ 0{,}2437} \quad [\mu m] \qquad (1)$$

These experimental values were

compared with the calculated data. Comparison of experimental and calculated data is shown in the Fig. 2.

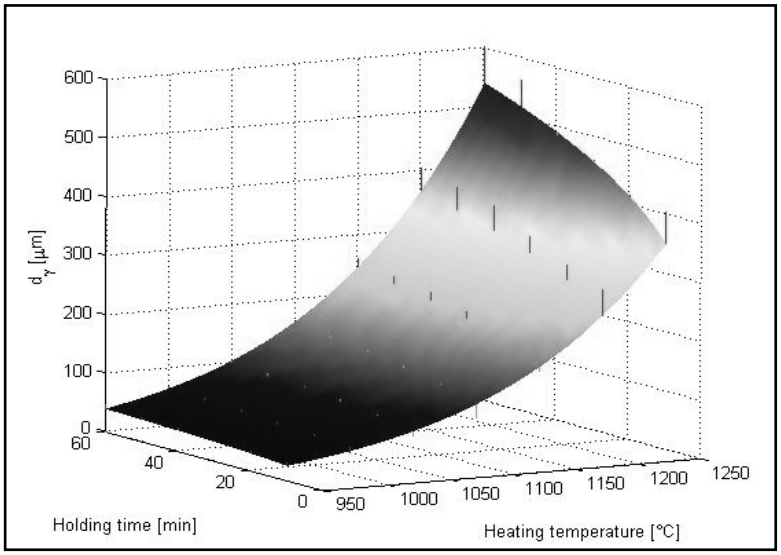

Fig.2. Graphical characterization of the Eq. 1

Experimental values are in good coincidence with calculated data with small deviations. Illustrated area corresponds with measured experimental values and it gives a possibility to define different grains size for the other calculated temperatures and times.

3.2 Determination of Phase Transformation from the Simulation and the Dilatometers Test

Simulation of phase transformation in Hardenability Database shows a good coincidence comparative with the dilatometers test (see Fig.3). Temperatures A_{c3} = 727ºC and A_{c1}=860ºC from simulation of Hardenability Database are a bit different that temperatures from dilatometers test A_{c1}=738,9ºC and A_{c3}=867,1ºC. The shapes of curves are similar too.

Cooling rates of the experimental dilatometers test were from 0,018ºC/s to 4,27ºC/s (see Fig. 3**).** It coincident with [11] the A_{r3} temperature decreased as the cooling rate and the Nb content increased.

4. Conclusion

From these results we make following conclusions:

- average AGS increased with increasing temperature
- the abnormal high AGS is achieving after the exceeded of precipitation dissolution temperature where the microalloying elements are in solution
- the good coincidence of phase transformation temperatures of Hardenability database and dilatometers test

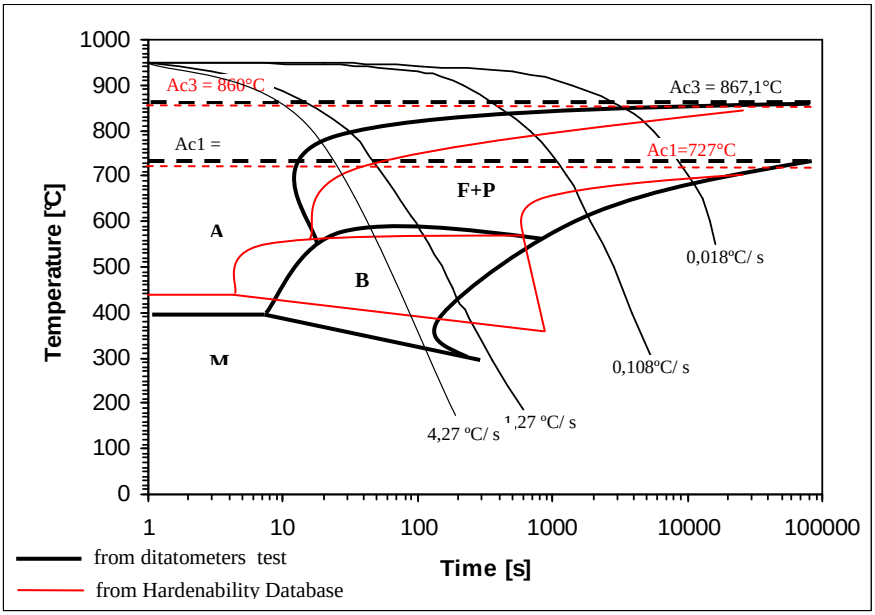

Fig. 3. CCT diagrams designed by Hardenability Database and dilatometers test

Acknowledgement

This research was supported by the grant EUREKA E!4092 MICROST.

References

[1] www.autosteel.org/AM/TemplateRedirect.cfm?Template=/CM/ContentDisplay.cfm&ContentFileID=9298
[2] DEARDO, A.J.: Microalloyed strip steels for 21st century, Materials Science Forum Vols. 284-286 (1998), p. 15-26
[3] KORCHYNSKY, M.: Advanced Metallic Structural Materials and a new role for microalloyed steels, Materials Science Forum Vols.500-501 (2005), p.471-480
[4] RODRIGUEZ-IBABE, J.M.: Thin slab direct rolling of microalloyed steels, Materials Science Forum Vol. 500-501 (2005), p. 49-62
[5] www.oulu.fi/elme/ELME2/PDF/Diplomityot/Masters_Thesis_Albert_Satorres%20.pdf
[6] KVAČKAJ, T: Vplyv riadeného valcovania na vlastnosti konštrukčných mikrolegovaných ocelí, KDP, Košice, október 1982
[7] ZEMKO, M.: Výskum plastických deformácií pomocou MKP, PhD. práca, jún 2006
[8] KLEIN, M., SPINDLER, H., LUGE, A., RAUCH R., STIASZNY, P., EIGELSBERGER, M.: Thermomechanically hot rolled high and ultra high strength steel grades – processing, properties and applications, Material Science Forum Vols. 500-501 (2005), p. 543-550
[9] software HARDENABILITY DATABASE, year 2008
[10] SELLARS, C.M.: Modeling strain induced precipitation of niobium carbonitrides during hot rolling of microalloyed steel, Materials Science Forum Vols. 284-286 (1998), p. 73-82
[11] KANG, NAMHYUHN, P., JIN, J., SANGHO, B., LEE, Y., CHO, K-M.: Effect of finishing rolling temperature on the microstructural behavior for Fe-0,1C steel as a function of niobium content, Advanced Materials Research Vols. 26-28 (2007), p. 55-60

Transcom 2009, 22-24 June 2009
University of Žilina, Žilina, Slovak Republic

Cutting Conditions and Surface Integrity during Grinding.

[*]Martin Novak, [*]Frantisek Holesovsky
[*]J. E. Purkyne University in Usti nad Labem, Faculty of Production Technology and Management, Department of Technology and Material Engineering, Pasteurova 3334/7, 400 01 Usti nad Labem, Czech Republic. {novak, holesovsky}@fvtm.ujep.cz

Abstract. This text deals with problems of cutting conditions during grinding and subsequently evaluation of surface quality. This text arises from research of surface integrity during hardened steels grinding and subsequently dynamic loading with monitoring of changes of quality surface in normal and corrosive surrounding.

Keywords: Cutting conditions, grinding, surface quality, dynamic loading, corrosive surrounding

1. Introduction

Fundamental of this experiment is evaluation of surface quality of parts, which are in samples shape with heat treatment by hardening and drawing to hardness 62 [HRC]. These samples are grounded by same cutting conditions and subsequently is evaluated surface quality in observe components of surface integrity. These prepared and evaluated samples are subsequently dynamic loaded in corrosive surrounding make by corrosion chamber.

2. Implementation of Experiment

The experiment was made in laboratory of faculty including heat treatment, machining and dynamic loading in different surrounding. Material of samples was steel 14 109.6 (mark: CSN 42 0002), bearing steel.

2.1. Prepare of Samples, Machining

The samples were circle's profile. The samples were heat treatment by hardening and drawing to harness 62 [HRC]. They were all by same cutting conditions grounded inclusive:

- cutting speed of tool, 37 [m.sec^{-1}];
- cutting speed of workpiece, 20 [m.min^{-1}];
- feed, 0,26 [mm.min^{-1}];
- cutting surrounding (with cutting fluid)

Changes of cutting conditions were in kind of abrasive tool used:

- SG grain
- CBN grain

Half of samples were prepared by SG grain and the second half was prepared by CBN grain. This intention was induced by effort find out how the quality of surface hanged in depend on used kind of abrasive grain and subsequently changes of surface quality in depend on number of dynamic loads cycles. This experiment was backup the claim on dynamic load in corrosive surrounding.

2.2. Cutting Conditions

During grinding process is workpiece strained more than by conventional methods of machining by defined edge geometry. Seeing that during grinding process isn't material of workpiece removal evenly by one edge but one is removal by large quantity of grain (edges) at a time, is happening to grow of cutting forces and load larger of same tool and workpiece. Total cutting force composed of particular components of force as:

- normal force, Fp
- tangential force, Fc
- feed force, Ff

In Fig. 1 is shown allocation of components of forces during grinding and in Fig. 2 is shown real size of Fp and Fc components of force during grinding measured by Kistler dynamic force sensor. These forces were measured on hardened steel ground with cutting speed 37 [m.sec^{-1}] and feed rate 0,26 [mm.min^{-1}].

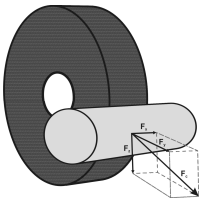

Fig. 1. Allocation of components of forces during grinding.

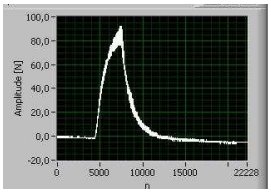

Normal component of force

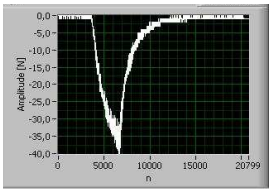

Tangential component of force

Fig. 2. Real forces during grinding.

2.3. Heat by Grinding

With grow of forces by grinding related to heating. The heat is generated from relative working of abrasive tool and workpiece. Heat affect fundamentally follows using proprieties of parts and their durability. At machined zone of surface rising layer by defined depth which is affected of these forces and heat. Total of heat quantity is given sum of elements:

- heat transfer into workpiece
- heat transfer into tool
- heat leaving in chips
- heat extracting by cutting fluids
- excitation heat

In Fig. 3 is shown heat-field distribution on abrasive tool with SG and CBN grain and heat-field on workpiece, hardened steel. This heat is during grinding with cutting speed 37 [m.sec^{-1}] and feed rate 0,26 [mm.min^{-1}].

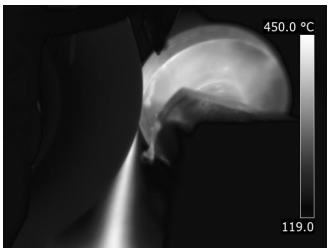

heat field of SG grain during grinding

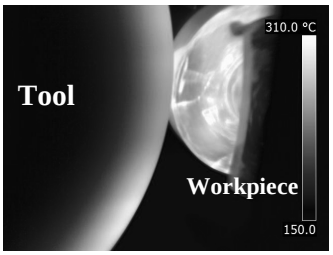

heat field of CBN grain during grinding

Fig. 3. Heat-field by grinding.

3. Surface Integrity

Surface integrity is very important part of total quality surface evaluation of machined parts. In our experiments we evaluate total seven components of surface integrity:

- roughness, material portion
- geometrical accuracy (roundness)
- hardness
- residual stress
- structure of material
- heat changes
- cracks

By components of surface integrity we evaluate quality of surface by parameters of same components of surface integrity. The parameters are given by CSN EN ISO standard.

For show of influence of cutting conditions on surface quality will be compared three components of surface integrity:

- roughness, profile of surface and material portion of surface profile, Fig. 4.
- roundness, Fig. 5.
- residual stresses, Fig. 6.

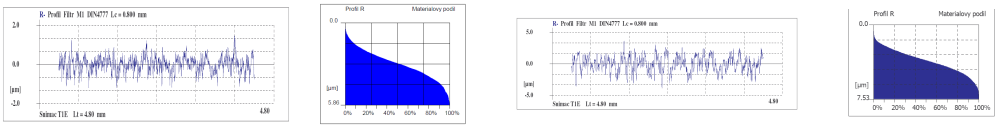

SG grain (Roughness R_a 0,28 μm)

CBN grain (Roughness R_a 0,86 μm)

Fig. 4. Profile of surface and roughness, parameter Ra with two abrasive wheels using by same cutting conditions, cutting speed 37 [m.s^{-1}], feed rate 0,26 [mm.min^{-1}].

SG grain

CBN grain

Fig. 5. Geometrical accuracy (roundness) of workpiece with two abrasive wheels using by same cutting conditions, cutting speed 37 [m.s^{-1}], feed rate 0,26 [mm.min^{-1}].

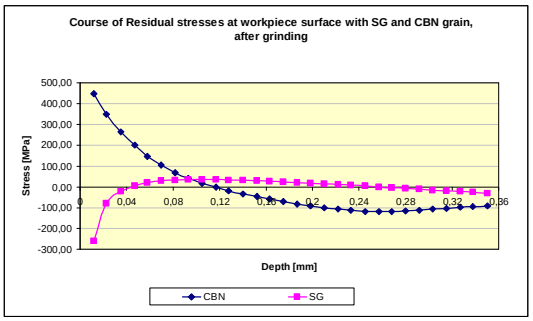

Fig. 6. Course of residual stresses at workpiece surface with two abrasive wheels using by same cutting conditions, cutting speed 37 [m.s^{-1}], feed rate 0,26 [mm.min^{-1}].

4. Dynamic Loading

In our experiments are the Workpieces exposed to dynamic loading after grinding. We pursue changes of quality of surface in depend on number of dynamic load cycles and in depend on dynamic load surroundings. Changes on surface of workpiece dynamic loaded in corrosive surrounding are shown on Fig. 7.

Surface of workpiece loaded at corrosive surrounding

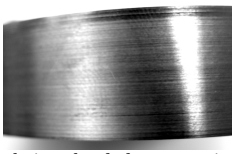

Surface of workpiece loaded at corrosive surrounding with oil supply

Fig. 7. Workpieces loaded in corrosive surrounding.

In the Fig. 7, left side we can see changes on surface in form of abrasion wear, pitting and crack formation. This problem is due to corrosive surrounding caused and its activity during dynamic loading.

In the Fig. 7, right side we can see surface of workpiece loaded in corrosive surrounding too, but with oil supply. On surface we can see no crack formation, abrasive wear and pitting. It's due to action of inactive oil incoming into area of workpiece and ceramics wheel contact. Ceramics wheel loaded workspaces in special machine by same loaded force.

5. Conclusion

On base of our experiments with cutting conditions, surface quality and changes of surface dynamic loaded Workpieces on bearing steels, we can make the conclusion, that surface quality and cutting conditions along with relate. This fact is supported by dynamic loaded workspaces in different surrounding and changes of surface integrity components evaluate in depend on cutting conditions of workspaces and loaded surrounding.

This experiment and other following researchers of this problem is very important for construction of new tools, using of new tools material, cutting fluids reduction, high speed grinding, reduction of production coast and many others.

References

[1] HOLEŠOVSKÝ, F., NOVÁK, M. *Process coolant influence at grinding*. In III.Mezinárodní konference Strojírenská technologie – Plzeň 2009. Plzeň : ZU v Plzni. 2009. s.52. ISBN 978-80-7043-750-6.

[2] MÁDL, J., HOLEŠOVSKÝ, F., RÁZEK, V., KOUTNÝ, V., VILČEK, I., MICHNA, Š., NÁPRSTKOVÁ, N., NOVÁK, M. *Integrita obrobených povrchů z hlediska funkčních vlastností*. M. Sláma. Ústí n. Labem : FVTM UJEP Ústí n. Labem. 2008. 230 s. ISBN 978-80-7414-095-2.

[3] MASLOV, J., N. Teorie broušení kovů. Praha : SNTL, 1979. 246 s.

[4] NÁPRSTKOVÁ, Nataša, NÁPRSTEK Vladimír. Monitoring of proces values in grinding. In *7th International Scientific Conference Automation inproduction planning and manufacturing*. Žilina-Valča, 2.-4.5.2006, Sborník přednášek. Žilina: 2006, TU Žilina. ISBN 80-8070-537-2.

[5] NOVÁK, M., HOLEŠOVSKÝ, F. *Studium změn broušené povrchové vrstvy při dynamickém zatěžování*. In Manufactorig Engineering. 2008. Prešov : FVT TU Košice, 2008. Studium změn broušené povrchové vrstvy při dynamickém zatěžování. s. 11-13. ISSN 1335-7972.

[6] NOVÁK, M., HOLEŠOVSKÝ F. *Vliv brousícího nástroje na kvalitu povrchu a povrchové vrstvy*. ITC 2009 – VII. Mezinárodní nástrojařská konference 2009 [CD-ROM]. Zlín : 2009. ISBN 978-80-7318-794-1.

Transcom 2009, 22-24 June 2009
University of Žilina, Žilina, Slovak Republic

Boiling Heat Transfer on Fins Covered with Thin Wire Mesh Structure

[*]Tadeusz Orzechowski, [*]Anna Zwierzchowska, [*]Sylwia Zwierzchowska
[*]Kielce University of Technology, Al. Tysiąclecia PP7, 25-314 Kielce, Poland, {todek, annazw, sylwiazw}@tu.kielce.pl

Abstract. This investigation was conducted for non-isothermal surfaces of phase-change heat exchangers to establish the possibility of increasing the heat transfer rate. The experiments involved measuring the distribution of surface temperature along the centerline of a long fin with and without a wire mesh structure. The data were represented graphically as boiling curves. The analysis shows that this technology of surface enhancement contributes to an increase in the heat transfer rate.

Keywords: heat transfer, boiling, fin, wire mesh structure, thermovision.

1. Introduction

In response to the energy crisis, we are faced with the necessity to look for alternative energy sources, especially renewable ones. Higher prices of fossil fuels inspire new solutions to boost energy efficiency and reduce consumption. Efficient use of energy is particularly important, for instance, in the case of compact heat exchangers, as they have to operate efficiently at small temperature differences. The most suitable solution is to apply phase-change devices such as thermosyphons and heat pipes, which are now frequently used in solar panels, recuperators, condensers and evaporators in heat pumps, etc. One of the factors limiting the development of such devices is insufficient knowledge of the physics of boiling. In consequence, there exist no appropriate computation procedures to be used, especially if surfaces with microcoverings are applied to increase the heat transfer rate.

The majority of investigations dealing with boiling heat transfer focus on surface enhancement and improvement with respect to the heat transfer coefficient. Surface enhancement is a passive technique. One of the earliest surface modification technologies was matt sanding by means of sandpaper with different grits. The treatment leads to a distinct increase in the number of active nuclei on the heating surface, as shown in Ref. [1]. The detachment of vapor bubbles intensifies convective movements. The process results in mass transfer and heat flux removal. This type of treatment, however, does not cause considerable changes in the critical heat flux, when compared with a smooth surface. The method effectiveness is therefore limited [2].

However, the rise in the heat transfer rate is insufficient with respect to the constantly increasing demand. It was necessary to develop new techniques to intensify the heat transfer process. Different layers may be deposited by thermal spraying of powder or sintering of capillary-porous layers made of metal fibers. The industrially produced structures include High Flux (Union Carbide), Thermoexcel-E (Hitachi), Gewa-T, -TX, -TXY (Wieland), etc.. References [3] and [4] provide an extensive review of the techniques used.

Effective surface enhancement can be achieved by applying wire mesh layers. They are produced by depositing one layer over another. In the past, the layers were pressed together by taking advantage of their natural elasticity (for instance, in heat pipes). Sometimes, specially designed holders had to be used. A disadvantage of such a design was high contact resistance leading to impeded heat transfer along the fin centerline. At present, sintered coatings are frequently applied to improve the performance of the heating surface. It should be noted that a wire mesh structure can be used to produce a capillary porous structure with pre-determined diameters of pores. When pores are uniformly distributed over the surface, it is easier to model and analyze the effects of selected parameters on phase-change heat transfer. There exists relatively extensive literature describing the heat transfer on mesh structures made of different materials. The data are presented in the form of correlations. Their use, however, is limited due to differences in the technologies of joints. Isothermal surfaces are generally horizontally oriented and thus difficult to measure.

The purpose of the study was to determine the effect of surface enhancement on the boiling heat transfer process by applying wire mesh structures on the non-isothermal fin surface.

2. Results

The experiments were conducted using a special measurement facility, the main element of which was a copper fin with a thickness of 3 mm and a length of about 80 mm. The side in contact with the boiling fluid was covered with a wire mesh structure intensifying the heat transfer. The measured quantity was the distribution of surface temperature using a Jenoptik VarioCAM HR thermovision camera. Figure 1 presents a thermogram obtained for the fin.

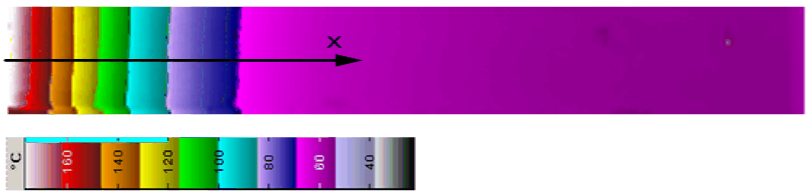

Fig. 1. Thermogram of the element under analysis

The analysis was conducted for long fins covered with a one- or two-layer copper wire mesh structure with a wire thickness of 0.2 mm and a mesh opening size of 0.40 mm. The influence of the mesh structures on the heat transfer process was determined by comparing the results with those obtained for the smooth surface. Fig. 2 shows a distribution of temperature along the centerline of the fin for water. A more rapid drop in temperature along the fin centerline testified to a considerable increase in the heat transfer rate for the mesh structures compared to the smooth surface.

The measured distributions of temperature in Fig. 1 shows that the heat transfer on the fin can be treated as a one-dimensional problem. In such a case, the boiling curve can be determined assuming that the coefficient of heat transfer is in the form of a power series of superheat. The procedure is analyzed thoroughly in Ref. [5].

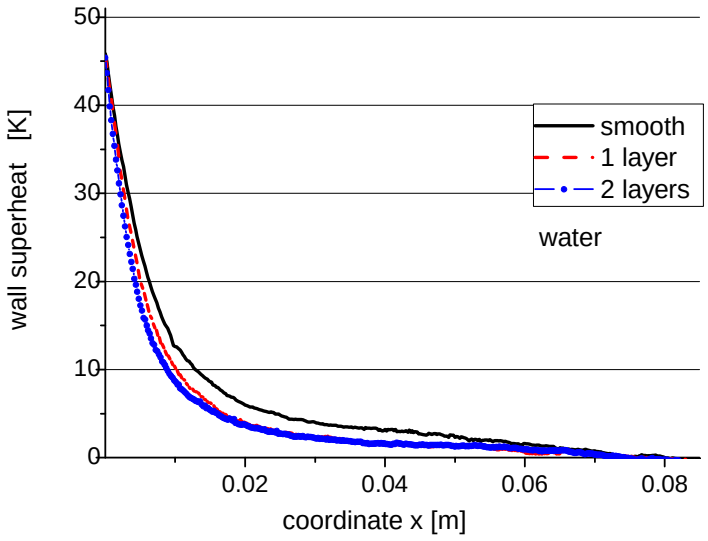

Fig. 2. Wall superheat along the fin centerline for water.

In Fig. 3 boiling curves for the wire mesh structures compared to the smooth surface.

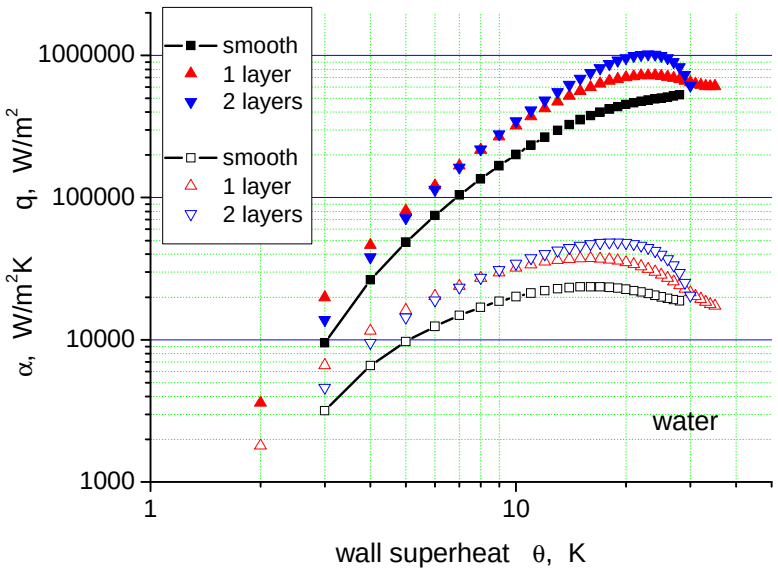

Fig. 3. Boiling curves for the smooth surface and the one- and two-layer wire mesh structures, with water as a heat transfer medium.

3. Conclusion

Compared to the smooth surface, the wire mesh structures are responsible for an increase in the heat transfer rate at boiling. The maximum heat flux of water in boiling heat transfer is 0.528 MW/m^2, 0.724 MW/m^2 and 1.023 MW/m^2 for the smooth surface, the one-layer mesh structure and the two-layer mesh structure, respectively. From Figs. 3 it is clear that nucleate boiling is initiated at lower superheat. For ethanol, the wire mesh structures contributed to a significant increase in heat transfer at low values of superheat, which was due to different wettability of the two fluids. Similar conclusions were drawn for the heat transfer coefficient.

Acknowledgement

The work has been financed with the funding for scientific research in the years 2006-2007 as a research project.

References

[1] KURIHARA, H.M., MYERS, J.E., The Effects of Superheat and Surface Roughness on Boiling Coefficients. AIChE J., Vol. 6, No. 1. 1960, pp. 83-91.

[2] RAMILSON, J.M., SADASIVAN, P., LIENHARD, J.H. Surface factors influencing on flat heaters, ASME J. Heat Transfer, Vol. 114, 1992, pp. 287-290.

[3] WEBB, R.L. Principles of Enhanced Heat Transfer, Wiley, New York, 1994.

[4] PONIEWSKI, M.E., THOME, J. R. Nucleate Boiling on Micro-Structured Surfaces, Heat Transfer Research, http://www.htri-net.com/ePubs/epubs.htm, 2008.

[5] ORZECHOWSKI, T. Local values of heat transfer coefficient determination on fin's surface. Experimental Thermal and Fluid Science, 31 Issue 8, 2007, pp. 947-955.

Transcom 2009, 22-24 June 2009
University of Žilina, Žilina, Slovak Republic

Evaluation of Boiling Heat Transfer Coefficients on Fin's Smooth Surface

[*]Tadeusz Orzechowski, [*]Anna Zwierzchowska, [*]Sylwia Zwierzchowska
[*]Kielce University of Technology, Al. Tysiąclecia PP7, 25-314 Kielce, Poland, {todek, annazw, sylwiazw}@tu.kielce.pl

Abstract. The investigation discusses boiling heat transfer on non-isothermal surfaces. Using the example of a long fin, it was possible to show that the correlations presented in the literature do not provide sufficiently accurate result.

Keywords: fin, boiling, thermovision, boiling heat transfer correlations.

1. Introduction

This paper is concerned with the experimental determination of the boiling heat transfer rate for smooth surfaces of finned elements in heat exchangers. Such systems are suitable for heating, ventilation and air-conditioning purposes as well as in devices where large amounts of heat are transferred at small temperature differences. The computation procedures required to establish the Nusselt number are based on different correlations. However, the results obtained in this way are not sufficiently accurate. This is probably due to the fact that the correlations usually concern heating surfaces with a constant temperature. In finned elements of heat exchangers, the temperature changes along the centerline. It is essential to individually determine the local value of the heat transfer coefficient.

There exist numerous correlations applied to different surfaces in the specialized literature [1]. The most popular and most common is that proposed by Rohsenow. It assumes that the heat transfer process is affected by the formation and movement of vapor bubbles. An increase in the number of bubbles results in liquid mixing and higher rate of convection. The derived relationship includes constant C_{sf} and the exponent n. Each quantity is selected individually, depending on the type of surface and material. A review of works dealing with similar experiments [2] shows that values of these constants are only given. The investigation results can also be described using other, more accurate correlations. An extensive analysis of the most common relationships can be found in Ref. [3].

The study was conducted with a view to assessing the applicability of selected correlations and then determining a boiling curve for systems with variable surface temperature. An example of such a surface is a fin.

2. Test facility

A special measurement facility was used. The main element was a thin smooth surface fin with a length of approximately 80 mm. The measurements were conducted in a closed bakelit vessel (Fig. 1.).

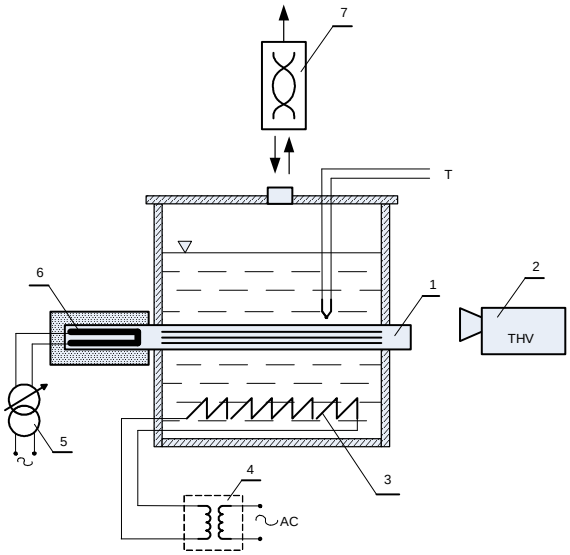

Fig. 1. Schematic diagram of the test apparatus: 1 – sample, 2 – thermovision camera, 3 – auxiliary heater, 4 - electrical current separation unit , 5 – transformer, 6 – main heater, 7 – cooling and condensate recovery system, T – thermocouple.

The element under study was the fin with a heater mounted at the system base. As the amount of heat leaving the system is not sufficient to maintain boiling in the whole volume, the system was equipped with an auxiliary heater, i.e. a spirally bound resistance wire at the bottom of the vessel. The temperature of a selected factor was controlled using a coat thermocouple. The measurement stand was also equipped with a cooling and condensate recovery systems. The vapor of the boiling fluid was condensed in the system of two radiators connected in series. After condensation, the medium is gravity-fed to the vessel. The design assumes that there is atmospheric pressure inside the vessel. The Jenoptik VarioCAM HR thermovision camera applied to the measurements equipped with a microbolometric matrix (640 x 480 piksels) operates in the long-wave infrared range (7.5 … 14 μm). The quantity measured was the distribution of temperature along the fin centerline. According to the procedure presented in Ref. [4], the data is then used to determine a boiling curve.

3. Results

The tests were conducted for fins 80 mm in length made of copper and aluminum. Their surfaces were polished with sandpaper no 1200. After the fins were fitted in the measurement facility (Fig. 1), the thermovision camera was employed to determine the distribution of temperature. Basing on the data, it was possible to draw a boiling curve. Each of the measurements was conducted for four different values of power of the main heater and for the same power of the auxiliary heater. Very good repeatability of results was obtained. Selected results are presented in Figs. 2 and 3. The figures include the curves drawn on the basis of the Rohsenow, Labuntsov and Kruzhilin correlations available in the literature. The values of the constants used were selected according to Ref. [3].

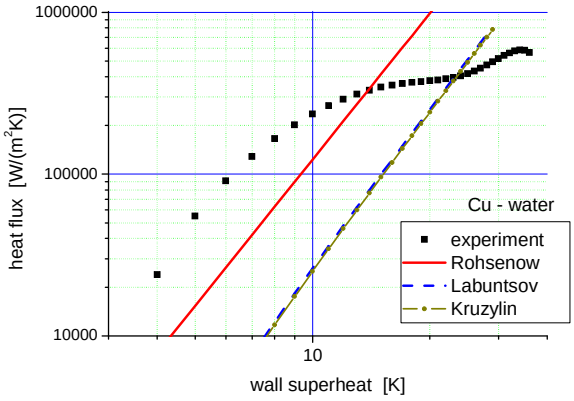

Fig. 2. Boiling curve for water at ambient pressure.

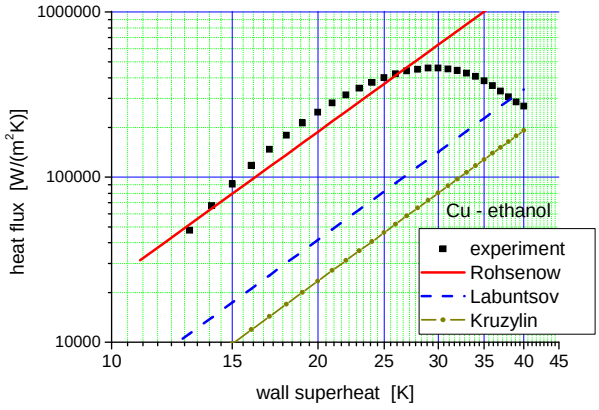

Fig. 3. Boiling curve for ethanol at ambient pressure.

4. Conclusion

The measurement data were used to draw boiling curves for smooth copper and aluminum surfaces operating with water or ethanol medium at ambient pressure. In the nucleate boiling regime, corresponding curves were calculated basing on the appropriate correlations, for which the values of certain parameters were established according the procedure found in Ref. [2].

The differences between the results obtained in the experiments and those of the calculations related to the correlations are responsible for the changes in temperature along the fin centerline. Of importance is the vertical orientation of the heating surface.

Nishikawa [5] suggests that a change in the orientation of the surface from horizontal to vertical results in an over 200% increase in heat flux. The phenomenon is characteristic of low values of wall superheat. For high values of wall superheat, the differences are smaller. The correlations analyzed in the study were those of Rohsenow, Labuntsov and Kruzhilin. The best approximation, however, was obtained for the Rohsenow correlation. The other two provided even lower values of the heat flux. Similar conclusions concerning these correlations were drawn in Ref. [3]

Acknowledgement

The work has been financed with the funding for scientific research in the years 2006-2007 as a research project.

References

[1] WEEB, R. L. *Principles of Enhanced Heat Transfer*. Wiley, New York.

[2] PIORO, I. L. *Experimental evaluation of constants for the Rohsenow pool boiling correlation*. International Journal of Heat Transfer 42, 1999, 2003-2013.

[3] PIORO, I. L., ROHSENOW, W., DOERFER, S. S. *Nucleate pool-boiling heat transfer. II: assessment of prediction methods.* International Journal of Heat Transfer 47, 2004, 5045-5057.

[4] ORZECHOWSKI, T. *ocal values of heat transfer coefficient determination on fin's surface.* Experimental Thermal and Fluid Science, 31 Issue 8, 2007.

[5] NISHIKAWA, K., FUJITA, Y. *Nucleate Boiling Heat Transfer and Its Augmentation*. Hartnett J.P., Irvine, Jr., T.F.(ed.), Academic Press, Advances in Heat Transfer, 20 (1990), pp.1-82.

Transcom 2009, 22-24 June 2009
University of Žilina, Žilina, Slovak Republic

Production Technological Procedures of Capillary Soldering Copper Tubes

[*]Peter Pallo, Miloš Mičian, Miloš Varga
*University of Zilina, Univerzitná 1, 010 26 Zilina, Slovak Republic, tel. 00421-513 2771,
e-mail: peter.pallo@fstroj.uniza.sk

Abstract. This article deals with production technological procedures of capillary brazing copper tubes. It is oriented for working-out methodics of production procedures brazing copper manifolds. On suggest configuration were made chosen non-destruction and destruction tests of brazing joints.

Keywords: Capillary soldering, soldering,flux, solder,

1. Introduction

Soldering is used mostly for a connection of the copper tubes. Using copper is suitable for distributions of cold and hot water, for distributions in heating systems, in solar systems, distributions of oil, in gas distribution systems and also in refrigerating system. Copper tubes are also exploited of the transport medical and laboratory-technical gases etc. This technology provides high quality of the brazing joints, decreases the total costs, redeployment etc.

Abstract of brazing is defined as the way of the metallurgical connection of metal components by fused solder, when jointed surfaces are not melted, but only wet by used solder. Important condition is a good wetness of the connected material by a fluid solder. Surface atoms of the parent metal and fluid solder are very close each other; they afford properties for action of the adhesive and cohesive forces. Most often the result is mutual melting and diffusion jointed metals. The result of influence of capillary pressure, which manifests with gaps smaller than 0,5 mm, is flowing of solder (or flux) in the gap of connection by all directions. Minimal width of soldering gap must be 0,02 mm. For soldering is very important the surface tension in the contact flats between metal, fluid solder and flux (or protective atmosphere, vacuum). Condition of formation of diffusion at soldering, is removing atoms of solder and parent metal, this is conditional non-homogenity of chemical composition. Gradient of concentration defines direction of movement.

During soldering is in mutual touch the fluid solder and solid parent metal for definitely time (some seconds or minutes – according to kind of heating). According to solder kind and parent metal in limit their touch can start up one of following reactions:

- Adhesive connection,
- Mutual diffusion of solder elements and parent metal,
- Melting parent metal by used solder,
- Reaction of solder components with surface oxid of parent metal.

2. Constructional Plan of Soldering Nests

There is a dimensional drawing of designed soldering nest on the Fig. 1. For a project of this nest we used copper tubes, copper and brass adapting pipes of diameters 15, 18 and 22 mm. Connections are made by a capillary soldering, a brazing capillary soldering and by a pressing. Pressed connections are used because of a complexity solder nest. Individual used diameters of the tubes, adapting pipes and used kinds connection are designed, because they are the most used diameters of tubes, adapting pipes and kinds connections in the technical praxis. This soldering nest serves for execution destructive and non-destructive tests, and if these tests are suitable, it can serve for certification jointers according to a norm STN EN 13134.

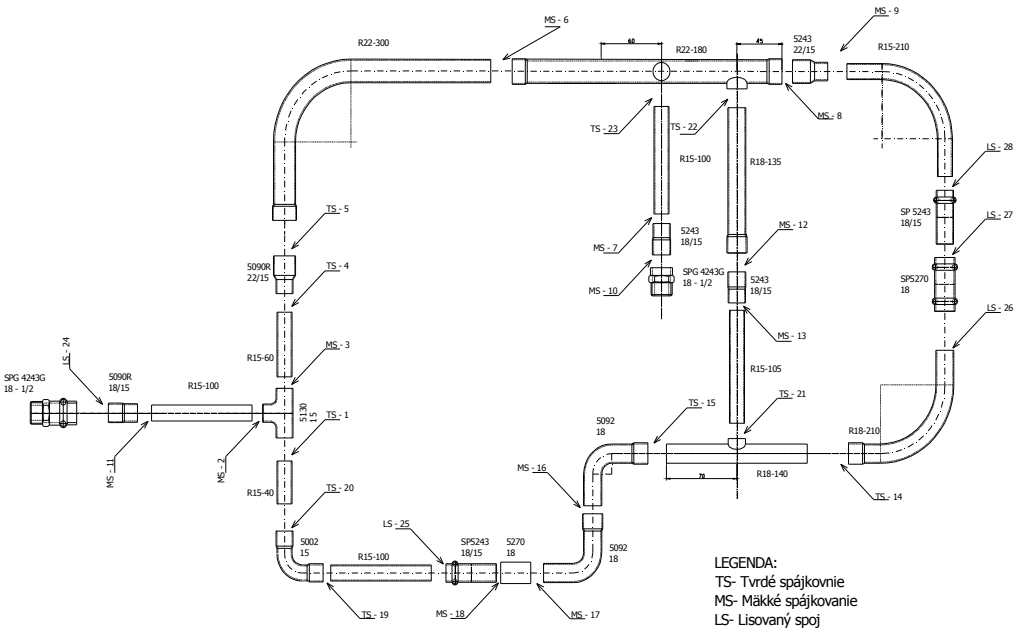

Fig. 1. Soldering nests

2.1. Basic material

Material of tubes is the copper by phosphorus desoxided with big cleanness (Cu + Ag min 99,90% a 0,015 < P < 0,040%), mark of this material quality is Cu-DHP or CW024A. Tubes are made in the level of hardness, in a limp, a half-hard or a hard one. Copper tubes are made in the rolls or in the straight pieces, with a plastic film or without it. Norm STN EN 1057 deals with the seamless copper tubes of circular conjunction for water and gas in the sanitarian and in the heating installation. Norm specifies terms, composition, properties, sampling, test methods and delivery conditions for the seamless copper tubes.

For construction made nest we used copper tubes with certificate concord SK03-ZSV-0126 issued by Technical tested institute Piešťany š.p. Producent copper tubes is Buntmetal Amsteten G.m.b.H. Fabrikstrase 4,A-3300, Amsterten Austria. At a merge material according to the norm STN-CR-ISO 15608 is kind of material, which we used, classified into the group 31. Specification individual variants of the tubes, which we used: SUPERSAN half-hard (R250) Ø 15x1; 18x1; 22x1 mm. The tubes SUPERSAN are assigned for the installer purposes in the distributions drink water, central heating and gas mediums on base hydrocarbons and their allied substances (natural gas, propane, butane, biogas etc.). Copper

tubes with smaller thickness of the wall than 1,0 mm are not generally suitable for distribution drink water and gas.

2.2. Filler materials for soldering

Filler materials used for soldering are divided according to the temperature of melting into the solders and the brazing solders. Characteristic property of the solders is their temperature of melting lower than 450ºC. Characteristic property brazing solders is melting temperature higher than 450ºC. Brazing solders are accessible in form of the sticks, wires, foils (or others semi-products) or in the form of powder. But not all materials are accessible in these forms. Brazing solders are made and marked according to norm STN EN 1044.

We use the filler metal with commercial name Rems Lot Cu3 for soldering on the nest machined by us. Identification this solder according to the norm STN EN 9453 is S-Sn97Cu3. chemical composition of solder is 97% Sn, 3% Cu **(mass%).** Listed solder does not contain plumbum, it follows, that it does not damage the human health and the environment. It does not contain silver. Melding temperature is in interval from 230 to 250°C. It is uses for soldering of the copper tubes with copper, bronze, brass adapting pipe, for installation of hot and cold water and for installation of heating with temperature of heating medium < 110ºC. Solder is in form of a wire with diameter 3 mm spooled on reel.

We used as the filler metal for capillary brazing the brazing solder with commercial name REMS LOT P6. Identification according to STN EN 10044 is B-Cu94P-710/890, melting zone in interval from 710 to 890°C. Chemical composition of used solder is 94% Cu, 6% P (mass %). Brazing solder without silver in the composition, is of lower operating temperature. It is used at brazing soldering of copper tubes with copper, bronze, brass adapting pipe, for installation of hot and cold water, installation of gas, of cooling and conditioning technology. It is delivered in the form of the square rods 2x500 mm.

2.2. Soldering flux

Flux according to the norm STN 050040 is a chemical medium, which helps at soldering by eliminating oxides and the other metal compounds from soldering area, protects this area against the next oxidation and influences favourably the surface tension of solder. Flux is a homogenous mixture of molten and non-molten chemical allied substances (organic and anorganic), a solution or a paste emulsion of matters in a dissolvent. Flux dissolves oxides and before all it inhibits their formation and the result is improvement of dipping of the parent metal by melting solder.

3. Hint of soldering procedure

Hint of soldering procedures begins preparation pre-defined procedure of soldering, called pBPS. It is soldering procedure, which is elaborated by the producer according to his previous experiences. By its formation one emanates from product, which will be produced. Pre-defined procedure of soldering is elaborated according to the norm STN EN 13134, which defines it as avowed by producer, but not accredited procedure. Test pieces needed for accrediting of soldering procedure – BPS must be produced on the ground of pBPS.

After execution of non-destructive and destructive tests of soldering procedure one elaborates record about the test of soldering procedure (BPAR) and consequently record of defined procedure soldering (BPS). Record about procedure test of soldering (BPAR) is tests notation of each testing lump including checking. Record must contain detailed entry of all inconvenient results of the tests. If there are not found differences, examiner or agent of testing organization must undersign, that the samples, made according to specific procedure of

soldering, satisfy agreed criteria for valuation samples and testing. Defined procedure of soldering (BPS) is a document, which contains needed information about definitive parameters of soldering, which are needed for attainment qualitative solder connection for defined application.

3.1. Destructive testing soldering connections

Norm STN EN 12797 deals with destructive tests solder connections. It describes procedures destructive tests and kinds of test pieces needed to execution tests on solder connections. We employed metallographic tests as microstructure observation.

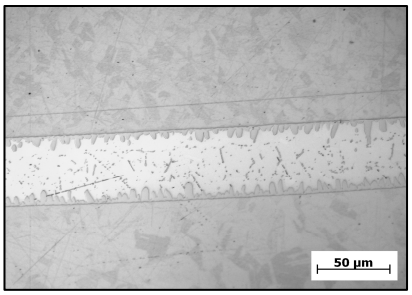

Fig. 2. Microstructure shot of the solder joint Identification of parent metal: copper tubes Cu + Ag min 99,90% s 0,015 < P < 0,040%, Identifications of filler metal: S-Sn97Cu3, etchant: without etching

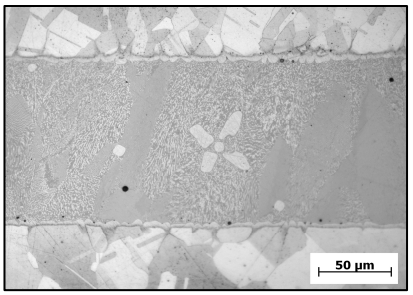

Fig. 3. Microstructure shot of the brazing solder joint Identification of parent metal: copper tubes Cu + Ag min 99,90% s 0,015 < P < 0,040%, Identifications of filler metal: B-Cu94P-710/890, etchant: $K_2Cr_2O_7$

4. Conclusion

Technology of the capillary soldering of the copper tubes gives high quality connections, decreases total costs, improves work-bench etc. Because of many advantages, which are by sequel alleged in the former clause, it is possible to evaluate this technology as one of the most best-fit for using to all kinds installations of the technical machines of buildings.

Acknowledgement

This work has been supported by Scientific Grant Agency of Ministry of Education of Slovak republic, grand VEGA No V-08-046-00.

References

[1] LEŽDÍK, V. - MIČIAN, M.- ŠKYBRAHA, J. - BOHINSKÝ, J. : *Tvorba postupov zvárania kovových materiálov*. Ikv s.r.o., Žilina, 1.vyd., 2007, 77 s.

[2] RUŽA, V.: *Pájení*. 2. vyd. SNTL Praha, 1988, 452 s

[3] LEŽDÍK, V. – BOHINSKÝ, J. – ŠTENCHLÁK, B.: *Spájkovanie medených rúrok* – [skriptum]. Vzdelávacie stredisko SPP,a.s. Žilina, 2007, 38 s.

[4] PALLO, P.: *Tvorba technologických postupov kapilárneho spájkovania medených rúr*. Diplomová práca. Žilina 2008

[5] EN 13134:2000 zavedená v STN EN 13134: *2002 Tvrdé spájkovanie*. Skúška postupu spájkovania (05 0048)

[6] EN 12797: 2000 zavedená v STN EN 12797: *2002 Tvrdé spájkovanie*. Deštruktívne skúšky spájkovaných spojov (05 0046)

Transcom 2009, 22-24 June 2009
University of Žilina, Žilina, Slovak Republic

Fatigue Threshold Analysis of quenched, Tempered and shot Peened steels

I. Fernández Pariente[*], S. Bagheri Fard[**]

[*] Universidad de Oviedo, Dpto. Ciencia de los Materiales e Ingeniería Metalurgica. Campus de Viesques, Edificio de Energía, 33203 Gijón (Spain), inesfp@uniovi.es,
[**] Politecnico di Milano, Dip.to di Meccanica, Via La Masa, 34, 20156 Milano (Italy), sara.bagherifard@mail.polimi.it

Abstract. Fatigue failure is one of the most important cases of damages in industrial components. Most of these failures occur on the surface where there are various kinds of defects such as mechanical scratches, welding cracks, forging or casting defects, decarburization, etc. Shot peening (SP) is a surface treatment usually used to increase the fatigue strength of mechanical components. In this work the fatigue strength of quenched, tempered and shot peened (Q&T+SP) low allow steel with small surface defect was studied. Two different series of 15 sandglass specimens with a micro-hole in the minimum section introduced after Q&T+SP treatments were considered, acting as a pre-existent crack. Also a formula previously proposed by the authors to predict ΔK_{th} in nitrided and shot peened steel was verified with the experimental data. Experimental results are in agreement with ones obtained with the proposed formula.

Keywords: quench and temper, shot peening, scratch, micro-hole, fatigue bending test.

Introduction

Fatigue failure is one of the most important cases of damages in industrial components. In structural engineering applications, nucleation and propagation of fatigue cracks are some of the most important characteristics in the mechanical properties of metals. Fatigue failures of metallic materials mostly occur on the surface where there are various kinds of defects such as mechanical scratches, welding cracks, forging or casting defects, decarburization, deficiencies in alloying elements, nonmetallic inclusions, etc., as well as residual stresses caused by cold or hot working.

The need of improved performances and more rational use of materials are making more and more popular the use of treatments to improve mechanical behavior of structural and machine elements [1]. Quench and temper (Q&T) processes are the most common form of hardening and strengthening heat treatment in medium-carbon steels. It is also known that these treatments provide good combination of high strength and toughness causing a small deviation of mechanical properties of steels. This reason makes them highly used in mechanical components of machines. Many researchers have extensively characterized the common properties and problems of quenched and tempered steels [2–5].

However in many cases the surface strength obtained by Q&T is not sufficient and some other surface treatments are used to improve fatigue performances of materials. Shot peening, a process used to cold working surface layer of material, is commonly used with this aim [6]. It consists of shooting a flow of small shots to a metallic surface under controlled conditions, with an impact energy able to cause plastic deformation on the surface layer of material, thus introducing compressive residual stresses and material hardening in and just under the free surface. The effects of this treatment are responsible for improved fatigue behavior of the shot

peened parts. This improvement is more pronounced in the case of notched elements, due to the severe gradient of the applied stresses [7, 8]. Its main effect consists of arresting crack propagation more than preventing crack initiation. Bearing this fact in mind it is important to investigate the behavior of shot peened samples containing surface cracks and defects [8, 9].

In this work the fatigue behavior of two series of sandglass steel specimens quenched, tempered and shot peened Q&T+SP, with two different sizes of defects in the minimum section was studied. All the samples were submitted to rotating bending fatigue tests. The effect of defect dimension on fatigue behavior is assessed in terms of ΔK_{th} by means of stair case method and checked with a theoretical formula proposed by the authors in [10] for nitrided and shot peened samples. From the obtained results it seems that the proposed correction of Murakami's formula is effective also for predicting the ΔK_{th} in Q&T+SP steels.

2. Experimental work

The material studied in this work is the 39NiCrMo3 (UTS=1053MPa, Yield Strength=940 MPa, Elastic Modulus E=206˙000 MPa, Elongation A=20%). Two different series of 15 sandglass specimens were considered, being both of them quenched and tempered (quench in oil 850ºC; tempered 2h, 550ºC) and then shot peened with an Almen intensity equal to 12 A. To investigate the fatigue strength of materials with small surface defects it is common to perform tests on samples where small hole has been artificially introduced [11]. For this reason a micro-hole in the minimum section of all the specimens, after quenching, tempering and shot peening, was done (fig. 1), with the help of an indentator using 600 N load, thus simulating a damage due to a mechanical impact or scratch on the surface material, common on real components during their life span. In both cases, these micro-holes act like a pre-existent defect and were introduced to have a preferential site for fatigue crack initiation, being the aim to determine the value of ΔK_{th} in the field of short cracks.

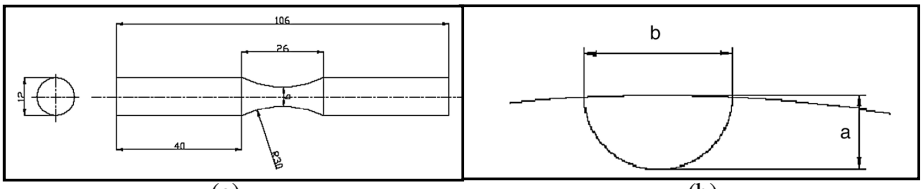

(a) (b)

Figure 1. Specimen used for rotating bending fatigue tests: a) Specimen geometry b) particular of the micro-hole

Rotating bending fatigue tests were carried out on both series of specimens. The tests were stopped after 3E+06 cycles, and the specimens not broken after this number of cycles were considered run-out. The tests allowed analyze the effect of defects dimension on fatigue behavior, in terms of ΔK_{th} using the stair case procedure.

The sub-surface layer of material was characterized also by measuring the residual stresses by means of an AST XStress 3000 X-ray diffractometer (radiation Cr Kα, {211} diffraction planes of the α–Fe phase, irradiated area 1 mm^2, $\sin^2\psi$ method, 11 angles of measurement). Electro-polishing device was used to remove material in order to know residual stresses trend in-depth. The results were corrected by using the method described in [12]. The XRD measurements allowed to obtain also the full width of diffraction peak at half maximum (FWHM), an index parameter of hardening, grain distortion and dislocation density [13]. Micro-hardness tests were also done on the sample surface with a weight of 100g. SEM observations were executed on broken and run-out specimens and the presence of arrested cracks was detected on these latter. Besides it was possible to measure the effective dimension of the created defects.

3. Results

Hardness value on Q&T+SP samples surfaces was 291 HV. In Figures 2 and 3 it is possible to see the residual stresses and the FWHM trend of the samples after Q&T treatment and after Q&T+SP , both of them in the longitudinal direction (0°) of the samples (the other two directions, 45 and 90° are similar). It is clear the increase of residual stresses and FWHM values after shot peening treatment.

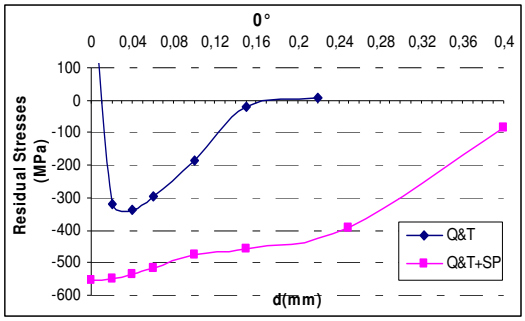

Fig 2. In-depth residual stress trend after Q&T and after Q&T+SP treatment of the samples in the longitudinal direction

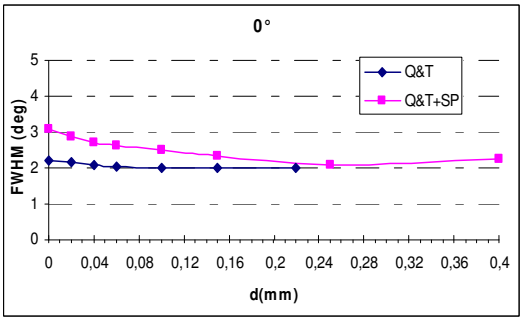

Fig. 3. In-depth FWHM trend after Q&T and after Q&T+SP peening treatment of the samples in the longitudinal direction

The results from fatigue bending test on both series of samples were analyzed by means of the stair case procedure. Prediction of the fatigue limit was also assessed using formula (1) proposed by the authors [10] for nitrided and shot peened materials, that is a modified version of the Murakami's one [14].

$$\Delta K_{th}=3.3*10^{-3} * (HV+120)*(\sqrt{area})^{(1/3)} *((1-R)/2)^{\alpha} * (FWHM_{Q\&T+SP} /FWHM_{Q\&T}) \qquad (1)$$

Where $\alpha=0.226+HV\cdot10^{-4}$, $\sqrt{area}$ is the projected shape of the initial defect which was suggested in [10], R is the stress ratio, and HV is the measured hardness. $FWHM_{Q\&T}$ and $FWHM_{Q\&T+SP}$ are the values obtained from the diffractometer measurements in Q&T and Q&T+SP samples respectively. This formula takes into account the peculiar behavior of "short crack" due to the dimension of the considered defects (series 1: $\sqrt{area}_1$ = 170µm, series 2: $\sqrt{area}_2$ = 438µm). Figures 4 and 5 show SEM images of defects in each series. The agreement between experimental and prediction results are satisfactory for the two series considered, as it is shown in Table 1.

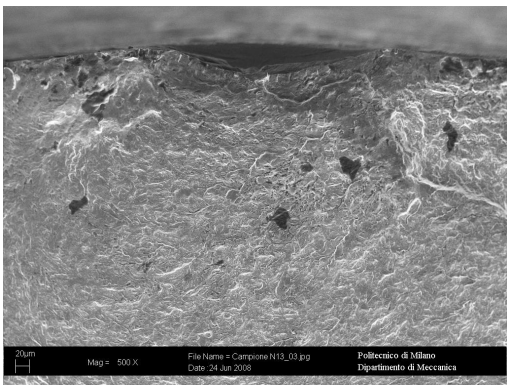

Fig. 4. Micro-hole in Q&T+SP $_1$

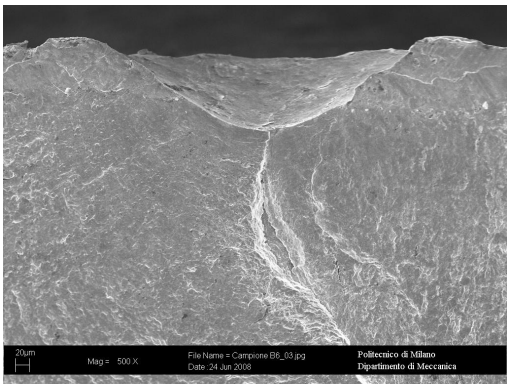

Fig. 5. Micro-hole in Q&T+SP $_2$

	Q&T+SP $_1$	Q&T+SP $_2$
ΔK_{th}(MPa√m) **[Experimental]** Stair-Case	13.08	20.26
ΔK_{th} (MPa√m) **[Prediction]** [10]	13.36	21.83

Table 1. ΔK_{th} obtained by stair case procedure and using formula (1) series 1 and 2

Conclusions

In this research fatigue crack propagation behavior of a low alloy steel quenched, tempered and then shot peened was investigated. On the tested samples a small micro-hole was generated by indentation, thus simulating the presence of a pre-existent defect. The XRD measurements show the strong effect of shot peening in terms of residual stress and of surface hardening until a depth of about 0.2mm.

Fatigue results show that the threshold value of the stress intensity factor is related to the defect dimension and it increases with this latter quantity. This means that for the tested materials and defects with the dimension considered we are in the field of the short cracks, where crack propagation properties depend on the microstructure of the material. The results were elaborated according to a modified version of the Murakami formula of ΔK_{th}, developed by the authors for taking into account the modification induced by shot peening on the properties of the materials [10]. The formula, originally proposed for nitrided and shot peened steels, is in good agreement with the experimental results also in this case. This relative importance of the surface hardening induced by shot peening (considered in the formula by means of the ratio of the quantity FWHM) suggests that for this kind of steel grain distortion due to the impact of the shots is the main factor of the improved behavior due to shot peening.

References

[1] MARSH, K.J. (1993): Shot Peening: Techniques and Applications. *EMAS, London*.
[2] J. P. WISE, J. SPICE, S. G. DAVIDSON, W. E. HEITMANN and G. KRAUSS, *Scripta Mater*. 44 (2001) 299.
[3] K. KAWASAKI, Y. SETO and T. YAMAZAKI, *Tetsu-to-Hagane* 71 (1985) 100.
[4] K. KAWASAKI, T. CHIBA, N. TAKAOKA and T.YAMAZAKI, *ibid.* **73** (1987) 2290.
[5] K. KAWASAKI, T. CHIBA and T. YAMAZAKI, *ibid.* **74**(1988) 334.
[6] MARSH K.J., 1993. Shot Peening: Techniques and Applications. Ed. EMAS, London.
[7] MURAKAMI Y., Metal Fatigue: effects of Small Defects and Nonmetallic Inclusions, Elsevier, 2002, pp. 173–178.
[8] GUAGLIANO M., VERGANI L., Engineering Fracture Mechanics 71 (2004) 501–512
[9] COLOMBO C., GUAGLIANO M., VERGANI L., 'Fatigue Crack Growth Behaviour of nitrided and Shot Peened Specimens, SID, vol.1, no.4, pp.253-265, 2005.
[10] FERNÁNDEZ- PARIENTE I., GUAGLIANO M., Surf. Coat. Technol. 202 (2008) 3072
[11] MURAKAMI Y., Metal Fatigue: effects of Small Defects and Nonmetallic Inclusions, Elsevier, 2002, pp. 35–74
[12] MOORE M.G., EVANS W.P., SAE Transact. 66 (1958) 340.
[13] NOYAN I.C., COHEN J.B., Residual Stress- Measurement by Diffraction and Interpretation, Springer-Verlag, New York, 1987
[14] MURAKAMI Y., Metal Fatigue: effects of Small Defects and Nonmetallic Inclusions, Elsevier, 2002, pp. 57–74.

Transcom 2009, 22-24 June 2009
University of Žilina, Žilina, Slovak Republic

Al-Mg-Si Alloy Crack Properties After Various Mechanical Processing

[*]Rastislav Poliak, Peter Palček, Mária Chalupová
[*]University of Žilina, Faculty of Mechanical Engineering, Department of materials engineering, Univerzitna 1, 01026 Žilina, Slovakia, {rastislav.poliak, peter.palcek, maria.chalupova}@fstroj.uniza.sk

Abstract. Changes on the crack surface of aluninium alloy Al-Mg-Si after impact test has been studied. The aluminium alloy was delivered in two states, extruded and rolled and tests alone were realisated at 22 °C and 100 °C. The results show some changes of crack surface e.g. pits size and orientation or crack propagation in dependence on enhanced test temperature.This paper also deals with basic crack surface analysis of aluminium Al-Mg-Si alloy.

Keywords: Al-Mg-Si alloy crack properties, mechanical processing

1. Introduction

Development and emergence of novel metallic materials to meet the stringent demands of almost every brunch of industry are largely driven by a need to satisfy economic motivations while concurrently ensuring scientific and technical advancement. Much emphasis is put on issues like precision, life-cycle designs, durability, reliability, cost-effectiveness and last but not least lower weight [1, 2]. As a result of their good physical and chemical properties (corrosion, formability, weldability, internal damping, etc.) 6xxx series Al-alloys are widely used [3]. Al-Mg-Si alloys have been studied extensively because of their technological importance and their exceptional increase in strength obtained by precipitation hardening. They are mostly used in extruded Al products in Western Europe, as well as for construction and automotive purposes [4].

The temperature is one of the factors having significant influence on the final properties of the alloy. It also influences the behavior of the material during operation. It is very important to know the response of the used material to the applied loading, mechanical or thermal or combination of both. Following the results of the tests we have the chance to predict the failures and malfunction of the products and hence we can prevent a danger of an accident. On the other side, understanding the material behavior supports the effort to improve the manufacture qualities of the materials and it provides the essential information for further research and development [5-8].

2. Experimental material and procedure

For this study was used commercial heat treatable Al-Mg-Si aluminium alloy, in two conditions (after rolling and extrusion). Chemical composition of used alloy specified by producer is given in Tab. 1. Extruded material was supplied in a form of bars with diameter of 21 mm, and rolled in a form of solid plates 500 x 100 x 15 mm.

element	Mg	Si	Fe	Cu	Mn	Zn	Ti	Cr	Al
content (wt %)	0.76	0.88	0.35	0.04	0.45	0.04	0.03	0.04	balance

Tab. 1. Chemical composition of used aluminium alloy.

Metallographic analyses for each state was done in longitudinal direction (Fig.1,2). The microstructure was invocated by use of chemical and electrochemical etching, with Tucker's and Barker's reagent, and evaluated on Carl Zeiss AxioImager A1m light microscope. The microstructure of used aluminium alloy after extrusion and rolling (Fig.1,2) consits of deformed polyedric grains of substitue solid solution of alloying elements in aluminium, elongated in the extrusion or rolling direction. The microstructure after extrusion is markedly finer in compare with rolling.

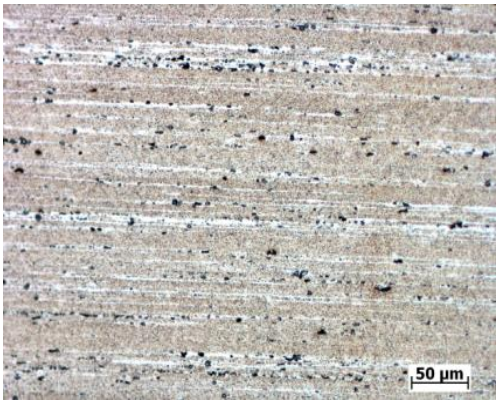

Fig. 1. The microstructure of Al-Mg-Si alloy after extrusion, etched Tucker, longitudinal direction.

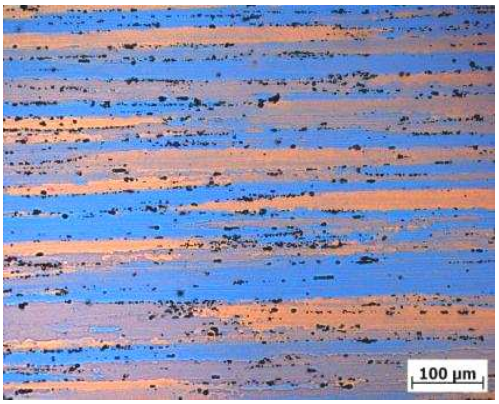

Fig. 2. The microstructure of Al-Mg-Si alloy after rolling, etched Barker, longitudinal direction.

Notched test bars with 2 mm deep V shape notch were assigned for impact tests. They were made from supplied aluminium bars and solid plates by usual machining methods. Shape and dimensions of test bars are specified in STN EN 10045-1. Impact tests were realised at two various temperatures (22 °C and 100 °C). Test bar temperature was mesured by Cu-Ko termocouple with accuracy of 2 °C.

3. Results and discussion

The results of impact tests are shown in Tab. 2. These data are average values of multiple measurements.

state / temp.	22 °C	100 °C
extruded	48 J	47 J
hot rolled	23 J	29 J

Tab. 2. Impact energy values of extruded and rolled aluminium alloy

We can observe, that impact energy values of extruded alloy, with increasing of temperature aren't changing in a large extent like peak values of rolled alloy. It's probably in context with various material behaviour in decreasing of strength limit in dependence on mechanical processing.

In comparison the crack surfaces of extruded and rolled alloy, from macroscopic point of view it's clear that extruded alloy has significantly softer texture (Fig. 3,4). Crack surface of extruded alloy is less segmented and lining is less significant thas in rolled alloy. From macroscopic point of view the crack surface in both alloys is created by transcrystaline ductile failure with pits' morphology. Inequality of pits is caused by direction of major loading, pits are orientating mostly in this direction (Fig 5,6). At the temperature of 22 °C these pits have approximately the same size for both alloys, however the pits of extrusion alloy seem shallower, more equiangular and on the walls there is observed more significant corrugation (Fig 5,6).

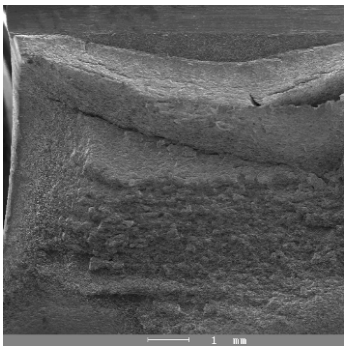

Fig. 3. Crack surface of extruded aluminium alloy.

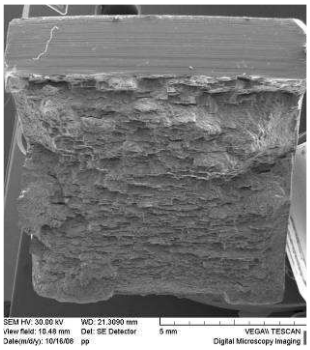

Fig. 4. Crack surface of rolled aluminium alloy.

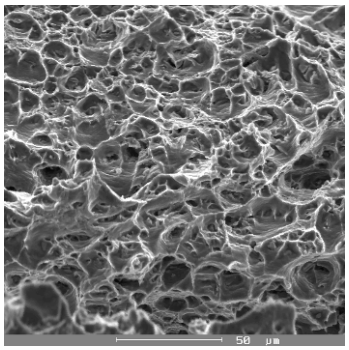

Fig. 5. Transcrystaline ductile failure of extruded alloy.

In both cases, there are observable two types of pits, the main large pits creating the major part of crack surface and the softer pits, in order smaller pits appearing locally. These soft pits prove presence of softer intermetallic phase, probably eutectic $\alpha + Mg_2Si$. Their appearance, on the crack surface of the rolled pattern is quite rare. In comparison of both crack surfaces is obvious that rolled alloy was damaged locally as well as intergranulary and that caused increase in lining. Intergranular failure is incurred by essentially larger grain size as well as bigger share of grain boundaries presented at the crack surface. On the intergranular part of crack surfaces of rolled alloy are observable very soft pits, this proves the fact that the progress of the intergranular crack as well in this case went ductile (Fig 7).

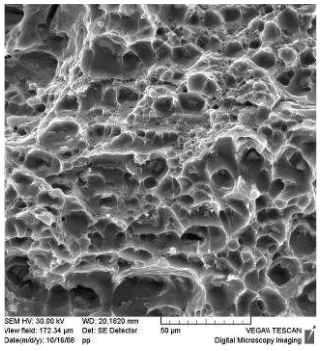

Fig. 6. Transcrystaline ductile failure of rolled alloy, pits on the crack surface

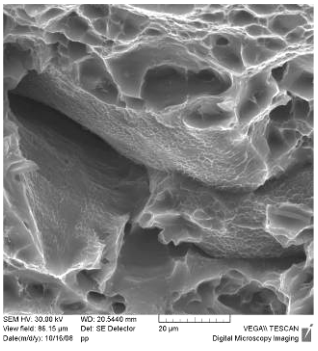

Fig. 7. Intercrystaline ductile failure, small pits on intercrystaline crack surface

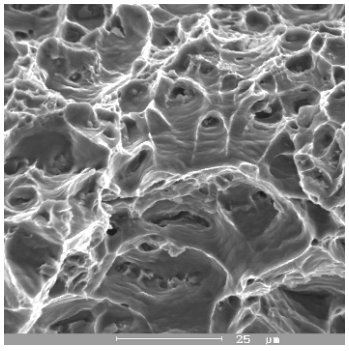

Fig. 8. Preoriented pits and crawling on pit surface in extruded alloy, 100 °C

At the temperature of 100 °C in both alloys is comparable dulcification of the main pits. On the top of that, in extrusion alloy the pits are significantly orientating in direction of the main loading and the corrugation of their walls appears as more clear. The corrugation of the rolled alloy remained unchanged, however the share of pits and intergranular crack increased. This implies that also the lining itself is more significant (Fig. 8). Impact energy values at 100 °C in extruded alloy are comparable with values at 22 °C but rolled alloy show obvious changes. These changes are caused by expressive degradation of strength with increasing of temperature in rolled alloys.

4. Conclusion

- The micorstructure of both (extruded and rolled) Al-Mg-Si alluminium alloy fine-grained with grains oriented in extrusion or rolling direction. Observed intermetallic phases have alignemt in this directions.
- The impact test results at 22 °C or 100 °C show different crack morphology in rolled and extruded aluminium alloy.
- Crack surface of rolled aluminium alloy has a character of transcrystaline ductile failure with pits' morphology and local intergranular ductile failure.
- Crack surface of extruded aluminium alloy has a character of transcrystaline ductile failure with pits' morphology.
- With increasing of impact test temperature increase ratio of pits and intergranular crack in rolled alloy. In extruded alloy appears corrugation of pit walls as more clear.

Acknowledgement

The part of the results of this work was supported by Slovak-Czech cooperation, project No. SK-CZ-0085-07 and Scientific Grant Agency of Ministry of Education and Slovak Academy of Science, SK, Grant No. 1/0249/09.

References

[1] POLMEAR,I.: Light Alloys, From Traditional Alloys to Nanocrystals, 4th edition, 2006.

[2] NOVÝ, F., PALČEK, P., CHALUPOVÁ, M.: Kovové materiály, 43, 2005, p. 447-456.

[3] MARIONARA, C.D. et al.: *Acta materialia 49*, 2001, p. 321-328.

[4] GREGÁŇ, P., HADZIMA, B., TILLOVÁ, E.: In.: Transcom 2003, Eds.: Skočovský, P. et al.: ŽU v Žiline, Žilina, 2003, p. 99.

[5] POLIAK, R., RESETERIČOVÁ, L., ŠKORÍK, V., PALČEK, P.: Alluminium 2007: 5th International Conference, Czech Republic, 2007, pp. 141-146.

[6] RESETERIČOVÁ, L., POLIAK, R., PALČEK, P.: Damping capacity of Al-Mg-Si alloy in different times of artifical aging, Materials Engineering, Vol. 15, 2008, No. 2a, Special Issue.

[7] POLIAK, R., RESETERIČOVÁ, L., PALČEK, P., CHALUPOVÁ, M.: The effect of temperature on properties of extruded AW6082 aluminium alloy, 25th Danubia-Adria Symposium on Advances in Experimental Mechanics, Czech Republic, 2008, pp. 209-210.

[8] ČINČALA, M., NOVÝ, F., TŐRŐK, P.: Mechanical-property anisotropy in Al-Zn-Mg-Cu alloy extrusions. In: Nowe technologie i osiągnięcia w metalurgii iinżynierii materiałowej : VIII międzynarodowa konferencja naukowa, Wydawnictwo Wydziału Inżynierii Procesowej, Materialowej i Fizyki Stosowanej Politechniki Częstochowskiej, Częsztochowa, may 25, 2007, Poland, p. 75-78, - ISSN 1234-9895.

Transcom 2009, 22-24 June 2009
University of Žilina, Žilina, Slovak Republic

Mechanical Properties of Bone Cements

[*]Róbert Seewald, [**]Henrietta Lelovics, [***]Libor Nečasr
[*]University of Žilina, Fakulty of Mechanical Engineering, Department of Materials Engineering
Univerzitná 1, 01026 Žilina, Slovakia, robert.seewald@fstroj.uniza.sk
[**]University of Žilina, Fakulty of Mechanical Engineering, Department of Materials Engineering
Univerzitná 1, 01026 Žilina, Slovakia, henrietta.lelovics@fstroj.uniza.sk
[***]Orthopedics and Traumatology Clinics, Teaching Hospital in Martin, Kolárova 2, 03659 Martin, Slovakia, necas@mfn.sk

Abstract. The aim of this work is to evaluate the influence of mixing technique and some of the mechanical properties of bone cements used in today's orthopedic surgery (SMARTSET^{TM}HV, OSTEOBOND$^{®}$, Palacos$^{®}$R). Specimens prepared by hand mixing were used for impact test and bending test, then the porosity of the fracture surfaces after the impact tests was evaluated. All the experiments were performed on the device Dynstat.

Keywords: bone cement, bending moment, porosity, impact energy, diffraction angle.

1. Introduction

The evolution of science in the 21.th century and revelation of new materials, such as bone cements, avoid a life quality growing for patients with congenital defects and for patients suffering after accidents or diseases. Bone cement is used in orthopedic surgery for fixation of total endoprostheses of hip, knee and elbow joints.

Since the 60's of the last century, when first experiments were done on bone cements, they went under different modifications in they structure and quality. They consist of two basic components (powder and liquid) which are mixed together under the conditions recommended by manufacturer which vary for each type of cement. After mixing the components the exothermal polymerization reaction and hardening begins [1]. The endoprosthesis is inserted into the bone canal which is filled with polymerizing bone cement. Bone cements have much less modulus of elasticity like the metal endoprosthesis, but they are stiff enough and are fully biocompatible. The main role of bone cements is to distribute the loads from the metal endoprosthesis into the surrounding bone and tissues [2].

Patients after the surgical treatment are able for extensive moving and can perform ordinary services. The more increasing the number of institutes where the chirurgical treatments using bone cements are done the more patients can get back into the normal life without permanent suffering [3, 4].

2. Experimental materials, methods and conditions

To determine the impact and bending properties of small polymer samples made mainly with cutting from final products the device Dynstat (Fig. 1) can be used.

The aim of the impact strength test is to determine the energy required to break the samples which is a measure of the material resistance to impact straining. During the bending test the bending moment M_o and the diffraction angle α are measured.

Three kinds of bone cements were used for tests: SMARTSET^{TM}HV, OSTEOBOND$^{®}$ and Palacos$^{®}$R. The components of the cements were mixed together at room temperature and atmospheric pressure using 2 techniques of mixing: a) liquid into the powder, b) powder into the liquid (the manufacturers recommend only one of these methods).

Fig. 1. Device Dynstat**.**

To simulate the real in vivo hardening conditions was necessary to design special mould where the required pressure for cement hardening (more then 16kPa) was provided by weights. The scheme of the muddle is presented in Fig. 2. The samples obtained from the muddle had 4x4mm cross section and were cut into 15mm length.

Fig. 2. Scheme of the muddle for sample preparation.

3. Results and discussion

The aim of this paper was to establish possibly connections between the mixing techniques and mechanical properties of the prepared samples. The values measured for samples prepared by recommended mixing technique are marked with symbol (•).

In Fig. 4. the averaged energies measured during the impact tests are presented. After the impact strength tests the porosity of the fracture surfaces was established, the results are presented in Fig. 5. and some of the fracture surfaces in Fig. 3a,b,c.

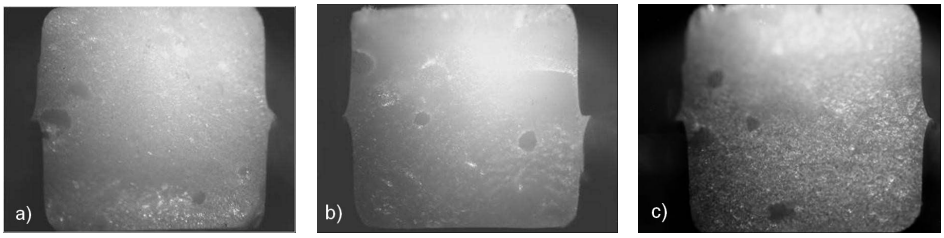

Fig. 3. Fracture surfaces of the bone cements prepared by mixing technique powder to liquid. a) SMARTSETTMHV, b) OSTEOBOND®, c) PALACOS®R.

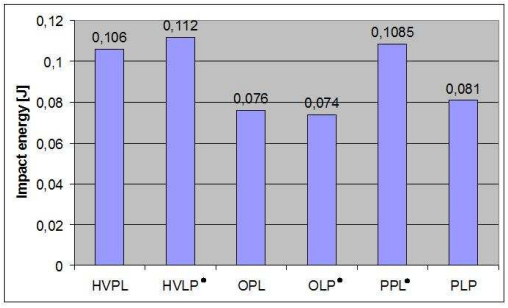

Fig. 4. Averaged impact energies of the cements prepared by different techniques.

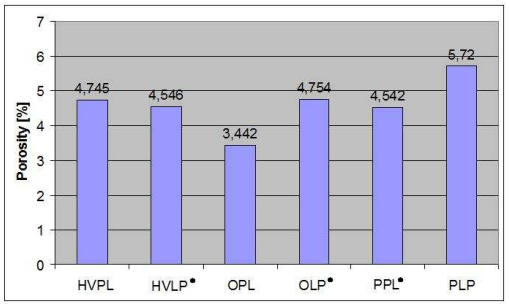

Fig. 5. Averaged porosities of the fracture surfaces after impact strength tests.

On the all fracture surfaces pores with diameter up to 0,5mm are visible which vary in shape and size. These pores cause stress concentration and can initiate fractures in cement mantle. The smaller is the sample porosity the higher is the energy required to break the samples.

The results of bending tests are presented in Fig. 6. and in Fig. 7. The vice-versa technique of mixing much more affected the diffraction angles but caused higher bending moments at bone cement PALACOS®R contrary of the other two cements.

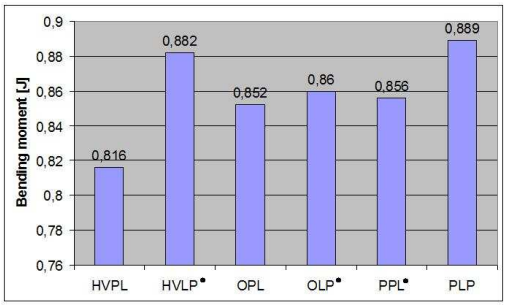

Fig. 6. Averaged bending moments of the samples prepared by different techniques.

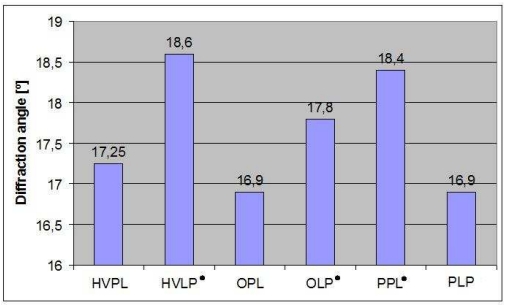

Fig. 7. Averaged diffraction angles of the samples prepared by different techniques.

4. Conclusions

In this paper the result of impact strength and bending test performed on bone cement samples are presented. The results show particularly how the mixing techniques influence the mechanical properties of tested bone cements.

It was shown, that in term of impact stress is necessary to reduce cement porosity, for example by vacuum mixing, to prevent the entrapment of air into the viscous cement mass during mixing.

The influence of the room temperature on the hardening time was also observed. The higher was the temperature the shorter was the setting time of the cement. Increasing the room temperature with $2^{o}C$ reduced setting time up to 2 min.

Acknowledgements

This research has been partially supported by Scientific Grant Agency of Ministry of Education of Slovak Republic and Slovak Academy of Sciences, grant No 1/0249/09. This support is gratefully acknowledged

References

[1] Constantz, BR., Ison Ira, C., Fulmer, MT., Poser, RD., Smith, ST., VanWagoner, M., Ross, J., Goldstein, St. A., Jupiter, JB., Rosenthal, DI.: Skeletal Repair by in Situ Formation of the Mineral Phase of the Bone. (1995) Science page: 267ff.

[2] Deb, S., Di Silvio, L., Vasquez, B., San Roman, J.: Water Absorption Characteristics and Cytotoxic and Biological Evaluation of Bone Cements Formulated with a Noval Aktivator, Biomaterials, year (1999), number 48, page: 719-725.

[3] Seewald, R.: Mechanické vlastnosti kostných cementov. diploma work, university of Žilina, 2008.

[4] Lelovics, H., Liptáková, T.: Comparison of Some Mechanical and Rheological Properties of Bone Cements, 25th Danubia-Adria symposium on Ad

Transcom 2009, 22-24 June 2009
University of Žilina, Žilina, Slovak Republic

Non-destructive Structuroscopy of Brake and Clutch Disks

Břetislav Skrbek, Vladimír Nosek
Technical University of Liberec, Faculty of Mechanical Engineering, Department of Material Science, Studentská 2, 46117 Liberec, Czech Republic, bretislav.skrbek@tul.cz

Abstract. Application of cast iron castings as mass production semiproducts of parts for power transmission from engines to car wheels and rail driving units is still frequently unreplaceable. Cast irons as a "composite" of steel matrix and graphite filler. Resistance scale against thermal and mechanical stress can be shown by Eichelberg factor EF. Quantities necessary for EF determination can be measured by NDT method directly on castings or finished disks in the frame of production material quality assurance. Measurement of intended local regions of disks. Matrix evaluation methods – method of magnetic point pole. Acoustic method of graphite parameters evaluation by initial elasticity modulus Eo determination. Calculation of R_m, $R_{p0,2}$. Vector expression of casting set structure in the [HB; E_o] plane offers visually remedy to manufacturing process quality improvement – examples. TELIT system developed for these complex evaluation in the frame of program project BONATRANS F1 – IM/001.

Keywords: magnetic method, structuroscopy, cast iron, clutch disks

1. Introduction

Parts of moving mechanism, which connect and disconnect power transferred to wheels of axles or on the contrary - brake, at both road and railroad vehicles have similar specific requirements for material and quality. There are coupling and braking disks (eventualy drums), flywheels and thrusting lamela plates. Twisting moment transer is performed by thrust force and by contact surfaces friction. Large amount of heat liberation and shear stress occur at mutual moving of these surfaces. Resistance against thermal shock can be specified by Eichelberg factor EF. Its value enables to compare mutualy suitability of varous technical materials at normal and operational temperatures.

$$EF = R_m \cdot \lambda/(\alpha \cdot E) \qquad (1)$$

Economy and technical optimum of materials for abovenentioned parts are graphitic cast irons. They own the highest EF values in the range of iron alloys. Cast irons creat "composite" from steel matrix, in which are placed variously oriented graphite formations with maximum size several tenths of mm. Excellent thermal conductivity of graphite causes high I values. Graphite transfers only compression loading. It has no tensile strength.It decreases cast iron rigidity considerably (it means elasticity modulus value E as well) in comparison with steels. Cast irons don´t shrink due to "graphite growth". It enables to cast substaially homogeneous castings of brake and coupling disks disimilarly from Al and Cu alloys. High shear strength values $SS=0,9R_m$ can be achieved by stable strong matrix - usually pearlite. Ferrite formation is not allowed. Shape of graphite and final matrix structure is determined by casting metallurgy. Casting metallurgy process reproducibility is influenced by raw material composition, process temperatures and duration senzitively. Effective checking of activity is necessary to ensure quality of cast iron casting with narrow tolerances of mechanical properties and homogeneity. Its effectivity is based on checking just onto casting

without its destruction and speed (it doesn´t brake manufacturing flow), that enables operative correction of eventual properties deflections from technical specifications.

2. Structuroscopy of Bonatrans Disks

Chapter exploits knowledge of internal report [1,2,4]. The aim of checking operations is to ensure the delivery of disks and hooks with mechanical properties within given tolerances. Boundary values of HB, R_m, R_p, A important for releasing of castings to delivery prescribe technical delivery conditions (TDC) TP 22 -112 - 04. In the years 2005 and 2006 in the frame of campaign of development melts were cast tens of testing disks of Y2 blocks and flat samples with large-scale structure. After non-destructive measurement were determined mechanical properties and metalography destructively. By regression analysis of both non-destructively and destructively measured data were determined mathematic models to memories of DOMENA and TELIT aparatuses.

2.1. Magnetic Structuroscopy - Domena B3

The aim of research was to determine linear equations (constants A, B) for calculation of mechanical properties inserted into memory of DOMENA B3 before measurement [3]. Optimum regime was set to magnetization M4 or M5. During the solution of project was made an effort for improvement of measurement reproducibility after reproduced measurement and measurement at low and high temperatures. (+-30^0C). On basis stability measurement results the manufacturer of DOMENA B3 (ELKOSO s.r.o. Brno) implemented technical changes to performance stability improvement. Generally:

$$HB=A \cdot M+B \tag{2}$$

Hardness measurement on castings and disks from cast iron with spheroidal graphite .

$$HB = 0,6 \cdot M + 100 \tag{3}$$

Measurement of mechanical properties on disks from cast iron with spheroidal graphite
Δ…medium verified measurement error Table 1

Property	Equation	Δ	K K^2
HB	0,8·M+128	10	0,958 0,918
F [%]	116 – 0,585·M	10	-0,932 0,868
R_m [MPa]	2,69·M+383	26	0,955 0,912
$R_{p(0,2)}$	1,81·M+242	32	0,931 0,867
A [%]	22,4-0,09·M	2	-0,89 0,787

Table 1. Measurement of mechanical properties on disks from cast iron with spheroidal graphite.

Measurement of R_m, R_p, A is qualified with satisfactory high value of elasticity modulus over 160 GPa, which ensures high share of spheroidal graphite in the structure. It is necessary to prove it by universal defectoscope USN35. This checking procedure is replacing measurement instead of TELIT.

2.2. Rigidity Eo of Cast Irons

The formulas serves both for general work with USN35 and iinsertion into memory of TELIT before measurement. After E_o value can be unambiguously determined quality rank of cast iron with spheroidal graphite for given wall-thickness. For cast iron with flake graphite SKS used still for BONATRANS disks is valid:

$$Eo = (446,1 \cdot L/L_u)^2 \tag{4}$$

Boundary values contains Table 2 in the report [4]. For disks is valid:

ČSN quality	Eo [GPa]	V_L [m/s]	L/L_u
Lower limit	97	4133	0,6982
42 2420	102,2	4242	0,7166
Boundary 20/25	111,1	4423	0,7472
42 2425	120	4597	0,7765
Boundary 25/30	126	4711	0,7957
42 2430	132	4821	0,8144

Table 2. Boundary values E_0 of cast iron according to ČSN

Values L/L_u serves for operative rapid checking.

Cast iron with spheroidal graphite:

$$Eo = (432{,}57 \cdot L/L_u)^2 \tag{5}$$

Average rigidity of disks BONATRANS (Figure 2) Eo = 171,7GPa. In foundry practice of ladle modification procedures is satisfactory to measure L/Lu of first and last casting cast from charge of modified cast iron of ladle usually. In SKS developed INMOLD modification requires to to prove modification efficiency of each casting from mold. Boundary values of sound velocity v_L resp. only rate L/Lu with regard to boundary values after EN for rapid estimation of cast iron with spheroidal graphite satisfactory nodularity is valid Table 3.

Quality after ČSN	Eo [GPa]	V_L [m/s]	L/Lu
42 2304,5	160	5475	0,9247
42 2306,7	170	5642	0,9532

Tab. 3. Boundary values E_0 of cast iron with spheroidal graphite according to ČSN

EN standards are ambiguous at allocating Eo values. Value of 160 GPa corresponds to 25-35% share of vermicular GIII at the expense of spheroidal GVI graphite in cast iron structure. Strict technical delivery conditions TP 22-112-04 requires to keep boundary value 170 GPa.

2.3. Checking by Utility Design TELIT

Equipment for non-destructive determination of material quality under type label TELIT, after utility design CZ17380 (Figure 1) measures input quantities M, L, L_u.

By mathematical models

$$HB = A \cdot M + B \tag{6}$$

$$Eo = (K \cdot L/Lu)^2 \tag{7}$$

$$Y = C \cdot (L/Lu)^D \cdot M^E \tag{8}$$

Then HB, E_o, Y where Y is R_m strength, R_p yield strength and A ductility.

For cast iron with spheroidal graphite castings is valid :

$$HB = 0{,}6 \cdot M + 100 \tag{9}$$

$$E_o = (446{,}1 \cdot L/L_u)^2 \tag{10}$$

$$R_m = 7{,}211 \cdot (L/L_u)^{2{,}278} \cdot HB^{0{,}75} \tag{11}$$

For disks from cast iron with spheroidal graphite:$(L/L_u)^{5{,}257} \cdot HB^{0{,}86}$ (12)

$$R_p = 9{,}3 \cdot (L/L_u)^3 \cdot HB^{0{,}756} \tag{13}$$

$$A = 132000 \cdot (L/L_u)^{13} \cdot HB^{-1{,}635} \tag{14}$$

Verified mean error R_m, R_p, A upto 10%

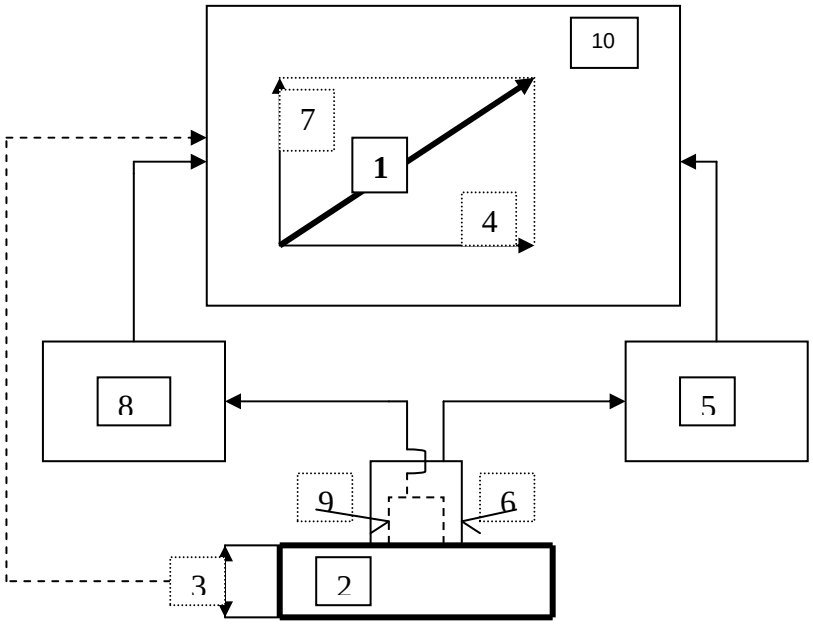

Fig. 1. TELIT: 1. vector of structure, 2. disk, 3. disk thickness, 4. cast iron rigidity, 5. impulsion magnetic hardnesstester, 6. magnetic reader, 7. constituent (hardness) of cast iron matrix, 8. ultrasound thicknessmeter, 9. ultrasound probe, 10. composing unit (PDA).

3. Conclusions

Average checking cadence with magnetic hardnestester DOMENA B3 is 3-5s and with combined structuroscope TELIT 5-20s (after parallel or seria regime of reader measurement). As-calculated mathematic models enable to measure mechanic properties with satisfactory accuracy. The solution of region of NDT of structure by project F-1M/01 shall ensure 100% production checking of both as-developed (from cast iron with spheroidal graphite) and existing BONATRANS disks. Series of particular knowledge exceeded specification range. Their appropriation and introduction to industrial practice of other foundry shops by project owner is of great importance.

Acknowledgement

This contribution was created under support of research plan MSM4674788501.

References

[1] ISSN 1213-3825. DVOŘÁK,J. *Nedestruktivní zkoušení – platné ČSN k 31.12.2004.* NDT Welding BULLETIN, II/2004, s.59-64, ISSN 1213-3825.

[2] DEUTSCH, V., PLATTE, M., VOGT, M. *Ultraschallprüfung : Grundlagen und industrielle Anwendungen.* Berlin : Springer Verlag, 1997. ISBN 3-540-62072.9.

[3] SKRBEK, B. *Impulzní magnetická kontrola výrobků z ocelí.* NDT Welding BULLETIN, III/2001, s.47-52,

[4] SKRBEK, B.: *Výběr a zpracování dat experimentálně změřených v SKS kampaních r.2006.* Interní zpráva 75-40SKS projektu F1-1M/01, SKS Krnov 2007, 24 s.

Transcom 2009, 22-24 June 2009
University of Žilina, Žilina, Slovak Republic

Analyzing the Technical Characteristics of EDM Tools

[*]Sławomir Spadło, [*]Dominik Dudek
[*] Kielce University of Technology, Chair of Vehicles and Mechanical Equipment, Aleja Tysiąclecia Państwa Polskiego 7, 25-314 Kielce, Poland, E-mail: dominik_dudek@op.pl

Abstract. The paper deals with the investigations of influence parameters of electrical discharge machining (EDM) on the surface microgcometry of machining parts. BP-95 machine with electonic generator type was used to perform EDM process. Kerosene was used as a dielectric. During EDM process different current of single discharge were utilised. The following parameters were determined: productivity of EDM process and surface roughness R_a. It was shown that energy (current) of the single discharge influences mainly on the EDM process running. The higher was energy of the single discharge the higher were the productivity of the process and roughness of the machining surfaces. State of the material surface after EDM was estimated on the base of the scanning microscope images. It has been noticed that at the material surface after EDM small, solid remelted areas occured. Their dimensions are growing up with increasing of the energy of a single discharge. This phenomenon signifficantly influences on the surface roughness parameters.

Keywords: electrical discharge machining, surface roughness, geometrical structure of surface.

1. Introduction

Processing electrical discharge machining is with ways one the removing from surface of worked object material. She uses the energy of electric discharges. Removing material follows in result of - over periodical flashes among worked object and working electrode. Process this runs in working center about properties of dielectric.

After achievement border electric breakdown follows between electrodes voltage. The accelerated in strong electric field electron crash from atoms of center, causing their ionization. Plasmas full with ions channel creates and electron. Temperature in plasmas channels achieves 14000K. The energy of ions striking in surface of grid electrode it changes hot. Gas blister about growing diameter round channel creates. The melting the surface of object in result of local growth of temperature follows local as well as her partial vaporization. Intensive influence of electric discharges cause throwing out liquid metal, which clots in figure of balls (spheres). Final effect these are discharges crater pipes.

The examining on roughness of got surface the influence of parameters of processing was the aim of investigations, as well as the examining on efficiency of processing the influence of temperature of dielectric. The obtainment the profiles of technological machine tools will make possible the proper selection of parameters of processing dressing with attention on got in process roughness of surface. The results of investigations of influence temperature dielectric on efficiency of process will make possible enlargement his efficiency across suitable selection of devices cooling. The got investigative material in future will make up the premise to optimum designing the arrangement of admission of machine tool the working liquid.

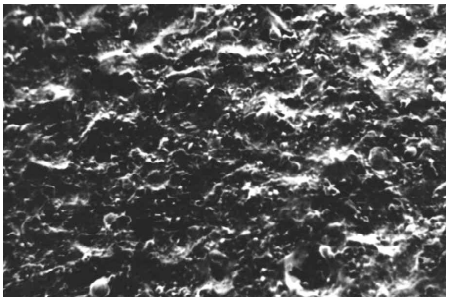

Fig. 1. The example geometrical structure of surface after EDM processing

2. Experimental Investigations of the Technological Characteristics of Electrical-discharge Machine

Investigations hugged two stages:

– the investigation of roughness of surface after processing the EDM as a function of parameters of processing (the value of intensity of current, time of duration of impulse, time of duration of pause);

– the investigation of efficiency of processing the WEDM in function of temperature of dielectric as well as the time of duration of impulse and the time of duration of pause.

Hugging experiment first investigations depended on qualification of dependence of value intensity current and the time of duration on got roughness of surface the pulse. The EDM process of type investigations were conducted on EDM machine BP95 - for two kinds of samples (steel C40 after carbureting and tempering, as well as from carbide H10). In investigations was applied circular specimen with diameter was 30 mm and thickness was 10 mm. Copper electrode in investigations as working electrode was used. It the range of changes parameters the processing was show in table 1. The example results of experiment were show on figure 2.

Value of intensity of current [A]	Time of duration of impulse T_i [µs]	Time of duration of pause T_p [µs]
2 12 24	5 1250 2500	15

Tab. 1. The parameters of processing experiment first

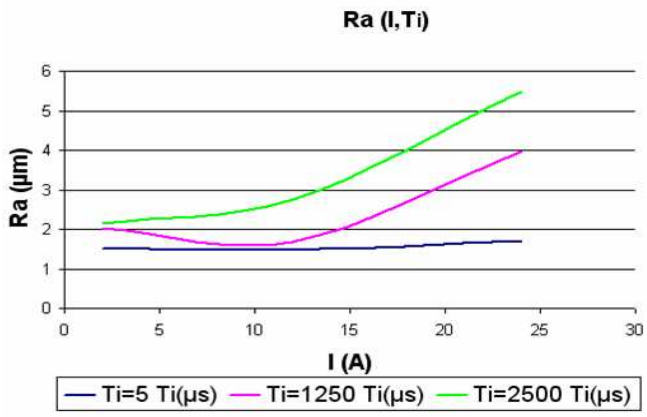

Fig. 2. The dependence the Ra in function of value of intensity current and the time of duration of impulse

He depended hugging experiment second investigations however on examining the influence of change of time duration of impulse, time of duration of pause as well as the temperature of dielectric on efficiency of processing the WEDM. Material stainless steel be worked. The locker of changeability of parameters processing was show in table 2. The example results of experiment were show on figure 3.

Time of duration of pause T_p[µs]	temperature of dielectric [^{o}C]	Time of duration of impulse T_i [µs]
40 50 60 80 100 150 200	15 22 30	1,5 2,0 2,5 3,0

Tab. 1. The parameters of processing experiment second

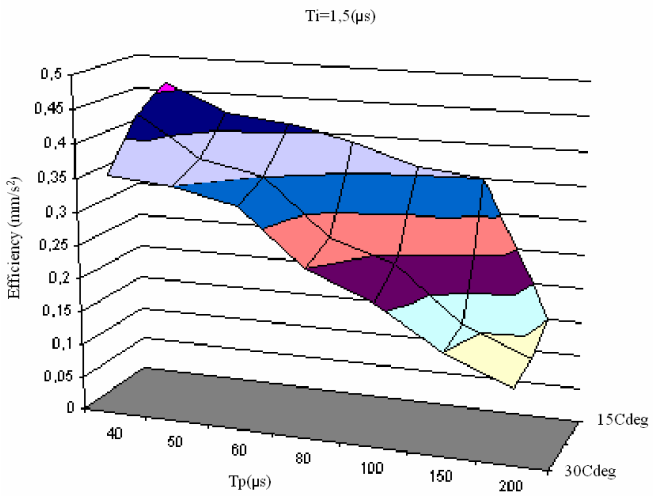

Fig. 3. The dependence of efficiency in function of times of pause the tp and the temperature of dielectric.

3. Conclusion

We notice the analysis results of experiment first, that the course of changeability of roughness as a function of value of intensity current and it shows the time of duration of impulse, that the roughness of surface with growth these two factors grows up together with. For time 5 µs dependence has linear character. For times 5 µs and 1250 µs the courses of changeability have linear t character. For time 2500 µs we observe the growth of roughness with growth of value of intensity current together with. This caused with drawing ahead during discharge phenomena is mainly the growth of energy of discharges.

We notice in second experiment analyzing got results, that the efficiency of process grows with fall of time of pause among impulses. This caused with this is, that reducing we enlarge between next impulses the time of pause. It was one should remember with time of pause between impulses it has to be sufficient on deionizations of dielectric. The efficiency of processing grows with fall of temperature of dielectric together with.

They after conducted experiences were advanced 4 following conclusions:

- The energy of impulses with growth of intensity of current grows with her the roughness of worked surface;
- With fall of time of duration of impulse together with the roughness of surface falls and the course for small times achieves approximate to linear;
- The Efficiency of process falls with growth the duration of pause together with;
- The Efficiency of process grows with fall of temperature together with;

References

[1] Albiński K.: *The Polarity of Electrodes in Electro-Discharge Machining. Proc.* ISEM - XI, Lausanne, 1995, pp. 95-104.

[2] Dauw F., Van Coppenolle B.: *On the evolution of EDM research. PART 2: From fundamental research to applied research. Proc.* ISEM-XI, Lausanne 1995, pp. 133-142.

[3] Miernikiewicz A.: *Doświadczalno-teoretyczne podstawy obróbki elektroerozyjnej (EDM)*, Praca habilitacyjna, Kraków, 1999

[4] Spadło S.: Teoretyczno - *Eksperymentalne aspekty obróbki elektroerozyjno – mechanicznej*, Kielce 2006.

[5] Spadło S., Dudek D.: *Badania eksperymentalne charakterystyk technologicznych obrabiarek elektroerozyjnych BP-95*. Zeszyty Naukowe Politechniki Świętokrzyskiej Nauki techniczne – Budowa i Eksploatacja Maszyn Z. nr 11/2008 s. 281-288, Kielce 2008.

[6] Zolotych B. N.: *Ways of Solving the Problem of Controlling Composition and Properties of Machine Parts Surface Layer Formed under EDM Influence*. 12 - th International Symposium for Electromachining ISEM, 1998

Transcom 2009, 22-24 June 2009
University of Žilina, Žilina, Slovak Republic

Dielectric Real-Time Analysis of the Photo-Curing and Post-Curing Behaviour of Dental Composite Fillings.

[*]Johannes Steinhaus, [*]Bernhard Möginger, [**]Matthias Frentzen, [***]Martin Rosentritt
[*]Bonn-Rhein-Sieg University of Applied Science, Department of Natural Sciences, von-Liebig-Str. 20, 53359 Rheinbach, Germany, {Johannes.Steinhaus, Bernhard.Moeginger}@h-brs.de
[**]University Hospital Bonn, Department of Periodontology, Operative and Preventive Dentistry, Welschnonnenstr. 17, 53111 Bonn, Germany, {Frentzen}@uni-bonn.de
[***]University Hospital Regensburg, Department of Dental Prosthetics, Franz-Josef-Strauss-Allee 11, 93053 Regensburg, Germany, {Martin.Rosentritt}@klinik.uni-regensburg.de

Abstract. Analysing the ion mobility of charged particles and dipole motion in an oscillating electrical field allows for the real-time characterisation of rapid photo-curing processes of dental composite filling materials as well as their post curing behaviour. The Dielectric Analysis (DEA) measurements match well to mechanical (DMA) and calorimetric (DSC) measurements in their corresponding time domains but require a much simpler sample preparation. The DEA is easy to handle, and it is a cost efficient method to investigate the curing kinetics of dental composites and special engineering resins as well as for quality insurance purposes.

Keywords: Dental materials, photo-curing composite filling, curing behaviour, dielectric analysis (DEA), ion mobility, ion viscosity

1. Introduction

Dental composite filling materials are highly filled acrylic resins having a paste-like consistency. After photo-curing they exhibit a stiffness of 10-15 GPa being close to the elastic modulus of teeth. The polymerisation mechanism of these materials can be separated into two curing phases. In the first phase the light-induced radical polymerisation builds up a rough polymer network within a few seconds consisting of monomers and oligomers. This process is started by a light activation of the curing agent and takes place during the dentist's direct treatment. After this primary curing phase remaining uncured monomers are trapped in the glassy polymer network more or less unable to find radicals as polymerisation partners. In this state the post curing phase begins. Now the curing process is proceeding much slower as it is driven by diffusion and rearrangement processes in the polymer network. The post curing can be described as chemical and physical ageing which occurs after the dentist's treatment during the utilization phase. Due to these processes the composite filling changes its mechanical properties towards equilibrium properties [1]. The ability to characterise a new filling material composition in its primary and post curing kinetics provides the knowledge to recommend the optimal curing light exposure and to predict the life time of the filling.

1.1. Theoretical Background of Dielectric Analysis (DEA)

Dielectric properties of polymers can be investigated using DEA as charged ions (e.g. Cl^- ions as impurities) and permanent dipoles in their chemical structure contribute to them. The charged ions are forced to move according to the applied external electrical field in the DEA

measuring device (Fig. 1, left) while the dipoles are forced to orient. Both processes contribute to an internal electric field which reduces the external one [2].

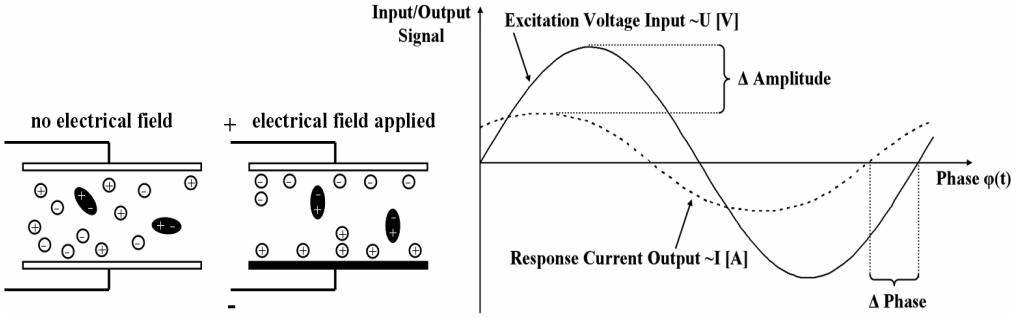

Fig. 1: Dipole orientation and charged ion motion in a polymer due to the external electric field (left) [2]. Voltage excitation and current response signal of a dielectric polymer between two electrodes (right) [2].

The energy transferred to the specimen is partly dissipated by internal friction due to ion migration and dipole oscillation in the viscous or viscoelastic polymer resin [3]. This leads to an amplitude loss of the excitation voltage input signal and a phase shift of the response current output signal (Fig. 1, right).

These two characteristic quantities yield the complex dielectric constant which depends both on the polymer viscosity and the measuring frequency. This allows for the precise characterisation of the polymer curing as the viscosity changes drastically shifting all dispersions to lower frequencies. The appropriate engineering quantity to trace the curing process is the ion viscosity μ depending reciprocally on the ion mobility u. Equation (1) shows their dependency of the dielectric loss ε'', frequency f and the dielectric constant ε_0 [1].

$$\mu(f) \sim \frac{1}{u(f)} = \frac{1}{2\pi\, f\, \varepsilon_0\, \varepsilon''(f)} \,. \qquad (1)$$

1.2. Dielectric Analysis (DEA) Measurement Device

To introduce the curing initiating light to the sample not both surfaces can be covered with electrodes. Therefore, flat dielectric sensors consisting of two comb-shaped electrodes embedded in an exactly defined insulating matrix are utilised. On this sensor surface the polymer specimen can be applied as a layer having a thickness of about 1 to 2 mm and easily light-cured (Fig. 2). The electrical field between the electrodes has a finite reach into the sample and penetrates the specimen to a depth being more or less identical to the electrode distance. Hence, the chosen electrode distance of the measurement device determines the effectively investigated part of the specimen.

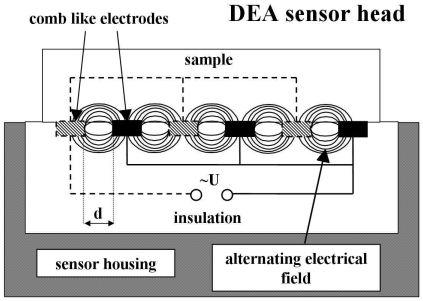

Fig. 2. Schematic design of the DEA sensor device with polymer specimen on top [4].

2. Dielectric Measurement Results of the Curing Process

The two curing phases, primary photo-curing and post curing have to be investigated with two different measuring techniques. The photo-curing process requires only a few seconds to transfer the acrylic resin to a rough polymer network. Hence, the dielectric measurement device needs to collect data for about 1 minute with a sampling rate of 10 to 20 data points per second. The post-curing process takes place in a time range lasting from several days to some years due to slow diffusion and rearrangement processes in the polymer network. The investigation of the post-curing process requires a very sensitive device to detect the small changes in the dielectric behaviour of the polymer specimen over a long time.

2.1. Measurement Results of the Primary Photo-Curing

During the photo-curing of a dental composite material the dielectric analysis (DEA) shows a rampant increase in ion viscosity directly after exposing to light. After approximately 8 seconds, the drastic increase of the ion viscosity has reached the saturation. The primary photo-curing phase is finished by the cross-linking of a rough polymer network. In Fig. 3 the ion viscosity progression is compared to a DSC-validation-measurement (Dynamic Scanning Calorimetry) of the curing reaction heat flow of a composite specimen.

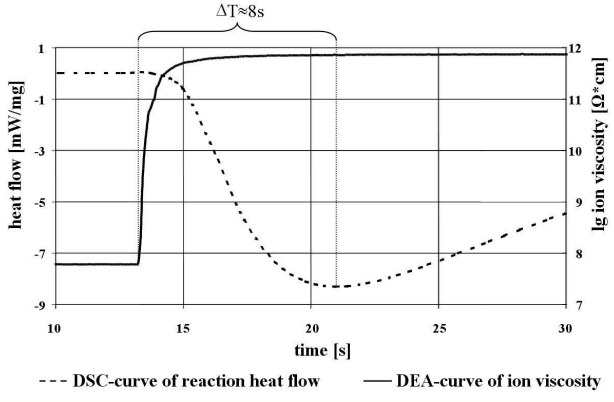

Fig. 3. Comparison of DEA and DSC measurement of the photo-curing process of a dental composite material.

The DSC-curve shows a minimum of the exothermal heat flow 8 seconds after the exposure. This can be interpreted in the way that the heat flow release due to the curing reaction has come to an end and that the relaxation of the heat flow to the base line is due to simple cooling. The DEA and the DSC measurements indicate that the saturation of ion viscosity or ion mobility coincides with the end of heat generation in the sample.

2.2. Measurement Results of the Post-Curing-Phase

After the photo-curing process dental composite materials show a slowly proceeding increase in stiffness. The time dependent elastic modulus measured by Dynamic Mechanic Analysis (DMA) shows that the stiffness rises approximately by 30% during 2 days (Fig. 4, right). In this post-curing phase the dielectric analysis (DEA) shows also a similar continuous increase of the ion viscosity after the exposure (Fig. 4, left).

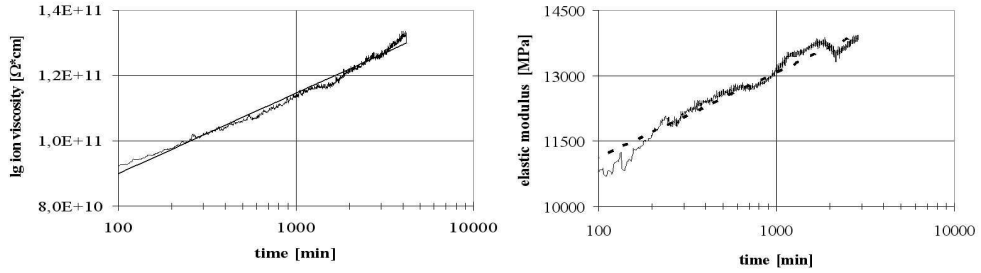

Fig. 4. Comparison of DEA (left) and DMA (right) measurements of the post-curing process of a dental composite

In the first approximation the time dependency of stiffness and ion viscosity, respectively, can be described by following equations

$$E(t) = E_0 + \Delta E \log t \tag{2}$$

$$\log \mu(t) = \log \mu_0 + \Delta(\log \mu) * \log t \tag{3}$$

with the initial modulus E_0, the change of modulus ΔE, the initial logarithmic ion viscosity μ_0, and the change of the logarithmic ion viscosity $\Delta(\log\mu)$. For the investigated dental composite material one gets the stiffness constants to E_0 = 7200 MPa and ΔE = 850 MPa and the ion viscosity constants to $\log \mu_0 = 4*10^{10}$ and $\Delta(\log \mu) = 1*10^{10}$.Both DEA and DMA measurements show a linear dependency of the post cure kinetics in the logarithmic time scale.

3. Conclusion

Hence, the DEA method allows for a precise and detailed view both on the short-term and long-term curing processes. It may provide characteristic data for the engineering of dental composite polymers and others with respect to curing light exposure conditions, minimal illumination times, and life time predictions. Furthermore the DEA is an easy to handle and cost efficient method to investigate curing kinetics of dental composite fillings and a powerful tool if assisted by other thermo-analytical methods.

Acknowledgement

The authors thank Dr. Reinhard Maletz and Dr. Martin Danebrock, Voco GmbH for supporting this work with supplying dental materials and photo-curing devices and Stephan Knappe, Netzsch Gerätebau GmbH for his very helpful suggestions concerning our DEA measuring setup.

References

[1] MOEGINGER, B., *Investigation of the Curing Behaviour of Photo-curing Dental Materials using DSC and DEA*, Proceedings of 34th NATAS Conf., Bowling Green, 2006

[2] ZAHOUILY, K., DECKER, C., KAISERSBERGER, E., GRUENER, M, *Real-time UV cure monitoring*, European Coatings Journal, 11/2003.

[3] MIJOVIC, J., FITZ, B. D., *Dielectric spectroscopy of reactive polymers*, Chapter 9, page 349-384 in "Dielectric Relaxation Spectroscopy; Fundamentals and Applications", Kremer, F., Schonals, A. Eds. Springer-Verlag, Berlin, 2002.

[4] STEINHAUS, J., *Curing kinetics investigation of dental photopolymers*. Diploma thesis, Bonn-Rhein-Sieg University of Applied Science, 2003

Transcom 2009, 22-24 June 2009
University of Žilina, Žilina, Slovak Republic

Study of Deformation after Heat Treatment and their Influence on Cutting Process

[*]Michal Šípek, [*]Miroslav Neslušan, [**]Vladislav Ochodek
[*]University of Žilina, Faculty of Mechanical Engineering, Department of Machining and Manufacturing Engineering, Univerzitna 8215/1, 010 26 Žilina, Slovakia,
{michal.sipek, miroslav.neslusan}@fstroj.uniza.sk
[**]VŠB-Technical University of Ostrava, Faculty of Mechanical Engineering, Department of Mechanical Technology, 17.listopadu 15, 708 33 Ostrava, Czech republic, vladislav.ochodek@vsb.cz

Abstract. This paper deals with deformations after heat treatment and their influence on stability of cutting process and precision of produced parts. There is presented comparison of deformations after heat treatment on martensite and bainite structure. The results of measurements show that deformation of bainite parts are lower than that for martensite one.

Keywords: heat treatment, deformations, turning, grinding, precision

1. Introduction

Process of roll bearing production includes heat treatment process to ensure the required properties of roll bearing rings. The convectional hardening process results into formation of hard structure of low toughness. Moreover, there are induced the tensile residual stresses, deformation of shape and dimensions of parts.

Nowadays, there is tendency to modify process of heat treatment, first of all the cooling phase of the process. The cooling phase of roll bearing parts is not realized in the oil of low temperature. This process is sometimes realized in the technical salt at temperature above 200 °C for several hours in the dependence on the processed material and required hardness. This process can result into formation of bainite structure [1]. Hardness of this structure is about 4 HRC lower that that for the martensite structure. On the other hand, toughness of the bainite structure is doubled in comparison with the martensite structure [2]. There are the next significant aspects of this process. There are significantly lower deformations of parts. In should be noticed that these deformation affects stability of cutting process and precision of produced parts. And so, this paper deals with deformations after heat treatment and their influence on stability of cutting process and precision of produced parts when application roll bearing steel 100Cr6.

2. Terms and Results of Experiments

Mechanical properties of roll bearing steel 100Cr6 of the different structure together with process of heat treatment are in Tab. 1. There were prepared 30 rings of external diameter 49,5 mm, internal diameter 40 mm and width 8 mm for each group of heat treatment process. These rings were machined before the heat treatment. There were measured their shape and dimension after machining and after the heat treatment. The measured data were processed in the software Q – DAS. Results of statistical analyze considering dimension of parts are

illustrates in Fig. 1. Results of statistical analyze considering deviation of roundness are illustrates in Fig. 2.

Parameters of heat treatment		Microstructure	Hardness HRC	toughness ($J.cm^{-2}$)		
Austenitization Tγ / τγ	Bainit transformation Tbt / τbt			-40°C	-30°C	20°C
Hardening for martensite 840 / 25 oil; tempering 160°C		Tempered martensite	62	13	16	23
860/ 5	240 / 3	Low bainite	59	35	45	55

Tab. 1. Properties of steel 100Cr6 after heat treatment [1].

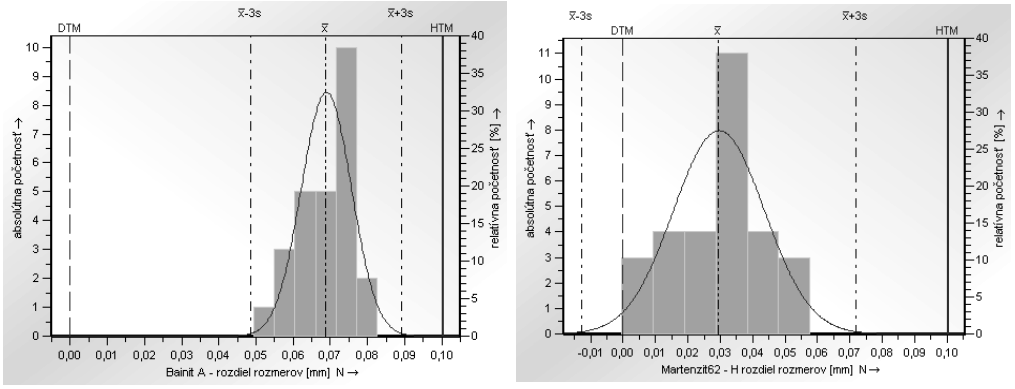

a) bainite b) martensite

Fig. 1. Statistic analyze of changes of ring diameter.

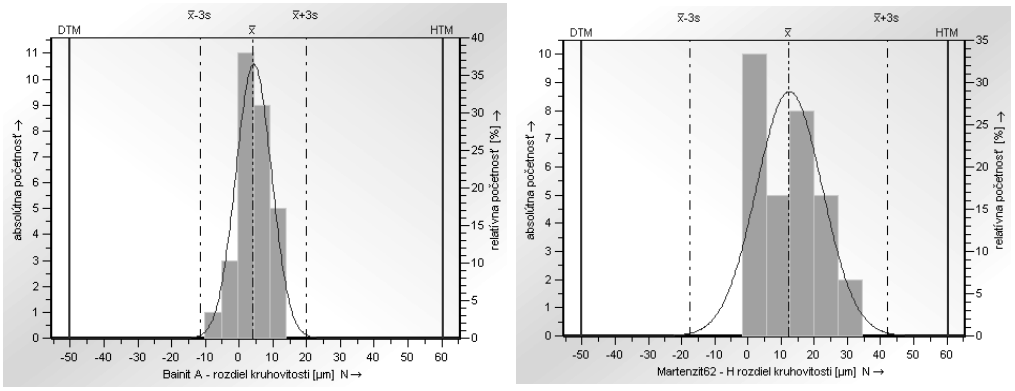

a) bainite b) martensite

Fig. 2. Statistic analyze of changes of roundness deviation.

Results of experiments are illustrated in Fig. 1 and 2. It is visible that the average value of roundness deviation changes about 4 µm for bainite structure, (interval ±3σ is only 35 µm) while the average value of roundness deviation changes is about 12 µm for martensite

structure, (interval ±3σ is 85 µm). On the other hand, average value of ring deformations is about 68 µm for bainite structure, (interval ±3σ is only 45 µm) while the average value of ring deformations are about 29 µm for martensite structure, (interval ±3σ is 90 µm). This aspect must be related to the different cooling rate and the different process of structure formation under the different conditions. The different cooling process leads to the different state of residual stress in the surface layers. There is formation of compressive stress in the bainite structure in comparison with the martensite structure and so the deformation of parts of bainite structure are lower that that for martensite structure.

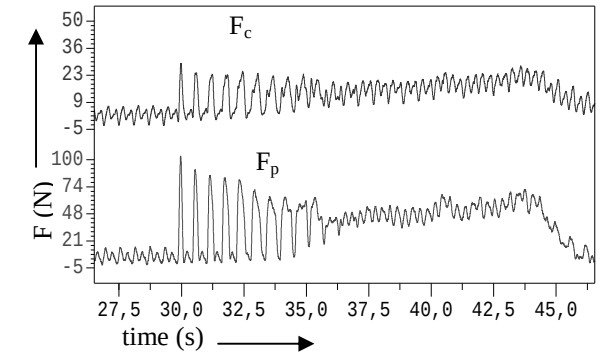

a) Record of cutting forces when grinding bainite parts
v_c = 30 m.s^{-1}
A99 80K 9V 350x20x127

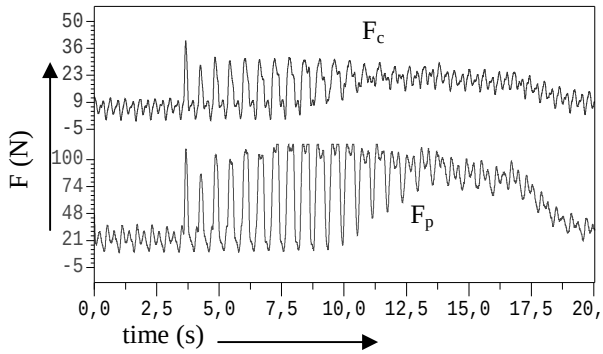

b) Record of cutting forces when grinding martensite parts
v_c = 30 m.s^{-1}
A99 80K 9V 350x20x127

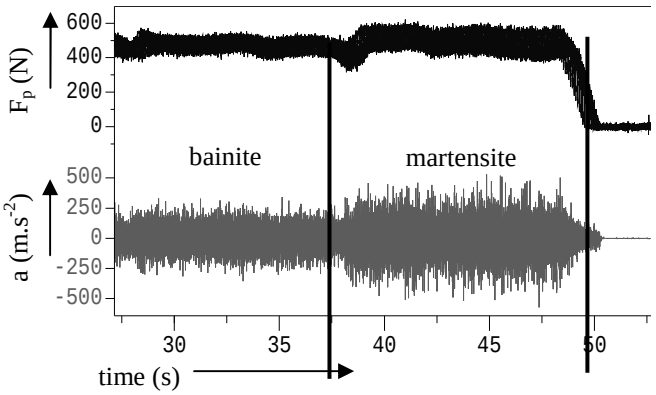

c) Record of F_p and acceleration during turning
v_c = 30 m.s^{-1}, f = 0,09 mm,
a_p = 0,25 mm
ceramic tool
DNGA150408 with TiN coating

Fig. 3. Record of cutting forces and acceleration during grinding (a, b) and turning (c).

Deformations of parts after heat treatment significantly affect the allowances for the following machining operation. This allowance must ensure to remove deformation after heat treatment and to ensure the required precision of parts (the main roles takes interval $\pm 3\sigma$). It is apparent that heat treatment for bainite structure enables to reduce deformation of parts. The allowances for machining operation and so the cycle times are shorter in comparison with conventional heat treatment. Moreover, the significant differences in deformations affect stability of the following cutting process, respectively the cycle times necessary for deformation removal. Fig. 3 illustrates that the grinding process is unstable in the first period of cycle (removal process of deformations after heat treatment). The next, there is visible the next period of full contact between grinding wheel and part. Moreover, Fig. 3 illustrates that the unstable period is longer because of the higher deformations after heat treatment for the martensite structure in comparison with bainite structure. The values of cutting forces are higher for martensite structure because of its higher hardness. The higher mentioned aspects affect the precision of produced parts.

The significant differences are visible during turning process. This is illustrates by Fig. 3c. The cutting process is more stable when turning bainite parts in comparison with martensite structure (RMS F_p 41 N for martensite, 27 N for bainite, RMS of acceleration is 130 $m.s^{-2}$ for martensite and 90 $m.s^{-2}$ for bainite). Turning process of hard turning is unstable because of deformation after heat treatment and quasi interrupted cutting contact between tool and workpiece. Precision of parts produced by grinding should be better that that for turning process. Turning process is realized per 1 pass while grinding process is realized by the consecutive repeated passes through the parts.

3. Conclusion

Nowadays, there is tendency to eliminate some undesirable aspects of conventional heat treatment through application of progressive methods or modification of cooling process. These approaches enable to eliminate the deformations of roll bearing ring, first of all of the light rings. The different process of heat treatment should be analyzed from the point of functional properties of produced parts. These experiments were carried out on some bearing made of steel 100Cr6 of bainite structure. Results of experiments show that the bainite structure can substitute the martensite one under the some conditions [2] from the point of noisiness and life time of roll bearing.

References

[1] HOZÁK, M - CHALUPOVÁ, M. - DURMIS, I.: *Izotermické zušľachťovanie Cr-Mn ocele na valivé ložiská.* In: Doksem 2004, Terchová – Šípková, 2004, s. 5 – 9.

[2] MINÁRIK, M. : *Brúsenie ocele 100Cr6 tepelne spracovanej na bainitickú štruktúru*, DDP, ŽU, SjF,2007

[3] PANDA, A.: *Využitie štatistickej regulácie výrobných procesov v praxi*, TD 2000-DIAGON ′99, VUT Brno, Zlín, 1999, s.188-192, ISBN 80-214-1328-X.

[4] NESLUŠAN, M. – TUREK, S. – BRYCHTA, J. – ČEP, R. – TABAČEK, M.: Experimentálne metódy v trieskovom obrábaní, EDIS Žilina 2007, ISBN 9788080707118

[5] JECH, J.: Oceli na valivé ložiska a jejich tepelné spracování, Praha: SNTL, 1968

[6] SKOČOVSKÝ, P. – VAŠKO, A.: Materiály a technológie. 1.vyd. EDIS, Žilina 2004. ISBN 80-8070-277-2

Transcom 2009, 22-24 June 2009
University of Žilina, Žilina, Slovak Republic

Titanium Alloy Implant Corrosion – Effect of Physiological Solution Temperature

[*]Lenka Škublová, [*]Branislav Hadzima
[*]University of Žilina, Faculty of Mechanical Engineering, Department of Materials Engineering,
Univerzitna 2, 01026 Žilina, {lenka.skublova, branislav.hadzima}@fstroj.uniza.sk

Abstract. Corrosion behaviour of biocompatible TiAl6V4 titanium alloy has been investigated by using electrochemical impedance spectroscopy in physiological solution (0.9 % solution of NaCl) at various temperatures. On the basic of type and shape of Nyquist curves obtained from EIS measurements there is assigned probable mechanisms of corrosion in specific corrosion system.

Keywords: EIS, corrosion resistance, biocompatibility, titanium alloy.

1. Introduction

Materials to be used as permanent implants in the human body must be biocompatible, corrosion resistant, tissue compatible, vital and elastic [1]. Metallic materials which combine these properties with good mechanical characteristics are chosen [2].

The primary use of metals is in the manufacture of orthopaedic implants [3]. For load-bearing joint replacement (e.g. hip or knee), metals are still chosen because of their mechanical stability. Thus, stainless steel, titanium alloys and cobalt-chrome alloys are the most widely used metallic components [4].

The good compatibility observed with titanium and titanium alloy implants in bony enviroments and the high fatigue strength of some Ti-alloys have increased the use of these metals in reconstructive surgery during the last decades. Amongst the various materials currently employed, the alloy Ti6Al4V has found extensive biomedical applications due to its good mechanical properties and ability for osseointegration, combined with an excellent corrosion behavior due to passivity. Passivity is due to the very stable and tenaciously adherent oxide films spontaneously formed over the surface, which reform very rapidly if removed or mechanically damaged [2, 5].

Currently, titanium alloys are commonly used for orthopaedic purpose but all metallic implant materials are denser, stronger and have higher elastic moduli than bone (E of compact human cortical bone is 5 times less than that of the Ti alloys). Titanium and its alloys also have the advantage of lower densities comparison with stainless steels. This is coupled with high strength and a very low rate of corrosion. The lower density reduces the weight of the implant and hence a reduced awareness of the implant by patient. The lower modulus of elasticity gives a „springier“ implant and reduces stresses around the implant, as it is more able to flex with the bone [3].

On some occasions, the high mechanical stiffness of metallic implants may result in stress shielding and bone resorption due to the mismatch of the elastic modulus of metals with that of bone. Other disadvantages of using metallic implants include the need for a second operation to remove temporary implants and the negative tissue response caused by the ions released from permanently implanted devices [6].

2. Experimental materials

The specimens from TiAl6V4 titanium alloy were used for the study. The standardized chemical composition of the alloys is in Tab. 1 [7]. All specimens were ground to 1200 grit and cleaned in ethanol before each corrosion testing.

element	N	C	H	Fe	O	Al	V	Ti
wt.%	0.05 max	0.08 max	0.15 max	0.4 max	0.2 max	5.50-6.75	3.50-4.50	rest

Tab. 1. Standardized chemical composition (wt %) of Ti-6Al-4V titanium alloy.

2.1. Microstructure analysis

Microstructural investigation has been done by optical microscope ZEISS AXIO Imager.A1m. The microstructure of TiAl6V4 specimens is (Fig.1) a two-phase structure created by polyedric grains of α phase (bright grains) and β phase (dark grains). The volume of α phase is ~80 %.

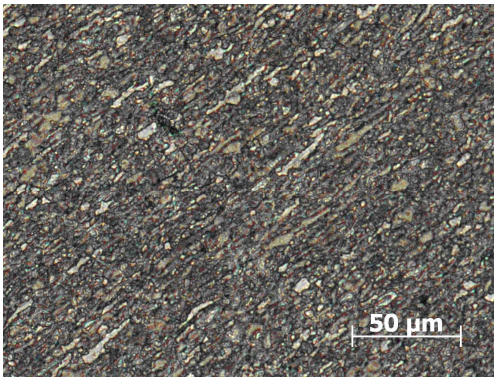

Fig. 1. Microstructure of TiAl6V4 titanium alloy; etch. HNO_3 + HF + ethanol.

3. Results and discussion

The electrochemical tests were performed using electrochemical impedance spectroscopy (EIS) in 0.9% NaCl solution at various temperatures (20, 30, 40 and 50 °C). The polarization resistance R_p and the Warburg impedance Z_w are electrochemical properties characterizing the material properties in the certain environment. The higher values of R_p and Z_w represent better corrosion resistance of the material in corrosion environment. The electrochemical experiments were performed in a conventional three-electrode cell system with a calomel reference electrode and a platinum auxiliary electrode using Voltalab 10 corrosion measuring system with PGZ 100 measuring unit. The scheme of circuit connection and measuring principle is described in detail elsewhere [8].

The time for potential stabilization between the specimen and electrolyte was set to 30 minutes. The measurement frequency ran in a range from 100 kHz to 20 mHz with 20-times frequency change pro decade. The amplitude of AC voltage was 40 mV. DC voltage component, by which the specimen was polarized during testing, was set to the measured value of free potential after 30 minutes of stabilization.

Temperature range (20-50°C) shows temperature influence on corrosion characteristics in temperature interval which can be attained in human organism.

Results of electrochemical impedance spectroscopy measurements as Nyquist diagrams for TiAl6V4 are in Fig. 3. The impedance spectrum for this alloy was fitted by computer using EC-Lab Software V9.32 obtained equivalent circuit (Fig. 2). The circuit is compound of the electrolyte solution resistance (R_Ω), and the electrical elements from the protective layer on the surface: the constant phase element (CPE), the polarization resistance (R_p) and the Warburg element (W). The constant phase element was introduced into the circuit instead of a capacitance in order to depict the nonhomogeneous quality of the deposited layer [9]:

$$CPE = A^{-1}(j\omega)^{-n}, \tag{1}$$

where A is a CPE coefficient, n is a fractional exponent (if n = 1.0, then A = C_{true}), and $\omega = 2\pi f$ is an angular frequency. The values for each element at various temperatures are in Tab. 2.

In Fig. 2 is a typical equivalent circuit represent mass transfer diffusion effects. The additional element, known as the Warburg impedance, is a complex quantity having real and imaginary parts which are equal. This impedance is proportional to the reciprocal of the square root of the frequency ($1/\sqrt{\omega}$). At high frequencies, therefore, this term is small and the diffusion process is only observed at low frequencies [9].

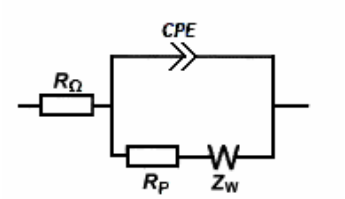

Fig. 2 Equivalent circuit for analysis of Nyquist plots of TiAl6V4 alloy

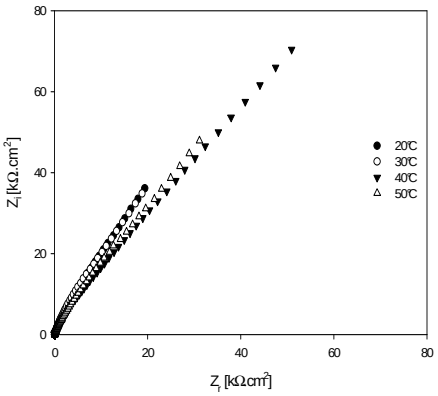

Fig. 3 Nyquist diagrams of TiAl6V4 in physiological solution at various temperatures

	20 °C	30 °C	40 °C	50 °C
Resistance, R_Ω (Ω cm^2)	20.5	15.9	12.8	12.6
Capacitance, CPE (μF/cm^2)	19.5	26.1	12.9	26.4
n	0.9	0.9	0.9	0.8
Resistance, R_p (Ω cm^2)	59.8	88.0	61.4	104.7
Warburg impedance, Z_W (Ω cm^2)	53449.5	58652.3	62189.4	59390.4

Tab. 2. The values of electrical elements for the measured specimens from EIS method.

Titanium alloy material has the ability to form protective layer on the surface. In contrast to stainless steel, the repassivation ability in oxidic solutions is much more effective on titanium alloy surface because it is possible to create three different oxidic layer (TiO_2 and Ti_2O_3, eventually also TiO) as a protection of surface from corrosion [10].

Measured values of equivalent electrical elements of TiAl6V4 titanium alloy show that influence of surrounding temperature on corrosion properties is minimal. Corrosion process for this titanium alloy is handled by diffusion in whole range of temperatures from 20°C to 50°C. It results from shape of measured EIS curves.

4. Conclusion

The metallographic and electrochemical investigations of surrounding temperature on the corrosion resistance of TiAl6V4 alloy have been carried out in 0.9% NaCl. The following conclusions can be drawn from this study:

- The metallographic evaluation confirms that microstructure of TiAl6V4 specimens is a two-phase structure created by polyedric grains of α phase (20%) and β phase (80%).
- The results of TiAl6V4 alloy confirmed that dependency of polarization resistance to surrounding temperature solution from 20 to 50°C has not any significant importance on material properties and this titanium alloy does not presence any risks joint with its implantation in vivo from corrosion properties point of view.
- Corrosion resistance of TiAl6V4 alloy does not change in term of different temperatures of solution in contrast of the corrosion properties of AISI 316L stainless steel [11].

The results depose that TiAl6V4 titanium alloy is much more suitable for long-term implantation than AISI 316L stainless steel in human body when human temperature range can achieve inflammatory temperature above 40°C. However, it is very important to tests this material before its using. Surface polishing and passivation of this biomaterial is prefered at production. Then biomaterial resists better to the corrosion in enviroment of body fluids.

Acknowledgement

The part of the results of this work was supported by Slovak-Hungary cooperation, project No. SK-MAD-030-06 (in Hungary TET-SK-11-2006). This work has been supported by Scientific Grant Agency of Ministry of Education and Slovak Academy of Sciences, grants No.1/4096/07 and No. 1/0203/08.

References

[1] EISENBARTH, E., VALTEN, D., MÜLLER, M., THULL, R., BREME, J.: *Biocompatibility of β-stabilizing elements of titanium alloys.* Biomaterials 25, 2004, p.5705-5713.

[2] SOUTO, R. M., LAZ, M. M., REIS, R. L. *Degradation characteristic of hydroxyapatite coatings on orthopaedic TiAlV in simulated physiological media investigated by electrochemical impedance spectroscopy.* Biomaterials 24, 2003, p.4213-4221.

[3] BARBER, D.C., LAWFORD, P.V., HOSE, D. R., SMALLWOOD, R.H., BROWN, B.H. *Medical Physics and Biomedical Engineering.* CRC Press, 1998, p.125.

[4] BORDJI, K., JOUZEAU, J.Y., MAINARD, D., PAYAN, E., DELAGOUETTE, J.P., NETTER, P. *Evaluation of the effect of three surface treatmens on the biocompatibility of 316L stainless steel using human differentiated cells.* Biomaterials 17, 1996, p.491-500.

[5] BRUNETTE, D.M. *Titanium in Medicine: Material Science, Surface Science, Engineering, Biological Responses and Medical Applications.* Springer, 2001.

[6] SHI, D. *Biomaterials and Tissue Engineering. Biological and Medical Physics, Biomedical Engineering.* Springer, 2004.

[7] ŠKUBLOVÁ, L., SUCHÝ, P., HADZIMA, B. *Biocompatibility of TiAl6V4 Titanium Alloy*. Transcom 2007, p.233-236.

[8] HADZIMA, B., LIPTÁKOVÁ, T. *Základy elektrochemickej korózie kovov*. EDIS ŽU v Žiline, Žilina 2008.

[9] ŠKUBLOVÁ, L., HADZIMA, B., V., BORBÁS, L., VITOSOVÁ, M. *The influence of temperature on corrosion properties of titanium and stainless steel biomaterials*. Materials Engineering, 15, 4, 2008, p.18-22.

[10] HUANG, Y.Z., BLACKWOOD, D.J. *Characterisation of titanium oxide film grown in 0.9% NaCl at different sweep rates*. Electrochimica Acta, 51, 6, 2005, p.1099-1107.

[11] HADZIMA, B., ŠKORÍK, V., BORBÁS, L., OLÁH, L. *Corrosion of biocompatible AISI316 stainless steel in physiological solution*. Materials Engineering, 15, 3, 2008, p.27-30.

Transcom 2009, 22-24 June 2009
University of Žilina, Žilina, Slovak Republic

Hard Turning with PCBN and Present Development Trends

Ľubomír Šupej, Michal Sporka, Dana Stančeková
University of Žilina, Faculty of Mechanical Engineering, Department of Machining and Manufacturing Engineering, Univerzitna 2, 01026 Žilina, Slovakia,
{ lubomir.supej, michal.sporka, dana.stancekova }@fstroj.uniza.sk

Abstract: The present work studies some aspects of the turning process applied on hardened steel using multilayer coated carbide, ceramic, cermet and polycrystalline cubic boron nitride tools at higher cutting speeds. The current literature reports many studies using PCBN on hardened steel of hardness 45 to 63 HRC. A significant pool of CBN tool wear studies has been surveyed, in an attempt to achieve better processing and tooling applications, and discussed from the tool wear pattern and mechanism perspectives. The article explain basic information from hard turning with polycrystalline cubic boron nitride, benefits this progressive technology of cutting material and present development trends.

Keywords: hard turning, grinding, polycrystalline cubic boron nitride, hardened material, roughness of surface

1. Introduction

Producers of machined components and manufactured goods are continually challenged to reduce cost, improve quality and minimize setup times in order to remain competitive. Frequently the answer is found with new technology solutions. Such is the case with grinding where the traditional operations involve expensive machinery and generally have long manufacturing cycles, costly support equipment, and lengthy setup times. The newer solution is a hard turning process, which is best performed with appropriately configured turning centers or lathes.

The clear attraction to hard turning is the possibility of eliminating grinding operations. For some shops, though, the process of repeatedly turning parts that are harder than 45 HRC to grinding-level accuracies is still a bit cloudy.

1.1. Hard turning

Hard turning is defined as the process of single point cutting of part pieces that have hardness values over 45 HRC. Typically, however, hard turned part pieces will be found to lie within the range of 58-68 HRC. The hard turning process is similar enough to conventional "soft" turning that the introduction of this process into the normal factory environment can happen with relatively small operational changes when the proper elements have been addressed. However, some shops misstep by initially using the wrong (that is, less expensive) tool insert for the application. Others may not be sure if their machine possesses the rigidity to handle cutting pressures that can be twice that of a typical turning operation [1].

Hard turning is best accomplished with cutting inserts made from either CBN (Cubic Boron Nitride), Cermet or Ceramic. Since hard turning is single point cutting, a significant benefit of this process is the capability to produce contours and to generate complex forms with the inherent motion capability of modern machine tools. High quality hard turning

applications do require a properly configured machine tool and the appropriate tooling. For many applications, CBN tooling will be the most dominant choice. However, Ceramic and Cermets also have roles with this process [4].

The range of applications for hard turning can vary widely, where at one end of the process spectrum hard turning serves as a grinding replacement process, and can also be quite effective for pre-grind preparation processes [4].

A properly dialed-in hard turning process can deliver surface finish of 0.0027 mm, roundness of 0.00022 mm and diameter tolerance of ±0.005 mm [5].

Fig. 1. Typical parts for technology of hard turning [5]

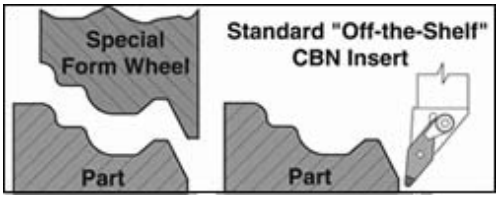

Fig. 2. A properly tuned hard turning system can reduce, and in some cases eliminate, grinding and its associated high tooling costs and long processing time [5]

The degree of machine rigidity dictates the degree of hard turning accuracy. Most machines made in the last 15 to 20 years have sufficient rigidity to handle some hard turning applications. In many cases, a machine's overall condition is more of a factor than its age. Even an old, well-maintained manual lathe can be a candidate for hard turning. However, as required part tolerances get tighter and surface finishes get finer, machine rigidity becomes more of an issue [1].

Harding has integrated a number of features in its turning centers to increase rigidity and damping characteristics for hard turning applications. These include machine bases with polymer composite reinforcement, direct-seating colleted spindles that locate the spindle bearing close to the workpiece and hydrostatic ways [4].

1.2. Experimental measurement roughness of surface by hard turning with PCBN

Material of workpiece was bearing steel the class 14209.4 with hardness 63 HRC. Measurement was done on apparatus MITUTOYO SURFEST 301, which independently evaluate the characteristics of roughness *Ra*, *Rq* and *Rz*. Measuring was done in three places on surface workpiece angle-wise 120°. Table 1 describe used the cutting parameters. From record values of roughness were computed arithmetical averages. From this one were created structural equations for all three parameters of roughness. The ternary graphs were crafted at the conclusion. These graphs describe influence cutting speed v_c, feed f and cutting depth a_p on roughness tooled surface.

Number	Quantity		
	a_p (mm)	f (mm)	v_c (m . min^{-1})
I.	0,3	0,102	50; 100; 300
II.	0,3	0,05; 0,102; 0,150	100
III.	0,1; 0,3; 0,5	0,102	100

Tab. 1. Cutting parameters

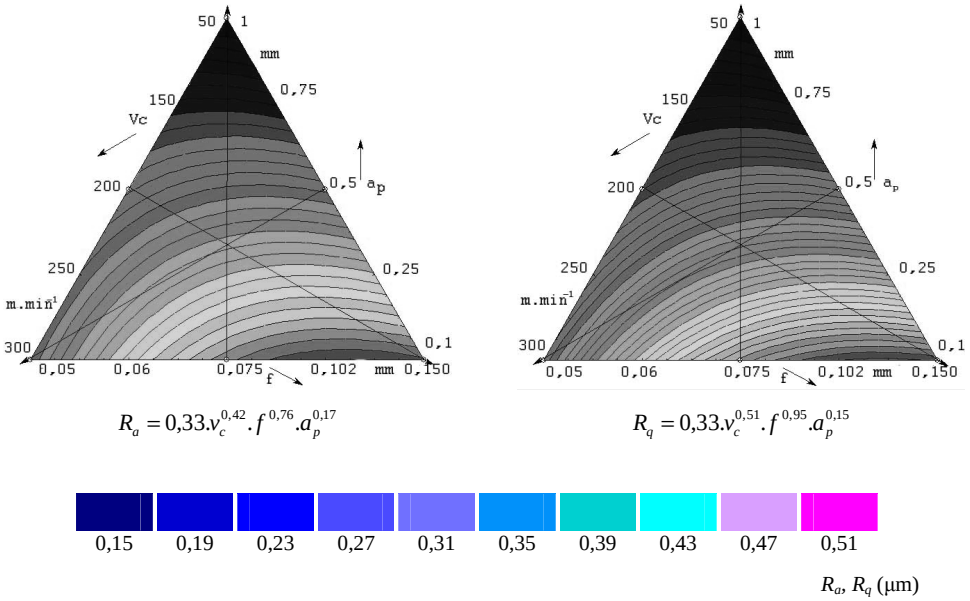

Fig. 3. Ternary graphs constructed from structural equations for *Ra* and *Rq*

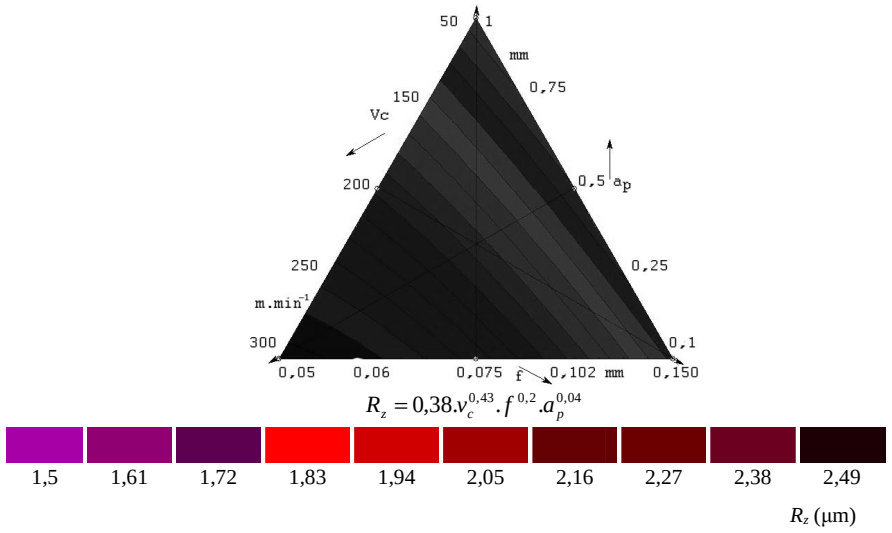

Fig. 4. Ternary graph constructed from structural equations for *Rz*

From result of measurement we can say: When cutting speed and feed increase, parameters roughness of surface will increase too. Feed has major influence and cutting depth has minimal influence on the quality of surface. Higher quality of tooled surface is possible to reach with correct combination of cutting speeds and feeds.

1.3. Present Development Trends for PCBN Tools

The development specific types cutting materials determine new information for all fields hard materials cutting. On the basis of trends from knowledge PCBN cutting materials we can say:

The cutting tools for hardened materials are burden with high mechanical and thermal stress during cutting process. From this reason known black types PCBN blades change for coating one. These coating can reduce intensity of wear and escalate lifetime tools. Blades from firm Iljin Inc are available with Ni coating for Resin bond wheel and Ti coating for Metal bond wheel to improve retention force [3].

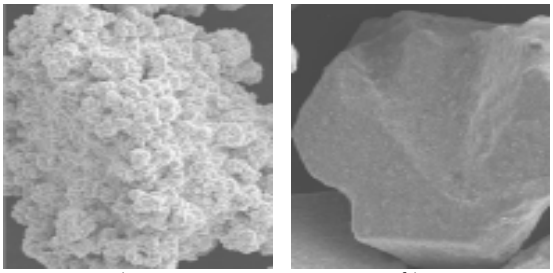

a) b)

Fig. 5. Illustration: a) Ni coating, b) Ti coating PCBN grains Iljin Inc [3]

Geometry of blade begin has significant function on increase of productivity. Kyocera how the first company developed blade with chipbreaker in combination with coated carbide. This blade improves the control of shape and way drain chip (fig. 6.) [2].

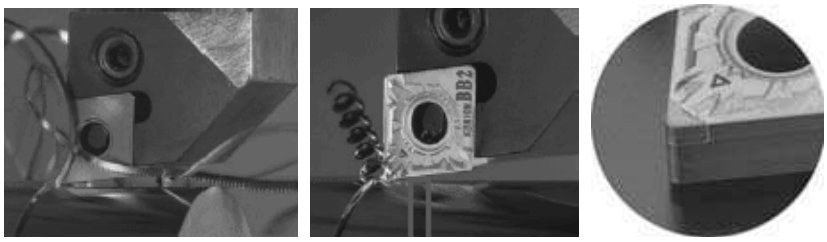

Fig. 6. Geometry of blade in left conventional blade, in right new type of blade company Kyocera [2]

Nowadays production is oriented on improve of quality PKNB from perspective homogeneity size grains. This improve can increase toughness of cutting blade. Other new type will be blades with higher content CBN grains for cutting cast iron.

2. Conclusion

This article describes technology of hard turning for hardened materials. This progressive technology has benefits economical and technological. Important task for technologists is correct choice cutting material. It should guarantee desired hardness of cutting material above hardness of workpiece. High strength cutting materials and their use in production process can substitute grinding of irregular- shaped components with easier and cheaper geometry defines tools.

References

[1] VASILKO, K. – HAVRILA, M. – NOVÁK-MARCINČIN, J. – MÁDL, J. – ZAJAC, J.: *Top trendy v obrábaní III./IV.- Technológia obrábania*, Žilina: MEDIA/ST, 2006, str. 154 - 157 a str. 166- 169.

[2] Internet : http://americas.kyocera.com

[3] Internet : http://iljindiamond.co.kr

[4] Internet : http://www.mikesmusic.co.uk/Aston%20Products/hard_turning.html

[5] Internet : http://www.mmsonline.com

Transcom 2009, 22-24 June 2009
University of Žilina, Žilina, Slovak Republic

The Influence of Shot-Peening and Nickel Plating on the Fatigue Endurance of S235JRG2 Steel in the Ultra-High Cycle Regime

[*]Veronika Valovičová, [**]Robert Ulewicz, [**]Piotr Bojanowicz
[*]University of Žilina, Faculty of Mechanical Engineering, Department of Materials engineering, Univerzitná 2, 01026 Žilina, Slovakia, {Veronika Valovičová}@fstroj.uniza.sk
[**]Czestochowa University of Technology, Faculty of Management, Department of Production Engineering, Czestochowa, Poland

Abstract. In this work the authors present original knowledge about the influence of shot-peening and nickel plating on the fatigue endurance of S235JRG2 steel in the ultra-high-cycle region of loading ($N = 6\times10^6 \div 10^{10}$ cycles) obtained at high-frequency fatigue testing ($f \approx 20$ kHz, $T = 20 \pm 3$ °C, $R = -1$). Shot-peening is a technological process and during this process the surface layer is exposed to plastic deformation which is caused by high speed shooting using small metallic or ceramic particles. Nickel plating is employed for final layers production or it can be used for production of inter-layers in chrome plating.

Keywords: Fatigue endurance, shot-peening, nickel plating.

1. Introduction

The fatigue endurance is one of the most important criteria determining the quality of components and structures [1]. More than 90% of all fractures are caused by fatigue in service [2, 3, 4]. Fatigue lifetime is investigated in the low-cycle region of loading ($N < 10^4 \div 10^5$ cycles), high-cycle region of loading ($10^4 \div 10^5 < N < 2.10^6 \div 10^7$ cycles) and in the ultra-high-cycle region of loading ($10^7 < N < 10^{10}$ cycles). In recent ten years, the ultra-high-cycle region of loading ($10^7 < N < 10^{10}$ cycles) is intensively investigated by several research teams. The aim of these experimental studies is to increase the endurance, safety and reliability of components and structures [3, 4]. The reason of this study is a fact, that the fatigue fractures occur more than $N = 10^7$ cycles of loading. Determination of fatigue characteristics is usually realized using usual frequencies, in the range from $f \approx 10$ Hz to $f \approx 200$ Hz. It takes a lot of time and it is expensive. On this account the new experimental methods working with a high frequency cyclic loading are employed ($f \approx 20$ kHz) [2, 5, 6].

The application of non-ferrous metal layers is used in engineering praxis with the aim to renovate the components, to increase the resistance against to the effect of aggressive environments, to increase the wear resistance and to produce layers with decorative purpose. Electrolytic deposition layers can cause decrease of endurance strength [7, 8].

Nickel plating is employed for final layers production or it can be used for production of inter-layers in chrome plating. The final nickel layers are suitable for light and extra-light corrosive environments. Nickel layers are not suitable for the middle and heavy corrosive environments. Nickel coatings without inter-layer are suitable for protection of chemical devices working in alkaline environments. They can be used for protection of some components, which need high wear resistance. Decorative coating with inter-layer is usually

used with three-coating version (copper-nickel-chrome). This version of three-coating improve anti-corrosive resistance of base material [8, 9].

The endurance strength of some components with nickel coatings or chrome coatings can be increase by shot-peening before electrolytic deposition of nickel layer for strengthening of surface layer. This procedure can lead to fatigue properties increase [7].

Shot-peening is a technological process. During this process the surface layer is exposed to plastic deformation which is caused by high speed shooting using small metallic or ceramic particles. The result of this process is strengthening of surface layer and formation of compression internal residual stresses in the surface layer. But on the other hand the results of this process can lead to the formation of rough surface. This surface roughness results in to the notches well known as stress concentrators. These facts can cause the increase of endurance strength up to 20%. They can also cause the decrease of fatigue lifetime [7, 11].

In this paper are present the results of fatigue endurance investigation of steel after shot-peening and results about fatigue resistance of the same steel with nickel layer. The results are obtained from fatigue tests in ultra-high-cycle region by means of methods and procedures of high-frequency loading.

2. Experiments

The S235JRG2 structural steel of common quality was used as an experimental material. The chemical composition of the steel is introduced in Tab. 1. From the experimental material were prepared specimens for mechanical tests and specimens for fatigue tests. The fatigue tests were performed on specimens with nickel coatings and on specimens after shot-peening.

C	Mn	P	S	Si	Ni	Cr	Cu	R_e [MPa]	R_m [MPa]	A_5 [%]
0.17	0.57	0.015	0.032	0.12	0.09	0.07	0.27	340	445.6	30.8

Tab. 1. Chemical composition [wt.%] and mechanical properties of S235JRG2 steel

The results from metallographic analysis are shown in the Fig. 1. For metallographic analysis was used light metallographic microscope NEOPHOT 32. The experimental steel has ferritic-perlitic fine-grained microstructure (Fig. 1), with grain size 10 (classified according to Slovak standard STN 42 0462). Tensile test (according to STN EN 10002-1) was performed using experimental universal mechanical testing machine ZWICK Z 50 (with loading range $F = 0 \div 50$ kN, temperature $T = 20 \pm 2$ °C). For tensile tests were used round standard specimens with diameter $D_0 = 6$ mm. The obtained results are present in the Tab. 1.

For fatigue tests was used experimental equipment KAUP-ŽU Žilina. Used testing methods and procedures are described elsewhere [3, 6]. The experiments were carried out on resonant high-frequency fatigue machine in the regime of controlled load using sinusoidal tension-compression loading with the frequency of 20 kHz. The stress ratio of R = -1 was used. Fatigue tests were performed at the ambient temperature ($T = 20 \pm 3$ ºC). Specimens were cooled by distilled water with anticorrosive inhibitor [12]. Shapes of specimens were described [3, 6]. The specimens with nickel coating were grinded and polished for elimination of surface roughness before the application of nickel coating.

The fatigue tests, dependence $\sigma_a = f(N)$, were performed in the range from $N = 6\times10^6$ cycles to $N = 10^{10}$ cycles. Fatigue tests were aborted in region of $N = 10^{10}$ cycles. For experiments were used three sets of specimens with ten specimens for

each set. The sets contained specimens from basic material, specimens after shot-peening and specimens with nickel coating. The results of fatigue tests are shown in Fig. 2.

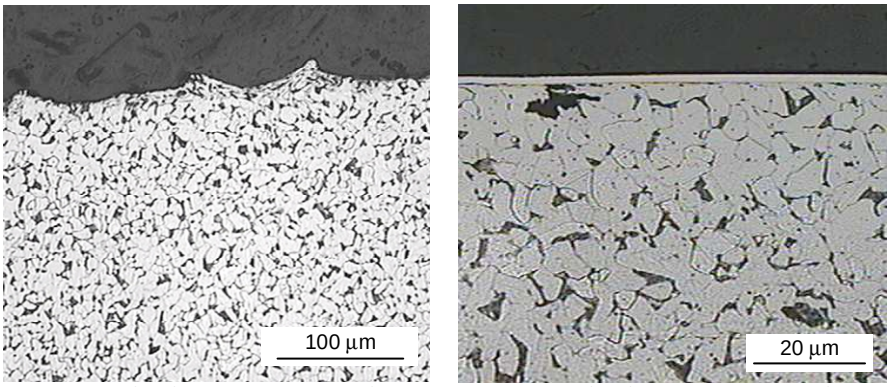

a.) Character of surface, S235JRG2 steel after shot-peening

b.) Character of surface, S235JRG2 steel after nickel electrolytic coating

Fig. 1. Microstructure of the S235JRG2 steel, etch. 3 % Nital

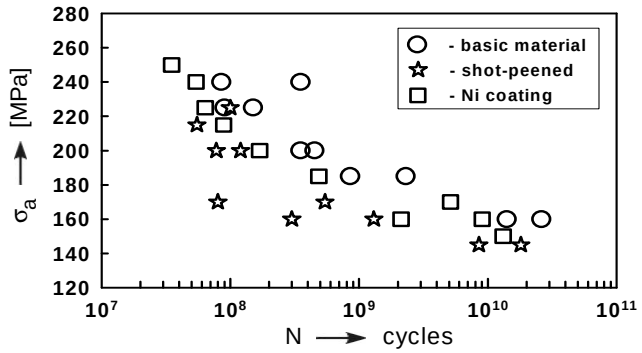

Fig. 2. The $\sigma_a = f(N)$ dependence, S235JRG2 steel, high frequency cyclic loading

From carried out tests results in which the stress amplitude σ_a decreases together with increase of cycles number N beyond conventional cycles border $N_c = 10^7$ cycles. The fatigue test always ends with fatigue fracture. In case of specimens without nickel layer coating the stress amplitude decreases of $\Delta\sigma_a = 160$ MPa ($N = 8\times10^7 \leftrightarrow N = 10^{10}$ cycles). Specimens with nickel layer coating indicate similar decrease of the stress amplitude like specimens without nickel coating ($\Delta\sigma_a = 180$ MPa, $N = 6\times10^6 \leftrightarrow N = 10^{10}$ cycles). In case of specimens after shot-peening the stress amplitude decreased of $\Delta\sigma_a = 70$ MPa (from $N = 5.19\times10^7$ cycles to $N = 1.73\times10^{10}$ cycles).

The shot-peening process had not a positive effect for fatigue life increase (Fig. 2). The experimental data from the fatigue tests determined on the sets of specimens after shot peening, are lower than the experimental data determined on other two sets of specimens. It is possible to say that expected positive effect of recorded compression stresses and strain hardening after shot-peening was exceeded with negative notch effects, i.e. with stress concentrators (Fig. 1a). The analogical knowledge was observed also by other authors [10, 11]. The presence of the compressive stresses in the heavy deformed surface layer is accompanied by the presence of tensile stresses in the area under this layer. The tensile

stresses have a negative effect on the fatigue endurance [13]. The data, noted above, are corresponding with fact that in the ultra-high regime of cycles loading the surface has not a critical role in the fatigue process, if this surface is smooth. In this case the fatigue crack initiation begins from the subsurface. The important role has a micropurity of experimental material, a number of microdefects, long grain bounds and so on [5, 14, 15].

3. Conclusion

From carried out experimental results the following conclusions can be drawn:

- The shot-peening process has not a positive effect for fatigue life increase. Surface roughness and notches after shot-peening were a primary initiation places for fatigue process.
- The electrolytic deposition of nickel coating led to the fatigue lifetime reduction in the low-cycle fatigue region. The influence of electro-plated nickel coatings on the fatigue endurance is not so strong in the high and ultra-high-cycle region.

Obtained results have a predicative value for an engineering praxis with respect to optimal choice of material and technological parameters for shot-peening and surface coatings.

Acknowledgement

This work was supported by Science and Technology Assistance Agency under the contract No. APVT-20-012804. This work has been partially supported by Scientific Grant Agency of Ministry of Education and Slovak Academy of Sciences, grant No. 1/4096/07. The authors gratefully acknowledge this support.

References

[1] BIDULSKÝ, R. - RODZIŇÁK, D.: Vplyv spevňovania povrchu na únavové vlastnosti spekanej ocele na báze Fe legovanej Cr a Mo s prídavkom 0,5% C, In: Zb. Letná škola únavy 2006, Žilina-Strečno, 2006, ŽU, p. 172.

[2] NICOLETTO, G. - BOKŮVKA, O. - KOPAS, P. - COLLINI, L. - BUJNOVÁ, P.: Transaction of FAMENA, Vol. 29, No. 1, Croatia, Zagreb 2005, p. 9.

[3] BOKŮVKA, O. - NICOLETTO, G. - KUNZ, L. - PALČEK, P. - CHALUPOVÁ, M.: Low and High Frequency Fatigue Testing, EDIS, ŽU Žilina, 2002.

[4] SKOČOVSKÝ, P. - BOKŮVKA, O. - KONEČNÁ, R. - TILLOVÁ, E.: Náuka o materiáli pre odbory strojnícke, EDIS, ŽU Žilina, 2001.

[5] BATHIAS, C. - PARIS, P. C.: Gigacycle Fatigue in Mechanical Practice. M. Dekker, N. York, 2005.

[6] BOKŮVKA, O. - NOVÝ, F. - KUNZ, L. - LUKÁŠ, P.: Únavová životnosť materiálov v oblasti veľmi vysokého počtu cyklov zaťažovania, In: Zb. Životnost materiálů a konstrukcí 2006, ÚFM Brno, 2006, p. 15.

[7] HOLZMAN, M. - KLESNIL, M.: Křehký a únavový lom materiálů a konstrukcí, SNTL Praha, 1972.

[8] KANDER, L.: Nízkocyklová únava funkčních galvanických povlaků na bázi Ni, In: Zb. Letná škola únavy materiálov 2004, ZUBEREC - ROHÁČE, 2004, p. 181.

[9] DORAZIL, E. - HRSTKA, J.: Strojírenské materiály a povrchové úpravy. VUT Brno, 1985.

[10] KUNZ, J. - NEDBAL, I. - SIEGL, J.: In: Proc. Fractography 91, Košice, ÚFM SAV, 1991, p. 361.

[11] KUNZ, J. - SIEGL, J. - NEDBAL, I. : Materials Engineering, Vol. 14, Issue 3, p.44.

[12] HADZIMA, B. - SUCHÝ, P.: Materials Engineering, Vol. 14, Issue 4, 2007, p.31.

[13] MIHALIKOVÁ, M. - KOVALOVÁ, K. - MICHEĽ, J.: Materials Engineering, Vol. 11, Issue 3, 2004, p. 13.

[14] NOVÝ, F. - BOKŮVKA, O. - CHALUPOVÁ, M. - MOTÝĽOVÁ, E.: Materials Engineering, Vol. 15, Issue 2a, 2008, p. 79.

[15] PRŠKOVÁ, V. - NOVÝ, F. - CHALUPOVÁ, M..: Materials Engineering, Vol. 15, Issue 2a, 2008, p. 97.

Transcom 2009, 22-24 June 2009
University of Žilina, Žilina, Slovak Republic

Welding of Plastic Material in Gas Industry

*Miloš Varga, *Miloš Mičian, *Peter Pallo
*University of Zilina, Univerzitná 1, 010 26 Zilina, Slovak Republic, tel. 00421-513 2771, e-mail: milos.varga@fstroj.uniza.sk

Abstract. The article is focused on the problem of creating the technological procedures of welding the plastic, destructive and not destructive examinations.

Keywords: welding, welding the thermoplastic, butt welding, electric sleeve welding, WPQR, WPS.

1. Introduction

In this article we deal with welding of plastic pipes from PE material. Two technologies had been chosen – butt welding and electric sleeve welding. Next, the tensile tests of the welded pipes were conducted and experimental protocols and welding procedures pWPS, WPQR and WPS were made. We issued from the norm STN EN 13067 which defines the type of welding and the type of testing for different pipe diameter, as it is shown in the chart number 1. Pipe diameter are integrated into subgroups[7].

Methods welding	Butt welding		Electric sleeve welding		
Subset material PE	3.4	3.5	3.6	3.7	3.8
Diameter pipe [mm]	D_n 110	D_n 400	D_n 90	D_n 315	D_n 32
Class test	Visual, Tensile		Visual, Flaking		

Tab. 1. Partition welding and class test depending up diameter pipe normative STN EN 13067.

2. Butt Welding

The machine which was used for butt welding is hydraulic in the pressure chops. The size of the fixative chops was for big pipe diameters (D_n=250 mm-500mm). The fixative chops which were situated on the frame of the machine, the sledge, were adjusted to the required welded pipe diameter D_n = 400 mm. The hydraulics of the machine was the part of the casing component. The plane was not the component of the machine but it was individual. The control unit which was solved as CNC machine evaluated and used the welding parameters for a required diameter of the welded pipe and type of the material itself. Only the divided pipe with the sawing brief which is adjustable for different diameters was used out of the apparatus.

2.1 Butt Welding Procedure

The welding material was the PE 100 pipe with the diameter D_n= 400 mm. The welding was carried out in the workroom conditions.

At first, the preparation of the welding was performed. It was focused on the execution of the safety conditions and health protection. After the control of the welding machinery, the

CNC machine was launched and after loading of the bar code from the chip card of every welder and inserting cards in the bar-code reader it was possible to proceed to other operations of preparation before the welding itself. The CNC machine gradually called the welder for further operations, which were necessary to conduct, on its display.

The next step was the preparation of the material which included expurgation from abrasive impurities. After the clamping work, the CNC machine brought the welded pipes closer to each other and visually checked the displacement.

After the displacement check, the planing of the pipe front followed by the help of the plane which was placed between the welded pipes. After the planing the displacement check was needed again.

After the expurgation, the mirror was placed between the pipe fronts as it is illustrated in the Fig. 2.

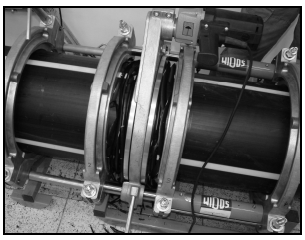

Fig. 1. Planning pipe through the medium plane

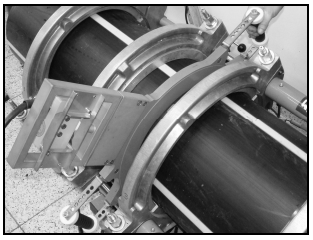

Fig. 2. Insertion mirror amid forehead pipe

The mirror temperature was 220 ºC. After placing of the mirror, the pipe fronts with the help of the sledge touched the warmed mirror and the heating followed. The heating time was 183 seconds. In this time the pipes were pressed by certain pressure which was evaluated by the CNC welder. In consequence a small veining was created as it is portrayed in the picture 3.

Then the converting followed when the sledge was removed and the mirror, which had to be put out very quickly, was very quickly released. The converting was followed by the connection where the welded surfaces touched and the pressure was gradually added until the complete welding pressure. The welding pressure was maintained constant during the cooling time as well. The cooling time was 28 minutes and 51 seconds. It depended on the depth and of the pipe as well. In this time, the veining was gradually produced as in is portrayed in the Fig. 4. The welding was finished after the cooling.

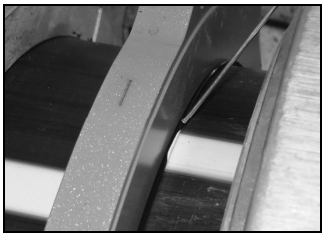

Fig. 3. Creating veining at warming

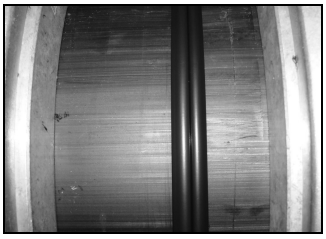

Fig. 4. Creating veining

3. Electric Sleeve Welding

The electric sleeve which was used for the welding was of diameter D_n=32 mm in the elbow form. The welding machine was of the brand FRIAMAT for welding the electric sleeve of different diameters.

3.1. Electric Sleeve Welding Process

The welding was realised in the workroom conditions PE 100 pipes with the diameter of D_n=32 mm were welded and the electric sleeve with the elbow form was used. The first phase was conducted. It was focused on the workplace check in the terms of safety, visual check of the material and welding machine condition (flexible cord condition, operation mode settings).

The welding phase itself followed. First, two welding parameters were loaded by the bar-code reader on the electric sleeve. It is portrayed in the Fig. 5. The heating of the welding surface started by the resistive wire loaded in the electric sleeve into the plasticizing state. The welding parameters were voltage U=328 V and frequency f =50 Hz. The time to achieve the weld was t =25 s. These welding parameters were evaluated by the welding machine itself regarding the ambient temperature which was 18 ºC. All this was possible to monitor on the welding machine display. After running out of the welding time the ending of the power supply, disconnection of the contacts and the visual check of the weld by the replacement of the pin indicator occurred. It is illustrated in the Fig. 6.

Finally, the cooling phase and the welding completion phase followed. Under the completion phase belongs identification symbol made with the permanent felt-tip pen next to the weld which is the welding date and time and the name of the welder. The welding process was completed.

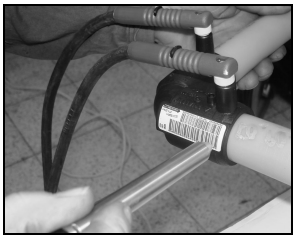

Fig. 5. Counting welder parameters

Fig. 6. Visual control weld through replacement pin welder indicator.

4. Testing of the Welded Joints

Testing of the welded joints was carried out according to the norm STN EN 13067. This norm defines the test type which is supposed to be conducted on the welded material according to the diameter of the welded pipe and the type of welding as it is portrayed in the chart 1.

The visual check was done according to the norm STN EN 13100 – 1: Not destructive testing of the welded joints of the thermoplastic semiproducts, part 1: the visual check. The check on the welded joints was conducted directly after the welding. The examiner had the testing and production documentation to his disposal. After the completion of the visual check, the check report was elaborated.

The tensile test was realised according to the norm STN EN 12814-2: Testing of the welded joints of the thermoplastic, part 2: The tensile test. The testing body was the PE 100 pipe with the diameter of D_n=400 mm and it was pulled in the direction of the longitudinal axis with the constant speed till the time of breaking or flowing of the material. During the test course the charging by which the body was strained was measured.

The flaking test is only done for the pipes welded by electric sleeve. This test is defined by the norm STN EN 12814 – 4. The test met because the break length in the weld is not

bigger than the distance between the first two windings of the electrofusion adapting pipe wire and the separation between the pipe and adapting pipe did not occur.

Macroscopic test was conducted according to the norm STN EN 12814 – 5: Macroscopic testing. The material which was exposed to this testing was the PE 100 pipe with the diameter of D_n=400 mm and pipe with the diameter of D_n=32 mm[4,5,6].

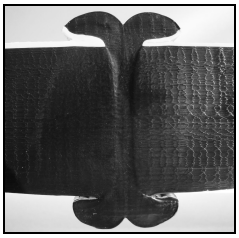

Fig. 16. Macrostructure pipe in diameter D_n = 400 mm

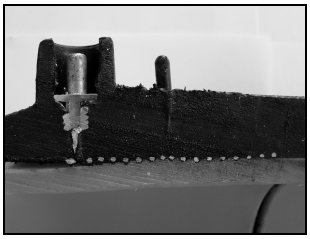

Fig. 17. Macrostructure pipe in diameter D_n=32mm

5. Accredited Protocol of the Welding Procedure (WPQR) and the Defined Welding Procedure (WPS)

The elaborated Accredited protocol of the welding procedure includes a predefined producer's welding procedure (pWPS), visual check protocol, the tensile test protocol and the macroscopic test protocol and A test of the basic material. Next, the defined welding procedure was elaborated. These protocols were elaborated for the averages of D_n=400 mm, D_n=315 mm, D_n=110 mm of the pipe samples welded on blankly hot body and averages D_n= 315 mm, D_n=110 mm, D_n=90 mm of the pipe samples welded by the electric-adapting pipe.

6. Conclusion

The main importance of creation of technological procedures of welding of the plastic is to improve significantly the quality of welding and the weld. Nowadays, the welding technology of the plastic pipes is at such a level that the mistakes which might occur while welding are minimal or none.

Acknowledgments

This work has been supported by Scientific Grant Agency of Ministry of Education of Slovak republic, grant VEGA N^o V-08-046-00.

References

[1] LEŽDÍK, V.-SOBOTA, M.-BEZÁK, J.: *Zváranie v plynárenstve.* 1. vyd. EDIS Žilina, 2001. 191 s. (ISBN 80-7100-902-4)
[2] LOYDA, M. a kol.: *Svařování termoplastů.* 1.vyd. UNO, s.r.o. Praha, 2001. 477 s. (ISBN 80 – 238 – 6603 – 6)
[3] VARGA, M.: *Tvorba technologických postupov pri zváraní plastov v plynárenskom priemysle.* Diplomová práca, Žilina 2008
[4] STN EN 12814 – 2. *Skúšanie zváraných spojov polotovarov z termoplastov. Časť 2: Skúška ťahom*
[5] STN EN 12814 – 4. *Skúšanie zváraných spojov polotovarov z termoplastov. Časť 4: Skúška odlupovaním*
[6] STN EN 13100 – 1: *Nedeštruktívne skúšanie zváraných spojov polotovarov z termoplastov. Časť 1: Vizuálna kontrola*
[7] SNT EN 13067 – *Personál pre zváranie plastov, skúšky odbornej spôsobilosti zváračov, zváranie spojov z termoplastov.*

Transcom 2009, 22-24 June 2009
University of Žilina, Žilina, Slovak Republic

Analysis of the Factors Influencing Microstructure and Mechanical Properties of Austempered Ductile Iron

[*]Alan Vaško, [**]Peter Kopas
[*] University of Žilina, Faculty of Mechanical Engineering, Department of Material Engineering, Univerzitná 8215/1, 010 26 Žilina, Slovakia, alan.vasko@fstroj.uniza.sk
[**] University of Žilina, Faculty of Mechanical Engineering, Department of Applied Mechanics, Univerzitná 8215/1, 010 26 Žilina, Slovakia, peter.kopas@fstroj.uniza.sk

Abstract. The paper deals with some factors influencing microstructure and mechanical properties of austempered ductile iron (ADI). Final structure and properties of ADI are obtained by exactly controlled process of heat treatment of nodular cast iron. The influence of conditions of isothermal heat treatment on microstructure and mechanical properties of austempered ductile iron, especially different temperature of isothermal transformation of austenite and different holding time at this temperature, is shown in the paper.

Keywords: austempered ductile iron, isothermal heat treatment, microstructure, mechanical properties

1. Introduction

Austempered ductile iron (ADI) is new, perspective construction material with an excellent combination of strength, plasticity and toughness. Special properties of ADI are given by unique structure of matrix which is created by acicular ferrite and retained austenite. Technical literature often describes this matrix as bainite (although it does not contain carbides). The structure of ADI is obtained by exactly controlled process of heat treatment of nodular cast iron (Fig. 1) [1,2].

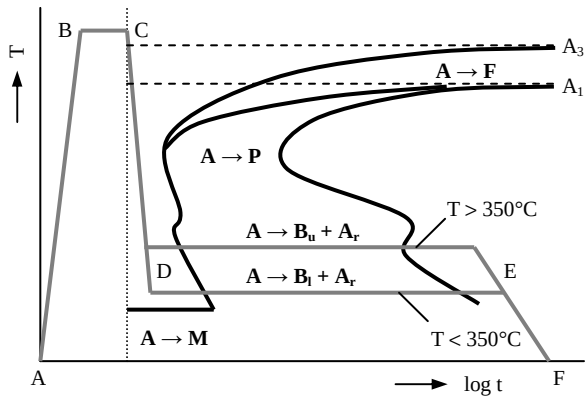

Fig. 1. Process of isothermal heat treatment in the diagram of isothermal transformation of austenite.

The isothermal heat treatment consists of the following stages:

- *heating to the austenitization temperature* (AB);
- *holding time at the austenitization temperature* (BC);
- *quick cooling to the temperature of isothermal transformation of austenite* (CD) so that no other transformation of austenite is carried out before reaching the temperature of isothermal transformation;
- *holding time at this temperature* (DE) until austenite is transformed into bainite;
- *cooling to the ambient temperature* (EF) which is usually realized slowly in order to prevent from formation of stress.

Final structure and properties of austempered ductile iron are dependent on the following metallurgical factors:

- *microstructure of initial nodular cast iron* – nodular cast iron has to have perfectly-nodular graphite with the nodularity higher than 80 % and the count of graphitic nodules higher than 150 mm^{-2} and it usually has fine-grained pearlite-ferritic matrix. The structure has to be without free carbide, segregation, porosity and other casting defects;
- *basic chemical composition* – the content of carbon and silicon is dependent on wallthickness of cast (the content of carbon is from 3,3 % for wallthickness 100 mm up to 3,7 % for wallthickness 5 to 25 mm, the content of silicon is from 1,9 % for wallthickness 100 mm up to 2,4 % for wallthickness 5 to 25 mm), the content of manganese should be lower than 0,2 % because it causes occurrence of martensite at grains boundaries;
- *austenitization temperature and holding time at this temperature* – they shall insure homogeneous austenitic matrix. The austenitization temperature is chosen in the range from 820 to 950 °C in dependence on content of carbon. Higher temperature causes higher hardness, lower temperature causes higher tensile strength and good elongation. Holding time at the austenitization temperature is usually from 1 to 3 hours and it depends on initial structure of nodular cast iron. High content of ferrite in matrix before the heat treatment lengthens the holding time; pearlitic matrix needs shorter holding time than ferritic;
- *cooling rate to the temperature of isothermal transformation of austenite* – cooling rate has to be quick enough in order to prevent from the occurrence of undesirable ferrite and pearlite;
- *temperature of isothermal transformation of austenite and holding time at this temperature* – they both determine the final structure and properties of ADI in a decisive way. The temperature of isothermal transformation is usually within 250 and 450 °C. At higher temperatures (350 to 450 °C) it is possible to obtain ADI with lower strength and hardness but higher elongation and toughness and better fatigue characteristics. At lower temperatures (250 to 350 °C) it is possible to get ADI with higher strength, hardness and abrasion resistance but lower elongation and toughness. The holding time at temperature of isothermal transformation of austenite is within 0.5 and 4 hours when austenite is transformed into upper or lower bainite;
- *alloying elements* – they have strong influence on quality and properties of ADI. Some of them (for example copper, molybdenum or nickel) decrease critical cooling rate by moving the diagram of isothermal transformation of austenite to the right [3,4].

2. Experimental material and methods

The influence of conditions of isothermal heat treatment on microstructure and mechanical properties of austempered ductile iron was searched on several sets of specimens which were different in temperature of isothermal transformation of austenite and holding time at this temperature.

Ferrite-pearlitic nodular cast iron was used as basic material for isothermal heat treatment. The austenitization temperature was 920°C and the holding time at this temperature was 30 minutes. The isothermal transformation of austenite was realized in AS 140 salt bath at the temperatures 420, 380, 320 a 250 °C and the holding time at this temperature was from 30 to 300 minutes (by 30 min.) [5,6].

3. Experimental results

From microstructural point of view the basic material (after casting) is ferrite-pearlitic nodular cast iron (Fig. 2) with content of ferrite in a matrix 57%, size of graphite within 15 and 60 μm and count of graphitic nodules 205 mm^{-2}. Graphite occurs only in a perfectly-nodular (80%) and imperfectly-nodular (20%) shape.

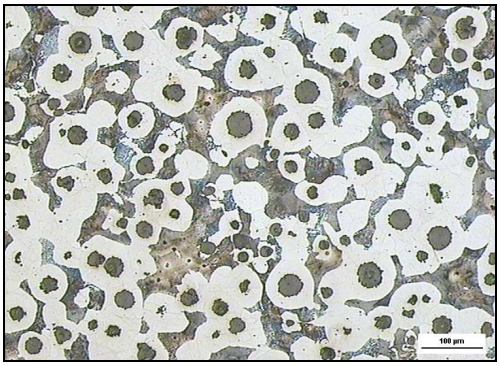

Fig. 2. Microstructure of basic material (after casting) – ferrite-pearlitic nodular cast iron, etched by 3 % Nital.

After isothermal heat treatment ADI was obtained. The specimens after isothermal heat treatment with the temperature of isothermal transformation of austenite 420 and 380 °C have matrix created by upper bainite and retained austenite (Fig. 3a). The specimens after isothermal heat treatment with the temperature of isothermal transformation of austenite 320 and 250 °C have matrix created by lower bainite and retained austenite (Fig. 3b). The content of retained austenite is slightly decreased with increasing holding time in all sets of specimens. The shape, size and count of graphitic nodules in the specimens after isothermal heat treatment are not changed in comparison with the specimen of basic material (after casting).

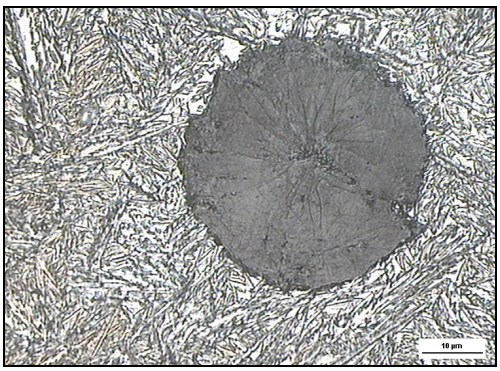

a) 380°C/ 60' – upper bainite and retained austenite

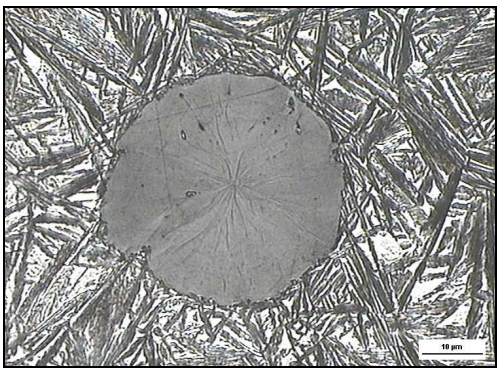

b) 320°C/ 60' – lower bainite and retained austenite

Fig. 3. Microstructure of specimens after isothermal heat treatment – austempered ductile iron, etched by 3 % Nital.

The tensile strength of basic material (ferrite-pearlitic nodular cast iron) is 711 MPa, the hardness of basic material is 24.6 HRC. The isothermal heat treatment has induced considerable improvement of tensile strength and hardness in comparison with basic material. The tensile strength and hardness of the specimens after isothermal heat treatment are increased with decreasing temperature of isothermal transformation of austenite (Tab. 1).

Fatigue strength of basic material is about 390 MPa. The isothermal heat treatment has induced decrease of fatigue properties in comparison with basic material. Fatigue endurance of the specimens after isothermal heat treatment is decreased with decreasing temperature of isothermal transformation of austenite.

Specimen	Matrix	R_m (MPa)	HRC	σ_c (MPa)
basic material	ferrite + pearlite	711	24.6	390
420 °C/ 60'	upper bainite + retained austenite	980	49.0	378
380 °C/ 60'		1040	50.6	361
320 °C/ 90'	lower bainite + retained austenite	1164	50.3	328
250 °C/ 60'		1551	52.9	276

Tab. 1. Mechanical properties of chosen specimens.

4. Conclusion

Final structure and mechanical properties of casts from ADI are markedly dependent on temperature of isothermal transformation of austenite and holding time at this temperature. Their influence on microstructure and properties of ADI can be summarized in following points:

- the specimens with higher temperature of isothermal transformation of austenite have matrix created by upper bainite and retained austenite and the specimens with lower temperature of isothermal transformation of austenite have matrix created by lower bainite and retained austenite;
- the content of retained austenite is decreased with increasing holding time at the temperature of isothermal transformation;
- the shape, size and count of graphitic nodules are not changed in dependence on the temperature of isothermal transformation of austenite and in dependence on the holding time at this temperature;
- the tensile strength and hardness of the specimens are increased with decreasing temperature of isothermal transformation of austenite, but the elongation and toughness is decreased;
- the fatigue strength is decreased with decreasing temperature of isothermal transformation of austenite.

Acknowledgement

This work has been supported by Culture and Educational Grant Agency of Ministry of Education of Slovak Republic, grant No. 3/6078/08 *Creation of a laboratory and textbooks for teaching of subject „Properties and using of materials"*.

References

[1] SKOČOVSKÝ, P., PODRÁBSKÝ, T.: *Grafitické liatiny*. Žilina, EDIS 2005.

[2] SKOČOVSKÝ, P., VAŠKO, A.: *Kvantitatívne hodnotenie štruktúry liatin*, Žilina, EDIS 2007.

[3] GEDEONOVÁ, Z., JELČ, I.: *Metalurgia liatin*. Košice, HF TU 2000.

[4] VĚCHET, S., KOHOUT, J., KLAKURKOVÁ, L.: *Fatigue properties of austempered ductile iron in dependence of transformation temperature*, Materials science (Medžiagotyra), 2008, Vol. 14, No. 4, p. 324-327.

[5] VAŠKO, A., KOPAS, P.: *Influence of conditions of isothermal heat treatment on microstructure and mechanical properties of austempered ductile iron (ADI)*. In: TRANSCOM 2007, Section 6, Žilina, 2007, p. 255-258.

[6] BELAN, J.: *Structural analyses of advanced materials for aerospace industry*, Materials science (Medžiagotyra), 2008, Vol. 14, No. 4, p. 315-318.

Transcom 2009, 22-24 June 2009
University of Žilina, Žilina, Slovak Republic

Chip Formation when Turning Internal Bearing Rings

Stanislav Veľas, Ján Šemcer
*University of Žilina, Faculty of Mechanical Engineering, Department of Machining and Manufacturing Engineering, Univerzitna 8215/1, 01026 Žilina, Slovakia, stanislav.velas@fstroj.uniza.sk

Abstract. This paper deals with chip formation when CNC production of parts for automotive industry. There are presented experiments connected with choice of the suitable toll and its coating. All options considering of the toll choice were related to the practice requirements.

Keywords: chip formation, tool choice, coating, cutting force

1. Introduction

New technologies of cutting tool production enable to apply the higher cutting speeds and feed and so to increase productivity of machining. Research and design of cutting tools is realized with he cooperation with the practice to ensure to full fill the its requirements [1, 2]. The next significant aspect of mechanical technology is shortening of the cycle times together with full filling requirement connected with quality and production costs [3, 4]. The full filling of the higher mentioned aspects ensures the competitiveness of a company. This paper deals with chip formation when turning internal bearing rings of the progressive bearings. Some problems were indicated when turning the internal surfaces of bearing rings (Fig. 1) connected with chip formation and so the decreasing of productivity.

Fig. 1. Bearing ring applied in the experiments made of steel C56 E2

2. Results and Discussion

There were applied four cutting inserts (Fig. 2) when turning bearing rings under the different cutting conditions presented in Table 1.

VBMT 120404 TT 8115 VBMT 120404 PF 4015 *VBMT 120404 PF 4225* *VBMT 120404 PR 4225*

Fig. 2. Applied cutting inserts

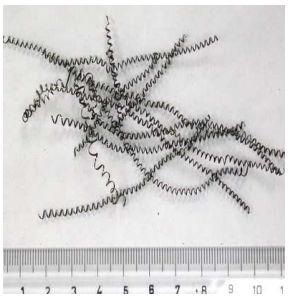

Fig. 3. Chip form

Chip formation was analyzed together with the cutting force measurements. On the base of realized experiments were indicated the best results were obtained when application cutting insert VBMT 120404 TT8115 in connection with the chip formation and range of cutting conditions (Fig. 3).

Analysis of cutting forces were carried out on the recorded signals as illustrated in Fig. 4 and 5. On the base of this signal, cutting forces in the 3 direction were evaluated and are presented in form presented in Fig. 6 and 7. Experimental measurements were carried out for cutting inserts 4015, 4225PF, 4225PR and TT8115 in connection with influence of cutting conditions. The values presented in Fig. 6 and 7 are the average values of were repeated experiments.

n.	a_p (mm)	f (mm)	v_c (m.min^{-1})
1	0,3	0,175	110
2	0,4	0,175	110
3	0,5	0,175	110
4	0,4	0,135	110
5	0,4	0,210	110

Tab. 1. Cutting conditions applied in the experiments

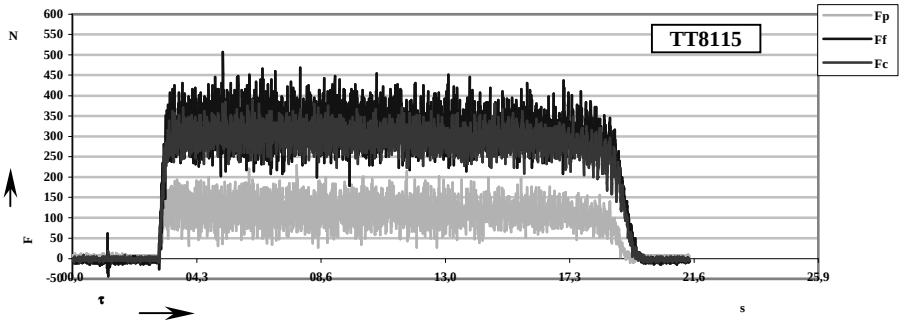

Fig. 4. Record of cutting forces for insert TT815 (applied condition n.2, tab.1)

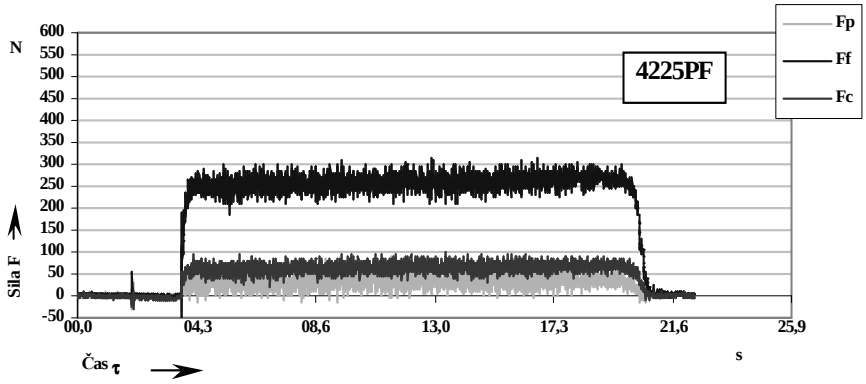

Fig. 5. Record of cutting forces for insert 4225PF (applied condition n.2, tab.1)

Fig. 6 and 7 presents influence of cutting condition of cutting force and its components. The best results were achieved when application cutting insert 4225PF. Application of this cutting insert leads to the lowest cutting force and its components. Elimination of cutting inserts is very important because of eliminates the dynamic aspects of cutting process and so affects tool life and the next related aspects of cutting process.

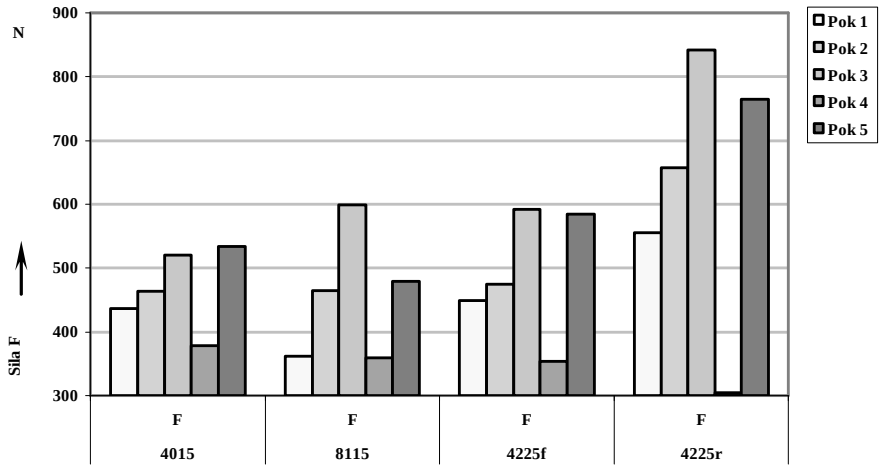

Fig. 6. Comparison of cutting force for the different cutting inserts

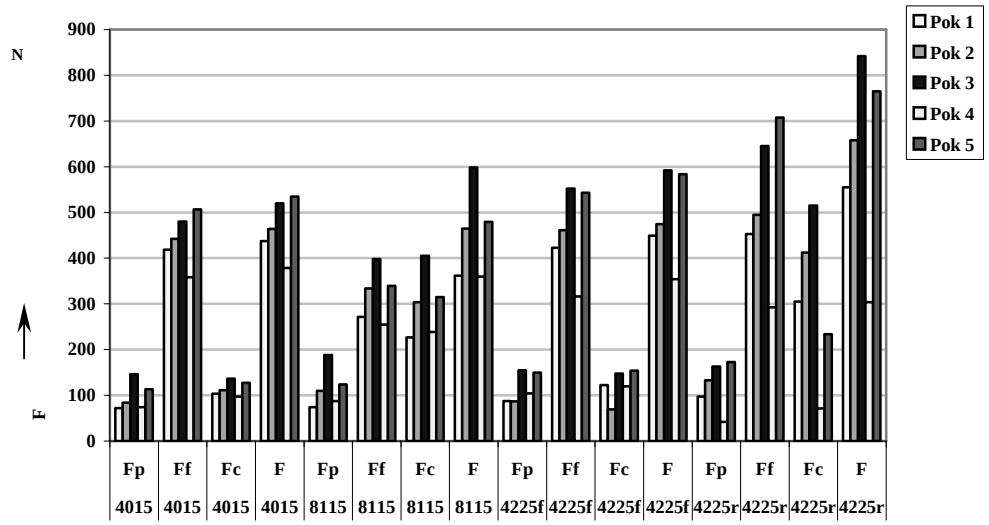

Fig. 7. Comparison of components of cutting force for the different cutting inserts

3. Conclusion

Application of the new generation of cutting tool enable to eliminates some problems related to the chip formations. The significant role takes the rake face of the tool. Application of Al_2O_3 coatings enable to eliminate the friction between the tool and workpiece. Application of cermets cutting tools enables to increases the tool life. Application of different cutting inserts could gives contradictory results (for example, while cutting forces for lower for insert VBMT 120404 PF 4225, the chip formation is difficult). The best choice among the higher applied cutting inserts is the cermet cutting insert VBMT 120404 TT8115 (combination of multicoating PVD and the surface layer Al_2O_3). The results and indication are applied in the practice.

References

[1] BEŇO J. - MAŇKOVÁ L: *Technologické a materiálové činitele obrábania*. Košice: Vienala 2004, str. 143 -145, 161 - 171, 178-179, 190-193,218-219, 194-220.
[2] JURKO J. - ZAJAC J.: *Top trendy v obrábaní*, 2 časť - Nástrojové materiály. Žilina : MEDIA/ST, 2006 ,
[3] BÁTORA, B, VASILKO, K.*: Obrobené povrchy*, Trenčín, GC-Tech, 2000
[4] BEŇO, J.: *Teória rezania kovov*, Vienala Košice 1999
[5] BEŇO J.: *Opotrebovanie rezných nástrojov*, Prešov:2005

Transcom 2009, 22-24 June 2009
University of Žilina, Žilina, Slovak Republic

The Influence of Mould on the Structure of the Alloy AlCu4MgMn

Viktorie Vajsová, Sylvia Kuśmierczak
Faculty of production technology and management, Jan Evangelista Purkyně University in Ústí nad Labem, Department of technology and Material Engineering

Abstract. A target of this experiment is to study the influence of two moulds (metal and bentonic) on the size of dendritic cells and their crystal inhomogeneity under the terms of individual dendrites themselves by typical gravitational casting of the alloy AlCu4MgMn. Intentionally was chosen the alloy with more alloyed elements, where is also a hypothesis of bigger crystal inhomogeneity, which can we uncover with the help of colour corroding of quantitative evaluation of the size of dendritic cells of both mould types.

Keywords: Crystal segregation, metal mould, bentonic shaping mixture, colour metallography, EDS analysis.

1. Introduction

The alloys of Al-Cu-Mg, chiefly duralumins AlCu4Mg, AlCu4Mg and AlCu4MgMn, reaching significant compactness after hardening by heat processing (R_m až 530 MPa). Maximal solubility of copper in stiff solution of aluminium is under steady conditions 5.7 hm.%Cu by temperature of eutectic reaction 548.2 ºC. The alloys of AlCuMg reach significant compactness after hardening; natural senescence is their advantage. Next alloyed element in industrial alloys of Al-Cu-Mg is Mn, which raises the compactness. In the alloy AlCu4Mg occur primarily a binary eutectic $\alpha + CuAl_2$ and small amount of ternary eutectics $\alpha + CuAl_2 + Cu_2Mg_2Al_5$, further Mg_2Si, $FeAl_3$, AlFeMnSi, AlCuFeMn etc.

The disadvantage if these alloys are low resistance against rust and proneness to significant crystal and zone segregation. Cause of establishment of crystal segregation is the selective hardening of crystal by gradual change of stiff phase composition. Important parameters influencing establishment and stage of crystal segregation are chemical composition of alloy, diffusion in solid and liquid phase, influence of cooling castings´ speed, to put it differently heat drain out of castings rate and that depends on chosen mould. Crystal segregation significantly influences mechanical and corrosive qualities of the alloy. Crystal segregation can be suppressed by homogeneous annealing, which will be subject of next experiment [1].

1.1. Casting of Al alloys and their forms

The ways of casting and right choice of mould has fundamental meaning on final structure and qualities of alloys. In majority industrial branches are to date used forms made of tool steel by classical or electro erosion machining. All metal forms are made on flake way on machine tool of steel solid or by stowing of steel parts to make a metal form. Material of metal forms must put up with quite high temperatures, in some cases about 400 to 600°C.

The most frequent material of forms for very exposing places is steel “CSN 42 0002”, alloyed elements Cr – V – Mo and it is meant for work by high temperatures. Big disadvantage by their production is mainly their high price and laboriousness. From this reason is profitable to product forms by cheaper technologies on basis of sand. Bentonic sands allow casting of big forms raw, because they are binding and well-permeable. In contrast to pouring into metal forms, they are cheaper, but castings from metal forms are characterized in that excellent internal compactness, higher smoothness of surface, good dimensioned values and mechanical qualities of castings [4].

2. Procedure of experimental casting

For preparation of alloy castings was used crude material supplied directly by producer, which was prepared in percentage proportion of chemical composition wickedly rule CSN 42 4250. Smelting given material realized in furnace by temperature 700°C, furnace temperature was scanned by digital thermometer with accuracy on ± 2°C. Parameters of prepared castings were 40 / 50 x 100 mm. The first casting was prepared by gravitational casting into metal form, which was treated with protective coat and preheated for working temperature about 220°C. The second casting was prepared under the same conditions and by the same chemical composition like the first casting. The casting was gravitational straight into bentonic form, which had room temperature.

Structure of prepared castings was evaluated by using metallographic methods into macrostructure and microstructure. Macrostructure was evaluated after mechanical grinding, polishing and corroding by NaOH by higher temperature. Microstructure of prepared castings was monitored in central area in corroding state by solution of orthophosphoric acid [3].

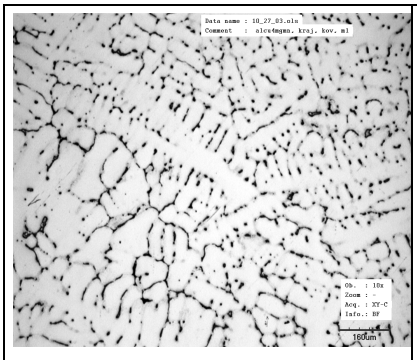

Fig.1.. Microstructure AlCu4MgMn - metal form x100

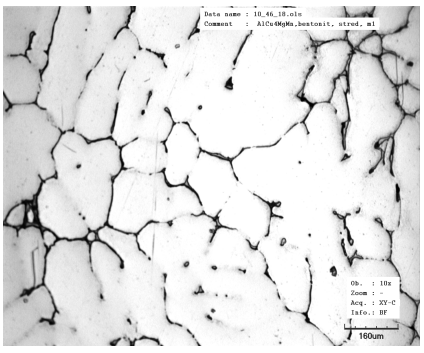

Fig.2.. Microstructure AlCu4MgMn - bentonic form x100

For colour identification were prepared metallographic sections from castings that were mechanical grinded, polished and colour corroding. Colour corroding was made by solution of potassium permanganate in alkaline surroundings of sodium hydroxide. Exemplars, prepared in this way, were watched by confocal laser optic microscope. This method enabled us, among others, to observe and document participating intermetallic phases and heterogeneity of chemical composition under the terms of dendritic cells on high-quality level. Individual colour shades after cell´s cross-section prove inhomogeneity of chemical composition[5].

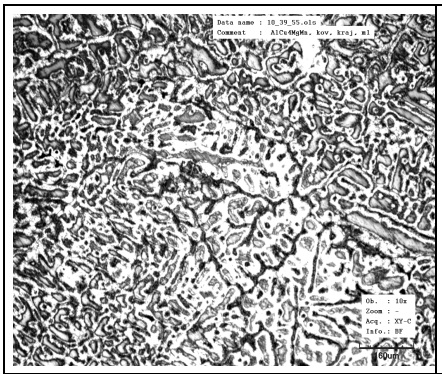

Fig.3. Microstructure AlCu4MgMn - metal form x100

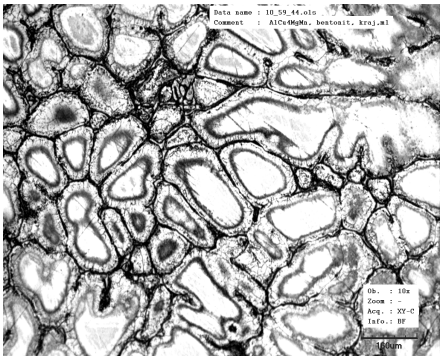

Fig.4.. Microstructure AlCu4MgMn - bentonic form x100

Chemical composition of basic structural components was realized on scanning electron microscope with help of EDS analysis. EDS is very suitable method for identification of all present elements, foreign particle and individual structural components in alloys. With the help of this method was determined chemical composition of eutectic and internal area of dendrite (Fig.5).

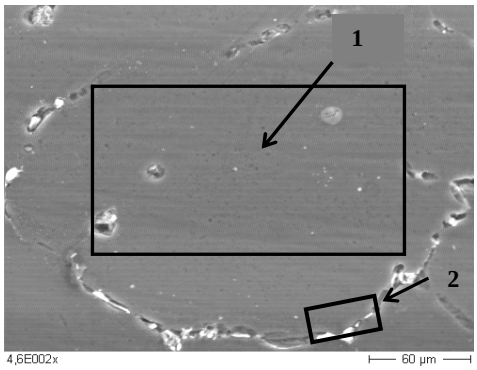

Fig.5. EDS analysis eutectic and internal area of dendrite

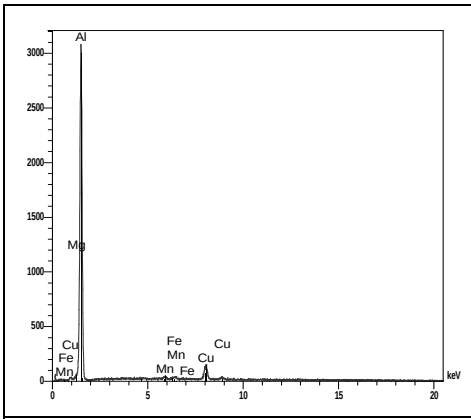

Fig.6. EDS analysis internal area of dendrite

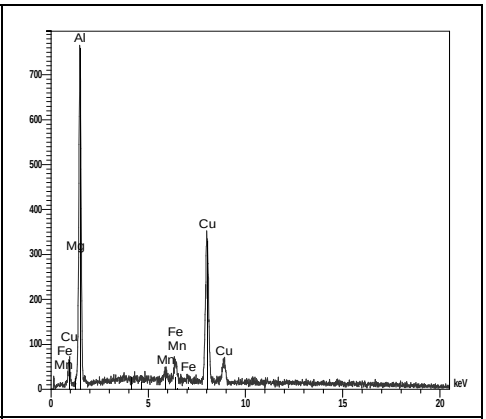

Fig.7.EDS analysis eutectic

	1 [weight %]		**2** [weight %]
Mg	1.53	**Mg**	1.16
Al	89.19	**Al**	64.46
Mn	0.58	**Mn**	0.59
Fe	0.51	**Fe**	1.83
Cu	8.19	**Cu**	31.97

Tab. 1. EDS analysis

3. Conclusion

From executed experiment, evaluation of macrostructures, EDS analysis results and quantitative evaluation of dendritic cell, it is possible to state following:

1. From point of executed macrostructures of differently prepared alloys is obvious, that size of dendrites by alloys casting into bentonic shaping mixture is bigger than by alloys casting into metal form.
2. By numerical evaluation of average size of dendritic cells was determined average (20 measures) size of cells. Average size of dendritic cells by alloys casting into metal form was 163 μm. By alloys casting into bentonic shaping mixture was determined average 356 μm. It follows, that size of dendritic cells is by alloys casting into bentonic form 2, 2 times bigger, than by alloys casting into metal forms. From results can be univocally states, that by casting into metal form it can be reached qualitatively the structure of pouring grain in contrast to casting into bentonic shaping mixture.
3. From EDS analysis of dendritic reticulation is clear, that it is mainly about binary eutectic $CuAl_2$ or ternary eutectic $\alpha + CuAl_2 + Cu_2Mg_2Al_5$. Except of above mentioned eutectics, cells reticulation is also formed by phases $CuAl_2$, AlFeMnSi, AlCuFeMn, etc.

References

[1] Michna,Š., Lukáč I.,Louda et al., *Aluminium materials and technologies from A to Z*, ISBN 978-80-8244-18-8, Printed by Adin, s.r.o.,Prešov 2007

[2] Náprstková, N., Kuśmierczak, S., Náprstek,V. *The Application of Computer Assistance for Structure Characteristics of Material.* In International Multididciplinary Konference, 6th edition. Scientific Bulletin Serie C, Volume XIX, 2nd Volume. Baia Mare: May 27-28, 2005, p.515-520. ISSN-1224-3264, ISBN 973-87237-1-X

[3] Michna,Š., Lukáč I., *Atlas struktur a vad u hliníku a jeho slitin*, Deltaprint, Děčín 1999, ISBN 80-238-4611-6

[4] Michna,Š., Lukáč I., *Technologie a zpracování kovových materiálů*, Adin, s.r.o.,Prešov 2008, ISBN 978-80-89244-38-6

[5] Michna,Š., Lukáč I., *Struktúra a mikrosegregácia zliatiny, AlCu4PbMgMn v liatom stave*, Slévárenství 2-3/2002, 2002, ISSN 0037-6825